University of Kentucky
UKnowledge

Theses and Dissertations--Toxicology and Cancer Biology

Toxicology and Cancer Biology

2018

MULTIVARIATE ANALYSIS TO IDENTIFY POTENTIAL BIOMARKERS FOR PROGNOSIS AND TREATMENT RESISTANCE IN HEAD AND NECK CANCER PATIENTS

Christina Ann Wicker
University of Kentucky, wickercaw@gmail.com
Author ORCID Identifier:
https://orcid.org/0000-0003-1018-8708

Digital Object Identifier: https://doi.org/10.13023/ETD.2018.001

Right click to open a feedback form in a new tab to let us know how this document benefits you.

Recommended Citation

Wicker, Christina Ann, "MULTIVARIATE ANALYSIS TO IDENTIFY POTENTIAL BIOMARKERS FOR PROGNOSIS AND TREATMENT RESISTANCE IN HEAD AND NECK CANCER PATIENTS" (2018). *Theses and Dissertations--Toxicology and Cancer Biology*. 19.
https://uknowledge.uky.edu/toxicology_etds/19

This Doctoral Dissertation is brought to you for free and open access by the Toxicology and Cancer Biology at UKnowledge. It has been accepted for inclusion in Theses and Dissertations--Toxicology and Cancer Biology by an authorized administrator of UKnowledge. For more information, please contact UKnowledge@lsv.uky.edu.

STUDENT AGREEMENT:

I represent that my thesis or dissertation and abstract are my original work. Proper attribution has been given to all outside sources. I understand that I am solely responsible for obtaining any needed copyright permissions. I have obtained needed written permission statement(s) from the owner(s) of each third-party copyrighted matter to be included in my work, allowing electronic distribution (if such use is not permitted by the fair use doctrine) which will be submitted to UKnowledge as Additional File.

I hereby grant to The University of Kentucky and its agents the irrevocable, non-exclusive, and royalty-free license to archive and make accessible my work in whole or in part in all forms of media, now or hereafter known. I agree that the document mentioned above may be made available immediately for worldwide access unless an embargo applies.

I retain all other ownership rights to the copyright of my work. I also retain the right to use in future works (such as articles or books) all or part of my work. I understand that I am free to register the copyright to my work.

REVIEW, APPROVAL AND ACCEPTANCE

The document mentioned above has been reviewed and accepted by the student’s advisor, on behalf of the advisory committee, and by the Director of Graduate Studies (DGS), on behalf of the program; we verify that this is the final, approved version of the student’s thesis including all changes required by the advisory committee. The undersigned agree to abide by the statements above.

Christina Ann Wicker, Student

Dr. Tadahide Izumi, Major Professor

Dr. Isabel Mellon, Director of Graduate Studies

MULTIVARIATE ANALYSIS TO IDENTIFY POTENTIAL BIOMARKERS FOR PROGNOSIS AND TREATMENT RESISTANCE IN HEAD AND NECK CANCER PATIENTS

DISSERTATION

A dissertation submitted in partial fulfillment of the
Requirements for degree of Doctor of Philosophy in the
College of Medicine at the University of Kentucky

By

Christina Ann Wicker

Lexington, Kentucky

Director: Tadahide Izumi

Lexington, Kentucky

2017

Copyright © Christina Ann Wicker 2017

ABSTRACT OF DISSERTATION

MULTIVARIATE ANALYSIS TO IDENTIFY POTENTIAL BIOMARKERS FOR PROGNOSIS AND TREATMENT RESISTANCE IN HEAD AND NECK CANCER PATIENTS

It is estimated that nearly 50,000 individuals in the United States will be diagnosed with head and neck cancer in 2017 (American Cancer Society www.cancer.org). Ninety percent of oral cancers are head and neck squamous cell carcinoma (HNSCC). Major obstacles in the treatment of HNSCC are recurrence and treatment resistance, which contributes to increased mortality. Therefore, there is increased need to determine genetic alterations in HNSCC that may be ideal novel drug targets, and biomarkers to improve diagnostic and prognostic testing.

Abnormal localization and overexpression of base excision repair protein and transcriptional regulator Apurinic/Apyrimidic endonuclease (APE1) has been associated with treatment resistance and poor prognosis. Therefore, we explored mechanisms for how APE1 contributes to treatment resistance and increased mortality in HNSCC.

Because oxidative stress heavily influences APE1's expression and transcriptional regulatory activities, we examined genes involved in oxidative stress management, including SOD3 and NRF2. PPARGC1A, a NRF2 transcriptional co-activator, was also examined as our lab previously observed a link between APE1 and PPARGC1A expression. This previous work also revealed that APE1 suppressed gene expression of tumor suppressor, decorin (DCN).

To examine possible mechanisms for how APE1 regulates expression of tumor suppressors and antioxidants, digital image analysis of immunohistochemistry staining was used to identify alterations in protein expression. Nuclear and total cellular protein expression of APE1, DCN, NRF2, PPARGC1A, and SOD3 were quantified in regions of proximal benign, carcinoma *in situ* (CIS) and invasive HNSCC. Patient survival analysis revealed that increased APE1, DCN, and PPARGC1A protein levels were significantly associated with reduced survival in CIS, benign, and invasive tissues respectively. Using multivariate analysis of protein expression, we identified that increased APE1 protein levels in the CIS of primary tumors were associated with the presence of cancer invaded lymph nodes. Elevated DCN and SOD3 protein levels in benign tissue were associated with poorly differentiated tumors as was reduced PPARGC1A in CIS.

Most importantly, potential prognostic biomarkers for use in early cancer development were identified. Identifying poor prognosis in early cancer development allows the possibility of improved treatment strategies, which could prevent invasive cancer development, and increase patient survival.

KEYWORDS: Head and Neck Squamous Cell Carcinoma, APE1, Digital Image Analysis, Biomarkers, oxidative stress, concomitant CIS with invasive

Christina Ann Wicker

Date 9/27/17

MULTIVARIATE ANALYSIS TO IDENTIFY POTENTIAL BIOMARKERS FOR PROGNOSIS AND TREATMENT RESISTANCE IN HEAD AND NECK CANCER PATIENTS

By
Christina Ann Wicker

Tadahide Izumi
Director of Dissertation

Isabel Mellon
Director of Graduate
Studies Date 9/27/17

Dedicated to my mentors, family, friends,

my 4 legged kids, and God.

Acknowledgements

I would like to first thank my primary advisor Dr. Tadahide Izumi. He provided far more than money and space for my work. He provided invaluable insight, guidance, and most of all patience. I was trusted to work largely independent and free of micromanaging. However, he knew when I needed prodding to get back on track and was never abusive in going about it. I have been blessed with the quality of my graduate school mentors.

I would like to express gratitude for my former and current lab members while at the University of Kentucky including Dr. Timothy Scott, Dr. Suganya Rangaswamy, and Bithika Dhar. Working together, we published the papers discussed in chapters 2 and 3. They were always there to lend help, advice, and even emotional support.

I am thankful for the input and guidance from my committee members Dr. John D’Orazio, Dr. Isabel Mellon, Dr. David Orren, and Dr. Hiroshi Saito. They made the perfect mix of basic and translational science. They have high standards but have always been fair. I am also grateful to Dr. Daret St. Clair for providing financial support through the T32 training grant. These individuals, our former chair Dr. Mary Vore, and the department itself went above and beyond supporting me throughout my studies. They maintained faith and continued supporting me when I stumbled from the sudden loss of my mother during my first year. Dr. Vore continues as a wonderful mentor even during “retirement", a time when most refuse to ever think about work again.

I am appreciative of the support and friendship from Dr. Alexandra Amaro-Ortiz, Dr. Stuart Jarrett, Dr. Janice Ortega and fellow classmates Kara Chan, Lu Dai, Nidhi Shukla, James Sledziona, and Chontida Yarana. I am glad to have worked with our collaborators Dr. Susanne Arnold, Dr. Yolanda Brill, Dr. Li Chen, Dr. Eric Durbin, Dr. Craig Horbinski, Dr. Mahesh Kudrimoti, Dana Napier, Dr. Thomas Pittman, Dr. Joseph Valentino, and Dr. Guoqiang Yu.

I continue to be indebted to previous advisors and lab mates especially Dr. Thomas L. Brown and Dr. Kashmira Kulkarni-Datar. They put up with me while I was a bumbling Master's student and I would never have made it this far if it were not for them. These individuals along with Chanel "#5" Keoni, Gwyn Isenhower, and Christopher Salyer continue to support and advise me in life.

I would like to acknowledge the support of my family, and my friends whom I have made my family. I'd list you all but there are just too many of you. Plus, it avoids the awkwardness of unintentionally forgetting someone or having to explain why I intentionally excluded someone. What I wrote in the acknowledgements of my Master's thesis still holds true but it is worth stating again. Thank you for putting up with my constant absence, and seamlessly reintegrating me on the rare occasions I see you. I would say that this will happen much less since I'm finishing my degree but we know that would be a lie. I will still be working more often than not. It's just the nature of research.

I want to thank my Dad for getting me into science into the first place. You were the first to introduce me to Mr. Wizard, Doctor Who, Star Trek and all the other geeky stuff that made me interested in science. It's all your fault. I probably could have been a lawyer by now and have a fancy car and home with a white picket fence and 2.5 dogs. Now I have to be satisfied with trying to improve survival and quality of life for cancer patients in a job I love doing despite all the hours and pay scale. Actually, that sounds like a much better deal so I'll stick with it. You have always been there to guide me whether it's letting me fall on my face to understand the consequences of my decisions, or reassuring me that people have survived much worse. I would like to thank my Mom for always pushing me to excel in school. She was the first in her family to complete high school and she wanted me to be the first to finish college. She told me when I was born that I would go to college and she knew before I did that I was better suited as a researcher and not as a physician. She was right as always (mostly). I wish she had lived long enough to see me graduate.

Finally, thanks to everyone who helped proofread at the very last minute including my dad, Nancy Fouts, and Dr. Daniel Diaz.

Table of Contents

Acknowledgements iii

List of Tables xiii

List of Figures xv

Chapter 1: Multivariate Analysis To Identify Potential Biomarkers for Prognosis and Treatment Resistance in Head and Neck Cancer Patients........................... 1

1.1 Introduction... 1

1.1.1 Overview of head and neck cancer 1

1.1.1.1 Current treatments for head and neck squamous cell carcinoma and their limitations... 3

1.1.2 Understanding the role of oxidative stress in head and neck cancer... 4

1.1.2.1 Origin of oxidative stress and its impact on cellular components .. 4

1.1.3 Repair of oxidative DNA damage 6

1.1.4 Antioxidant mechanisms to combat oxidative stress 8

1.1.5 Field cancerization in head and neck squamous cell carcinoma....... 10

1.1.6 Head and neck cancer risk factors and their contributions to oxidative stress…. 13

1.1.6.1 Reduction of SOD3 is associated with increased susceptibility to tobacco induced oxidative stress... 13

1.1.6.2 Human papillomavirus infection contributes to oxidative stress... 14

1.1.7 Head and neck cancer development is associated with an intricate network involving APE1 16

1.1.7.1 Aberrant APE1 expression is linked to increased metastasis and treatment resistance, which contributes to reduced patient survival 16

1.1.7.2 Loss of decorin enhances tumor development 18

1.1.7.3 PPARGC1A supports tumorigenesis and metastasis 19

1.1.7.4 NRF2 suppresses key antioxidant genes 19

1.2 Experimental Rationale 22

1.3 Methods 26

1.3.1 Chemicals and other reagents 26

1.3.2 Head and neck squamous cell tissues and clinical data sets 26

1.3.3 Immunohistochemistry for Head and Neck Squamous Cell Tissues . 27

1.3.4 High-resolution digitization of Immunohistochemistry Slides 27

1.3.5 Immunohistochemistry staining controls 28

1.3.6 Pearson correlation coefficient analysis 29

1.3.7 Univariate and multivariate analysis of protein expression data 29

1.3.8 Survival analysis 30

1.3.9 HNSCC gene expression analysis 31

1.4 Results 32

1.4.1 Differential protein and gene expression analysis in HNSCC 32

1.4.1.1 APE1 protein expression is upregulated in CIS, and invasive HNSCC…….. 33

1.4.1.2 APE1 protein expression is linked to reduced DCN protein levels in HNSCC 34

1.4.1.3 APE1 protein levels are linked to increased NRF2 protein levels 35

1.4.1.4 Suppression of superoxide dismutase upon increased APE1 expression 45
1.4.1.5 APE1 is positively linked to PPARGC1A gene and protein expression 46
1.4.1.6 NRF2 gene expression is linked to reduced gene expression of DCN, SOD2, SOD3 47
1.4.2 Survival Time in relation to APE1, DCN, NRF2, SOD3, and PPARGC1A expression 48
1.4.2.1 Patients with elevated APE1, and PPARGC1A expression had significantly shorter survival periods 48
1.4.2.2 DCN protein levels in benign tissue is linked to reduced survival 53
1.4.3 Multivariate analysis of protein expression within clinical groupings . 53
1.4.3.1 Elevated APE1 was associated with cancer invaded lymph nodes 57
1.4.3.2 Altered expression of DCN, SOD3, AND PPARGC1A in patients with poorly differentiated tumors 59
1.4.3.3 Alterations of SOD3 and PPARGC1A with tobacco usage 60
1.4.3.4 Reduced SOD3 in p16 positive tumors 63
1.4.3.5 Delayed cancer onset in patients with higher SOD3 65
1.5 Discussion 67
1.5.1 Potential biomarkers for identifying aggressive tumor phenotypes.... 67
1.5.2 SOD3 as a potential therapeutic target for patients at high-risk for developing HNSCC 70

1.5.3 Network of APE1 and associated factors 71

1.5.4 Limitations of this study 73

1.5.4.1 Limitations in the efficiency of protein expression analysis.......... 73

1.5.4.2 Limitations in obtaining clinical data from patients across the state ………………………………………………………….……….....… 74

1.6 Conclusions 75

Chapter 2: Analysis of RNA Expression of Normal and Cancer Tissues Reveal High Correlation of COP9 Gene Expressions with Respiratory Chain Complex Components 78

Synopsis 79

2.1.1 Background 79

2.1.2 Results 79

2.1.3 Conclusions 79

2.2 Introduction 80

2.3 Methods 83

2.3.1 Nomenclature of COP9 Genes 83

2.3.2 Data Obtained From TCGA 84

2.3.3 Generation of Correlation Coefficient Table Specific for Individual Genes… 84

2.3.4 Cytoband Plot and Generic Graphical Presentations 85

2.3.5 Interpretation of Functional Gene Annotation 85

2.3.6 Derivation of Enrichment Score (ES).. 86

2.4 Results... 86

2.4.1 A single gene expression analysis 86
2.4.2 Coordinated expressions of the COP9 genes in normal tissues........ 87
2.4.3 Loss of synergistic expressions of the COP9 genes in cancer tissues ………………………………………………………………………………93
2.4.4 Validation of the results with subgroups (age, anatomical sites, and smoking history) 93
2.4.5 Chromosome mapping of genes with expressions highly correlated with COPS5 100
2.4.6 Pathway analysis based on KEGG and GO revealed association of COPS5 expression with mitochondrial pathways 104
2.4.7 Alteration of COPS5 expression coordination in cancer tissues...... 109
2.4.8 Analysis of gene expression of other cancers in TCGA 113
2.5 Discussion 116
2.6 Conclusions 122
Chapter 3: Polyubiquitination of Apurinic/apyrimidinic Endonuclease 1 by Parkin …………………………………………………………………………..123
3.1 Synopsis 124
3.2 Introduction 125
3.3 Materials and Methods 127
3.3.1 DNA, Cell Culture And Transient Transfection 127
3.3.2 Immunoblot (Western blot) assay 129
3.3.3 Detection of Ubiquitinated APE1 in A549 131
3.3.4 Analysis of Localization of YFP-Parkin and APE1 131

3.3.5 Co-Immunoprecipitation (CO-IP) of Recombinant APE1-FLAG and Parkin ……132
3.3.6 Proximity Ligation Assay (PLA) 132
3.3.7 Tissue Extract Preparation 133
3.3.8 Immunohistochemistry for GBM and Control Tissues 134
3.3.9 Chemicals and Other Reagents 134
3.4 Results........ 135
3.4.1 Direct Involvement of Parkin in APE1 ubiquitination........ 135
3.4.2 Interaction of APE1 with Parkin 140
3.4.3 Ubiquitination and Degradation of Endogenous APE1 by Parkin and PINK1 ……147
3.4.4 Loss of Parkin is associated with elevated APE1 levels in GBM..... 149
3.5 Discussion 153
3.6 Chapter 3 acknowledgements 157
Chapter 4: Summary and Future Directions 158
4.1 Summary 158
4.1.1 Chapter 1 summary........ 158
4.1.2 Chapter 2 summary........ 160
4.1.3 Chapter 3 summary........ 161
4.2 Future directions........ 162
4.2.1 Explore if APE1 gene has a dominant physical effect on the transcription of nearby genes In HNSCC........ 162

4.2.2 Assessing if APE1 increases NRF2 activity to promote downregulation of DCN, and SOD3 167
Appendix A: List of Supplemental Figures and Tables 170
Appendix B: List of Abbreviations 172
Appendix C: Supplemental Material for Chapter 1 173
Appendix D: Chapter 2 Supplemental Material 180
Appendix E: Chapter 1 Summary of Conclusions 181
References 184
Vita 204

List of Tables

Table 1-1: NFE2L2 transcription factor binding sites within the DCN, and SOD3 promoter regions 21

Table 1-2: Correlation of TCGA HNSCC gene expression 40

Table 1-3: Pearson correlation analysis for APE1 and associated Factors in benign, CIS, and invasive HNSCC 42

Table 1-4: Patient Demographics 55

Table 1-5: Overall P values for clinical analysis........ 56

Table 2-1: Nomenclature of mammalian COP9 genes 81

Table 2-2: Correlation of expression of COP9 genes in normal oral tissues 88

Table 2-3: Correlation of let-7 miRNA and COP9 genes 92

Table 2-4: Loss of coordinated COP9 gene expression in HNSCC........ 94

Table 2-5: Loss of synchronized expression between COPS5 and the other COP9 genes in tumor tissues. 95

Table 2-6: Loss of COP9 expression coordination in tumor tissues independent of age. 97

Table 2-7: Synchronized COP9 expression in normal oral cavity tissues........ 98

Table 2-8: Synchronized COP9 expression in normal tongue tissues........ 98

Table 2-9: Synchronized COP9 expression in normal oral tissues of smokers .. 99

Table 2-10: Effect of relative distance in chromosomes on the gene expression correlation........ 103

Table 2-11: Association of COPS5 with mitochondrial pathways in normal oral tissues 105

Table 2-12: Loss of coordinated expression of COPS5 with mitochondria related genes in the tumor tissues 110

Table 2-13: Enrichment scores for the COPS5 gene on KEGG pathways 112

Table 2-14: ES for COP9 genes for all KEGG pathways 114

Table 2-15: ES for COP9 genes for the oxidative phosphorylation pathway ... 115

Table 2-16: Synchronized expression of the COP9 genes in the matched tissues of normal and lung squamous cell carcinoma 117

Table 3-1: Effect of Parkin and PINK1 on the stability of APE1 141

Table 4-1: Synchronization of DNA repair and survival genes physically located near APE1 in HNSCC 166

List of Figures

Figure 1-1: Disproportionate rates or oropharyngeal incidence and related mortality in the state of Kentucky 2

Figure 1-2: Base Excision Repair 7

Figure 1-3: Field Cancerization 11

Figure 1-4: Proposed Mechanism for APE1's role in HNSCC 24

Figure 1-5: Representative images of Hematoxylin and Eosin, and IHC for APE1, DCN, NRF2, SOD3, and PPARGC1A in benign, carcinoma *in situ*, and invasive HNSCC 37

Figure 1-6: Quantification of Total Cellular and Nuclear APE1, DCN, NRF2, SOD3, and PPARGC1A in benign, carcinoma *in situ*, and invasive HNSCC 38

Figure 1-7: Top significant survival curves based on protein expression 50

Figure 1-8: APEX1 gene expression survivals analysis 52

Figure 1-9: Analysis of protein expression and presence of lymph node invasion at diagnosis. 58

Figure 1-10: Analysis of protein expression and tumor grade at diagnosis. 61

Figure 1-11: Analysis of protein expression and tobacco usage. 62

Figure 1-12: Analysis of protein expression and P16 status. 64

Figure 1-13: Analysis of SOD3 Protein Expression and Age at Diagnosis. 66

Figure 1-14: Summary model of the role of APE1 and NRF2 in suppression of DCN, SOD2, and SOD3 77

Figure 2-1: Pair-wise plot of expressions of COP9 genes 89

Figure 2-2: Expressions of COP9 genes in normal oral tissues.......................... 90
Figure 2-3: Chromosomal mapping of genes with highly synchronized expression with the COPS5 gene. 101
Figure 2-4: Pair-wise plot for RNA expression 5 mitochondrial genes 108
Figure 2-5: Enrichment score for KEGG oxidative phosphorylation pathway .. 111
Figure 3-1: Dual expression vector pBi16-PaPi 130
Figure 3-2: Functional requirements for APE1 ubiquitination............................ 136
Figure 3-3: Parkin, PINK1, and APE1 Functional Domains 139
Figure 3-4: Interaction of APE1 with Parkin in the cytoplasm 142
Figure 3-5: Colocalization of YFP-Parkin and APE1... 144
Figure 3-6: APE1 and Parkin Interaction 146
Figure 3-7: Parkin targets APE1 for degradation 148
Figure 3-8: Effect of Parkin and PINK1 co-expression on APE1....................... 150
Figure 3-9: Parkin and APE1 expressions in GBM 151
Figure 4-1: Synchronized gene expression of genes involved in DNA repair and cisplatin-resistance 164

Chapter 1: Multivariate Analysis To Identify Potential Biomarkers for Prognosis and Treatment Resistance in Head and Neck Cancer Patients

1.1 Introduction

1.1.1 Overview of head and neck cancer

Head and neck cancer is the 8th most common malignancy in the United States, and an estimated 50,000 new cases will be diagnosed within the United States in 2017 (American Cancer Society www.cancer.org). Oral cancer disproportionally impacts Kentucky. Between 2009-2013, oral cancer incidence was roughly 1.2 fold higher than the national average and was highest in the nation (1,2) **(Figure 1-1)**. The age-adjusted incidence rate of oropharyngeal cancer was 11.3 per 100,000 people [95 % confidence interval (CI) 11.3 – 11.4] in the US and 13.8 per 100,000 people [95 % CI 13.3, 14.2] in Kentucky. Kentucky also has increased mortality as a result of head and neck cancer, with 2.9 per 100,000 deaths in the state versus 2.4 per 100,000 people in the nation (SEER & NPCR, Kentucky Cancer Registry) (1).

Approximately 90 % of head and neck cancers are squamous cell carcinoma, which are referred to as head and neck squamous cell carcinoma (HNSCC)(3). Impacted areas include the mouth, tongue, pharynx, nasal cavity, and sinuses. Major risk factors include tobacco and alcohol usage, and human papillomavirus (HPV) infection**.** These cancers have a high rate of recurrence and often develop treatment resistance.

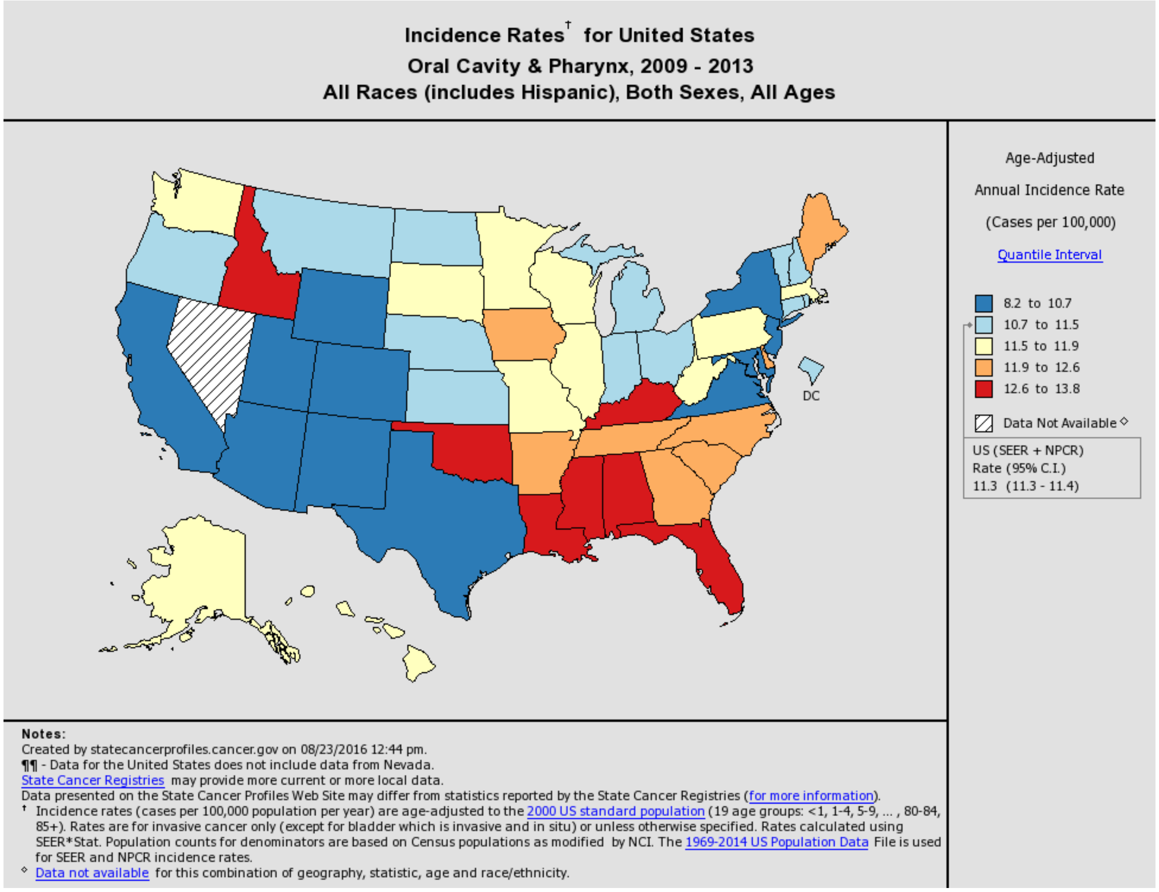
Incidence Rates† for United States
Oral Cavity & Pharynx, 2009 - 2013
All Races (includes Hispanic), Both Sexes, All Ages
Age-Adjusted
Annual Incidence Rate
(Cases per 100,000)
Quantile Interval
8.2 to 10.7
10.7 to 11.5
11.5 to 11.9
11.9 to 12.6
12.6 to 13.8
Data Not Available ◊
US (SEER + NPCR)
Rate (95% C.I.)
11.3 (11.3 - 11.4)
DC

Notes:
Created by statecancerprofiles.cancer.gov on 08/23/2016 12:44 pm.
¶¶ - Data for the United States does not include data from Nevada.
State Cancer Registries may provide more current or more local data.
Data presented on the State Cancer Profiles Web Site may differ from statistics reported by the State Cancer Registries (for more information).

† Incidence rates (cases per 100,000 population per year) are age-adjusted to the 2000 US standard population (19 age groups: <1, 1-4, 5-9, ... , 80-84, 85+). Rates are for invasive cancer only (except for bladder which is invasive and in situ) or unless otherwise specified. Rates calculated using SEER*Stat. Population counts for denominators are based on Census populations as modified by NCI. The 1969-2014 US Population Data File is used for SEER and NPCR incidence rates.

◊ Data not available for this combination of geography, statistic, age and race/ethnicity.

Figure 1-1: Disproportionate rates or oropharyngeal incidence and related mortality in the state of Kentucky

The state of Kentucky has one of the highest incidence and mortality rates associated with oropharyngeal cancer. Kentucky has an age-adjusted incidence rate of 13.8 [95 % CI 13.3-14.2] compared to the national rate of 11.3 [95 % CI 11.3-11.4]. Additionally, the mortality rate is increased at 2.9 [95 % CI 2.7-3.2] deaths per 100,000 people relative to the national rate of 2.4 [95 % CI 2.4-2.5] deaths per 100,000 people.

(Figures generated by statecancerprofiles.cancer.gov on 10/19/16).

1.1.1.1 Current treatments for head and neck squamous cell carcinoma and their limitations

Earlier stages of HNSCC are often successfully treated with surgery and radiation (4,5). Late stages can be resected and are typically treated with platinum-based chemotherapy, and radiation (5,6). Surgical resection is frequently used in disease management, but procedures can lead to compromised function and severe cosmetic damage. When possible, minimally invasive procedures are performed using laser therapy, and robotic assisted surgeries (4).

Radiation therapy occurs over the course of 7 weeks, with 5 doses of 2 Gy given over each week (4). However, radiation therapy is not without complications. Repeated radiation exposure damages healthy tissues, which can lead to delayed wound healing and can complicate recovery from any future operations (7-9). Radiotherapy can induce loss of function of the salivary glands, and thyroid. Patients may also experience dysphagia, forcing them to rely on feeding tubes (6).

There are multiple chemotherapeutic options including platinum-based compounds, antimetabolites, and taxanes (5,10). The immunotherapy drug Cetuximab is used to inhibit epidermal growth factor receptor (EGFR), which is commonly overexpressed in head and neck cancers (5,11). However, these drugs are not without risk, and treatment resistance is still an issue. Chemotherapy drugs are notorious for causing severe gastrointestinal disruption leading to rapid weight loss, as well as a weakened immune system that leaves individuals prone to deadly infections (12). Despite the many treatment options to combat head and neck cancer, treatment resistance is common and contributes to increased mortality. New and improved treatment options are needed to increase patient survival and quality of life.

1.1.2 Understanding the role of oxidative stress in head and neck cancer

1.1.2.1 Origin of oxidative stress and its impact on cellular components

Oxidative stress has been implicated in the development of cancer. This is thought to be a result of damage to key cellular components such as RNA, lipids, proteins, and DNA (13-18). Oxidative stress occurs as a result of imbalance between reactive oxygen species (ROS) with the antioxidant systems responsible for ROS neutralization (19-21). These groups are composed of both radical and non-radical compounds. Free radicals contain unpaired electrons and in an effort to become stable, remove electrons from other molecules (22). This process leads to the formation of additional free radicals that must be neutralized in order to prevent further damage (22). Non-radicals do not contain unpaired electrons. However, they can be converted into radical compounds. ROS radicals include superoxide ($O^{\bullet -}$), hydroxyl ($OH^{\bullet}$), alkoxyl radical ($RO^{\bullet}$), and peroxyl radical ($ROO^{\bullet}$) (22,23). Some of the non-radical ROS forms include hydrogen peroxide (H_2O_2), singlet oxygen ($^1O_2$), ozone (O_3), and organic peroxide (ROOH) (22,23). ROS are generated during normal metabolic reactions due to oxidative phosphorylation in the mitochondria (20,24). In addition, reactive oxygen species are generated in response to exogenous sources such as ultraviolet light, ionizing radiation, and lifestyle factors such as tobacco and alcohol usage (25).

Oxidative stress can damage critical cellular components including RNA, proteins, lipids, and DNA, and is thought to be involved in tumorigenesis. RNA is particularly prone to oxidative damage due to its close proximity to ROS created by the mitochondria. Unlike DNA, RNA is single stranded and there are few repair mechanisms compared to what DNA has. Damaged RNA can result in abnormal protein synthesis, but little is known about its role in cancer (13,17,26,27). Oxidative stress can also inactivate and induce proteolysis of proteins, including inactivation of antioxidant proteins (28,29). This likely exacerbates levels of oxidative stress and further increases cellular damage. Oxidative stress causes lipid peroxidation. This can result in disruption of cellular membranes and lead to the formation of malondialdehyde (15,30). Malondialdehyde, an active carbonyl, creates protein and DNA adducts (15). Significantly elevated levels of malondialdehyde been reported in head and neck cancer patients, which was linked to increased recurrence, and reduced survival (16,31,32). Oxidative stress can therefore damage numerous cellular components and disrupt normal cell function.

Oxidative stress can lead to DNA damage and cause the formation of single and double stranded DNA breaks. ROS damage the sugar-phosphate backbone of DNA, as well as pyrimidine and purine nucleotides (23,33). There are over 20 known forms of oxidized DNA nucleotides (23,33). Guanine is the most commonly oxidized nucleotide as it has the lowest oxidation potential of all nucleotides (34). The most prevalent forms of oxidized guanine include 8-oxoguanine (8-oxoG), and 2,6-diamino-4-hydroxy-5-formamidopyrimidine (FapyG) (20,34,35). Unrepaired DNA damage can lead to the formation of DNA mutations in key oncogenes and tumor suppressors, which contribute to tumorigenesis.

1.1.3 Repair of oxidative DNA damage

Repair of oxidative DNA damage is essential in preventing tumor development. Oxidative damage of lipids, RNA, and proteins are detrimental to the cell, but can be more easily removed and replaced. Oxidative damage to DNA is much more critical as DNA is the instructional foundation from which all other cellular components are made. Mutations within key oncogenes and tumor suppressors contribute to tumorigenesis (36,37). Therefore, it is of the utmost importance to correct oxidative DNA damage in order to prevent the formation of DNA mutations.

Base excision repair is largely responsible for repair of oxidative DNA damage including the repair of damaged nucleotides, abasic sites, and single strand breaks **(Figure 1-2)** (20,38-40). Damaged DNA bases are initially recognized by a family of enzymes called glycosylases (20,38-40). Apurinic/apyrimidic endonuclease 1 (APE1) then cleaves the phosphodiester bond in the sugar-backbone, which generates a 3’-OH termini (20,40,41). The deoxyribophosphodiesterase (dRpase) activity of polymerase beta creates a 5’-P through removal of the 5’-ribose moieties (20,38). Ligation occurs as the final step of base excision repair after polymerases fill in the break-site gap (20,40-44). Base excision repair is important in repairing oxidative DNA damage in order to prevent the formation of tumorigenic mutations.

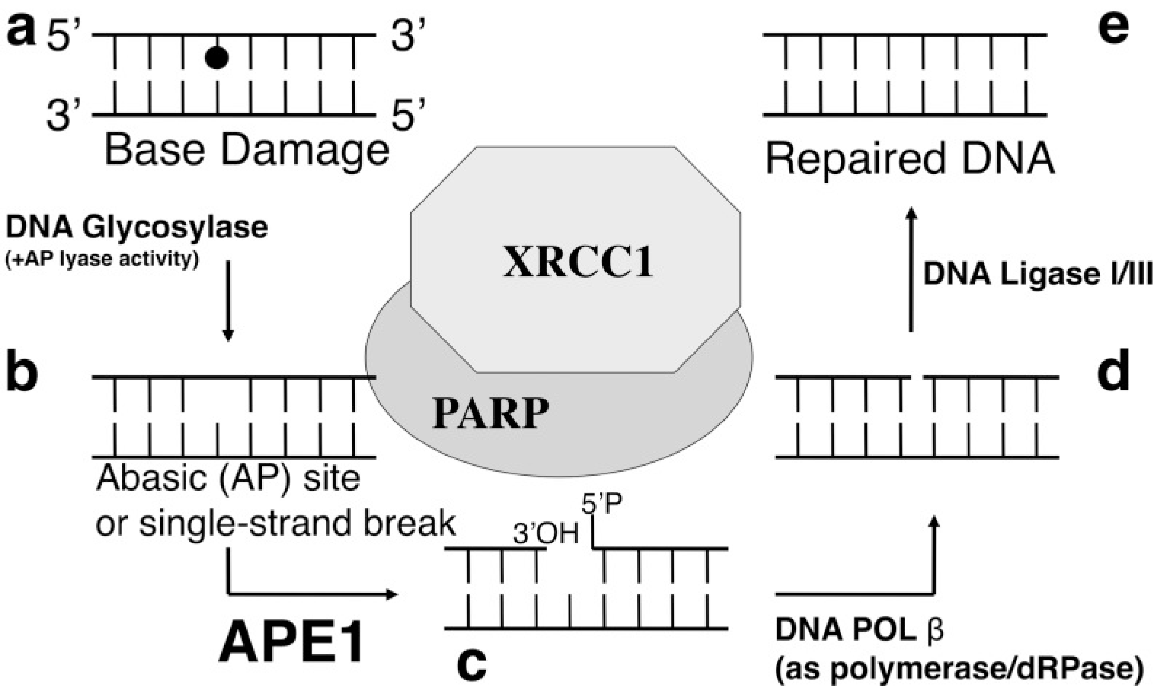
a
5'
3'
3'
5'
Base Damage
DNA Glycosylase
(+AP lyase activity)
b
Abasic (AP) site
or single-strand break
APE1
c
3'OH
5'P
XRCC1
PARP
DNA POL β
(as polymerase/dRPase)
d
DNA Ligase I/III
e
Repaired DNA

Reproduced from Scott, T.L.; Rangaswamy, S.; Wicker, C.A.; and Izumi, T. *Antioxidants & Redox Signaling*. 2014. 20(4): 708-26.

Figure 1-2: Base Excision Repair

A. DNA glycosylases recognize and remove damaged DNA bases. B. This leads to the creation of an abasic site or single strand break. C. APE1 processes 3' ends and creates the 3'-OH termini necessary for DNA polymerase activity. D. DNA polymerase beta generates 5'-P termini through removal of 5'ribose moieties, and fills in the gap. E. Finally, DNA is ligated with DNA ligase I or III.

1.1.4 Antioxidant mechanisms to combat oxidative stress

Although there are numerous DNA repair pathways to prevent the formation of DNA mutations, cells also have complex antioxidant systems to neutralize oxidative stress in order to prevent damage. Superoxide anions ($O^{\bullet-}$) are neutralized by the superoxide dismutase (SOD) family (22,45,46). They do so by dismutation of superoxide anions into oxygen and hydrogen peroxide ($O^{\bullet-} \rightarrow O_2 + H_2O_2$) (22,46,47). The hydrogen peroxide formed is relatively stable compared to radical ROS compounds. However, it undergoes conversion to hydroxyl radicals through Haber-Weiss or Fenton reactions, which leads to more oxidative stress-induced damage (22,23). To prevent the formation of hydroxyl radicals, hydrogen peroxide undergoes reactions involving the enzymes catalase and glutathione peroxidase. Catalase reduces hydrogen peroxide to water (H_2O) and oxygen (O_2) ($2H_2O_2 \rightarrow 2\ H_2O + O_2$) (22,46). Glutathione peroxidase along with antioxidant, glutathione (GSH), facilitates the conversion of hydrogen peroxide into water and glutathione disulfide (GS-SG), ($2GSH + H_2O_2 \rightarrow H_2O + GS\text{-}SG$) (46). All of the above processes help to minimize oxidative stress and lessens its negative impact of cellular health.

In humans, the superoxide dismutase family is comprised of 3 major isoforms including SOD1 (copper, zinc superoxide dismutase), SOD2 (manganese-containing superoxide dismutase), and SOD3 (extracellular superoxide dismutase) (46-48). Alterations of superoxide dismutases are linked to significant pathologies including neurological and cardiac dysfunction, as well as cancer (48-51). SOD1 is primarily located within the cytoplasm (48). While the roles of SOD1 in carcinogenesis have not been well clarified, alterations of SOD2 and SOD3 have been observed in cancer (51).

SOD2 is predominantly located within mitochondria (48). SOD2 has conflicting results as to its role in cancer (31,48,52-55). Reduction of SOD2 has been reported in pancreatic cancers as well as in invasive breast cancers (52,54,56). Increased cellular proliferation of pancreatic cancer cells was observed with reduction of SOD2 (54). However, elevated SOD2 has also been reported in gastric and lung cancer (53,55,57). In patients with gastric cancer, increased SOD2 was linked with increased lymph node metastasis, as well as reduced survival (52,53,55).

SOD3 is associated with the extracellular matrix and is also secreted into blood plasma and synovial fluids (36,58,59). Though primarily extracellular, there are also reports of SOD3 localization in the cytoplasm and nucleus (60,61). Oxidative stress induces nuclear translocation of SOD3 and this has been proposed as a means to protect nuclear elements from oxidative stress-induced damage (60,62,63). Secretion of SOD3 into blood plasma may be a means to replenish cells where SOD3 has been depleted by chronic oxidative stress (36,58,64). This seems probable, as uptake of recombinant SOD3 has been observed in *in vitro* cellular studies (61,62). Superoxide dismutase activity was reduced in the serum of head and neck cancer patients (31). This reduced superoxide dismutase activity likely contributes to oxidative stress and cellular damage in individuals with head and neck cancer. These studies underscore the importance of SOD3 in the development and progression of cancer.

1.1.5 Field cancerization in head and neck squamous cell carcinoma

Field cancerization contributes to the development of head and neck cancer. In 1953, Dr. Danely P. Slaughter first described the concept of field cancerization upon observation of the existence of multifocal squamous cell carcinoma in oral cancer. He posited this phenomenon occurs as a result of preconditioning by unknown carcinogens for long periods of time (65). With the discovery of DNA revealed only a few months prior to this 1953 paper, nothing was yet known as to the genetic underlying of this occurrence (66).

Field cancerization is common in head and neck cancers, and occurs when tissue areas are repeatedly exposed to DNA damaging agents including tobacco, and alcohol (67,68). This chronic exposure to DNA damaging agents leads to the formation of precancerous lesions within a field of tissue, which appears histologically normal **(Figure 1-3)**(67). Due to the undetectable nature of these lesions, precancerous fields may not be fully excised during surgery. This remaining precancerous field can progress into secondary primary tumors. Secondary primary tumors are not directly related to the initial primary tumor, but may contain overlapping mutations (67-70). Criteria defines that a secondary primary tumor have at least 2 cm of normal tissue between tumors or that the second tumor occurs a minimum of 3 years after the initial tumor (69). In addition, secondary field tumors that are more closely related to the initial primary tumor may develop **(Figure 1-3).** This extensive and histologically normal field of precancerous lesions are particularly problematic as it contributes to higher rates of disease recurrence (68,69).

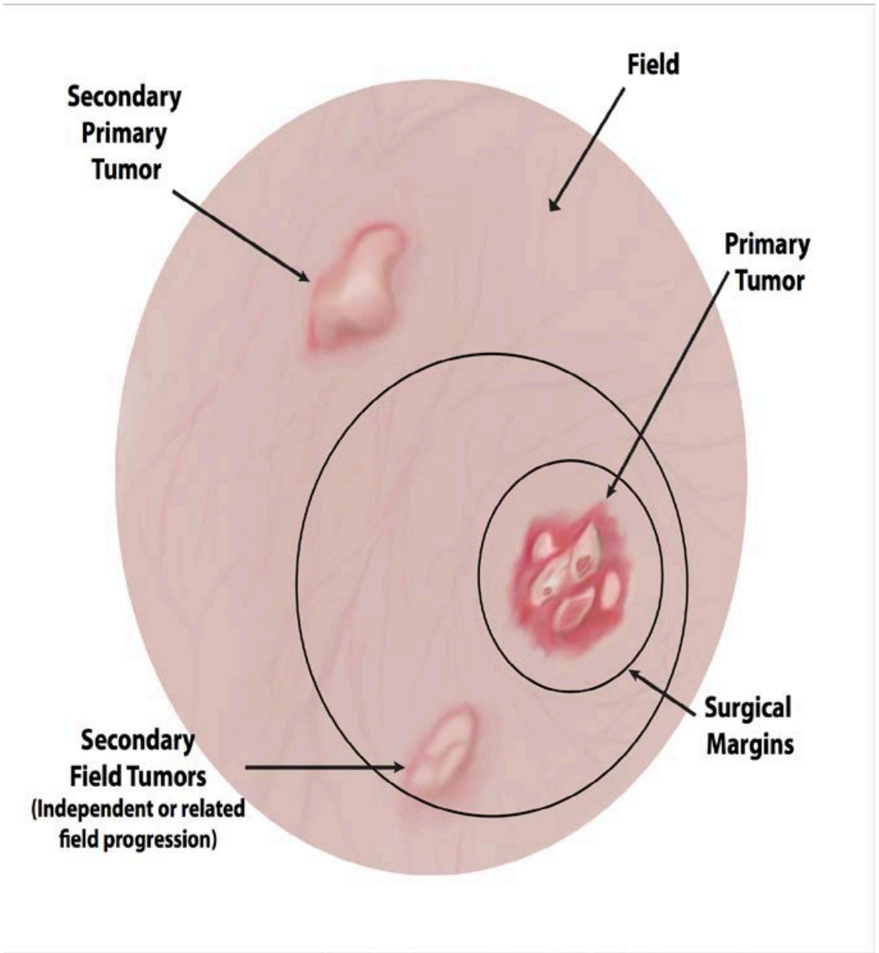
Field
Secondary Primary Tumor
Primary Tumor
Surgical Margins
Secondary Field Tumors (Independent or related field progression)

Figure 1-3: Field Cancerization

Long-term exposure of tissues to DNA damaging agents such as tobacco, alcohol, and UV can lead to mutations in large areas of tissue forming a precancerous field. This field appears histologically margin and can extend well beyond surgical margins. This field can develop secondary primary tumors that are independent of the initial primary tumor. Secondary field tumors that are independent or due to field progression can also occur.

Field cancerization leads to development of multifocal lesions due to widespread exposure to DNA damaging agents (68,69). Field cancerization can lead to a concomitant (i.e. simultaneous) existence of carcinoma *in situ* (CIS) and invasive cancer(71). CIS is early stage cancer that involves only the epithelial cell layers, whereas invasive cancer has disrupted the basement membrane (71). Reduced recurrence free survival and overall survival were observed in patients with concomitant CIS and invasive (Stage T1) bladder cancer (71,72). However, concomitant CIS and invasive tumor is a little studied phenomenon in head and neck cancer and thus it is unclear as to its clinical significance.

Several mechanisms have been proposed to explain the multifocal nature of head and neck cancer (67,73). It has been proposed that these tumors are monoclonal and are the result of intra-epithelia migration, or a transfer of sloughed cancer cells (67,73). It has also been proposed that these tumors are polyclonal, and developed more independent of one another (67,73). Either mechanism may explain the presence of concomitant invasive tumor with CIS. Both progressive genetic alterations that occur during intra-epithelial migration and the development of separate closely related cancerous tissues might result in concommitant CIS and invasive tumor within tissue fields.

1.1.6 Head and neck cancer risk factors and their contributions to oxidative stress

1.1.6.1 Reduction of SOD3 is associated with increased susceptibility to tobacco induced oxidative stress

Tobacco usage increases the risk of developing cancer including lung, pancreatic, and head and neck cancer (74,75). Tobacco combustion produces thousands of compounds, including nearly 100 carcinogens (74-79). Tobacco cigarettes produces free radicals that contribute to increased oxidative stress (22,23,79). This is supported by significantly increased levels of oxidative stress marker 8-hydroxy-2'-deoxyguanosine in smokers, and in bronchial epithelial cells treated with cigarette smoke extract (80). As previously mentioned, oxidative stress contributes to DNA damage. Uncorrected DNA damage can lead to mutations in critical oncogene and tumor suppressor genes, which can promote tumorigenesis.

Members of the cellular antioxidant system including glutathione, and superoxide dismutases are crucial in minimizing the DNA damaging effects of the free radicals found in cigarette smoke (81-83). Overexpression of SOD3 reduced the levels of oxidative stress in mouse macrophages exposed to cigarette smoke extract (84). SOD3 levels are significantly increased in individuals having the SOD3 R213G mutation, which was associated with reduced incidence of chronic obstructive pulmonary disease in smokers (81,82,85,86). In addition, reduction of SOD3 was observed in lung cancer tissues as compared to matched normal tissues (87). These studies highlight the importance of SOD3 in reducing the damaging effects of cigarette smoke.

1.1.6.2 Human papillomavirus infection contributes to oxidative stress

Human papillomavirus (HPV) is a growing risk factor for head and neck cancer and is associated with increased cellular proliferation and oxidative stress. HPV-associated oral cancers have increased 225% between 1988 and 2004 and this is thought to be associated with changing trends in sexual behaviors (88-92). High-risk HPV strains have been associated with several cancers including 70-90% of oral cancers (88-99). Head and neck cancer development is linked to HPV strains 16 and 18, increased sexual activity, and younger populations (6). HPV infects and replicates viral components within epithelial layers such as oral mucosal epithelia (100,101). High-risk strains of HPV encode viral proteins E6 and E7, which inactivate tumor suppressors p53 and retinoblastoma (Rb) (4,100-103). Inactivation of Rb induces overexpression of p16 (101,104). Typically, p16 inhibits cellular proliferation. However, the inactivation of tumor suppressor and cell cycle inhibitor Rb may override p16's attempts in halting cellular proliferation (105,106).

Overexpression of p16 protein as determined by immunohistochemistry (IHC), has been used as a surrogate marker for HPV infection. However, more direct methods including HPV *in situ* hybridization and PCR exist and these are often used to confirm p16 positive IHC results (4,6). There has been concern over the accuracy of using p16 as an indirect marker for HPV infection. Shi et al. analyzed 111 oral squamous cell carcinoma samples using IHC for p16, HPV16 *in situ* hybridization, and PCR amplification of E6 mRNA. IHC results for p16 were significantly in agreement with HPV16 *in situ* hybridization, and PCR amplification of E6 mRNA. Ninety-two percent of IHC p16 positive samples were HPV16 *in situ* hybridization positive, and 86% had positive PCR amplification of E6 mRNA (107). These results support that p16 overexpression as determined by IHC is an accurate surrogate to identify HPV infection.

Increased oxidative stress in HPV infected tissues has been attributed to the E6 and E7 viral proteins (25,104). Cervical cancer cells expressing E6 exhibited higher levels of ROS and 8-oxoguanine as compared to E6-negative cells (102). Transfection of E6 into oral keratinocytes induced higher levels of 8-oxoguanine, and DNA fragmentation as indicated by increased comet tail length (102). Elevated ROS and superoxide levels were identified in HPV-positive head and neck cancer cells as compared to HPV-negative cells (25,104). Artificial expression of E6/E7 in HPV-negative head and neck cells led to increased levels of ROS, and DNA fragmentation as assessed by comet assay (104). These results support that HPV E6/E7 viral proteins promote oxidative stress and DNA damage in infected tissues. This damage can lead to tumorigenic mutations and the development of cancer.

Patients with HPV-associated head and neck cancers have a more favorable prognosis, including increased survival and reduced rates of recurrence (108). Marur et al. demonstrated that patients with HPV-associated cancers have a 94 % [95% CI, 87-100] overall survival rate and 85 % [95% CI, 74-99] progression free survival rate in a 2 year period (6). HPV negative tumors were linked to only 58 % [95% CI, 49-74] overall survival, and 53% [95% CI, 36-67] progression free survival (6). This more favorable prognosis is likely due to increased treatment sensitivity, and earlier identification as compared to HPV-negative tumors(108). This improved treatment sensitivity is supported by increased DNA damage in HPV-positive head and neck cancer cells upon ionizing radiation (104). DNA damage was identified based on increased DNA fragmentation observed by DNA comet assay, and the presence of micronuclei (104). In addition, these studies demonstrated correlation between increased ROS and treatment sensitivity in HPV-associated cells and in cells where E6/E7 was artificially expressed (104). These observations may partly explain why HPV-associated head and neck cancers are more radiosensitive than HPV-negative tumors. Therefore, HPV is an important risk factor for the development of head and neck cancer, and HPV's surrogate biomarker p16 aids in predicting treatment response.

1.1.7 Head and neck cancer development is associated with an intricate network involving APE1

1.1.7.1 Aberrant APE1 expression is linked to increased metastasis and treatment resistance, which contributes to reduced patient survival

As a DNA repair protein, APE1 is predominantly located within the nucleus and mitochondria, and minimally so in the cytoplasm (20). However, aberrant overexpression and cytoplasmic localization have been identified in cancer tissues (109,110). This aberrant overexpression and cytoplasmic localization has been linked to metastasis, treatment resistance, and poor patient survival (20,109-112). APE1 overexpression may be linked to increased oxidative stress. Oxidative stress is typical of the tumor microenvironment and previous research using mammalian cell lines demonstrated that oxidative stress induces APE1 expression (19,113). Reduced levels of antioxidants are often observed within tumor tissues (52,114). This reduction in antioxidants may contribute to APE1 induction by through increased oxidative stress.

Overexpression of DNA repair proteins in cancer may limit the DNA damaging effects of chemoradiotherapy that are needed to effectively kill tumor cells. Chemoradiotherapy is used to kill tumor cells by inducing DNA damage. Overexpression of DNA repair proteins may therefore increase repair of DNA damage induced by chemoradiotherapy, which may allow tumor cells to survive treatment.

In addition to being a base excision repair protein, APE1 is also a redox dependent transcriptional regulator (39,115-119). APE1 regulates transcription of genes including nuclear factor kappa-light-chain-enhancer of activated B cells (NF-kB), hypoxia inducible factor 1 (HIF1), and Nuclear Factor, Erythroid 2-Like 2 (NRF2) (118). NF-kB is a prosurvival gene that is frequently upregulated in head and neck cancers and it has been associated with both treatment resistance and reduced patient survival (120). APE1 mediates hypoxia inducible factor 1 (HIF1) induction(118). HIF1-mediated induction of vascular endothelial growth factor (VEGF) leads to angiogenesis, which supports tumor growth (118). NRF2 is a transcriptional regulator that suppresses transcription of antioxidant genes such as SOD2 and SOD3 (121). Dr. Suganya Rangaswamy of Dr. Izumi's lab previously conducted microarray analysis comparing gene expression in cells with wildtype APE1 levels and in cells deficient in APE1 (122). This previously published study was conducted using mouse embryonic fibroblasts that are deficient in APE1. These fibroblasts were nullizygous for APE1, but contained a copy of the human APE1 gene in order to maintain cell viability (122,123). Increased APE1 expression was associated with increased levels of transcriptional co-activator, peroxisome proliferator-activated receptor gamma coactivator 1-alpha (PPARGC1A), and decreased levels of extracellular matrix protein, decorin (DCN) (122). Therefore, the redox transcriptional activities of APE1 may alter transcription of key tumor suppressor and antioxidant genes, which contributes increased tumor growth, metastasis, and reduced survival.

1.1.7.2 Loss of decorin enhances tumor development

DCN is a small, leucine-rich proteoglycan that acts as a tumor suppressor by preventing tumor growth and spread (124,125). Loss of DCN is associated with increased metastasis in patients having oral squamous cell carcinoma, lung, or breast cancer (126-132). DCN inhibits (VEGF-alpha) thereby inhibiting angiogenesis that is needed to support tumor growth (124,132). Increased VEGF-alpha protein expression, microvessel density, and lymph node involvement was associated with low DCN protein expression within oral squamous cell carcinoma (132). DCN also inhibits metastasis through upregulation of E-cadherin, which is needed to maintain cell adhesion. Maintaining cell adhesion prevents the epithelial-mesenchymal transition necessary for metastasis (120,125,126). During epithelial-mesenchymal transition, cells return to a more stem-like state, allowing their migration to distant sites where new tumors can form (120). This has been supported by increased colorectal tumor development in DCN null mice, which had significantly reduced E-Cadherin (120,125,133). Therefore, DCN is important in suppressing tumor development.

1.1.7.3 PPARGC1A supports tumorigenesis and metastasis

PPARGC1A is a transcriptional co-activator linked to mitochondrial biogenesis, oxidative phosphorylation, and has been implicated in tumorigenesis (134,135). The role of PPARGC1A in supporting tumorigenesis has been supported in Bhalla et al., which observed increased development of colon cancer in wildtype mice as compared to their PPARGC1A knockout counterparts (135). They also observed reduced tumor volume in mice injected with colon cancer cells that had PPARGC1A knockdown (135). Other studies in lung adenocarcinoma and oral squamous cell carcinoma have reported a paradoxical reduction of PPARGC1A in invasive tissues as compared to matched normal samples (134,136). LeBleu et al. discovered that PPARGC1A gene expression is increased in circulating cancer cells as compared to primary and metastatic tumors. They demonstrated that PPARGC1A knockdown inhibited metastasis without impacting cell proliferation within the primary tumor (137). Taken together, these studies support that increased PPARGC1A supports tumorigenesis and metastasis.

1.1.7.4 NRF2 suppresses key antioxidant genes

Nuclear Factor, Erythroid 2-Like 2 (NRF2) is a transcriptional regulator of antioxidant and cell proliferation genes (138,139). APE1 is a proposed NRF2 regulatory protein (140-142). This regulatory link is supported with the observation of reduced NRF2 in cardiac tissue where APE1 was knocked down (140). In this same study, physical interaction of NRF2 and APE1 was demonstrated in immunoprecipitation experiments (140). Increased NRF2-mediated transcription has been observed upon APE1's interaction with NRF2 (141). This would support that APE1 may not only increase NRF2 expression, but also NRF2 activity. In contradiction, one study observed a negative regulatory link between APE1 and NRF2. Knockdown experiments performed in pancreatic cancer cell lines demonstrated increased NRF2 expression, as well as increased expression of NRF2 downstream targets (142). It should be noted that these experiments were performed in various pancreatic cancer cell lines, and there might be some form of cell type specific regulation. APE1 and NRF2 are both upregulated in HNSCC (143-146). Therefore, it is likely that a positive regulatory link between APE1 and NRF2 exists in head and neck tissues.

As mentioned, NRF2 is an important regulator of antioxidant genes. SOD2, SOD3, and DCN gene downregulation was reported in type II alveolar cells with wildtype NRF2 as compared to their homozygous NRF2 knockout counterparts (121). Suppression of SOD2 protein was also observed in the skeletal muscle of aged wildtype mice as compared to the NRF2 homozygous knockout mice (147). In addition, NFE2L2 transcription factor binding sites were identified in the DCN and SOD3 promoter regions (**Table 1-1**)(148-150). Therefore, increased NRF2 expression and activity in HNSCC may increase suppression of superoxide dismutases leading to increased oxidative stress.

Table 1-1: NFE2L2 transcription factor binding sites within the DCN, and SOD3 promoter regions

NFE2L2 Transcription Factor Binding Sites

NFE2L2 Consensus Sequence

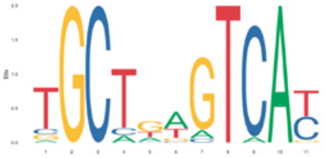

SOD3 Promoter

Sequence	Position (0-based)	Strand	Score	p-value	E-value
GTGACAAGGCT	324	+	8.98	0.000475	0.44
GGGACTCTGCA	335	+	8.52	0.00065	0.6

DCN Promoter

Sequence	Position (0-based)	Strand	Score	p-value	E-value
ATGACTTTGCT	215	+	11.22	0.0001	0.174
ATGACTCAGGC	1153	+	8.41	0.00065	1.13
ATTATATAGCA	225	-	8.33	0.00065	1.13
ATTATTTTGCA	1599	+	7.87	0.000775	1

NFE2L2 (MA0150.1) transcription factor binding sites were determined using LASAGNA-Search 2.0 with matrix-derived JASPER CORE models. NFE2L2 consensus logo obtained from JASPER.

1.2 Experimental Rationale

A major challenge concerning HNSCC is how to overcome treatment resistance and recurrence, which eventually leads to reduced patient survival (151). APE1 overexpression in tumors has been associated with metastasis, treatment resistance, and reduced patient survival (20,109-112). However, the mechanisms underlying this remain unclear. Previous microarray experiments suggest that APE1 significantly reduces gene expression of DCN (122). Reduced DCN expression has been associated with increased metastasis and mortality in cancer patients (126-132). The increased metastasis in patients with APE1 overexpression may be due to APE1 suppressing DCN levels. To explore how APE1 may be suppressing DCN, we looked at APE1's role as a redox dependent transcriptional regulator.

There are studies supporting that APE1 can increase NRF2's protein expression and transcriptional regulatory activity (140,141). Reddy et al. previously reported downregulation of DCN in NRF2 expressing cell lines (121). These observations warrant to test whether suppression of DCN by APE1 occurs indirectly through NRF2. In addition, NRF2 is linked to suppression of antioxidants SOD2, and SOD3 (121). PPARGC1A is a known co-activator of NRF2 and microarray analysis supports that APE1 positively regulates PPARGC1A gene expression (122). PPARGC1A as an NRF2 coactivator may support SOD2 suppression by NRF2. However, there is evidence that PPARGC1A is a positive regulator of SOD2 (152). Therefore, we decided to clarify the regulatory link between PPARGC1A and SOD2.

Chapter 1 will explore the hypothesis that APE1 expression downregulates tumor suppressor and antioxidant proteins and in doing so contributes to increased tumor development **(Figure 1-4).** We aim to gain insight into how APE1 influences survival, and also to identify potential biomarkers that aid in predicting aggressive tumor phenotypes, and survival. To test the proposed model, I measured protein expression of APE1, DCN, NRF2, SOD3 and PPARGC1A within HNSCC samples obtained from patients treated at the University of Kentucky. Digital slide image analysis was used to measure protein expression in benign, CIS, and invasive tissue subtypes based on immunohistochemistry staining intensity. To further support our proposed model, gene correlation analysis was performed using transcriptome data obtained from TCGA.

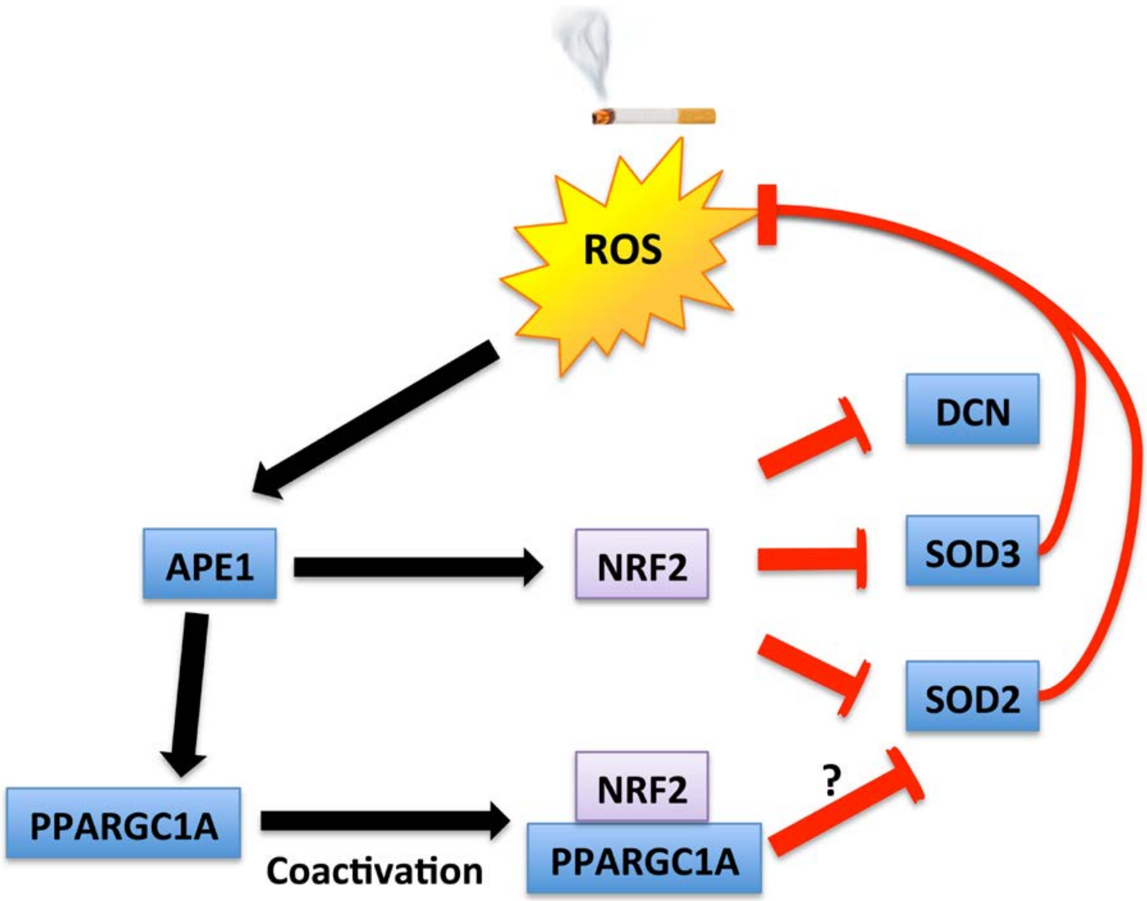
ROS
DCN
APE1
NRF2
SOD3
SOD2
?
PPARGC1A
Coactivation
NRF2
PPARGC1A

Figure 1-4: Proposed Mechanism for APE1's role in HNSCC

I hypothesize that oxidative stress in the tumor microenvironment increases APE1 levels. APE1 interacting with NRF2 drives suppression of DCN. NRF2 also leads to downregulation of SOD3. APE1 influences PPARGC1A driving SOD2 suppression. Downregulation of antioxidants SOD2 and SOD3 further elevates oxidative stress driving further APE1 overexpression.

I performed analysis to identify potential biomarkers that could predict patient survival and aggressive tumor phenotypes including increased metastatic potential. Kaplan-Meier survival analysis was performed where we compared differences in protein and gene expression levels. To understand how alterations of these proteins contributed to reduced patient survival, differences in protein expression were analyzed in relation to various clinical factors such as the presence of lymph node invasion, p16 status, and tumor grade. Understanding how APE1 overexpression contributes to increased cancer mortality could lead to the development of new and improved treatment strategies. Biomarkers that identify high-risk patients, particularly at early stages of tumor development, can potentially improve patient survival. I will discuss in depth some of the major limitations of the experiments in chapter 1 as well as ways to improve this in the future.

Chapters 2 and 3 are previously published first-author and co-first author manuscripts respectively (116,153). In chapter 2, we analyzed normal and cancer tissues to identify changes in genetic coordination between COP9 signalosome components and with components of the respiratory chain complex (153). Chapter 3 discusses post-translational modification of APE1 by tumor suppressor Parkin (116). The last chapter will summarize the findings and significance of chapters 1, 2, and 3. In addition, I discuss possible future directions to further develop the conclusions of this study.

1.3 Methods

1.3.1 Chemicals and other reagents

Antibodies used for this study include anti-APE1 (Santa Cruz, sc-55498), anti-DCN (Santa Cruz, sc-22753), anti-PGC1-alpha (Santa Cruz, sc-13067), anti-SOD3 (Santa Cruz, sc-67088), and anti-NRF2 (ABcam, AB31163). Our lab has previously used Western blotting to confirm the specificity of the anti-APE1, anti-DCN, anti-PGC1-alpha, and anti-SOD3 antibodies. Also utilized were anti-Ki67 (Dako IR626) and anti-desmin (Dako IR606). The Markey Cancer Center Biospecimen and Tissue Procurement Shared Resource Facility (BSTP SRF) has validated all antibodies listed above.

1.3.2 Head and neck squamous cell tissues and clinical data sets

Head and neck squamous cell tissue samples and de-identified clinical data were obtained from 77 patients at the University of Kentucky's Markey Cancer Center following IRB guidelines. Tissue specimens were obtained from the BSTP SRF.

Clinical data associated with these tissues were obtained from the Kentucky Cancer Registry with the help of Dr. Eric Durbin. Clinical data sets included information regarding patient age at diagnosis, tobacco usage, p16 status, time of survival, pathology and clinical staging, histology, tumor grade, presence of lymph node invasion, and whether the patient originated from the central or Appalachian region of Kentucky.

1.3.3 Immunohistochemistry for Head and Neck Squamous Cell Tissues

Formaldehyde-fixed paraffin embedded head and neck squamous cell carcinoma samples obtained from the BSTP SRF were used for immunohistochemistry. All samples were obtained prior to the patients starting chemoradiotherapy. Dana Napier of the BSTP SRF performed slide sectioning, and immunostaining.

Tissue sections with 5-µm thickness were deparaffinized and rehydrated step-wise through decreasing concentrations of ethanol and finally water. Antigen retrieval was performed using a Biocare Medical decloaking chamber and Dako antigen retrieval buffer. Following washing with TBS-Tween, endogenous peroxidase activity was quenched using the Dako peroxidase-blocking reagent. Slides were washed again in TBS-Tween and incubated with primary antibodies at room temperature. Slides were then incubated with polymer linked secondary antibody, either mouse (Dako K4007) or rabbit (Dako K4003). Diaminobenzidine was used for 1-10 minutes to produce color. Slides were subsequently counterstained with Meyer’s hematoxylin, and ammonia was used to blue slides. Slides were dehydrated stepwise through increasing concentrations of ethanol and cleared with xylene before coverslip fixation.

1.3.4 High-resolution digitization of Immunohistochemistry Slides

High-resolution digital image scans of our slides were obtained using the Aperio Scanscope XT (Leica) located in the Markesbery Neuropathology lab of the Sanders-Brown Center on Aging. Slides were scanned at 20X magnification with a resolution of 0.5 micrometer/pixel, which is equivalent to 50,000 pixels per inch (approximately 4 Giga Byte per slide). Immunohistochemistry staining was quantified using the Aperio ImageScope software (V 11.2.0.780) (154-156). Nuclear algorithm V9 was used to determine percentage of positively stained nuclei and calculated using the following formula [% total positive nuclei=(number of positive nuclei/total nuclei)*100%]. Total cellular staining was determined using the Positive Pixel Count algorithm V9 and calculated using the following formula [% total cellular staining=(number of positive pixels/total pixels)*100].

Dr. Yolanda Brill of the University of Kentucky's Pathology department visually inspected hematoxylin and eosin stained slides and annotated regions of benign, carcinoma *in situ*, and invasive tumor regions within slide sections. Areas from these marked locations were then selected for analysis with the Aperio ImageScope software.

1.3.5 Immunohistochemistry staining controls

Dr. Brill with the assistance of Dana Napier examined the immunohistochemistry test slides to identify the staining conditions necessary to minimize background staining. Factors considered included antibody dilutions, incubation periods, as well as the pH of the epitope retrieval buffer.

The accuracy of the Aperio algorithms was assessed by measuring the staining of Ki-67 and desmin, which are known to be predominantly located within the nuclei and cytoplasm, respectively **(Supplemental Figure C-1).** Test slides probed with either Ki-67 or desmin antibodies were assessed with both the nuclear algorithm V9 and the positive pixel algorithm V9.

1.3.6 Pearson correlation coefficient analysis

Pearson correlation coefficient (r) analyses was performed using SPSS 23 with significance determined as $p < 0.05$ (2-tailed). Pearson correlation coefficients are used to determine whether a positive or negative correlation between two factors exists. A positive correlation indicates that as one factor increases so does the second. A negative correlation indicates that as one factor increases, the other decreases. Data from 77 patients initially treated at the University of Kentucky were used to compare nuclear and total protein expression for individual proteins (for example APE1, SOD3) and between benign, carcinoma *in situ*, and invasive tissue subtypes.

1.3.7 Univariate and multivariate analysis of protein expression data

Both SAS and SPSS 23 statistical packages were used for statistical analysis. Dr. Li Chen of the Biostatistics and Bioinformatics Shared Resource Facility was instrumental in the univariate and multivariate statistical analysis. Initially, univariate mixed procedure was used to determine significance of protein changes across all 77 patient samples without regards to clinical data. Box and whisker graphs were generated with bars representing interquartile range, internal line representing the median, and whiskers representing the 95% CI. Multivariate mixed procedure was used to identify significant protein changes in respective clinical groups. Clinical data for the following were analyzed: p16 status, whether patients were from Appalachian Kentucky, tobacco usage, age at diagnosis, pathology stage, tumor grade, and presence of cancer infiltrated lymph nodes at the time of diagnosis. Overall p-values were generated based on linear mixed models with tissue and each variable as covariates, and with compound symmetric covariance structure. Significance was determined as $p<0.005$ after adjusting for examining 10 markers simultaneously, and $p<0.05$ without adjusting for examining 10 markers simultaneously. Categories where significance of the overall p-value was obtained were subjected to further analysis to determine significance of the variable effect (example benign, CIS, and invasive). Data were plotted with error bars representing standard error.

1.3.8 Survival analysis

The data from 77 different patients was used for survival analysis using protein expression data under Dr. Chen's supervision. Days of survival were determined as days between date of diagnosis and date of death, which was then converted to months of survival.

In order to perform Kaplan-Meier survival analysis, we first identified cutoff values for the proposed biomarkers based on previous research from other researchers (157,158). Cutoffs were determined for nuclear and total cellular levels for each individual protein and within each tissue subtype (example benign, CIS, and invasive). The quartiles of each biomarker were determined with low expression defined as the first quartile (Q1), and high expression defined as the third quartile (Q3).

Survival curves based on the Kaplan-Meier estimator were generated in R 3,3,1 GUI 1.68 Mavericks build 7238 (159). Additionally, xlsxjars, and rJava packages were used to import and generate the excel files needed for survival analysis (160-162). Survival, graphics and grDevices packages were used for generation of Kaplan-Meier graphs (159,163). Log Rank (Mantel-Haenszel), and Peto & Peto modification of the Gehan-Wilcoxon test, were used to determine statistical significance ($p<0.05$) (159). The Log Rank statistical test is sensitive in detecting differences in survival for long periods of time whereas the Wilcoxon test is better suited to detect differences at earlier time points (164).

1.3.9 HNSCC gene expression analysis

The Cancer Genome Atlas's online data portal was used to acquire gene expression data (mRNASe12, level3) and de-identified clinical data (example survival time, pathology stage, anatomical location) from 520 patients having head and neck squamous cell carcinoma (https://cancergenome.nih.gov). Gene expression and clinical data were initially organized with programs using command line applications developed with Swift (Xcode ver. 6) (153). Genes of interest were further isolated from the original data set of 15,857 different genes.

Gene expression data was utilized for correlation and survival analysis. Gene correlation was determined using TCGA RNA-Seq data from 43 matched non-neoplastic and HNSCC tissue. This data set was used to calculate Pearson correlation coefficients between individual genes (example APEX1, SOD3). For survival analysis based on gene expression, patient survival was compared between low expression (Q1) and high expression (Q3) of our genes of interest. Cutoff values were determined using same method as with protein expression. There were 44 patients in both low and high gene expression groups.

1.4 Results

1.4.1 Differential protein and gene expression analysis in HNSCC

In this study we examined whether and how APE1, DCN, PPARGC1A, SOD3, and NRF2 expression coordinated with one another, and how expression changed between non-neoplastic and HNSCC tissues. Analysis included gene expression analysis of data obtained from TCGA, and protein expression analysis based on IHC staining of HNSCC obtained from the University of Kentucky. TCGA database contains a large quantity of RNA-Seq data for HNSCC samples, approximately 10% of which have data from matched non-neoplastic tissues (153). Our lab previously reported the use of TCGA's transcriptome database in the discovery of discoordinated gene expression of COP9 subunits with mitochondria-related genes in cancerous tissues as compared to non-neoplastic tissue **(Chapter 2)** (153). We applied the same methods to analyze expression of genes for APE1, DCN, PPARGC1A, SOD2, SOD3, and NRF2 changes in non-neoplastic and HNSCC tumor tissues. APE1 gene name is designated APEX1 and NRF2 gene name is designated NFE2L2. To investigate gene coordination, Pearson correlation coefficients were calculated between genes of interest in non-neoplastic and tumor tissues.

Because gene expression does not always directly correlate to protein expression, we examined protein levels of APE1, DCN, NRF2, SOD3, and PPARGC1A. To do so, we analyzed protein levels in tissue specimens from 77 patients treated at the University of Kentucky's Markey Cancer Center. To objectively measure IHC staining, we utilized digital slide image analysis using the

Aperio ImageScope software. This software was used to calculate total cellular and nuclear protein expression within benign, CIS, and invasive HNSCC. Importantly, a pathologist who specializes in head and neck cancer independently identified regions of benign, CIS, and invasive HNSCC. This helped ensure that regions were accurately analyzed, and minimized bias in selecting regions of analysis using the Aperio ImageScope software. Data from the protein expression levels in proximal benign, CIS and invasive tissue were converted into box and whisker plots. Bars represent the interquartile range, and whiskers represent the 95% confidence intervals. To determine coordination between proteins and within each tissue type, Pearson correlation coefficients were generated.

1.4.1.1 APE1 protein expression is upregulated in CIS, and invasive HNSCC

We first examined if APE1 expression increases in HNSCC, in order to confirm previous studies that demonstrated APE1 overexpression in tumor tissues (109,110,165). APE1 protein expression in benign, CIS, and invasive HNSCC was determined using digital image analysis of IHC staining. Protein expression analysis revealed significantly increased total cellular APE1 in CIS, and invasive tissues as compared to benign ($p<0.001$ for both). In addition, APE1 protein expression was significantly increased in invasive tissue as compared to CIS ($p<0.05$). Nuclear APE1 protein expression was also elevated in both CIS and invasive HNSCC ($p<0.001$, $p=0.0023$ respectively) **(Figure 1-6).** This confirms prior research that demonstrated increased APE1 in cancer tissues (109,110,165).

However, to the best of our knowledge this is the first study to observed increased APE1 protein expression in not only invasive HNSCC but also in CIS.

1.4.1.2 APE1 protein expression is linked to reduced DCN protein levels in HNSCC

Based on our previous gene expression profiling using the wild-type and APE1-knockdown mouse embryonic fibroblasts described in the introduction and in Suganya et al. 2015 (122), we hypothesized that elevated APE1 leads to reduced DCN expression in HNSCC **(Figure 1-4**). To determine whether APE1 expression corresponds to DCN suppression, we performed correlation analysis at both protein and gene expression levels. Total and nuclear DCN protein levels were determined in benign, CIS, and invasive HNSCC using digital image analysis of IHC staining. Total and nuclear DCN protein levels were significantly decreased in both CIS and invasive HNSCC as compared to benign tissue ($p<0.001$ for all) **(Figure 1-5, Figure 1-6).** APE1 protein expression corresponded to significantly decreased DCN protein expression in CIS ($p<0.01$) **(Table 1-3**). Unexpectedly, there was a positive correlation between total cellular APE1 and DCN protein levels in benign tissue. It is not clear as to why, but these results support dysregulation between APE1 and DCN expression in tumor tissues.

We hypothesized that the reduction of DCN expression was a result of APE1's redox transcriptional regulatory activity. To examine whether APE1 gene expression corresponded to decreased DCN gene expression, we calculated Pearson correlation coefficients using RNA-Seq data obtained from TCGA. Gene expression analysis revealed no significant link between APE1 and DCN **(Table 1-**

2). This was unexpected as previously published microarray analysis in MEF cell lines exhibited significantly reduced DCN gene expression in mouse embryonic fibroblasts with wildtype APE1 as compared to cells with APE1 knockdown (122). This difference may be due to heterogeneity of tissues versus an immortalized, monoculture cell line. Further work is needed to determine whether APE1 impacts DCN gene regulation.

1.4.1.3 APE1 protein levels are linked to increased NRF2 protein levels

We hypothesized that APE1 indirectly downregulates DCN and SOD3 by modulating NRF2's transcriptional regulatory activity **(Figure 1-3**). APE1 is known to regulate NRF2 expression as well as increase NRF2's transcriptional regulatory activities (140,141). We first determined overall changes of NRF2 protein expression in benign, CIS, and invasive HNSCC using digital image analysis of IHC slides. Total cellular NRF2 protein levels were increased in invasive HNSCC as compared to benign tissue ($p<0.05$) and to CIS ($p=0.0002$) **(Figure 1-6)**. Gene expression coordination was investigated between NFE2L2, DCN, SOD2, and SOD3. To examine this coordination, we calculated Pearson correlation coefficients in non-neoplastic and tumor tissues using TCGA RNA-Seq data from patients with HNSCC. In non-neoplastic tissues, NFE2L2 gene expression was negatively correlated with DCN, SOD2, and SOD3 ($p<0.01$) **(Table 1-2).** This supports that NRF2 may negatively regulate transcription of DCN, SOD2, and SOD3. Additionally, we analyzed coordination between protein levels of NRF2, DCN, and SOD3. Overall, there was a trend toward negative correlation between nuclear NRF2 and DCN protein levels. However, NRF2 protein had a positive correlation with nuclear DCN and SOD3 in invasive tissues ($p<0.05$). Overall, these results support that NRF2 may be involved in suppressing transcription of SOD2, SOD3, and DCN.

Next, we explored coordination between NRF2 and APE1 protein expression in benign, CIS, and invasive HNSCC by calculating Pearson correlation coefficients. Investigation of protein expression demonstrated a positive correlation between nuclear APE1 and NRF2 in benign ($p<0.01$) and invasive tissue ($p<0.01$) **(Table 1-3 A).** Additionally, a positive correlation was found between nuclear APE1 protein levels in benign tissue and nuclear NRF2 protein levels in CIS ($p<0.05$) **(Table 1-3 A).** These results signify that increased APE1 protein expression in benign and invasive tissue corresponds to increased NRF2 protein expression in benign and invasive tissues. These initial results supported that APE1 may positively regulate NRF2 levels in HNSCC.

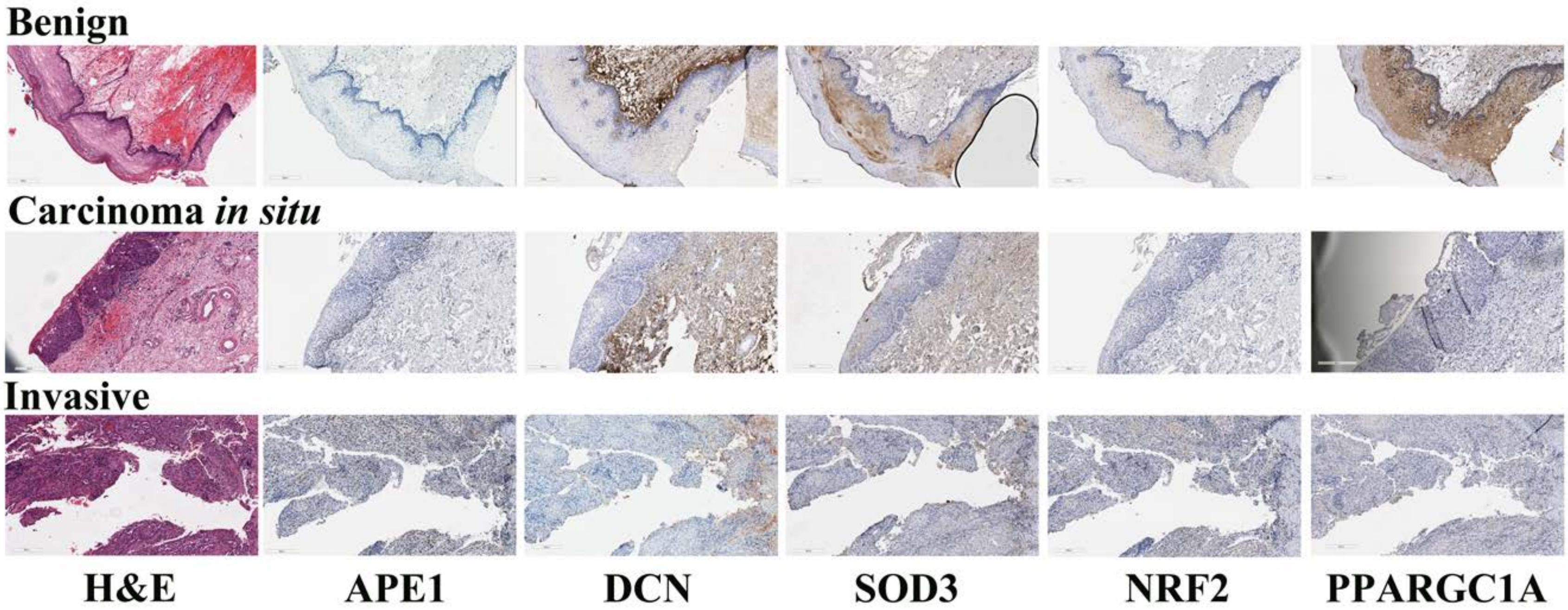
Benign
Carcinoma *in situ*
Invasive
H&E
APE1
DCN
SOD3
NRF2
PPARGC1A

Figure 1-5: Representative images of Hematoxylin and Eosin, and IHC for APE1, DCN, NRF2, SOD3, and PPARGC1A in benign, carcinoma *in situ*, and invasive HNSCC

Digital image scans of benign, carcinoma *in situ*, and invasive HNSCC from a single patient. Serial sections were used for hematoxylin and eosin (H&E) staining, and immunohistochemistry staining to detect APE1, DCN, SOD3, NRF2, and PPARGC1A.

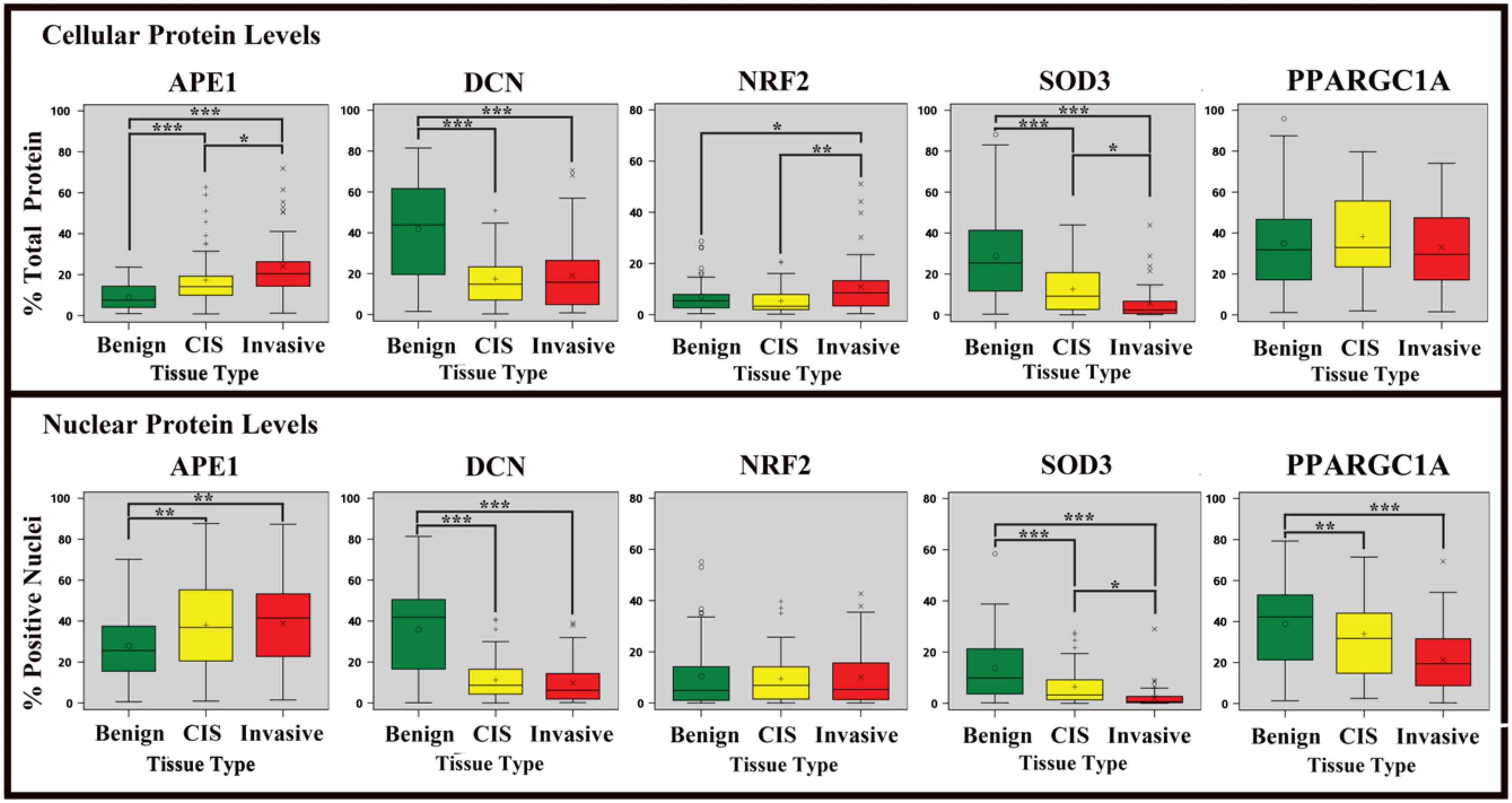

* p<0.05, **p<0.01, ***p<0.001

Figure 1-6: Quantification of Total Cellular and Nuclear APE1, DCN, NRF2, SOD3, and PPARGC1A in benign, carcinoma *in situ*, and invasive HNSCC

Immunohistochemistry staining was analyzed with Aperio software to determine protein levels of APE1, DCN, NRF2, SOD3, and PPARGC1A in benign, CIS, and invasive HNSCC. Bars represent the interquartile range and whiskers represent the 95% confidence intervals. Data is representative of 77 patients.

Table 1-2: Correlation of TCGA HNSCC gene expression

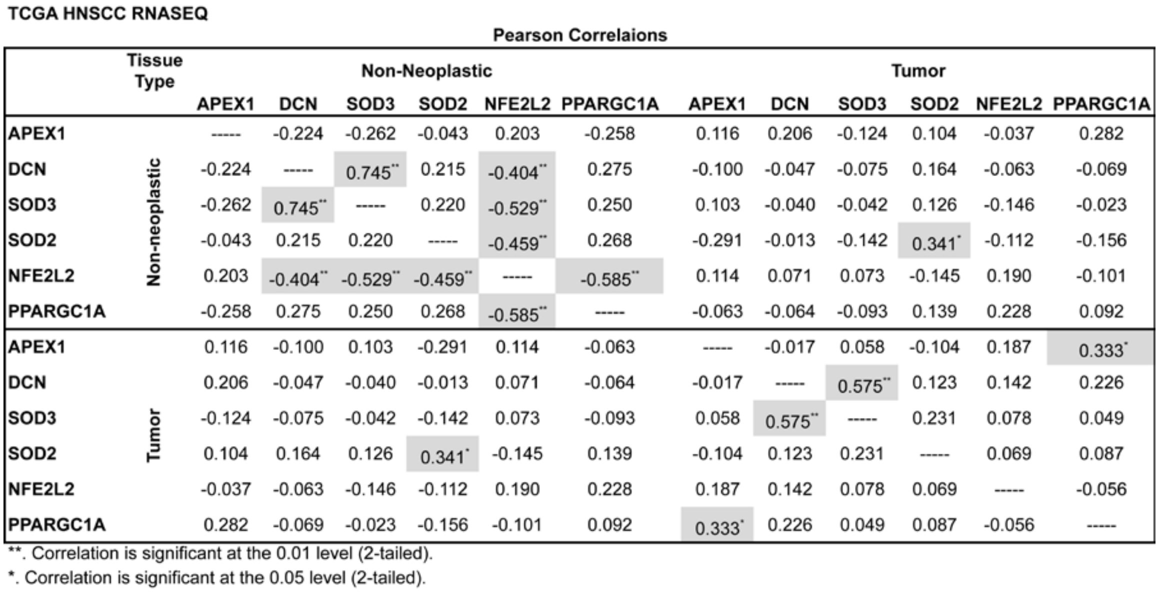

TCGA HNSCC RNASEQ

Pearson Correlaions

	Tissue Type	**Non-Neoplastic**						**Tumor**					
		APEX1	**DCN**	**SOD3**	**SOD2**	**NFE2L2**	**PPARGC1A**	**APEX1**	**DCN**	**SOD3**	**SOD2**	**NFE2L2**	**PPARGC1A**
APEX1	**Non-neoplastic**	-----	-0.224	-0.262	-0.043	0.203	-0.258	0.116	0.206	-0.124	0.104	-0.037	0.282
DCN		-0.224	-----	0.745**	0.215	-0.404**	0.275	-0.100	-0.047	-0.075	0.164	-0.063	-0.069
SOD3		-0.262	0.745**	-----	0.220	-0.529**	0.250	0.103	-0.040	-0.042	0.126	-0.146	-0.023
SOD2		-0.043	0.215	0.220	-----	-0.459**	0.268	-0.291	-0.013	-0.142	0.341*	-0.112	-0.156
NFE2L2		0.203	-0.404**	-0.529**	-0.459**	-----	-0.585**	0.114	0.071	0.073	-0.145	0.190	-0.101
PPARGC1A		-0.258	0.275	0.250	0.268	-0.585**	-----	-0.063	-0.064	-0.093	0.139	0.228	0.092
APEX1	**Tumor**	0.116	-0.100	0.103	-0.291	0.114	-0.063	-----	-0.017	0.058	-0.104	0.187	0.333*
DCN		0.206	-0.047	-0.040	-0.013	0.071	-0.064	-0.017	-----	0.575**	0.123	0.142	0.226
SOD3		-0.124	-0.075	-0.042	-0.142	0.073	-0.093	0.058	0.575**	-----	0.231	0.078	0.049
SOD2		0.104	0.164	0.126	0.341*	-0.145	0.139	-0.104	0.123	0.231	-----	0.069	0.087
NFE2L2		-0.037	-0.063	-0.146	-0.112	0.190	0.228	0.187	0.142	0.078	0.069	-----	-0.056
PPARGC1A		0.282	-0.069	-0.023	-0.156	-0.101	0.092	0.333*	0.226	0.049	0.087	-0.056	-----

**. Correlation is significant at the 0.01 level (2-tailed).

*. Correlation is significant at the 0.05 level (2-tailed).

RNA-Seq data from 43 matched non-neoplastic and HNSCC samples was obtained from TCGA. Pearson correlation coefficients were generated from this data to examine gene coordination between APEX1, DCN, SOD2, SOD3, NFE2L2, and PPARGC1A in non-neoplastic and HNSCC tumor tissues. ** Correlation is significant p<0.01 (2-tailed). *Correlation is significant p<0.05 (2-tailed).

Because gene expression analysis revealed no correlation between NFE2L2 and APEX1, the positive correlation observed between APE1 and NRF2 protein expression may not be due to increased gene expression of NRF2 **(Table 1-2, 1-3)**. These results do not discount the possibilty of increased NRF2 activity through interaction with APE1, which has been observed in other systems (141). Future *in vitro* studies will be needed to confirm whether APE1 is increasing NRF2 activity. Determining if APE1 increases NRF2 activity in head and neck cancer is necessary to understand how APE1 suppresses DCN and SOD3 in tumor tissues.

Table 1-3: Pearson correlation analysis for APE1 and associated Factors in benign, CIS, and invasive HNSCC

A: Comparison between Nuclear Protein Expression of APE1 and Associated Genetic Factors

		Pearson Correlaions														
		APE1			PPARGC1A			NRF2			DCN			SOD3		
		% Positive Nuclei														
% Positive Nuclei		Benign	Invasive	CIS	Benign	Invasive	CIS	Benign	Invasive	CIS	Benign	Invasive	CIS	Benign	Invasive	CIS
APE1	Benign	-----	0.275	0.066	0.190	-0.130	0.027	0.274*	0.113	0.392**	-0.158	0.038	-0.014	-0.142	-0.146	-0.025
	Invasive	0.275	----	0.402*	0.345*	0.329*	0.069	0.284	0.271*	0.244	-0.011	0.186	0.242	0.257	0.221	0.213
	CIS	0.066	0.402*	----	0.222	0.179	-0.050	-0.204	0.062	0.235	-0.161	0.069	-0.029	0.164	0.081	0.067
PPARGC1A	Benign	0.190	0.345*	0.222	----	0.210	0.338*	0.408**	0.179	0.256	-0.219	0.315*	0.152	-0.049	0.124	-0.015
	Invasive	-0.130	0.329*	0.179	0.210	----	0.622**	0.251	0.250	0.206	0.145	0.236	-0.105	0.011	0.374**	0.240
	CIS	0.027	0.069	-0.050	0.338*	0.622**	----	0.152	0.352*	0.123	0.128	-0.144	0.020	-0.050	0.254	0.109
NRF2	Benign	0.274*	0.284	-0.204	0.408**	0.251	0.152	----	0.104	0.182	-0.001	0.226	-0.005	-0.102	0.137	0.042
	Invasive	0.113	0.271*	0.062	0.179	0.250	0.352*	0.104	----	0.472**	-0.062	0.313*	-0.061	0.167	0.301*	0.109
	CIS	0.392**	0.244	0.235	0.256	0.206	0.123	0.182	0.472**	----	-0.121	0.396*	-0.009	-0.070	-0.039	0.113
DCN	Benign	-0.158	-0.011	-0.161	-0.219	0.145	0.128	-0.001	-0.062	-0.121	----	-0.011	-0.261	0.082	0.180	-0.057
	Invasive	0.038	0.186	0.069	0.315*	0.236	-0.144	0.226	0.313*	0.396*	-0.011	----	0.078	0.232	0.162	0.299
	CIS	-0.014	0.242	-0.029	0.152	-0.105	0.020	-0.005	-0.061	-0.009	-0.261	0.078	----	0.176	0.166	0.367**
SOD3	Benign	-0.142	0.257	0.164	-0.049	0.011	-0.050	-0.102	0.167	-0.070	0.082	0.232	0.176	----	-0.005	0.452**
	Invasive	-0.146	0.221	0.081	0.124	0.374**	0.254	0.137	0.301*	-0.039	0.180	0.162	0.166	-0.005	----	0.540**
	CIS	-0.025	0.213	0.067	-0.015	0.240	0.109	0.042	0.109	0.113	-0.057	0.299	0.367**	0.452**	0.540**	----

**. Correlation is significant at the 0.01 level (2-tailed).

*. Correlation is significant at the 0.05 level (2-tailed).

Table 1-3: Pearson correlation analysis for APE1 and associated factors in benign, CIS, and invasive HNSCC (Cont.)

B. Comparison of Total Cellular Protein and Nuclear Protein Expression for APE1 and Associated Genetic Factors

Pearson Correlaions

% Total Cellular Protein		APE1			PPARGC1A			NRF2			DCN			SOD3		
		% Positive Nuclei														
		Benign	Invasive	CIS	Benign	Invasive	CIS	Benign	Invasive	CIS	Benign	Invasive	CIS	Benign	Invasive	CIS
APE1	Benign	0.551**	-0.139	0.084	-0.039	-0.134	-0.239	0.132	-0.160	0.210	0.164	0.076	-0.140	-0.344*	-0.147	-0.225
	Invasive	0.377*	0.515**	0.410*	0.153	0.003	-0.147	0.090	-0.028	0.223	0.137	0.067	0.015	0.202	-0.062	-0.018
	CIS	-0.099	0.011	0.688**	0.101	0.021	-0.161	-0.144	-0.245	0.006	-0.143	-0.235	-0.079	-0.042	-0.156	-0.158
PPARGC1A	Benign	0.145	0.289	0.199	0.632**	0.361*	0.327*	0.226	0.214	0.197	-0.095	-0.071	0.098	-0.140	0.248	-0.137
	Invasive	0.065	0.368**	0.270	0.490**	0.654**	0.366*	0.413**	0.156	0.345*	-0.018	0.260	0.039	0.089	0.262	0.207
	CIS	0.094	0.271	0.275*	0.462**	0.543**	0.638**	0.249	0.125	0.126	0.207	-0.190	-0.145	-0.106	0.054	-0.060
NRF2	Benign	0.142	0.238	0.205	0.271*	0.132	-0.092	0.488**	-0.045	0.165	0.062	0.131	0.117	-0.128	-0.036	-0.207
	Invasive	0.131	0.392**	0.322*	0.268	0.125	0.018	0.228	0.561**	0.424**	-0.052	0.250	-0.181	0.050	-0.027	-0.013
	CIS	0.262	0.324*	0.279*	0.353*	0.174	0.186	0.303*	0.237	0.741**	0.163	0.102	-0.077	-0.115	0.167	-0.089
DCN	Benign	-0.024	-0.020	-0.070	-0.309*	-0.030	-0.055	-0.027	-0.143	-0.233	0.789**	-0.039	-0.152	0.140	-0.018	-0.086
	Invasive	0.060	-0.114	0.023	0.330*	0.205	-0.097	0.341*	0.008	0.064	0.099	0.664**	0.223	0.036	0.060	0.327
	CIS	-0.187	0.012	-0.234	0.095	-0.071	0.096	-0.003	0.138	0.116	0.058	0.296	0.569**	0.125	0.141	0.255
SOD3	Benign	-0.142	0.112	0.142	-0.075	0.016	-0.050	-0.147	0.112	-0.119	0.189	0.133	0.127	.832**	-0.096	0.263
	Invasive	-0.233	0.206	-0.026	0.059	0.373**	0.144	0.185	0.401**	-0.022	0.088	0.176	0.059	0.159	0.843**	0.513**
	CIS	-0.115	0.232	0.012	0.043	0.299	0.196	0.089	0.249	0.032	-0.030	0.327	0.358**	0.477**	0.571**	0.877**

**. Correlation is significant at the 0.01 level (2-tailed).

*. Correlation is significant at the 0.05 level (2-tailed).

Table 1-3: Pearson correlation analysis for APE1 and associated factors in benign, CIS, and invasive HNSCC (Cont.)

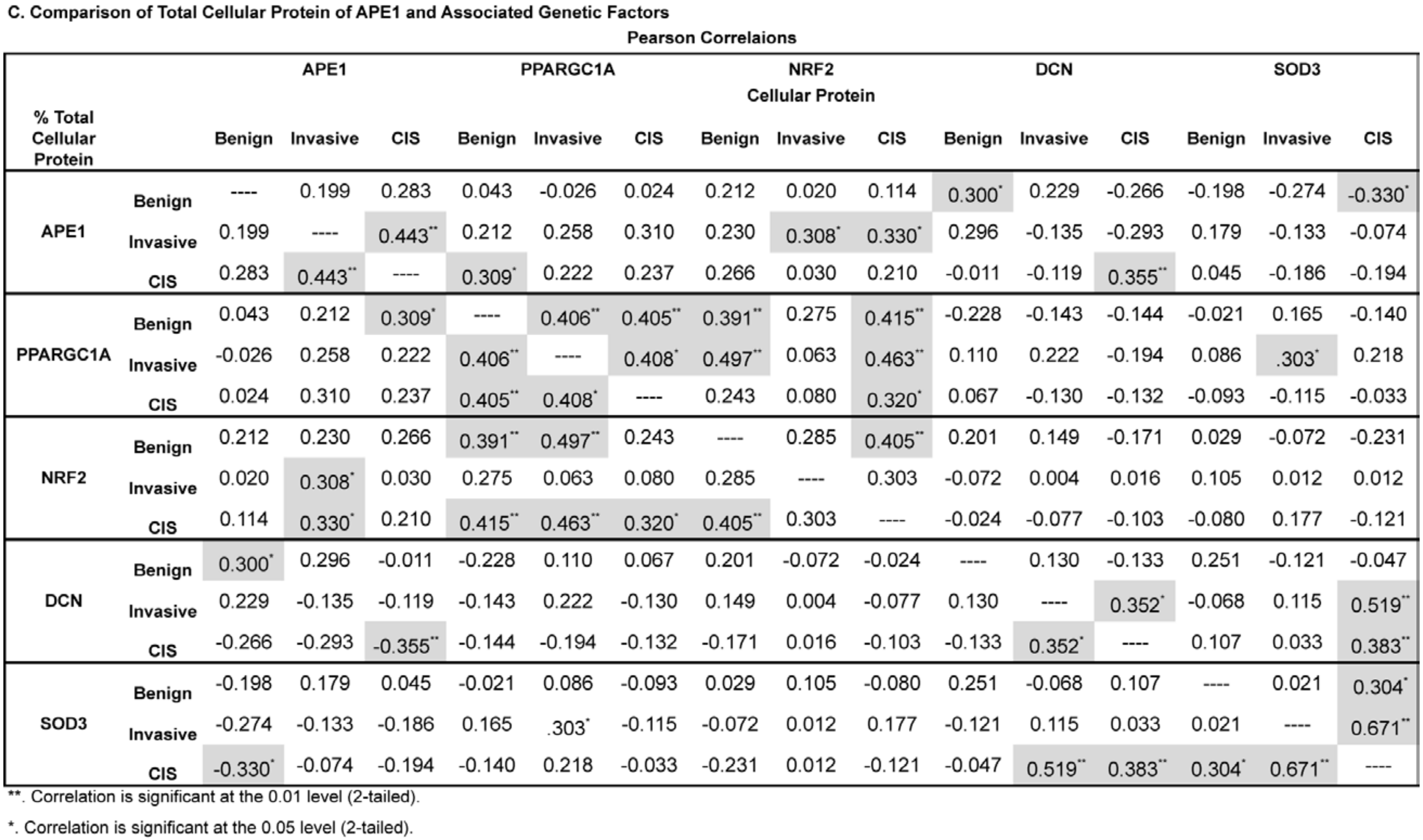

C. Comparison of Total Cellular Protein of APE1 and Associated Genetic Factors

Pearson Correlaions

		APE1			PPARGC1A			NRF2			DCN			SOD3		
									Cellular Protein							
% Total Cellular Protein		Benign	Invasive	CIS	Benign	Invasive	CIS	Benign	Invasive	CIS	Benign	Invasive	CIS	Benign	Invasive	CIS
APE1	Benign	----	0.199	0.283	0.043	-0.026	0.024	0.212	0.020	0.114	0.300*	0.229	-0.266	-0.198	-0.274	-0.330*
	Invasive	0.199	----	0.443**	0.212	0.258	0.310	0.230	0.308*	0.330*	0.296	-0.135	-0.293	0.179	-0.133	-0.074
	CIS	0.283	0.443**	----	0.309*	0.222	0.237	0.266	0.030	0.210	-0.011	-0.119	0.355**	0.045	-0.186	-0.194
PPARGC1A	Benign	0.043	0.212	0.309*	----	0.406**	0.405**	0.391**	0.275	0.415**	-0.228	-0.143	-0.144	-0.021	0.165	-0.140
	Invasive	-0.026	0.258	0.222	0.406**	----	0.408*	0.497**	0.063	0.463**	0.110	0.222	-0.194	0.086	.303*	0.218
	CIS	0.024	0.310	0.237	0.405**	0.408*	----	0.243	0.080	0.320*	0.067	-0.130	-0.132	-0.093	-0.115	-0.033
NRF2	Benign	0.212	0.230	0.266	0.391**	0.497**	0.243	----	0.285	0.405**	0.201	0.149	-0.171	0.029	-0.072	-0.231
	Invasive	0.020	0.308*	0.030	0.275	0.063	0.080	0.285	----	0.303	-0.072	0.004	0.016	0.105	0.012	0.012
	CIS	0.114	0.330*	0.210	0.415**	0.463**	0.320*	0.405**	0.303	----	-0.024	-0.077	-0.103	-0.080	0.177	-0.121
DCN	Benign	0.300*	0.296	-0.011	-0.228	0.110	0.067	0.201	-0.072	-0.024	----	0.130	-0.133	0.251	-0.121	-0.047
	Invasive	0.229	-0.135	-0.119	-0.143	0.222	-0.130	0.149	0.004	-0.077	0.130	----	0.352*	-0.068	0.115	0.519**
	CIS	-0.266	-0.293	-0.355**	-0.144	-0.194	-0.132	-0.171	0.016	-0.103	-0.133	0.352*	----	0.107	0.033	0.383**
SOD3	Benign	-0.198	0.179	0.045	-0.021	0.086	-0.093	0.029	0.105	-0.080	0.251	-0.068	0.107	----	0.021	0.304*
	Invasive	-0.274	-0.133	-0.186	0.165	.303*	-0.115	-0.072	0.012	0.177	-0.121	0.115	0.033	0.021	----	0.671**
	CIS	-0.330*	-0.074	-0.194	-0.140	0.218	-0.033	-0.231	0.012	-0.121	-0.047	0.519**	0.383**	0.304*	0.671**	----

**. Correlation is significant at the 0.01 level (2-tailed).

*. Correlation is significant at the 0.05 level (2-tailed).

1.4.1.4 Suppression of superoxide dismutase upon increased APE1 expression

We hypothesized that APE1 drives SOD3 suppression in HNSCC **(Figure 1-4**). We first determined whether SOD3 decreases in HNSCC in benign, CIS, and invasive HNSCC by using digital image analysis of IHC slides. Both total and nuclear SOD3 protein levels were decreased in CIS and invasive tissues as compared to benign tissues ($p<0.0001$). SOD3 protein levels were additionally reduced in invasive HNSCC as compared to CIS ($p<0.05$) **(Figure 1-6)**

We next investigated correlation between APE1 and SOD3 protein levels in benign, CIS, and invasive HNSCC. Correlation between proteins was determined by calculating Pearson correlation coefficients. There was an overall trend of negative correlation between APE1 and SOD3 protein levels in tissue subtypes. A significant negative correlation was observed between total APE1 protein in benign tissue with total SOD3 protein in CIS ($p<0.05$) **(Table 1-3 C).** Additionally, there was a significant negative correlation between total APE1 and nuclear SOD3 protein in benign tissue ($p<0.05$) **(Table 1-3 B).** Gene coordination between APEX1 and SOD3 had an overall negative trend. In non-neoplastic tissues, there was a slight negative correlation observed between APEX1 and SOD3 ($p=0.09$) **(Table 1-2)**. There was also a negative correlation between APEX1 and SOD2 gene expression in non-neoplastic tissue ($p=0.059$) **(Table 1-2).** This data partially supports that APE1 is involved in suppression of antioxidants SOD2 and SOD3. Larger data sets need to be analyzed to determine if there is a statistically significant reduction of SOD3 gene expression in tissues with elevated APE1. This is important, as oxidative stress is known to induce APE1 expression. APE1 suppressing superoxide dismutases and subsequent increased oxidative stress may further drive APE1 overexpression in tumor tissues.

1.4.1.5 APE1 is positively linked to PPARGC1A gene and protein expression

We examined whether APE1 is linked to altered PPARGC1A expression in HNSCC because our lab previously identified increased PPARGC1A expression in MEF cells with wildtype APE1 expression (122). First, we examined total cellular and nuclear PPARGC1A protein levels in benign, CIS, and invasive HNSCC using digital image analysis of IHC staining. We observed a significant decrease in nuclear PPARGC1A protein in cancerous tissues ($p<0.001$ benign versus invasive, $p<0.05$ benign versus CIS) **(Figure 1-6).** This reduction of PPARGC1A in tumor tissues supports previous research, which demonstrated loss of PPARGC1A protein in invasive tumor as compared to benign tissue (137).

We next calculated Pearson correlation coefficients to investigate coordination between APE1 and PPARGC1A protein levels. There was a significant positive correlation of nuclear APE1 protein in invasive with nuclear PPARGC1A protein in both benign and invasive tissue ($p<0.05$) **(Figure 1-6)**. A positive correlation was also observed between APE1 protein in CIS and PPARGC1A protein in benign tissue (**Table 1-3**). These results support a positive correlation between APE1 and PPARGC1A protein levels. Next, we investigated whether there was also a positive correlation between APEX1 and PPARGC1A gene expression. There was a significant positive correlation between APEX1 and

PPARGC1A gene expression in tumor tissue ($p<0.05$), but not in non-neoplastic tissues **(Table 1-2).** This suggests that APEX1 and PPARGC1A gene coordination becomes altered in cancerous cells. This positive correlation supports previous work performed in MEF cells (122).

1.4.1.6 NRF2 gene expression is linked to reduced gene expression of DCN, SOD2, SOD3

We hypothesized that NRF2 mediated transcriptional downregulation of DCN, SOD2, and SOD3 **(Figure 1-3).** Gene expression coordination was investigated between NFE2L2, DCN, SOD2, and SOD3. To examine this coordination, we calculated Pearson correlation coefficients in non-neoplastic and tumor tissues using TCGA RNA-Seq data from patients with HNSCC. In non-neoplastic tissues, NFE2L2 gene expression was negatively correlated with DCN, SOD2, and SOD3 ($p<0.01$) **(Table 1-2).** This supports that NFE2L2 may negatively regulate transcription of DCN, SOD2, and SOD3. Additionally, we analyzed coordination between protein levels of NRF2, DCN, and SOD3. Overall, there was a trend toward negative correlation between nuclear NRF2 and DCN protein levels. However, there was a positive correlation between nuclear NRF2 and nuclear DCN protein levels in invasive tissue ($p<0.05$ **(Table 1-3 A).** In addition, there was a positive correlation between nuclear NRF2 and nuclear SOD3 in invasive tissue **(Table 1-3 A).**

1.4.2 Survival Time in relation to APE1, DCN, NRF2, SOD3, and PPARGC1A expression

Biomarkers that predict patient survival may provide insight into novel drug targets, which could lead to improved therapeutics and increased patient survival. Therefore, we investigated whether APE1, DCN, NRF2, SOD3, or PPARGC1A expression could predict patient survival. To do this we performed Kaplan-Meier survival analysis using the protein expression data obtained from 77 patients with HNSCC. We first calculated the quartiles for each protein and within each tissue subtype. Survival was then compared between low protein expression (Q1) and high protein expression (Q3). We next examined survival of patients with stage T4a HNSCC with regards to APEX1, DCN, NFE2L2, SOD3, and PPARGC1A gene expression using TCGA RNA-Seq data. We then compared patient survival between low protein expression (Q1) and high protein expression (Q3).

1.4.2.1 Patients with elevated APE1, and PPARGC1A expression had significantly shorter survival periods

Previous research has observed reduced survival in patients whose tumors had aberrant APE1 expression (20,109-112). To confirm that reduced survival is associated with elevated APE1 levels, we created Kaplan-Meier survival plots for total cellular and nuclear APE1 protein expression in benign, CIS, and Invasive tissues. In CIS, increased total cellular APE1 protein was linked to decreased survival (LR $p<0.05$, GW $p<0.05$) **(Figure 1-7**). To the best of our knowledge, this is the first study where high APE1 protein expression in CIS was linked to decreased patient survival. We next determined whether elevated APE1 gene expression was associated with reduced survival, as we had found with protein expression. Gene expression analysis using TCGA data for HNSCC (pathology stage T4a) also revealed reduced survival in patients with elevated APE1 (LR p=0.0148, GW p=0.0101) **(Figure 1-8).** Patients with high total PPARGC1A in invasive tissue had significantly reduced survival (LR p<0.05, GW p=0.0575) **(Figure 1-7).**

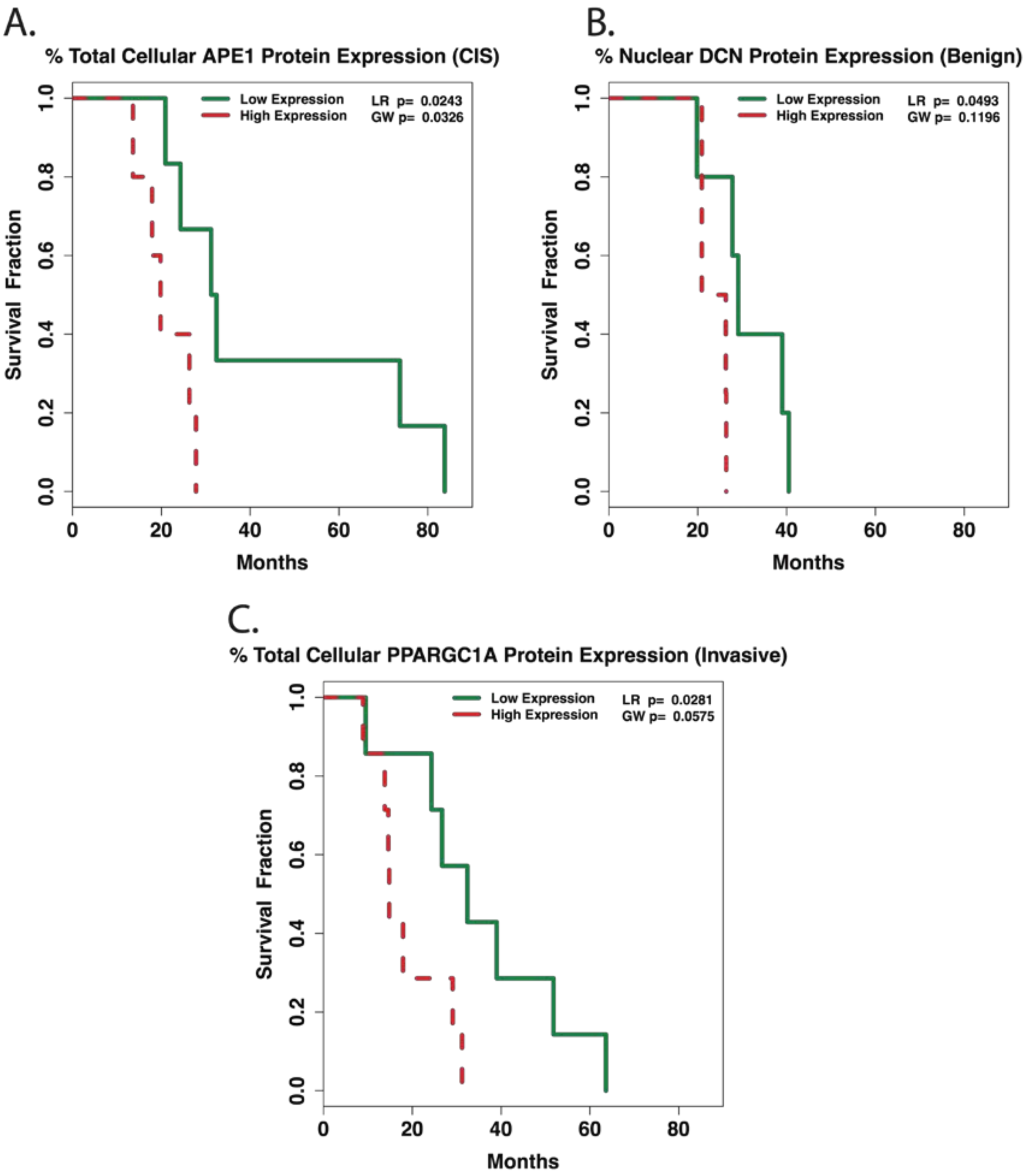

Figure 1-7: Top significant survival curves based on protein expression

Kaplan Meier survival curves were generated comparing low protein expression (Q1) versus high protein expression (Q3) in the samples of deceased patients. These graphs represent the top significant results as determined by LR: Mantel-Haenszel Log-Rank, GW: Peto & Peto modification of the Gehan-Wilcoxon statistical tests ($p<0.05$). **A:** % Total Cellular APE1 protein expression in CIS **B.** % Nuclear DCN Protein Expression in benign tissue **C.** % Total Cellular PPARGC1A protein expression in invasive tissue.

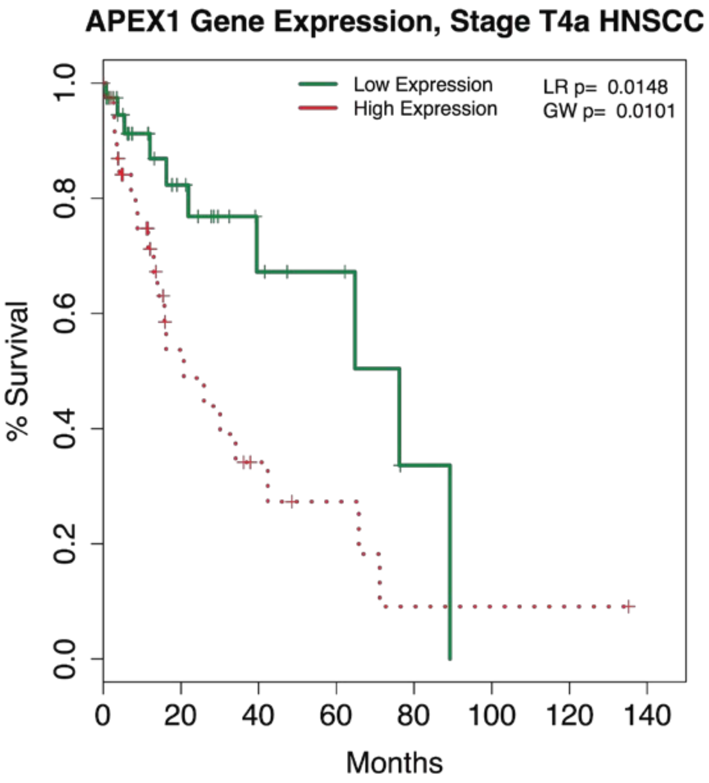

Figure 1-8: APEX1 gene expression survivals analysis

RNA-Seq data from 520 patient samples were used to generate Kaplan Meier survival curves. Differences in survival were determined between individuals with low APE1 gene expression (Q1) versus high APE1 gene expression (Q3). Statistical significance was determined using LR: Mantel-Haenszel Log-Rank, and GW: Peto & Peto modification of the Gehan-Wilcoxon statistical tests.

1.4.2.2 DCN protein levels in benign tissue is linked to reduced survival

We analyzed DCN protein expression to confirm previous reports that reduced DCN was linked to poor survival (126-132). To do so, we plotted Kaplan-Meier survival curves for total cellular, and nuclear DCN protein levels in each of the tissue subtypes. There appeared to be reduced survival in patients with low DCN expression in CIS. However, there were too few events (i.e. patient deaths) to obtain a statistically significant result. We suspect that low DCN protein expression in CIS corresponds to reduced survival, but a larger data set will be needed to confirm the link between low DCN protein levels and reduced survival. Unexpectedly, overexpression of DCN in benign tissue was linked to poor survival (LR p=0.0493)**(Figure 1-7).**

1.4.3 Multivariate analysis of protein expression within clinical groupings

Clinical data from the patients whose samples were used for protein expression analysis were obtained from the Kentucky Cancer Registry. Major categories examined were p16 status, whether patients were from Appalachia Kentucky, tobacco usage, tumor grade, presence of cancer positive lymph nodes, age at diagnosis, tumor size, pathology stage, and location of primary tumor **(Table 1-4)**. Initially, overall p-values were calculated to identify significant differences of each protein within clinical groups **(Table 1-5).** For clinical factors that were found to have significant overall p-values, additional statistical analysis was performed to identify if there was significant difference at the variable effect (i.e. benign, CIS, invasive). There were no significant differences of APE1, DCN, NRF2, SOD3, or PPARGC1A regarding location of the primary tumor, tumor size, whether a patient was from Appalachia Kentucky, or upon comparing patients having pathology stage 2/3 versus stage IV **(Table 1-5**).

Table 1-4: Patient Demographics

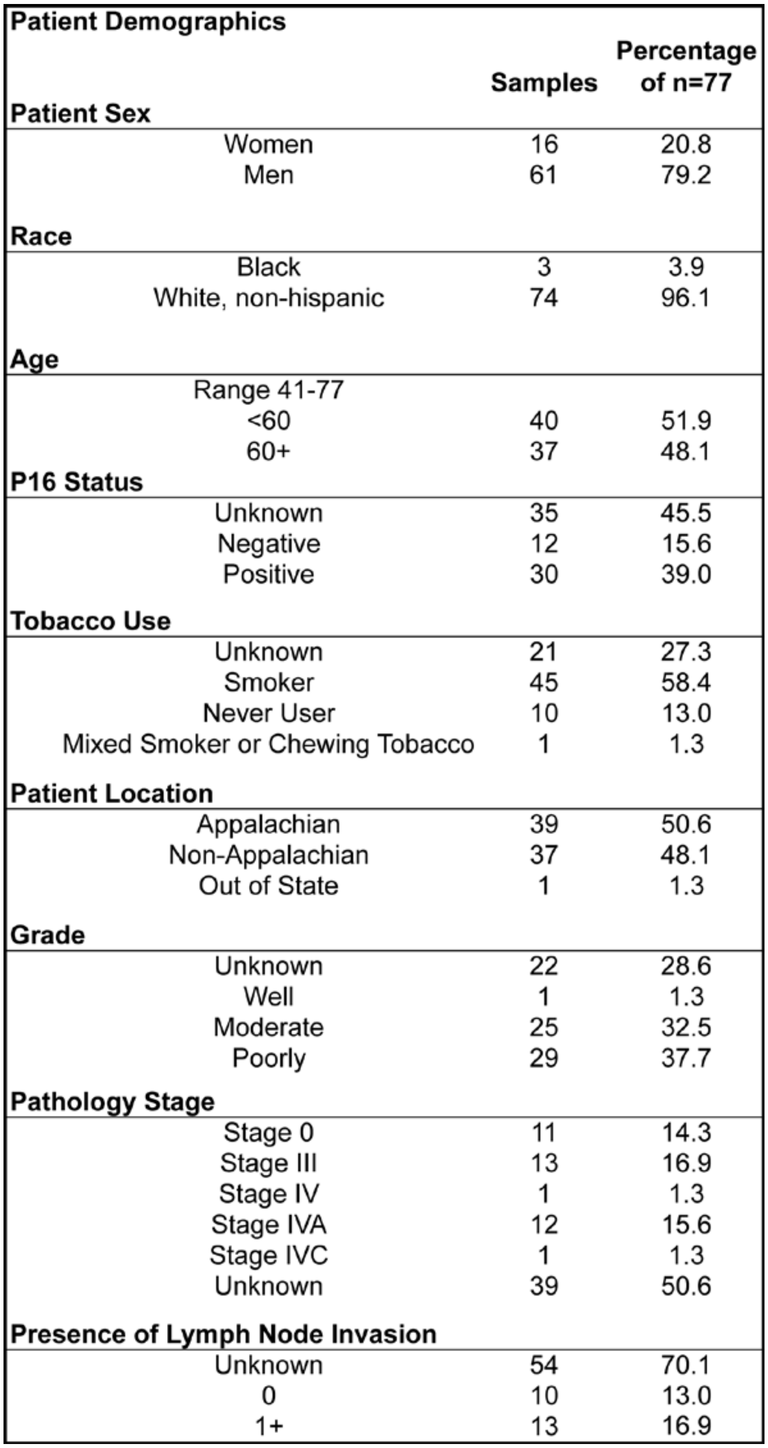

Patient Demographics		Samples	Percentage of n=77
Patient Sex			
	Women	16	20.8
	Men	61	79.2
Race			
	Black	3	3.9
	White, non-hispanic	74	96.1
Age			
	Range 41-77		
	<60	40	51.9
	60+	37	48.1
P16 Status			
	Unknown	35	45.5
	Negative	12	15.6
	Positive	30	39.0
Tobacco Use			
	Unknown	21	27.3
	Smoker	45	58.4
	Never User	10	13.0
	Mixed Smoker or Chewing Tobacco	1	1.3
Patient Location			
	Appalachian	39	50.6
	Non-Appalachian	37	48.1
	Out of State	1	1.3
Grade			
	Unknown	22	28.6
	Well	1	1.3
	Moderate	25	32.5
	Poorly	29	37.7
Pathology Stage			
	Stage 0	11	14.3
	Stage III	13	16.9
	Stage IV	1	1.3
	Stage IVA	12	15.6
	Stage IVC	1	1.3
	Unknown	39	50.6
Presence of Lymph Node Invasion			
	Unknown	54	70.1
	0	10	13.0
	1+	13	16.9

Table represents demographics of the 77 patients whose samples were utilized for immunohistochemistry

Table 1-5: Overall P values for clinical analysis

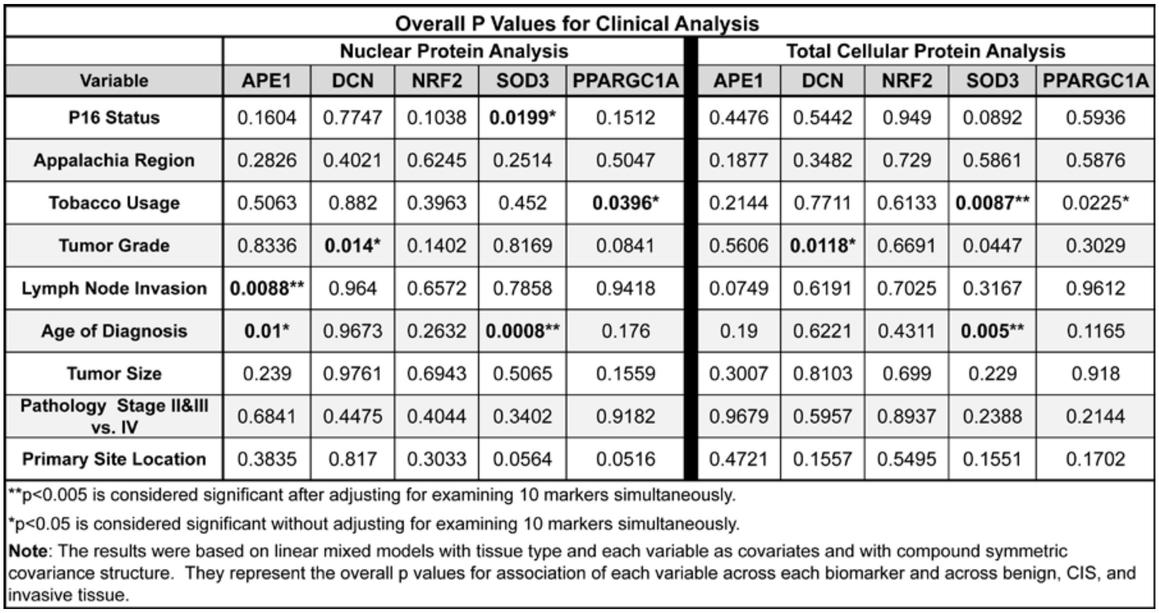

Overall P Values for Clinical Analysis										
	Nuclear Protein Analysis					Total Cellular Protein Analysis				
Variable	**APE1**	**DCN**	**NRF2**	**SOD3**	**PPARGC1A**	**APE1**	**DCN**	**NRF2**	**SOD3**	**PPARGC1A**
P16 Status	0.1604	0.7747	0.1038	0.0199*	0.1512	0.4476	0.5442	0.949	0.0892	0.5936
Appalachia Region	0.2826	0.4021	0.6245	0.2514	0.5047	0.1877	0.3482	0.729	0.5861	0.5876
Tobacco Usage	0.5063	0.882	0.3963	0.452	0.0396*	0.2144	0.7711	0.6133	0.0087**	0.0225*
Tumor Grade	0.8336	0.014*	0.1402	0.8169	0.0841	0.5606	0.0118*	0.6691	0.0447	0.3029
Lymph Node Invasion	0.0088**	0.964	0.6572	0.7858	0.9418	0.0749	0.6191	0.7025	0.3167	0.9612
Age of Diagnosis	0.01*	0.9673	0.2632	0.0008**	0.176	0.19	0.6221	0.4311	0.005**	0.1165
Tumor Size	0.239	0.9761	0.6943	0.5065	0.1559	0.3007	0.8103	0.699	0.229	0.918
Pathology Stage II&III vs. IV	0.6841	0.4475	0.4044	0.3402	0.9182	0.9679	0.5957	0.8937	0.2388	0.2144
Primary Site Location	0.3835	0.817	0.3033	0.0564	0.0516	0.4721	0.1557	0.5495	0.1551	0.1702

**p<0.005 is considered significant after adjusting for examining 10 markers simultaneously.

*p<0.05 is considered significant without adjusting for examining 10 markers simultaneously.

Note: The results were based on linear mixed models with tissue type and each variable as covariates and with compound symmetric covariance structure. They represent the overall p values for association of each variable across each biomarker and across benign, CIS, and invasive tissue.

Values represent overall P-value for clinical analysis of patient P16 status, patient geographic location, tobacco usage, tumor grade, lymph node invasion, age at diagnosis, tumor size, pathology stage, and primary site location. These results were based on linear mixed models with tissue type and each variable as covariates and with compound symmetric covariance structure. They represent the overall p values for association of each variable across each biomarker and across benign, CIS, and invasive tissue. ** p<0.005 denotes significance after adjusting for examining 10 markers simultaneously. * p<0.05 denotes significance without adjusting for examining 10 markers simultaneously.

1.4.3.1 Elevated APE1 was associated with cancer invaded lymph nodes

It is estimated that at least 90% of cancer-related deaths are a direct result of metastasis (166). During metastasis, cancer cells break away from the primary tumor and spread throughout the body (166). This leads to compromised functions of vital organs, eventually leading to death. A biomarker that identifies increased risk for metastasis could improve patient survival by allowing physicians to tailor the aggressiveness of treatment, or increase surveillance in order to identify metastasis sooner.

To identify a potential biomarker for increased risk for metastasis, we examined whether altered expression of our proteins of interest corresponded to the presence of cancer within a patient's lymph nodes. Given that metastatic cells originate from the primary tumor, we compared protein expression changes in the primary tumors of patients who had lymph node invasion at the time of diagnosis to those that did not. Out of the cohort of 77 patients, 13.0% had no lymph nodes that were positive for cancer (n=10), and 16.9 % had 1 or more cancer positive lymph nodes (n=13). Excluded from analysis were individuals whose lymph nodes were not assessed at the time of sample collection (n=54)(**Table 1-4**). Biomarkers that predict aggressive phenotypes (i.e. lymph node invasion) would be most useful if identified in early tumor development, such as in CIS. To determine if alterations in CIS could be linked to the presence of lymph node invasion, we examined alterations in protein expression. There were significantly higher levels of both total and nuclear APE1 in CIS in patients that had lymph node invasion at the time of diagnosis ($p<0.05$) **(Figure 1-9).**

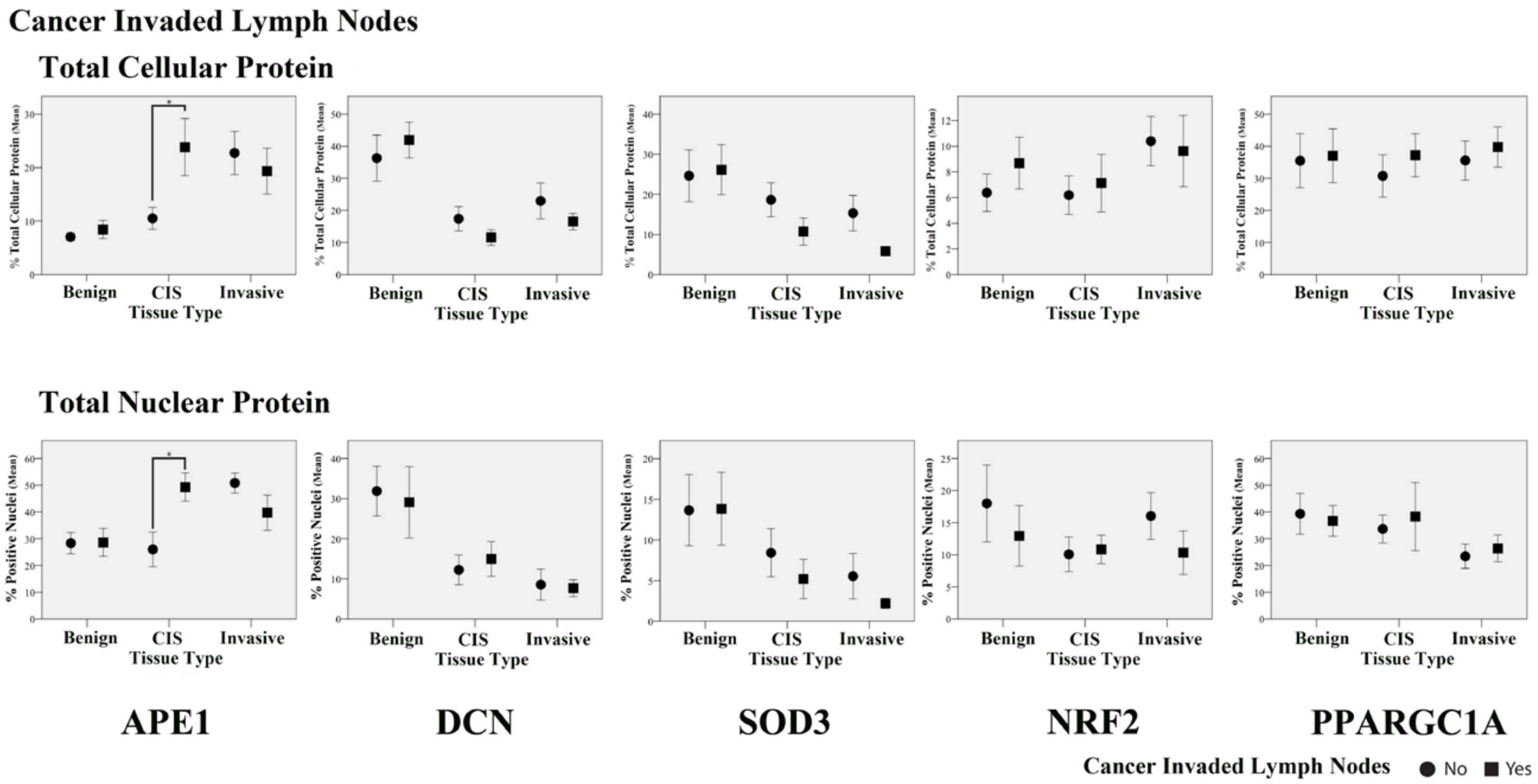

Figure 1-9: Analysis of protein expression and presence of lymph node invasion at diagnosis.

Nuclear and total cellular APE1, DCN, SOD3, NRF2, and PPARGC1A protein levels were determined in benign, CIS, and invasive HNSCC within the primary tumor. Values were compared between 10 patients with no lymph node invasion to 13 patients that had lymph node invasion at the time of diagnosis. * Denotes statistical significance ($p<0.05$).

1.4.3.2 Altered expression of DCN, SOD3, AND PPARGC1A in patients with poorly differentiated tumors

Tumor grade (i.e. the level of cellular differentiation) also influences prognosis. Tumor tissues vary between well differentiated, moderately differentiated and poorly differentiated. Well-differentiated tumors most closely resemble normal tissue, whereas poorly differentiated tumors are more stem-like (167). The latter of which is associated with poor patient survival. Our goal was to determine if altered expression of APE1, DCN, SOD3, NRF2, and PPARGC1A could identify patient prognosis, or understand how altered expression of these proteins influence tumor grade. Out of the cohort of 77 patients, 37.7 % had poorly differentiated tumors (n=29), and 32.5 % had moderately differentiated tumors (n=25). Excluded from analysis were individuals with unknown tumor grade (n=22) and an individual with a well-differentiated tumor (n=1)(**Table 1-4**). Benign tissue and CIS proximal to the invasive HNSCC were analyzed for protein expression as measured by immunohistochemistry staining intensity.

DCN protein decreased in CIS, and invasive tissue as compared to benign. However, there was no significant difference of SOD3 protein expression between patients with moderately and poorly differentiated tumors. Unexpectedly, patients with poorly differentiated tumors had significantly higher levels of DCN protein in benign tissue as compared to patients with moderately differentiated tumors ($p<0.05$) **(Figure 1-10)**. Poorly differentiated tumors had elevated total SOD3 in benign tissue ($p<0.05$)(**Figure 1-10**). Nuclear PPARGC1A was significantly decreased in CIS tissue of patients with poorly differentiated tumors ($p<0.05$)(**Figure 1-10**).

1.4.3.3 Alterations of SOD3 and PPARGC1A with tobacco usage

Tobacco usage is associated with increased risk of numerous cancers including lung, and oral cancer (74,75). Lung and oral cancers have higher incidence rates in Kentucky as compared to the national average (1,2). This increased incidence of oral cancer is likely linked to Kentucky having higher tobacco usage compared to the rest of the U.S. Therefore, we examined whether tobacco use altered expression of our proteins of interest to identify how these changes could contribute to cancer incidence. Out of the cohort of 77 patients, 58.4% were smokers (n=45), and 13.0% were never users of tobacco (n=10). Individuals with unknown tobacco usage (n=21) or with mixed tobacco usage (n=1) were excluded from analysis (**Table 1-4**). Total cellular SOD3 protein was significantly higher in the benign tissues of never users as compared to smokers ($p<0.05$) **(Figure 1-11).** However, upon tumorigenesis SOD3 protein decreased to similar rates between smokers and never users. Never users may have increased ability to combat oxidative stress in healthy tissues. Additionally, total and nuclear PPARGC1A protein levels were significantly lower in CIS tissue of never users ($p<0.05$) **(Figure 1-11).**

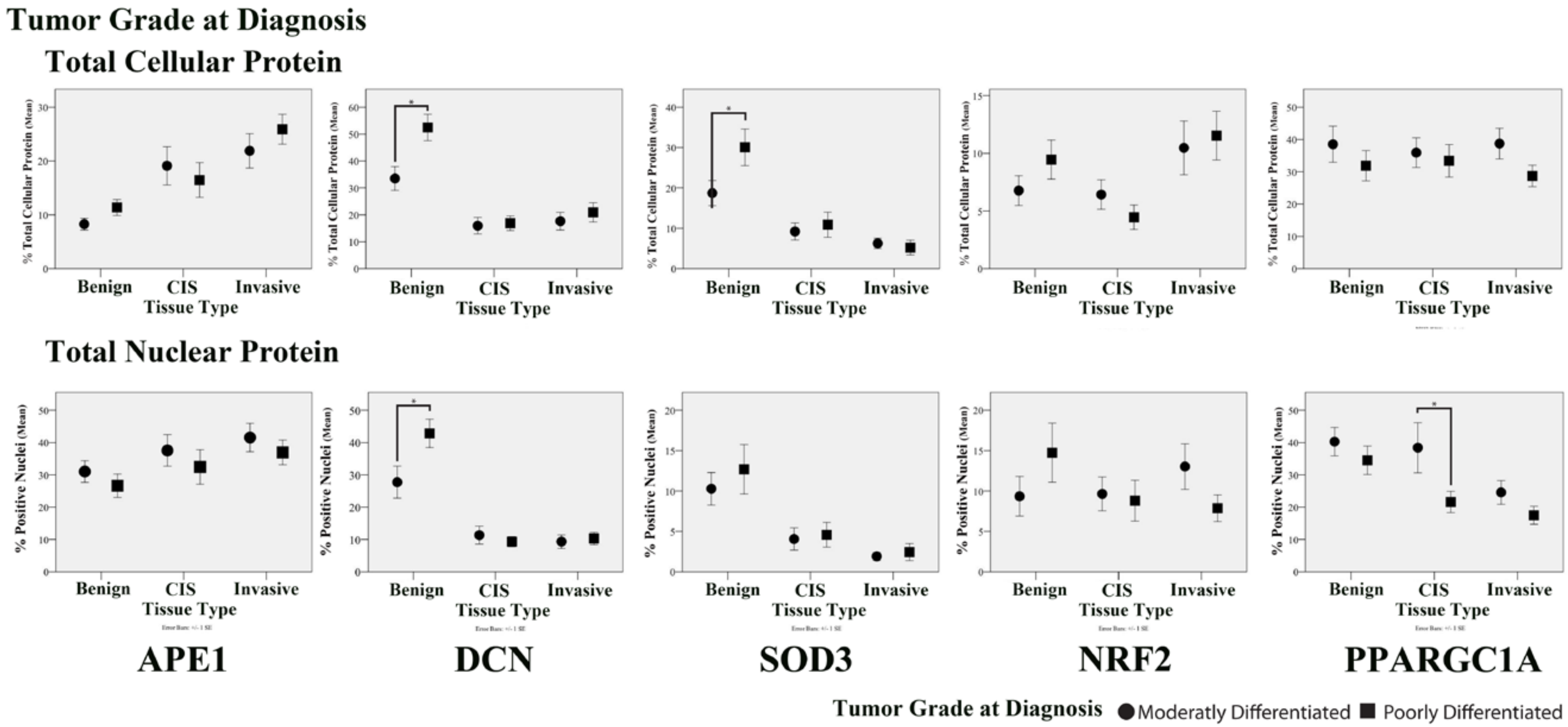

Figure 1-10: Analysis of protein expression and tumor grade at diagnosis.

Nuclear and total cellular APE1, DCN, SOD3, NRF2, and PPARGC1A protein levels were in invasive HNSCC, as well as in benign and CIS. Differences in protein markers were assessed between 29 samples with poorly differentiated tumors to 25 samples with moderately differentiated tumors. * Denotes statistical significance ($p<0.05$).

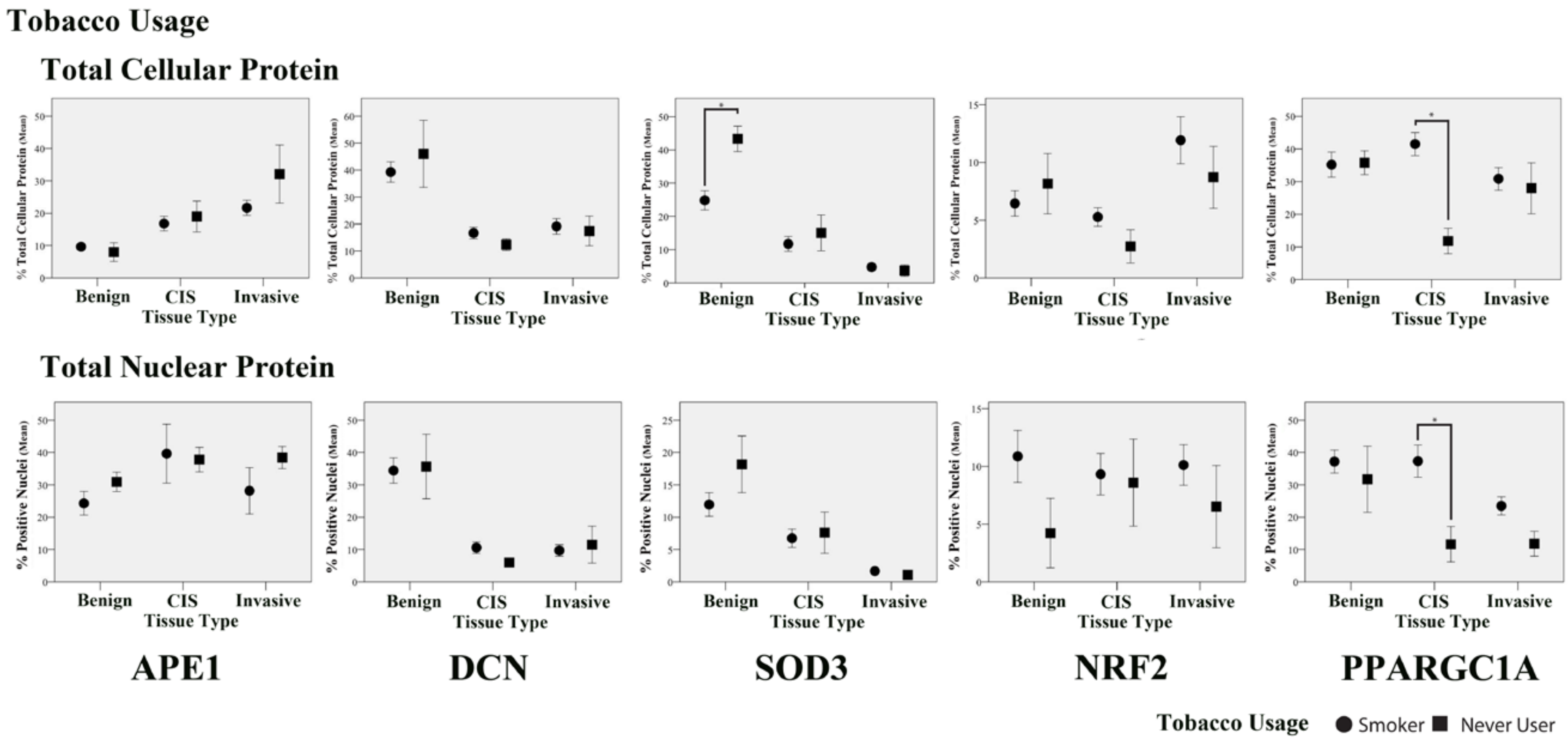

Figure 1-11: Analysis of protein expression and tobacco usage.

Nuclear and total cellular APE1, DCN, SOD3, NRF2, and PPARGC1A protein levels were determined in benign, CIS, and invasive HNSCC. These protein levels were compared for differences between 45 smokers and 10 never users. *Denotes statistical significance (p<0.05).

1.4.3.4 Reduced SOD3 in p16 positive tumors

Strains of human papillomavirus (HPV) have been associated with the development of oral cancer (6). As previously discussed in the introduction, p16 overexpression is an accurate surrogate marker for HPV infection (107). Because HPV-induced p16 overexpression is linked to improved treatment response, pathologists routinely determine the p16 status of oral cancers (107,168). Therefore, we examined differences in APE1, DCN, NRF2, SOD3, and PPARGC1A protein expression between p16 positive and p16 negative tumors. Out of the cohort of 77 patients, 15.6% were p16 negative (n=12) and 39.0% were p16 positive. Thirty-five patients were excluded from analysis due to unknown p16 status (**Table 1-4**). We observed no significant difference of APE1, DCN, NRF2, and PPARGC1A between p16 negative and p16 positive tissues. In benign tissue, there was significantly lower total cellular SOD3 protein in patients with positive P16 status ($p<0.05$) **(Figure 1-12).** Patients with positive p16 status also had reduced SOD3 protein in CIS, and invasive tissue as compared to patients with negative p16 status **(Figure 1-12**). However, this difference was not statistically significant. Although speculative, the increased oxidative stress that has been attributed to HPV may lead to depletion of antioxidant SOD3 in benign tissues (25,102,104).

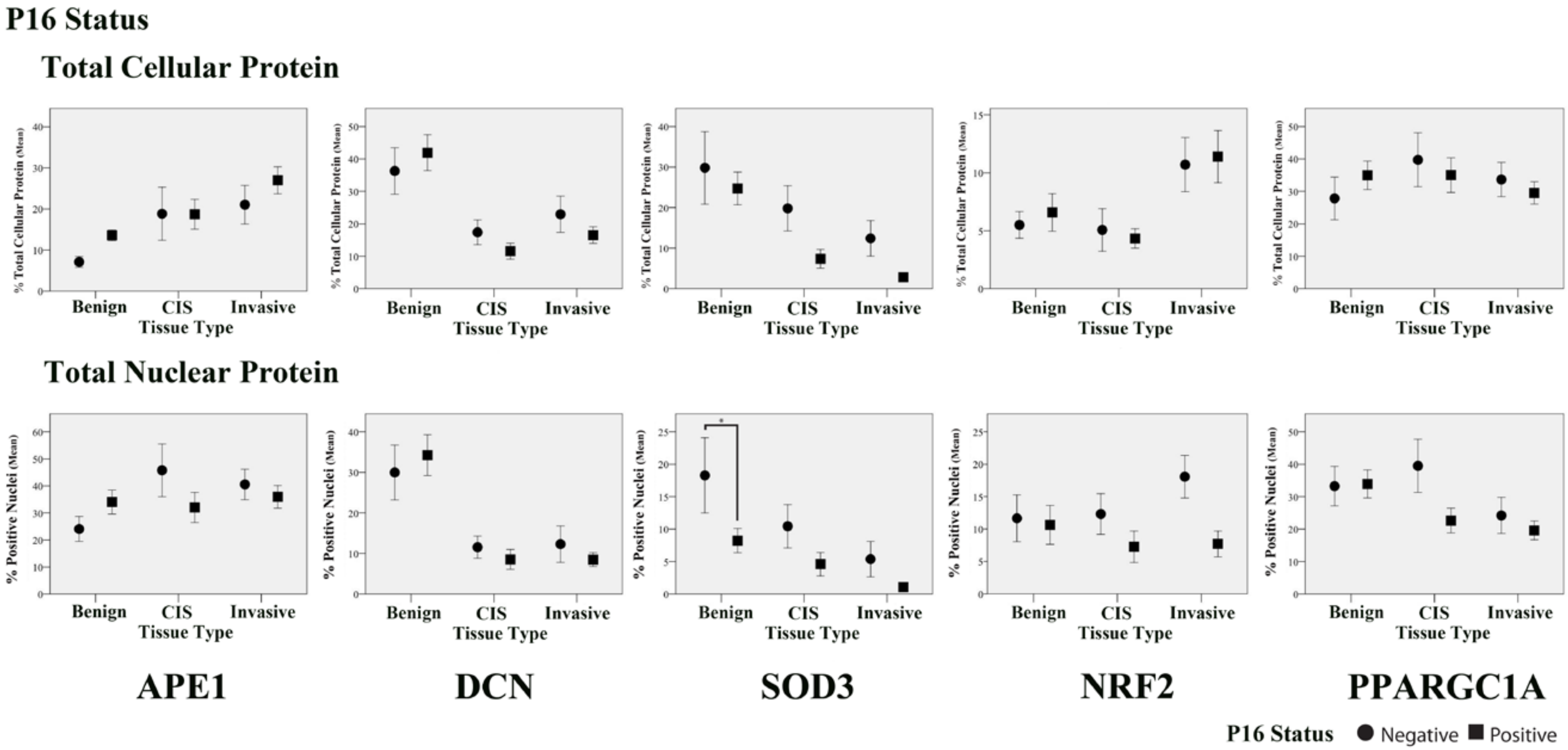

Figure 1-12: Analysis of protein expression and P16 status.

Nuclear and total cellular APE1, DCN, SOD3, NRF2, and PPARGC1A protein levels were determined in benign, CIS, and invasive HNSCC. Differences in protein levels were compared between 12 patients with p16 negative tumors and 20 patients with p16 positive tumors. * Denotes statistical significance ($p<0.05$).

1.4.3.5 Delayed cancer onset in patients with higher SOD3

Cancer is largely a disease of age. Every year of life leads to accumulation of genetic damage from oxidative stress that can lead to tumorigenesis. There has been increased interest in whether antioxidant supplements can reduce age related damage, and tumorigenesis (169). Therefore, we examined if patients who developed cancer earlier in life had reduced levels of the antioxidant, SOD3. Tissue samples were obtained from patients whose ages ranged from 41 to 77 (**Table 1-4**). Scatter plots were generated for total cellular or nuclear SOD3 levels in benign, CIS, and invasive HNSCC, with age as a continuous variable **(Figure 1-13).** Individuals who developed cancer later in life were found to have significantly higher levels of total and nuclear SOD3 protein in benign tissue ($p<0.05$) **(Figure 1-13).** It is unknown if these individuals maintained increased levels of SOD3 throughout their life or if other factors contributed to their delayed cancer onset. Though speculative, the increased SOD3 levels in benign tissues may have delayed tumorigenesis by reducing oxidative stress in tissues.

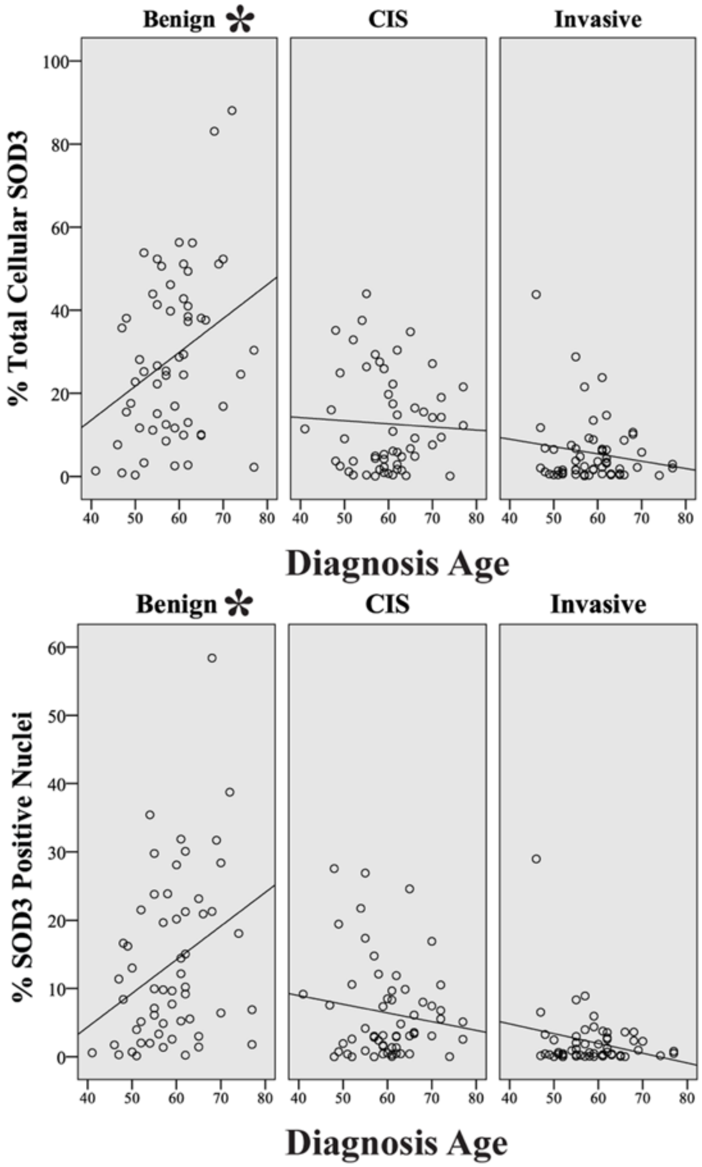

Figure 1-13: Analysis of SOD3 Protein Expression and Age at Diagnosis.

Total cellular and nuclear SOD3 protein levels were determined in benign, CIS, and invasive HNSCC. SOD3 protein levels were plotted against the patient's age at diagnosis. * Denotes statistical significance ($p<0.05$).

1.5 Discussion

1.5.1 Potential biomarkers for identifying aggressive tumor phenotypes

One of the purposes of this study was to identify potential diagnostic and prognostic biomarkers for use with HNSCC. We examined if altered expression of APE1, DCN, NRF2, PPARGC1A, and SOD3 proteins correlated with reduced survival, presence of lymph node invasion, and tumor grade. Identifying biomarkers for these factors can alert physicians to individuals who are more likely to have aggressive forms of cancer. This knowledge may alter treatment strategies, and improve a patient survival.

Overexpression of APE1 in cancer tissues has been previously associated with increased metastasis and reduced patient survival (20,109-112). In this study, we identified that increased APE1 protein expression in CIS was associated with decreased survival **(Figure 1-7, Supplemental Figure C-2).** Examining whether APE1 protein in CIS correlates to poor survival is important, because improvement of prognosis in the early stages of cancer may lead to improved treatment strategies that could potentially prevent the formation of invasive cancer. Additionally, this study identified that increased expression of total and nuclear APE1 protein within CIS of the primary tumor was significantly associated with the presence of lymph node invasion (**Figure 1-9**). Therefore, the reduced survival in patients with increased APE1 protein in CIS is likely linked to the significantly higher incidence of lymph node invasion in individuals with higher APE1 protein in CIS (**Figure 1-7**). Due to the effect of field cancerization, there is substantial overlap of mutations over a large tissue area. Because of this, early stage HNSCC may reflect genetic alterations that are present in proximal invasive cancers. Therefore, identification of mutations associated with aggressive tumor phenotypes in CIS may be useful in predicting lymph node invasion. Recently there was a reported correlation between increased APE1 in the serum of individuals with gastric cancer and the presence of lymph node invasion (170).

Analysis of gene expression in stage T4a HNSCC obtained from TCGA demonstrated that increased APE1 was associated with reduced survival **(Figure 1-8).** This not only confirms that elevated APE1 is associated with significantly reduced survival, but also indicates that this alteration occurs at the transcriptional level. Further studies are needed to identify what increases APE1 transcription in cancer tissues. Doing so could identify measures that prevent the APE1 overexpression that contributes to cancer progression and poor prognosis. This study supports our observation that increased APE1 is associated with lymph node invasion. Most importantly, these results support the potential of APE1 as a biomarker for identifying patients at risk for increased metastatic potential.

Reduced DCN expression in tumors has been attributed to increased mortality in cancer patients (126-132). Although there was a clear trend of diminished survival in patients with low DCN protein expression in CIS, there were not enough events to determine statistical significance (**Supplemental Figure C-3**). An increased sample size will be needed to confirm whether reduced DCN expression in cancer tissues is associated with significantly reduced survival. Unexpectedly, increased DCN protein expression in benign tissue was associated with reduced survival **(Figure 1-7).** The reduced survival in patients with increased

DCN protein in benign tissue may be related to our observation that DCN protein in benign tissue was significantly elevated in patients with poorly differentiated tumor tissues (**Figure 1-10**). These results were unexpected, as many studies have associated poor survival to decreased DCN expression. However, a differential proteomics study performed using breast cancer samples demonstrated that increased DCN expression in the stroma and epithelium was significantly associated with reduced overall survival (128). Thus, DCN protein expression in benign tissue may still be a valuable biomarker in HNSCC.

Increased SOD3 expression in benign tissue proximal to the primary tumor was associated with poorly differentiated tumors **(Figure 1-10).** Although SOD3 may be a valuable biomarker to identify patients who may be at risk for poorly differentiated tumors, it is unclear as to how increased SOD3 protein in benign tissue contributes to the development of poorly differentiated tumors. Although SOD3 is recognized as a tumor suppressor, the SOD3 rs699473 single nucleotide polymorphism has been associated with increased risk of high-grade or poorly differentiated prostate cancer as well as an increased risk for adult brain cancer (171-173). The exact role of how the SOD3 rs699473 polymorphism contributes to the development of poorly differentiated cancers is unclear (173). The SOD3 rs699473 polymorphism is located within the SOD3 promoter region, but it is unknown whether this polymorphism alters SOD3 protein expression (173). To the best of our knowledge, there are no studies reporting this polymorphism within HNSCC. Given that this SOD3 rs699473 has been implicated in poorly differentiated tumors, future studies should examine whether this mutation is prevalent in HNSCC and if it is associated with increased SOD3 expression in benign tissues.

1.5.2 SOD3 as a potential therapeutic target for patients at high-risk for developing HNSCC

Tobacco usage is linked to increased oxidative stress in tissues (22,23,79). Oxidative stress in lung tissues has been linked to depletion of the antioxidant, SOD3 (64). Because chronic oxidative stress contributes to the development of potentially oncogenic DNA mutations, we examined differences in SOD3 protein in smokers versus never users. SOD3 was significantly elevated in the benign tissues of individuals who never used tobacco as compared to smokers. Both groups of individuals had HNSCC. However, the reduced levels of SOD3 in smokers may further increase oxidative stress-induced cellular damage. As previously mentioned in the introduction, chronic oxidative stress can lead to both inactivation and depletion of SOD3 (29,64). In addition, we identified increased PPARGC1A protein in the CIS of smokers as compared to never users (**Figure 1-11**). Although the obvious step to prevent tobacco related lung and oral cancers is to avoid tobacco usage, the highly addictive nature of tobacco limits successful cessation. Therefore, understanding the changes that occur may allow for development of other preventative measures to reduce the cancer burden in this state and globally. Though speculative, supplementing the depleted SOD3 levels in smokers may reduce oxidative stress and subsequent cellular damage.

HPV has been associated with increased oxidative stress within tissues (25,104). As previously mentioned, oxidative stress can lead to the depletion of

SOD3. We identified a significant decrease in SOD3 protein in the benign tissue adjacent to p16 positive tumors (**Figure 1-12**). Identifying which antioxidants are depleted in individuals at high-risk for HNSCC would support the development of treatments to supplement antioxidant levels to minimize the development of oncogenic mutations.

Cancer development can occur at any stage in life, but is typically related to increased age. We identified that individuals who developed HNSCC later in life had increased SOD3 protein in benign tissue, whereas individuals with decreased SOD3 in benign tissue developed cancer at an earlier age. Though speculative, individuals with increased SOD3 expression may have had better protection against oxidative stress, which delayed cancer development. Supplementation of SOD3 in individuals with depleted SOD3 may protect against early cancer development.

1.5.3 Network of APE1 and associated factors

In this study, we examined how APE1 overexpression contributes to HNSCC development and decreased patient survival. We hypothesized that APE1's role as redox dependent transcriptional regulator mediates suppression of tumor suppressors and antioxidants. Previous research by our lab found that DCN gene expression was suppressed by APE1 in mouse embryonic fibroblasts (122). Loss of DCN has been associated with increased metastasis and mortality (126-132). Therefore, we hypothesize that tumor development is supported by decreased DCN expression in tissues overexpressing APE1.

We identified elevated APE1 expression in tumor tissues, which is consistent with previous observations (109,110). We also observed significantly increased APE1 protein expression in CIS. To the best of our knowledge, APE1 overexpression has not been identified in the CIS of patients with HNSCC.

APE1 protein overexpression in cancer tissues appeared to downregulate DCN. This was based on results demonstrating significant reduction of DCN protein in cancer tissues alongside increased APE1 protein expression in cancer tissues. There was also a significant negative correlation between APE1 and DCN protein levels in CIS. However, analysis using transcriptome data obtained from TCGA demonstrated no correlation between APEX1 and DCN gene expression in either non-neoplastic or HNSCC (**Table 1-2**). This contradicts our IHC results and previous results based on microarray analysis of mouse embryonic fibroblasts (122). It is unclear as to why there was no significant correlation between APE1 and DCN gene expression in HNSCC tissues. However, it is possible these differences are due to heterogeneity of tissues as compared to the immortalized, monoculture cell lines.

We hypothesized that APE1 mediated downregulation of DCN and SOD3 through NRF2's transcriptional regulatory activity. This hypothesis was based on previous research supporting APE1 increases NRF2 activity, and research demonstrated NRF2-mediated downregulation of DCN, SOD2, and SOD3(121). We were able to observe a negative correlation of DCN and SOD3 protein levels in relation to APE1 protein levels. In addition, we observed a positive correlation between APE1 and NRF2 protein levels (**Table 1-3**). An inverse relationship of

DCN, SOD2, and SOD3 gene expression relative to NRF2 was observed (**Table 1-2**). Upon searching for transcription factor binding sites within the DCN and SOD3 promoter regions, we identified NRF2 binding sites in both DCN and SOD3 promoter regions (**Table 1-1**) (148-150). Therefore, APE1 and NRF2 may be involved in reducing expression of DCN, SOD2, and SOD3.

1.5.4 Limitations of this study

1.5.4.1 Limitations in the efficiency of protein expression analysis

The protein expression analysis performed in this study is not yet optimal for clinical usage. For this study, regions of benign, CIS, and invasive tumor had to be first marked on each hematoxylin and eosin stained slide by a pathologist. After immunohistochemistry staining, these regions had to be manually selected for analysis using the Aperio ImageScope software. Analysis produced numerous individual spreadsheets containing raw data, which needed to be carefully labeled with the specimen and regions of analysis. These spreadsheets had to be merged for each sample along with clinical data before any downstream analysis could be performed. There is a long time delay between initial slide staining and final results. Clinical testing must be rapid and accurate so as not to delay patient treatment, which could result in increased mortality. In order to be practical for clinical analysis, this process needs to be expedited without compromising data quality. Currently, Aperio ImageScope software contains an algorithm to automatically identify regions of tumor within a tissue sections. However, it is unknown whether this can accurately determine regions of CIS. It is likely that a separate algorithm would need to be developed to automatically differentiate between benign, CIS, and invasive tissue.

Samples were stained in large batches to minimize variance in staining that otherwise would bring difficulty in assessing significant changes in protein levels. This was important for preliminary identification of potential biomarkers. However, these conditions would not be likely in a clinical setting. Collected specimens would need to be assessed in a timely manner and would be stained individually or in small batches. Specific protein expression cut off values are needed to group patients as low or high risk.

1.5.4.2 Limitations in obtaining clinical data from patients across the state

Due to certain limitations of clinical data collection, we were unable to obtain details of all clinical data. The University of Kentucky is the only NCI designated cancer treatment center in the state of Kentucky and therefore has a substantial catchment area. This leads to many patients being initially assessed and treated at the university but with their follow-up care completed closer to home. Due to this, it is not always possible to obtain a patient’s complete medical records. P16 status, tobacco usage, and lymph node assessment was not known for all patients included in this study. Significant results were still found in these categories even when excluding all unknowns. However, we may have obtained stronger statistical power if expanded. In addition, there were no details on administered treatments only as to whether a patient had chemotherapy, radiotherapy, and/or immunotherapy. We were therefore unable to clearly determine if protein expression correlated to a specific treatment resistance. To ensure access to complete treatment history, future studies can include individuals whose entire treatment was performed at the University of Kentucky.

1.6 Conclusions

This study examined the role of APE1 in HNSCC development including inhibition of tumor suppressors and antioxidants. APE1 is a key base excision repair protein and is important in repairing oxidative DNA damage that may lead to oncogenic mutations (20,38-40). Paradoxically APE1 overexpression has also been reported to disrupt DNA repair coordination, and is associated with tumorigenesis due to increased genomic instability (174). This genomic instability has been attributed to accumulation of single strand breaks, which APE1 creates as a normal part of base excision repair (174). We identified increased APE1 protein expression in early stage cancer, which supports that APE1 overexpression occurs early in tumor development (**Figure 1-6**). Though speculative, APE1 overexpression in early stage cancer may increase genomic instability and subsequent mutations leading to progression to invasive cancer. Risk factors for head and neck cancer such as tobacco usage or HPV infection can increase oxidative stress within tissues. We propose that this oxidative stress disrupts the finely controlled balance of APE1 expression and contributes to tumorigenesis. Though not certain from this study, APE1 overexpression may lead to increased NRF2 activity. Increased NRF2 activity subsequently inhibits transcription of DCN, SOD2, and SOD3. NRF2 transcriptional co-activator PPARGC1A may support NRF2's suppression of DCN, SOD2, and SOD3. The loss of antioxidants SOD2 and SOD3 leads to increased oxidative stress within the tumor microenvironment, which further drives APE1 overexpression (**Figure 1-14).**

Although not all details of the ROS network were identified in this study, we did identify several potential biomarkers for use in patients with HNSCC. In this study, we identified biomarkers that were associated with aggressive tumor phenotypes such as shortened survival time, poorly differentiated cancer, and increased metastatic potential. Patient survival may be improved by the use of biomarkers that identify patients with aggressive tumor phenotypes. Physicians may more accurately tailor treatment, and increase surveillance of patients with aggressive tumor phenotypes. In addition, biomarkers can identify potential novel drug targets. APE1 inhibitors are currently being explored as to whether they can effectively sensitize tumors to chemoradiotherapy (175). Improved treatment strategy through characterization of tumor phenotypes, and identification of novel drug targets may improve patient survival.

Digital image analysis of IHC slides allows the unique opportunity to objectively measure altered protein expression in proximal benign, CIS, and invasive tumors and often within the same slide. There are currently no clinically validated algorithms for automatic detection of CIS, and the methods used in this study are not timely enough to be used for clinical diagnostics. However, the development of new algorithms may allow for more accurate and rapid identification of biomarkers in the future.

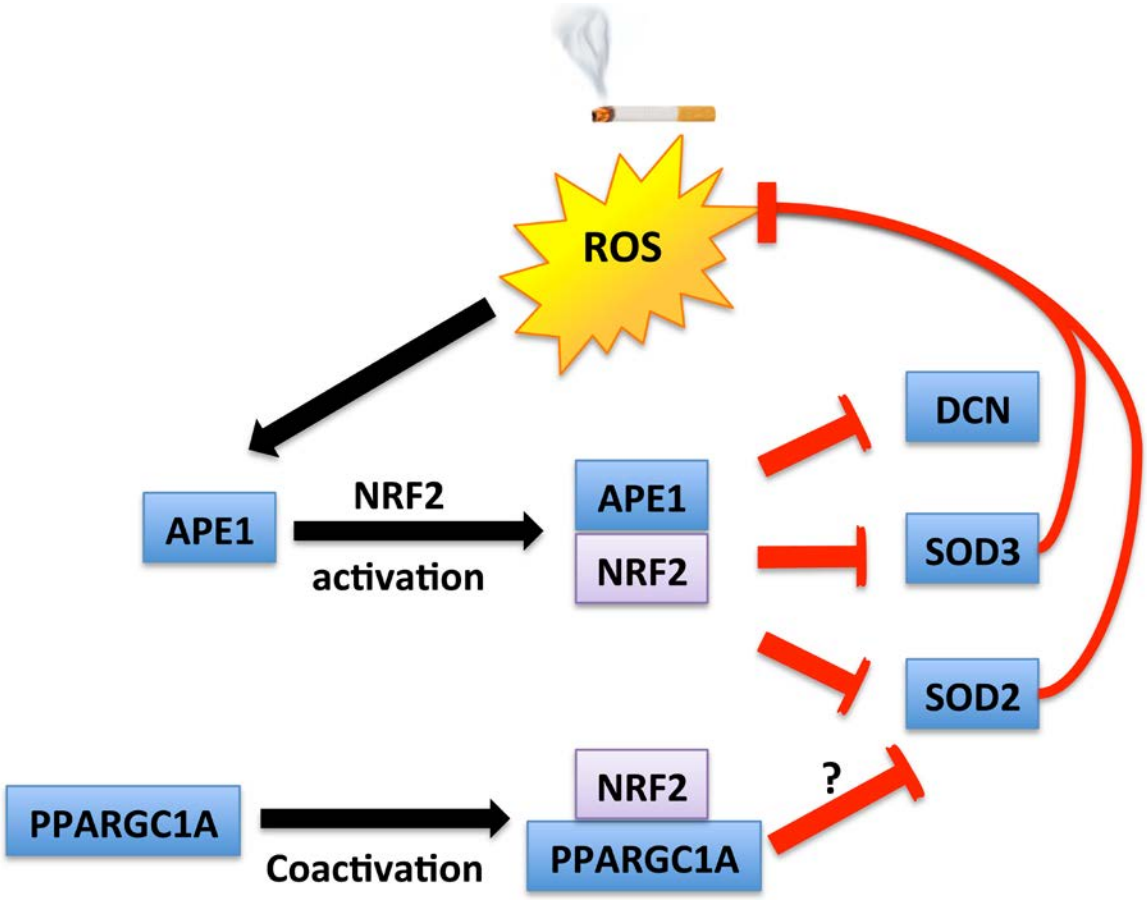
ROS
DCN
APE1
NRF2
activation
APE1
NRF2
SOD3
SOD2
?
PPARGC1A
Coactivation
NRF2
PPARGC1A

Figure 1-14: Summary model of the role of APE1 and NRF2 in suppression of DCN, SOD2, and SOD3

We propose that oxidative stress promotes APE1 overexpression. APE1 binding to NRF2 may increase NRF2's transcriptional regulatory activities. NRF2 suppresses transcription of DCN, SOD2, and SOD3. PPARGC1A as a coactivator potentially mediates NRF2's inhibition of SOD2. Reduction of the superoxide dismutases contributes to increased oxidative stress, which further drives APE1 overexpression.

Chapter 2: Analysis of RNA Expression of Normal and Cancer Tissues Reveal High Correlation of COP9 Gene Expressions with Respiratory Chain Complex Components

Original citation: Wicker, CA; Izumi, T. Analysis of RNA expression of normal and cancer tissues reveals high correlation of COP9 gene expression with respiratory chain complex components. *BMC Genomics*. 2016 DEC 1; 17(1): 983.

https://doi.org/10.1186/s12864-016-3313-y

This original publication is Open Access and licensed under the Creative Commons Attribution License 4.0.

Document is verbatim to that of published paper except for minor clarification, and meeting ETD formatting requirements.

Copyright © Christina Ann Wicker 2017

Synopsis

2.1.1 Background

The COP9 signalosome, composed of 8 subunits, is implicated in cancer genetics with its deneddylase activity to modulate cellular concentration of oncogenic proteins such as IkB and TGFβ. However, its function in the normal cell physiology remains elusive. Primarily focusing on gene expression data of the normal tissues of the head and neck, The Cancer Genome Atlas (TCGA) database was used to identify groups of genes that were expressed synergistically with the COP9 genes, particularly with the COPS5 (CSN5), which possesses the catalytic activity of COP9.

2.1.2 Results

Expressions of seven of the COP9 genes (COPS2, COPS3, COPS4, COPS5, COPS6, COPS7A, and COPS8) were found to be highly synergistic in the normal tissues. In contrast, the tumor tissues decreased the coordinated expression pattern of COP9 genes. Pathway analysis revealed a high coordination of the expression of COPS5 and the other COP9 genes with mitochondria-related functional pathways, including genes encoding the respiratory chain complex.

2.1.3 Conclusions

The results indicate that mRNA expression data for the matched normal tissues available in TCGA are statistically reliable, and are highly useful to assess novel associations of genes with functional pathways in normal physiology as well as in the cancer tissues. This study revealed the significant correlation between the expressions of the COP9 genes and those related to the mitochondrial activity.

2.2 Introduction

The constitutive Photomorphogenesis (CSN) 9, or COP9 signalosome, is a critical multi-functional structure in cells (176,177). COP9, originally discovered in *Arabidopsis thalania* as a negative regulator of photomorphogenesis, was later found to be highly conserved across many species (178,179). COP9 is a 450-550 kDA holocomplex composed of 8 subunits whose official gene symbols are listed in **Table 2-1** (176,180). COP9 has catalytic activity to remove Nedd8, a small-ubiquitin like modifier, to regulate cullin-RING ubiquitin E3 ligases, and thus protein degradation pathways mediated by cullin complexes (176). COP9 regulates phosphorylation of proteins such as tumor suppressor p53, and neddylation essential to ubiquitin-mediated proteolysis of key proteins including tumor suppressor HIF-1α (181-185). Thus, COP9 has been an important focus in cancer genetics (180,185-188).

Despite intense studies in the past, the exact essential role of COP9 still remains unknown largely due to COP9's promiscuous property to interact with a variety of cullin complexes and others, and to affect stabilities of a number of cellular factors. Additionally, subforms of COP9 complexes were reported (177,189,190). Dubiel et al. proposed that such flexible conformation enables the broad range of substrates.

Table 2-1: Nomenclature of mammalian COP9 genes

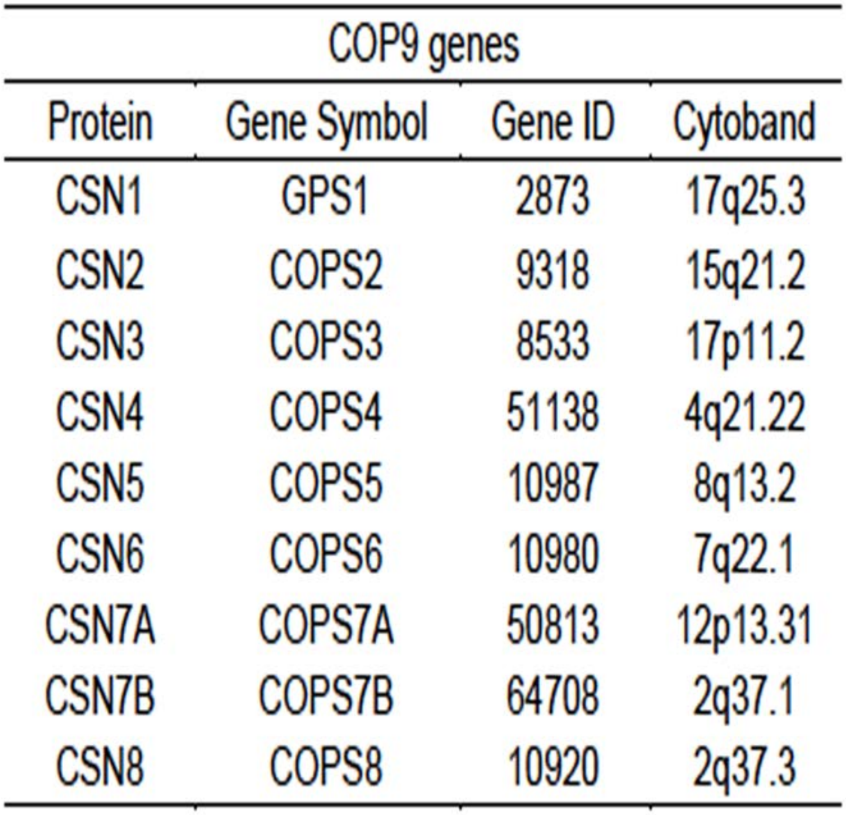

COP9 genes			
Protein	Gene Symbol	Gene ID	Cytoband
CSN1	GPS1	2873	17q25.3
CSN2	COPS2	9318	15q21.2
CSN3	COPS3	8533	17p11.2
CSN4	COPS4	51138	4q21.22
CSN5	COPS5	10987	8q13.2
CSN6	COPS6	10980	7q22.1
CSN7A	COPS7A	50813	12p13.31
CSN7B	COPS7B	64708	2q37.1
CSN8	COPS8	10920	2q37.3

Table contains protein and gene names for COP9 subunits, their gene ID and chromosomal location.

Among the 8 subunits, COPS5 is the most extensively studied subunit which has numerous critical functions including deneddylation reactions (176) (185). It is commonly over-expressed in cancers leading to increased deneddylation within cells (191). Other subunits have been shown to possess unique functions. For example, CSN1/GPS1 is involved in stabilization of p53 (185,188). Over-expression of COPS2 is linked to chromosome instability (188,192). Both COPS2 and COPS3 knockout are embryonic lethal at E3.5 and E8.5 respectively (185,188). COPS6 is frequently over-expressed in cancer (185). COPS8 knockout is also embryonic lethal (E7.5) with impaired growth and differentiation (185). Although these reports convincingly indicate that all the subunits have essential functions in mammalian cells, how these reported functions contribute to COP9 activity remains largely unknown.

Identification of functional groups with which COP9 signalosome may interact with in normal physiology may provide an important clue to understand how dysregulation of COP9 may facilitate tumorigenesis.

Deficiency in even one subunit leads to COP9 destabilization. Down-regulation of COPS5 in mouse embryonic fibroblasts drastically decreased the stability of COPS1, COPS3, and COPS8 (193-195). Therefore, it is plausible that coordinated expression of COP9 genes is needed to maintain necessary amounts of COP9 and imbalance may be associated with disease (196). To elucidate this possibility, a statistically adequate number of normal tissues must be analyzed with precision for their gene expressions. Using cultured cell lines is not appropriate for this investigation, because the cell lines established *in vitro* are all transformed and thus expressions of the COP9 genes are likely altered from cells in normal *in vivo* conditions.

The Cancer Genome Atlas (TCGA) has procured specimens from more than 500 human tumor tissues from various cancers for comprehensive analyses of tumor tissues and advanced cancer genomics. Importantly, matched normal tissues have been analyzed for about 10% of each cancer type. Using the TCGA database, we elucidated the possibility that expression of the COP9 genes are synchronized in the normal cells, and such coordinated gene expression is impaired in tumors. We found that the quality of the data from normal tissues was sufficiently high to test this possibility. Indeed the COP9 gene expressions were in synergy in the normal tissues, but this fine coordination was lost in the tumor tissues. Furthermore, the analysis led to the unexpected observation that the expressions of the COP9 genes were highly synchronized with those involved in mitochondrial biogenesis, particularly those of respiratory chain complex.

2.3 Methods

2.3.1 Nomenclature of COP9 Genes

Although the gene names from CSN1 to CSN8 are intuitive and have been accepted as the names for the COP9 subunits (197), the TCGA uses the official gene symbols (**Table 2-1**). For the simplicity, this study used the official gene symbols as the subunit names.

2.3.2 Data Obtained From TCGA

The mRNA expression data of normal and tumor tissues were obtained through TCGA's online data portal site (http://cancergenome.nih.gov). The cancer tissues chosen for this study are 44 normal and 522 cases of head and neck squamous cell carcinoma, lung adenocarcinoma (50 normal and 502 tumor). Normalized gene expression results (mRNASeq2 level3) were collected. Each set of mRNA expression data contained 20,531 gene entries, which were linked to annotations through DAVID functional gene annotation database (Database for Annotation, Visualization and Integrated Discovery; https://david.ncifcrf.gov), yielding 20,154 analyzable gene lists. The information linked to the mRNA data is chromosome cytoband and gene ontology (GOTERM_BP_FAT, GOTERM_CC_FAT, GOTERM_MF_FAT, and KEGG_PATHWAY).

Similarly, the de-identified clinical information including anatomical sites and smoking history were retrieved from TCGA. Data processing and analysis were carried out using R (ver 3.1.2) and series of command line programs developed with the Swift language using Xcode ver. 6.

2.3.3 Generation of Correlation Coefficient Table Specific for Individual Genes

Gene expression data of normal and tumor tissues from donors were assembled into a single table file consisting of columns of tissues and rows of genes. Genes that show zero mRNA values in more than 5% of the tissues analyzed were excluded. Pearson correlation coefficient (*r*) values between expressions of a target gene (example COPS5) and each of all the other genes were determined, and the genes were then sorted based on *r*-values. Significance of *r*-values were assessed with p values calculated with cor.test function in R, i.e., cor.test (A, B, method = "Pearson", alternative = "two.sided") where A and B are two mRNA expression vectors with an equal dimension (= number of samples). Pair and boxplots were drawn for particular gene sets using R.

2.3.4 Cytoband Plot and Generic Graphical Presentations

Genes ranked within 500 highest |*r*| values were pooled, and the cytoband information was processed into float values by the simple formula as following. For a gene with cytoband of ApB.N or AqB.N, a float value was generated by A - (B.N)/100 or A + (B.N)/100, respectively. For example, 8p11.2 was converted to 8 - 11.2/100 = 7.888, and 8q11.2 was to 8.112. Values of (x, y) = (cytoband, r) was plotted using R. X and Y chromosomes were shown in one column as all analyzed genes mapped in X chromosome were also found in Y chromosome.

2.3.5 Interpretation of Functional Gene Annotation

Top 1000 genes with the highest |*r*| values were pooled with each gene accompanying gene ontology (GO) and KEGG pathway information. Over-represented pathways are sorted by the p values based on binomial distribution: 1 - pbinom (n, 1000, μ) (in R), where n is the actual count occurring in the 1000 genes, and μ is the average of finding the particular pathways, and calculated with the whole gene set of 20,154.

2.3.6 Derivation of Enrichment Score (ES)

The ES scores were calculated by the method described previously (198). For example, for ES of oxidative phosphorylation (KEGG pathway hsa00190), the COPS5 correlation coefficient table with gene annotations was scanned based on association with "hsa00190" to generate P_{hit} - P_{miss}. ES was provided as the maximum value of P_{hit} - P_{miss} as described (198). A histogram of ES values was calculated with randomly chosen N_h genes for iteration of 1000, and the distribution was used to assess the statistical significance. Enrichment scores and corresponding *p* values were calculated for all genes and then false discovery rates were determined as described above.

2.4 Results

2.4.1 A single gene expression analysis

COPS5 (official gene symbol of CSN5) is responsible for the deneddylation activity of the COP9 signalosome, and also known as Jab1 to activate c-Jun (Jun-activating/binding protein). Thus, most COP9 studies have focused on the activity of COPS5 (199) and its influence on biological activities including tumorigenesis. Because of the pivotal role of COPS5 for the COP9 signalosome in mammalian cells, this study primarily focused on COPS5 to investigate the possibility of coordinated expression of the COP9 subunits in the normal and tumor tissues. Our primary interest was the head and neck squamous cell carcinoma (HNSCC), where effects of smoking and influences of major genetic factors, including p53, p16, AKT1 and K-Ras could be addressed due to its established cancer etiology involving these genes. In addition, HNSCC data in TCGA included a few distinct anatomical sites including oral cavity, tongue and larynx, and thus effects of tissue sites for the gene expression could be elucidated with the clarified clinical record. Therefore, this study mainly focused on the HNSCC. For the simplicity, the official gene symbols will be used in this study instead of more commonly used protein names (**Table 2-1).**

Expression of the COPS5 gene was examined using the data of 44 normal head and neck tissues available in TCGA. COPS5 expression in normal tissues showed mean value of 1261.0 with standard deviation (sd) 328.83 and coefficient of variation (sd/mean) 0.26. As a comparison, mean coefficient of variation of the 15,660 gene set was calculated, and found to be 0.693 (± 0.575). Therefore, the COPS5 gene expression appeared to be relatively stable among normal oral tissues.

2.4.2 Coordinated expressions of the COP9 genes in normal tissues

Expression patterns of COPS5 and other COP9 genes were elucidated by comparing correlation coefficients (expressed as *r* thereafter), using the RNA expression data (RNAseqV2 level 3). High positive correlations were found among the COP9 gene expressions. Specifically, relative to COPS5, all the other COP9 genes except COPS7B showed statistically significant positive *r-values* (**Table 2-2** and **Figure 2-1**). GPS1/CSN1 showed a smaller *r*-value than the others, namely COPS2, COPS3, COPS4, COPS6, COPS7A, and COPS8. The lower correlation of gene expression of GPS1 vs. COPS5 was found to be a

Table 2-2: Correlation of expression of COP9 genes in normal oral tissues

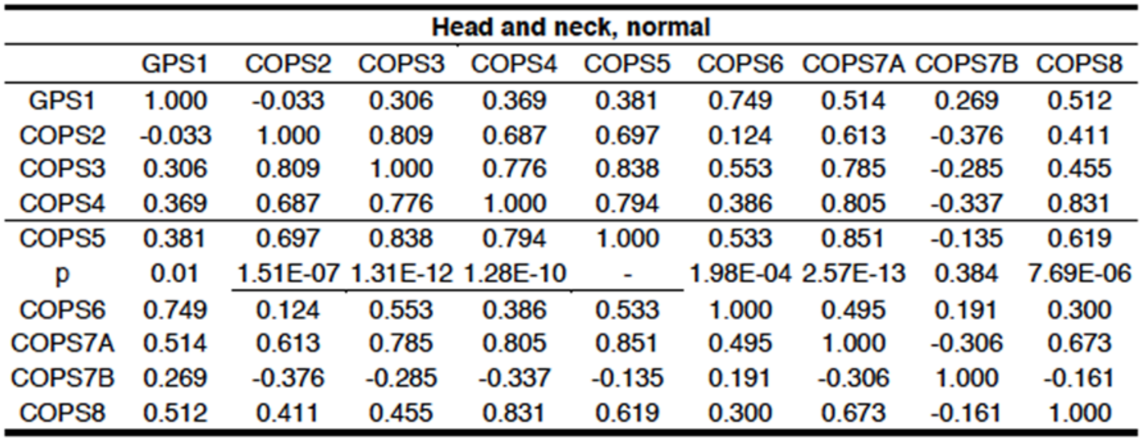

	Head and neck, normal								
	GPS1	COPS2	COPS3	COPS4	COPS5	COPS6	COPS7A	COPS7B	COPS8
GPS1	1.000	-0.033	0.306	0.369	0.381	0.749	0.514	0.269	0.512
COPS2	-0.033	1.000	0.809	0.687	0.697	0.124	0.613	-0.376	0.411
COPS3	0.306	0.809	1.000	0.776	0.838	0.553	0.785	-0.285	0.455
COPS4	0.369	0.687	0.776	1.000	0.794	0.386	0.805	-0.337	0.831
COPS5	0.381	0.697	0.838	0.794	1.000	0.533	0.851	-0.135	0.619
p	0.01	1.51E-07	1.31E-12	1.28E-10	-	1.98E-04	2.57E-13	0.384	7.69E-06
COPS6	0.749	0.124	0.553	0.386	0.533	1.000	0.495	0.191	0.300
COPS7A	0.514	0.613	0.785	0.805	0.851	0.495	1.000	-0.306	0.673
COPS7B	0.269	-0.376	-0.285	-0.337	-0.135	0.191	-0.306	1.000	-0.161
COPS8	0.512	0.411	0.455	0.831	0.619	0.300	0.673	-0.161	1.000

Pearson correlation coefficients were calculated using RNA expression data collected from TCGA. Data from 44 patient specimens were analyzed. P values were calculated as described in methods.

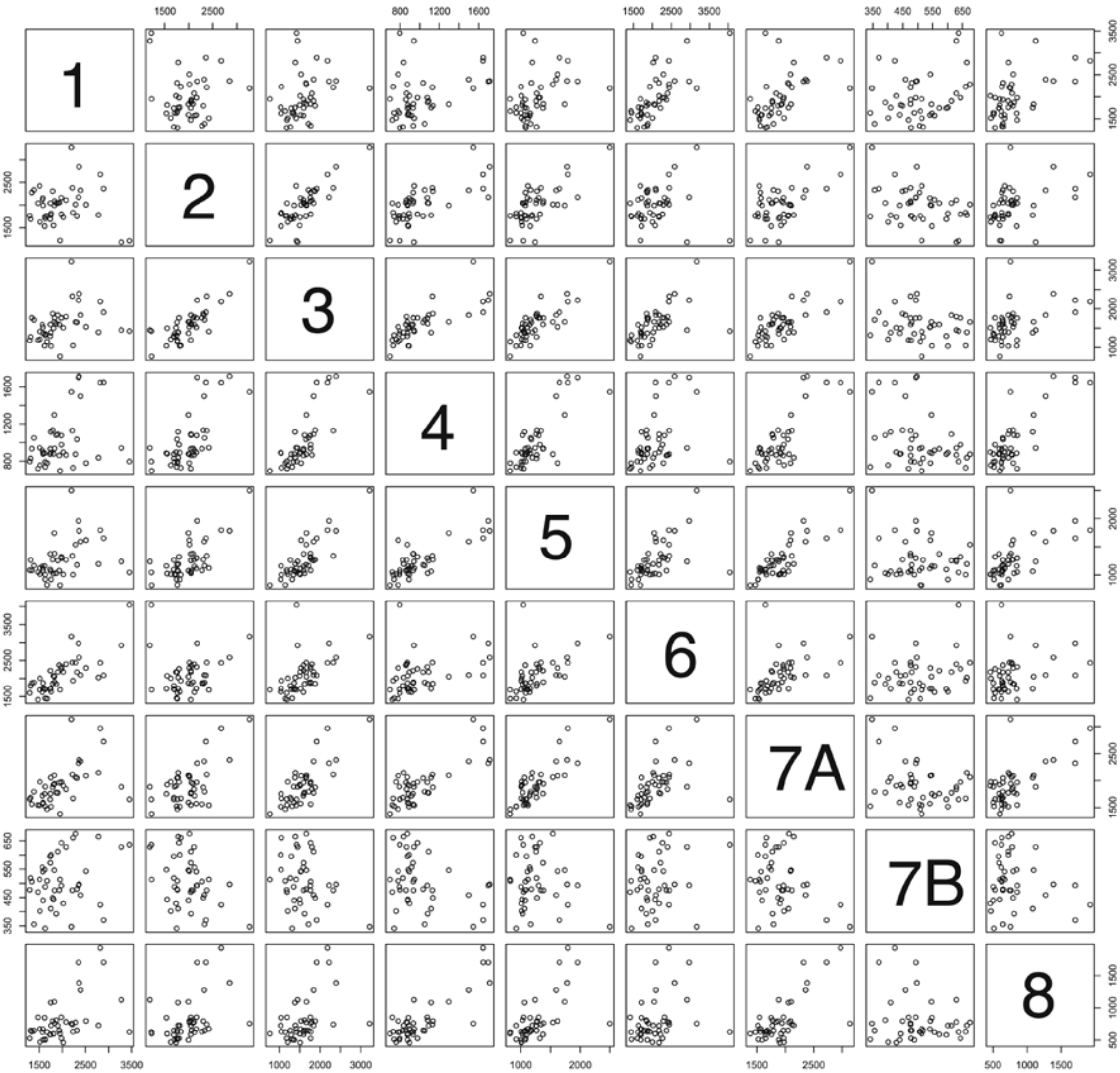

Figure 2-1: Pair-wise plot of expressions of COP9 genes

The RNA expression results from normal 44 oral tissues are plotted. 1: GPS1, 2: COPS2, 3: COPS3, 4: COPS4, 5: COPS5, 6: COPS6, 7A: COPS7A, 7B: COPS7B, 8: COPS8.

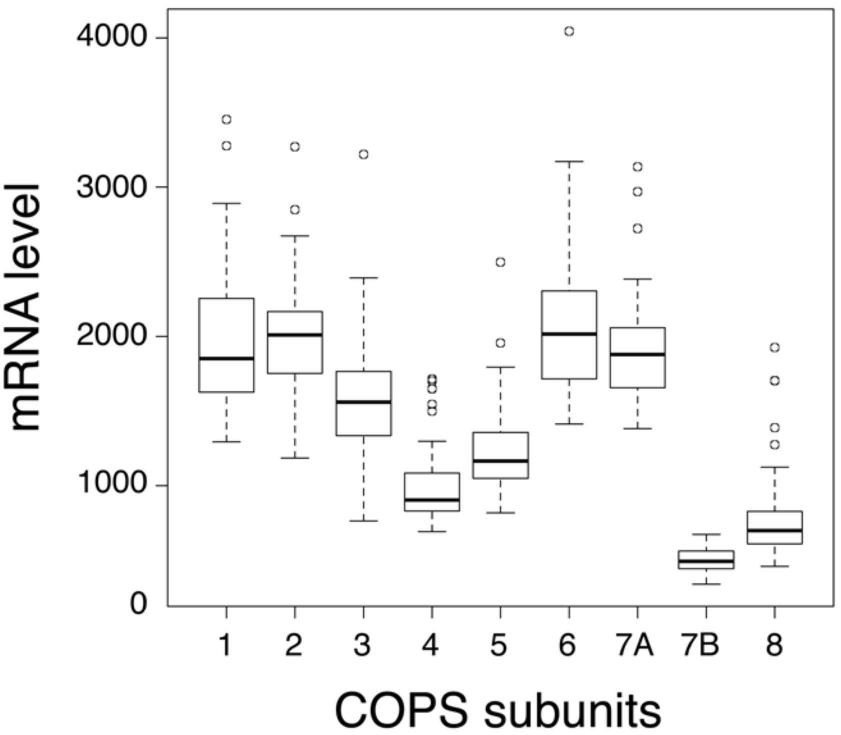

Figure 2-2: Expressions of COP9 genes in normal oral tissues

The RNA expression levels (y-axis) of COP9 genes from 44 normal oral tissues are shown. Horizontal lines in the boxes: median values. Top and bottom whiskers denote the first and the third quartile (Q1 and Q3). Outliers (> Q3 + 1.5 * (Q3 - Q1) and < Q1 - 1.5 * (Q3 - Q1)) are shown as individual dots.

general characteristic through our analyses in this study. However, the positive correlation between GPS1 and COPS5 was still statistically significant (p = 0.011). In addition to the low *r*-value relative to the other COP9 genes, the level of COPS7B expression was significantly lower compared to COPS7A (**Figure 2-2**).

These results indicated that the expressions of COP9 genes were synchronized in human normal oral tissues. Leppert et al. recently observed that mRNA levels of COP9 genes were regulated by an miRNA let-7 for synchronization (196). To probe the importance of the regulatory mechanism by miRNA, the TCGA miRNA dataset was used to determine the gene expression correlation of COP9 genes and the let-7 miRNA species (**Table 2-3**). There were statistically significant negative correlations between let-7 isoforms (7a, 7b, 7c, 7e, 7f-2, 7g) and COP9 genes (GPS1, COPS5, COPS6, and COPS8), which was consistent with previous work.

Table 2-3: Correlation of let-7 miRNA and COP9 genes

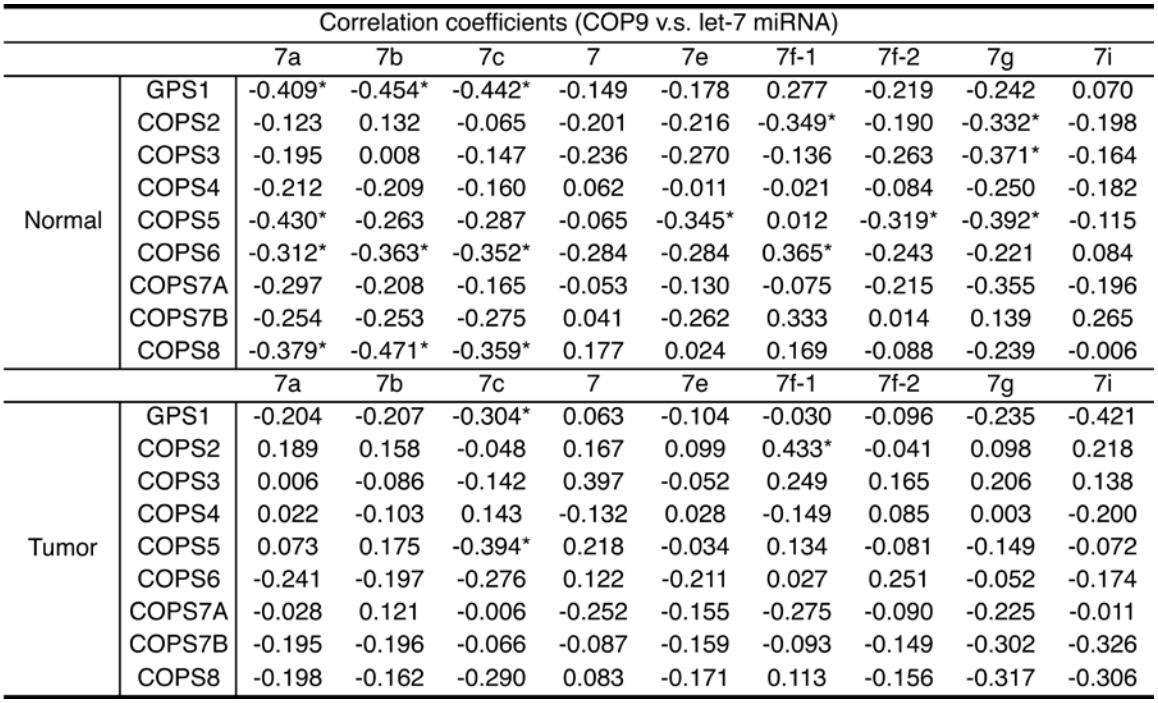

Correlation coefficients (COP9 v.s. let-7 miRNA)										
		7a	7b	7c	7	7e	7f-1	7f-2	7g	7i
Normal	GPS1	-0.409*	-0.454*	-0.442*	-0.149	-0.178	0.277	-0.219	-0.242	0.070
	COPS2	-0.123	0.132	-0.065	-0.201	-0.216	-0.349*	-0.190	-0.332*	-0.198
	COPS3	-0.195	0.008	-0.147	-0.236	-0.270	-0.136	-0.263	-0.371*	-0.164
	COPS4	-0.212	-0.209	-0.160	0.062	-0.011	-0.021	-0.084	-0.250	-0.182
	COPS5	-0.430*	-0.263	-0.287	-0.065	-0.345*	0.012	-0.319*	-0.392*	-0.115
	COPS6	-0.312*	-0.363*	-0.352*	-0.284	-0.284	0.365*	-0.243	-0.221	0.084
	COPS7A	-0.297	-0.208	-0.165	-0.053	-0.130	-0.075	-0.215	-0.355	-0.196
	COPS7B	-0.254	-0.253	-0.275	0.041	-0.262	0.333	0.014	0.139	0.265
	COPS8	-0.379*	-0.471*	-0.359*	0.177	0.024	0.169	-0.088	-0.239	-0.006
		7a	7b	7c	7	7e	7f-1	7f-2	7g	7i
Tumor	GPS1	-0.204	-0.207	-0.304*	0.063	-0.104	-0.030	-0.096	-0.235	-0.421
	COPS2	0.189	0.158	-0.048	0.167	0.099	0.433*	-0.041	0.098	0.218
	COPS3	0.006	-0.086	-0.142	0.397	-0.052	0.249	0.165	0.206	0.138
	COPS4	0.022	-0.103	0.143	-0.132	0.028	-0.149	0.085	0.003	-0.200
	COPS5	0.073	0.175	-0.394*	0.218	-0.034	0.134	-0.081	-0.149	-0.072
	COPS6	-0.241	-0.197	-0.276	0.122	-0.211	0.027	0.251	-0.052	-0.174
	COPS7A	-0.028	0.121	-0.006	-0.252	-0.155	-0.275	-0.090	-0.225	-0.011
	COPS7B	-0.195	-0.196	-0.066	-0.087	-0.159	-0.093	-0.149	-0.302	-0.326
	COPS8	-0.198	-0.162	-0.290	0.083	-0.171	0.113	-0.156	-0.317	-0.306

The let-7 expression profile was obtained from TCGA for the matched normal and tumor tissues of head and neck. Correlation coefficients for individual let-7 isoforms relative to COP9 genes are shown. (*) Asterisks indicate statistical significance ($p < 0.05$).

2.4.3 Loss of synergistic expressions of the COP9 genes in cancer tissues

To determine whether the synergistic expressions of the COP9 genes are maintained in the cancer tissues, 42 tumor tissues matched to the normal cases were pooled (2 normal cases could not be matched based on the id tag), and determined their correlation coefficients (**Table 2-4**). High positive *r*-values were observed among COP9 genes in normal tissues as expected. In contrast, the correlations of expressions among COP9 genes diminished in the matched tumor tissues (**Table 2-4 and Table 2-5**). Moreover, the negative effect of let-7 miRNA observed in the normal tissue dataset was diminished in the matched tumor tissues (**Table 2-3**). These results demonstrated that the coordinated expression of COP9 genes was lost in these tumor tissues.

2.4.4 Validation of the results with subgroups (age, anatomical sites, and smoking history)

HNSCC is an age-related disease. The majority of specimens in TCGA are from elderly patients (median = 61; the first quartile = 53, the third quartile = 69), and less than 4% of the patients are younger than 40 years old. Thus, the loss of the coordination of the COP9 gene expressions may be due to the age-related degeneration of the coordination. However, we analyzed the COP9 expression in the 31 tumor tissues that were 42 years old or younger to the 30 tumor tissues that were 80 years old or older **(Table 2-6 A and B).** With this analysis, we found similar loss of the coordinated expressions in specimens from both the young and elderly patients. In addition, there were no significant differences of the expression levels of each COP9 gene between the young and RNA-Seq data

Table 2-4: Loss of coordinated COP9 gene expression in HNSCC

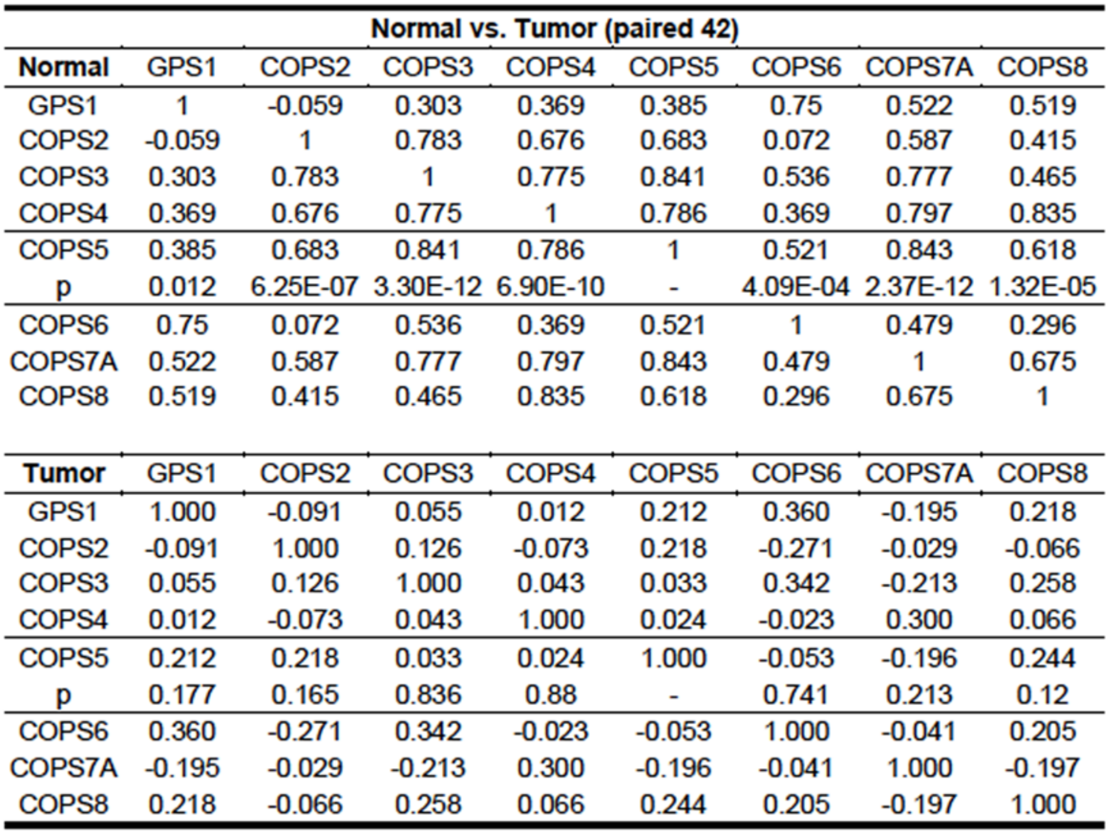

Normal vs. Tumor (paired 42)

Normal	GPS1	COPS2	COPS3	COPS4	COPS5	COPS6	COPS7A	COPS8
GPS1	1	-0.059	0.303	0.369	0.385	0.75	0.522	0.519
COPS2	-0.059	1	0.783	0.676	0.683	0.072	0.587	0.415
COPS3	0.303	0.783	1	0.775	0.841	0.536	0.777	0.465
COPS4	0.369	0.676	0.775	1	0.786	0.369	0.797	0.835
COPS5	0.385	0.683	0.841	0.786	1	0.521	0.843	0.618
p	0.012	6.25E-07	3.30E-12	6.90E-10	-	4.09E-04	2.37E-12	1.32E-05
COPS6	0.75	0.072	0.536	0.369	0.521	1	0.479	0.296
COPS7A	0.522	0.587	0.777	0.797	0.843	0.479	1	0.675
COPS8	0.519	0.415	0.465	0.835	0.618	0.296	0.675	1

Tumor	GPS1	COPS2	COPS3	COPS4	COPS5	COPS6	COPS7A	COPS8
GPS1	1.000	-0.091	0.055	0.012	0.212	0.360	-0.195	0.218
COPS2	-0.091	1.000	0.126	-0.073	0.218	-0.271	-0.029	-0.066
COPS3	0.055	0.126	1.000	0.043	0.033	0.342	-0.213	0.258
COPS4	0.012	-0.073	0.043	1.000	0.024	-0.023	0.300	0.066
COPS5	0.212	0.218	0.033	0.024	1.000	-0.053	-0.196	0.244
p	0.177	0.165	0.836	0.88	-	0.741	0.213	0.12
COPS6	0.360	-0.271	0.342	-0.023	-0.053	1.000	-0.041	0.205
COPS7A	-0.195	-0.029	-0.213	0.300	-0.196	-0.041	1.000	-0.197
COPS8	0.218	-0.066	0.258	0.066	0.244	0.205	-0.197	1.000

Normal and matched HNSCC tissues (sample number = 42) were compared for their correlation coefficient values among the COP9 genes.

Table 2-5: Loss of synchronized expression between COPS5 and the other COP9 genes in tumor tissues.

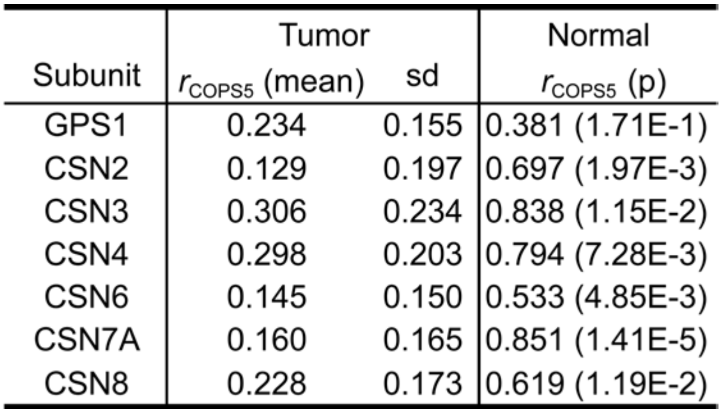

	Tumor		Normal
Subunit	r_{COPS5} (mean)	sd	r_{COPS5} (p)
GPS1	0.234	0.155	0.381 (1.71E-1)
CSN2	0.129	0.197	0.697 (1.97E-3)
CSN3	0.306	0.234	0.838 (1.15E-2)
CSN4	0.298	0.203	0.794 (7.28E-3)
CSN6	0.145	0.150	0.533 (4.85E-3)
CSN7A	0.160	0.165	0.851 (1.41E-5)
CSN8	0.228	0.173	0.619 (1.19E-2)

To support the result of Table 2-4, which included 42 cases of matched head and neck tumor tissues, 2 additional normal head and neck tissues were included to calculate correlation of expressions among the COP9 genes. To compare the results with the tumor specimens, correlation coefficients of COP9 genes versus COPS5 (rCOPS5) were determined from randomly selected 44 tumor specimens from the entire pool of 511. The calculations were repeated for 10,000 times to obtain their averages and standard deviations. The distributions followed normal distribution pattern, which were used to compare the difference from rCOPS5 of normal tissues.

from young (30 specimens) and elder patients (31 specimens) were used to calculate the correlation coefficients among the COP9 genes in aged populations **(Table 2-6 C).** Therefore, we conclude that the age is not a factor that affected the low coordination of the COP9 genes in the tumor specimens.

The oral tissues in TCGA were taken from different anatomical sites (oral cavity, tongue, etc.). The synergistic expression of COP9 subunit genes may vary depending on the exact site of oral tissues. To assess this possibility, the data set was arranged into subgroups based on the sites. The major groups were the oral cavity (14 specimens) and the oral tongue (13 specimens). The data sets of the two subgroups were used to determine correlation coefficients of the COP9 genes. These values were similar to those of the entire dataset **(Supplemental Table 2-7** and **Table 2-8**), indicating that the synergistic expressions of the COP9 genes are maintained regardless of the sites of the oral tissues. Similarly, there appeared to be no clear effects of smoking, because analyzing the normal tissues from eleven current smokers identified highly similar synergistic RNA expressions of COP9 genes (**Table 2-9**).

Table 2-6: Loss of COP9 expression coordination in tumor tissues independent of age.

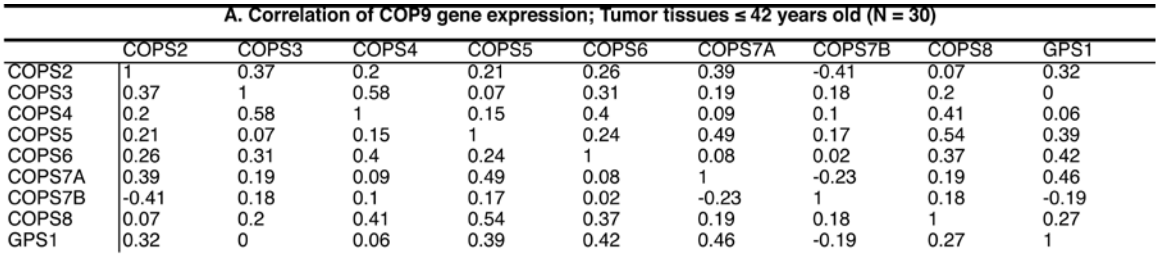

A. Correlation of COP9 gene expression; Tumor tissues ≤ 42 years old (N = 30)

	COPS2	COPS3	COPS4	COPS5	COPS6	COPS7A	COPS7B	COPS8	GPS1
COPS2	1	0.37	0.2	0.21	0.26	0.39	-0.41	0.07	0.32
COPS3	0.37	1	0.58	0.07	0.31	0.19	0.18	0.2	0
COPS4	0.2	0.58	1	0.15	0.4	0.09	0.1	0.41	0.06
COPS5	0.21	0.07	0.15	1	0.24	0.49	0.17	0.54	0.39
COPS6	0.26	0.31	0.4	0.24	1	0.08	0.02	0.37	0.42
COPS7A	0.39	0.19	0.09	0.49	0.08	1	-0.23	0.19	0.46
COPS7B	-0.41	0.18	0.1	0.17	0.02	-0.23	1	0.18	-0.19
COPS8	0.07	0.2	0.41	0.54	0.37	0.19	0.18	1	0.27
GPS1	0.32	0	0.06	0.39	0.42	0.46	-0.19	0.27	1

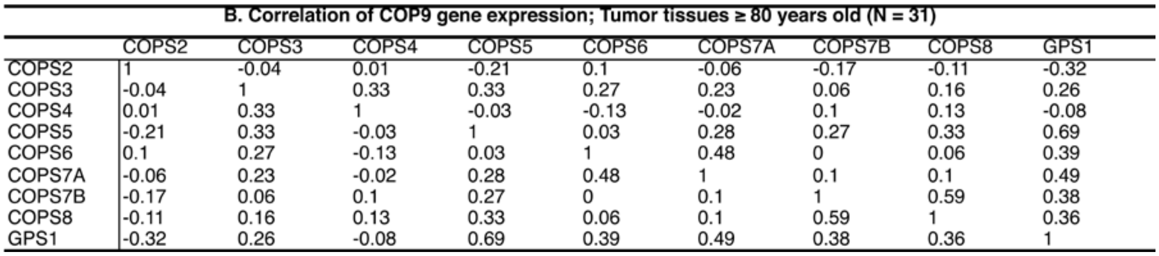

B. Correlation of COP9 gene expression; Tumor tissues ≥ 80 years old (N = 31)

	COPS2	COPS3	COPS4	COPS5	COPS6	COPS7A	COPS7B	COPS8	GPS1
COPS2	1	-0.04	0.01	-0.21	0.1	-0.06	-0.17	-0.11	-0.32
COPS3	-0.04	1	0.33	0.33	0.27	0.23	0.06	0.16	0.26
COPS4	0.01	0.33	1	-0.03	-0.13	-0.02	0.1	0.13	-0.08
COPS5	-0.21	0.33	-0.03	1	0.03	0.28	0.27	0.33	0.69
COPS6	0.1	0.27	-0.13	0.03	1	0.48	0	0.06	0.39
COPS7A	-0.06	0.23	-0.02	0.28	0.48	1	0.1	0.1	0.49
COPS7B	-0.17	0.06	0.1	0.27	0	0.1	1	0.59	0.38
COPS8	-0.11	0.16	0.13	0.33	0.06	0.1	0.59	1	0.36
GPS1	-0.32	0.26	-0.08	0.69	0.39	0.49	0.38	0.36	1

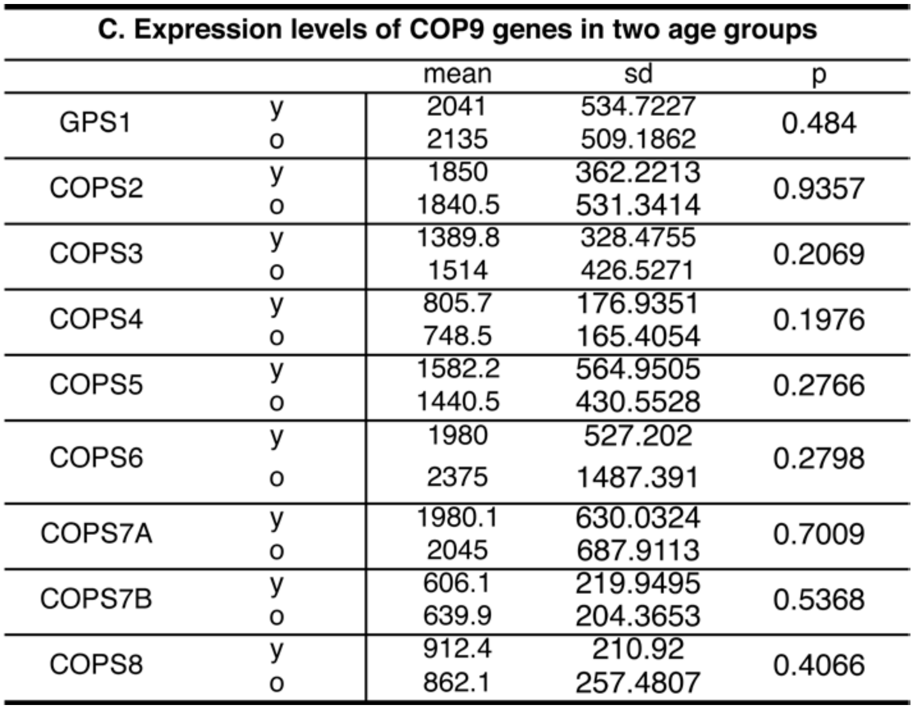

C. Expression levels of COP9 genes in two age groups

		mean	sd	p
GPS1	y	2041	534.7227	0.484
	o	2135	509.1862	
COPS2	y	1850	362.2213	0.9357
	o	1840.5	531.3414	
COPS3	y	1389.8	328.4755	0.2069
	o	1514	426.5271	
COPS4	y	805.7	176.9351	0.1976
	o	748.5	165.4054	
COPS5	y	1582.2	564.9505	0.2766
	o	1440.5	430.5528	
COPS6	y	1980	527.202	0.2798
	o	2375	1487.391	
COPS7A	y	1980.1	630.0324	0.7009
	o	2045	687.9113	
COPS7B	y	606.1	219.9495	0.5368
	o	639.9	204.3653	
COPS8	y	912.4	210.92	0.4066
	o	862.1	257.4807	

RNAseq data from young (30 specimens) and elderly patients (31 specimens) were used to calculate the correlation coefficients among the COP9 genes.

Table 2-7: Synchronized COP9 expression in normal oral cavity tissues

	Oral cavity, normal (N = 14)							
	GPS1	COPS2	COPS3	COPS4	COPS5	COPS6	COPS7A	COPS8
GPS1	1.000	-0.181	0.168	0.333	0.386	0.681	0.546	0.564
COPS2	-0.181	1.000	0.849	0.725	0.770	0.327	0.710	0.253
COPS3	0.168	0.849	1.000	0.783	0.915	0.715	0.841	0.307
COPS4	0.333	0.725	0.783	1.000	0.765	0.536	0.859	0.725
COPS5	0.386	0.770	0.915	0.765	1.000	0.783	0.929	0.401
p	0.17	1.27E-03	4.61E-06	1.43E-03	-	9.21E-04	1.55E-06	0.15
COPS6	0.681	0.327	0.715	0.536	0.783	1.000	0.732	0.352
COPS7A	0.546	0.710	0.841	0.859	0.929	0.732	1.000	0.612
COPS8	0.564	0.253	0.307	0.725	0.401	0.352	0.612	1.000

14 normal tissues from the oral cavity were pooled based on the clinical data in TCGA, and correlation coefficients as well as p values for COPS5 were calculated as described in the main article.

Table 2-8: Synchronized COP9 expression in normal tongue tissues

	Tongue, normal (N = 13)							
	GPS1	COPS2	COPS3	COPS4	COPS5	COPS6	COPS7A	COPS8
GPS1	1.000	-0.263	0.137	0.280	0.230	0.809	0.356	0.364
COPS2	-0.263	1.000	0.822	0.646	0.645	-0.253	0.714	0.494
COPS3	0.137	0.822	1.000	0.723	0.788	0.252	0.744	0.544
COPS4	0.280	0.646	0.723	1.000	0.917	0.134	0.877	0.950
COPS5	0.230	0.645	0.788	0.917	1.000	0.222	0.830	0.877
p	0.45	1.73E-02	1.36E-03	1.05E-05	-	0.47	4.39E-04	8.25E-05
COPS6	0.809	-0.253	0.252	0.134	0.222	1.000	0.132	0.174
COPS7A	0.356	0.714	0.744	0.877	0.830	0.132	1.000	0.829
COPS8	0.364	0.494	0.544	0.950	0.877	0.174	0.829	1.000

Data based on the 13 normal tongue tissues were pooled based on the clinical data in TCGA, and correlation coefficients as well as p values for COPS5 were calculated as described in the main article.

Table 2-9: Synchronized COP9 expression in normal oral tissues of smokers

	Smokers, normal (N = 11)							
	GPS1	COPS2	COPS3	COPS4	COPS5	COPS6	COPS7A	COPS8
GPS1	1.00	-0.11	0.47	0.54	0.56	0.89	0.59	0.72
COPS2	-0.11	1.00	0.67	0.69	0.52	-0.11	0.53	0.43
COPS3	0.47	0.67	1.00	0.82	0.85	0.56	0.82	0.64
COPS4	0.54	0.69	0.82	1.00	0.84	0.50	0.93	0.91
COPS5	0.56	0.52	0.85	0.84	1.00	0.67	0.87	0.77
p		0.10	8.15E-04	1.19E-03	-	2.53E-02	4.82E-04	5.51E-03
COPS6	0.89	-0.11	0.56	0.50	0.67	1.00	0.55	0.59
COPS7A	0.59	0.53	0.82	0.93	0.87	0.55	1.00	0.87
COPS8	0.72	0.43	0.64	0.91	0.77	0.59	0.87	1.00

11 normal tissues from smokers were pooled based on the clinical data in TCGA, and correlation coefficients as well as p values for COPS5 were calculated as described in the main article.

2.4.5 Chromosome mapping of genes with expressions highly correlated with COPS5

To elucidate the tumor-associated disintegration of the COP9 gene expression in detail, we focused on the COPS5 gene. We generated a "correlation table" of the COPS5, in which expressional correlation coefficients relative to the COPS5 gene (r_{COPS5}) were calculated for all the analyzable genes (about 14,000 genes). By cross-referring the results to gene ontology provided with DAVID, we noticed that genes with high r_{COPS5} of the tumor tissues were mapped in the same chromosomal location as the COPS5 gene (8q13.2, **Table 2-1)**. We thus speculated that the loss of the coordination of the COP9 expressions in the tumor tissues was not due to unpredictably disorganized expressions of the COP9 subunit genes, but rather there was a dominant effect of the physical locations of the genes on their expressions. To illustrate this possibility, chromosomal locations of 500 genes with top $|r_{COPS5}|$ values were plotted based on the chromosome 8 based on the cytoband (**Figure 2-3**, top). The genes with high $|r_{\mathrm{COPS5}}|$ in the normal tissues were distributed through all the chromosomes; among the top 100 genes, only 7 genes were mapped at 8q, near the COPS5 chromosomal location (8q13.2). In contrast, genes with high $|r_{\mathrm{COPS5}}|$ in the tumor tissues were concentrated near COPS5's chromosomal region (**Figure 2-3**, bottom); 56 genes out of the top 100 genes were bound to 8q.

We sought to assess the chromosomal cis-effect on the COPS5 gene expression more objectively. To this end, we determined the enrichment score (ES) (198) based on the $|r_{cops5}|$ for the genes located within 1 mega base pairs

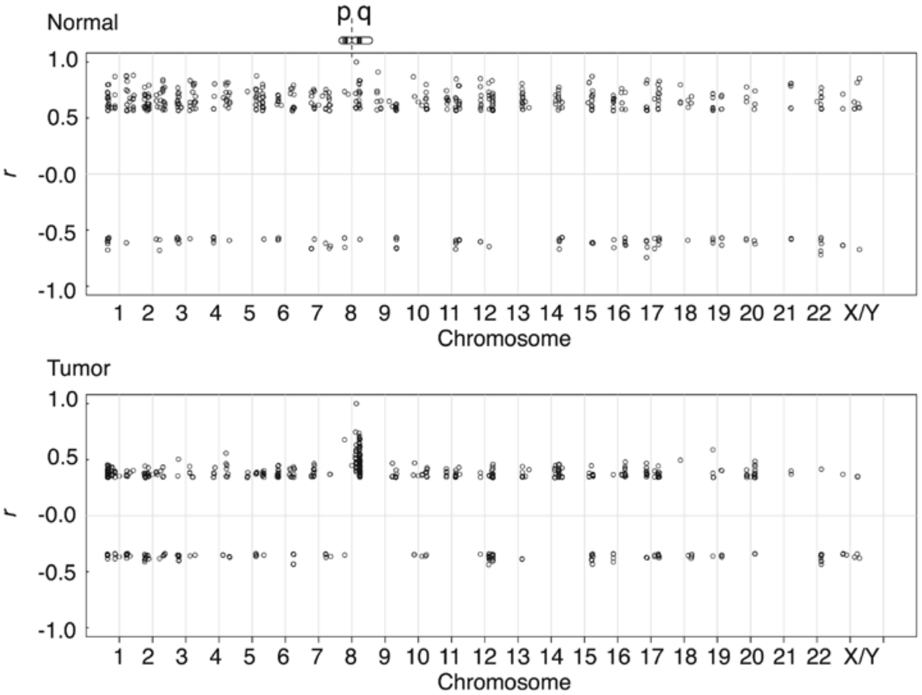

Figure 2-3: Chromosomal mapping of genes with highly synchronized expression with the COPS5 gene.

The 500 highest ranked genes based on $|r_{\text{COPS5}}|$ were pooled, and mapped on to chromosomal locations based on their cytoband information. In the top panel, a cartoon denotes the chromosome 8 (at 8 in x-axis) where the COPS5 gene is located (8q13). The major grid marks on the x-axis (1 - 22 and X/Y) depict location of centromeres dividing p and q arms at the left and the right sides, respectively. X and Y chromosomes are combined, because all genes analyzed in the figure are mapped in both X and Y.

(Mbp) from the COPS5, and obtained a p-value based on the null hypothesis that these ES values were not different from that calculated for genes outside 1 Mbs from the COPS5. We have also determined such ES values for all the genes in the chromosome 8 to determine false discovery rate (FDR, q). The ES value for the COPS5 with the tumor tissues (ES = 0.65, p = 0.02, q = 0.043) was significantly higher than that with the normal tissues (ES = 0.39, p = 0.27, q = 0.49). The procedure was applied for the other COP9 genes, and revealed significant links to the chromosomal cis-effect in case of the tumor tissues (**Table 2-10**). Therefore, we conclude that the COP9 expression in the tumors is disintegrated because the chromosomal cis-effect becomes a dominant force to express each subunit gene. Furthermore, these results indicated that analysis of the COP9 expressions in the normal tissues rather than tumor tissues is pivotal for understanding the COP9's role *in vivo*, and such an analysis is possible using the RNA-Seq data in the normal tissues available from TCGA.

Table 2-10: Effect of relative distance in chromosomes on the gene expression correlation

Gene	Matched HNSCC 42 tissues											
	Normal						Tumor					
	Nh	ES	mean	sd	p	q	Nh	ES	mean	sd	p	q
GPS1	46	0.510	0.202	0.080	6.079E-05	1.979E-03	46	0.764	0.267	0.090	1.575E-08	3.288E-07
COPS2	11	0.329	0.261	0.158	0.333	0.630	11	0.587	0.382	0.133	0.062	0.168
COPS3	21	0.224	0.174	0.107	0.321	0.630	21	0.637	0.348	0.114	0.006	1.894E-02
COPS4	13	0.541	0.277	0.147	0.036	0.203	13	0.904	0.271	0.146	7.013E-06	2.249E-04
COPS5	11	0.385	0.284	0.164	0.268	0.490	11	0.647	0.356	0.142	0.020	0.043
COPS6	52	0.482	0.187	0.076	4.936E-05	0.001	52	0.815	0.285	0.074	2.884E-13	1.777E-11
COPS7A	45	0.122	0.237	0.091	0.897	0.964	45	0.752	0.296	0.089	1.391E-07	3.051E-06
COPS7B	14	0.509	0.217	0.136	0.015	0.144	14	0.794	0.254	0.142	7.118E-05	9.864E-04
COPS8	9	0.374	0.304	0.172	0.344	0.637	9	0.837	0.349	0.176	0.003	0.014

Nh: number of genes found within 1 Mbp of each COP9 gene; mean, sd, p and q values were determined as described in materials and methods. Overall, highly significant ties of the gene expression correlation with the chromosomal locations were found in tumor tissues, while in normal tissues there were no such effects of the chromosomal locations on the gene expression co-expression (except for GPS1 and COPS6).

2.4.6 Pathway analysis based on KEGG and GO revealed association of COPS5 expression with mitochondrial pathways

Genes that belong to particular cell pathways may be over-represented in the COPS5 correlation coefficient table. Identifying such pathways should provide important clues as to COP9's roles under the normal physiology. Based on the results above, such functional association should be elucidated with the data derived from normal tissues, and the large pool of high-quality gene expression data in the TCGA database prompted us to investigate this possibility. Genes with the top 1,000 $|r_{\mathrm{COPS5}}|$ values in the normal tissues were pooled, and functional pathways available through GO and KEGG database were associated to each gene **(Supplemental Table D-1**). The GO and KEGG pathways were then ranked based on the over-representation, and the 20 most over-represented pathways are shown in **Table 2-11** (the expanded list is shown in **Supplemental Table D-2**). Unexpectedly, the pathways belonged to those related to mitochondrial functions and components. For example, 61 genes belonging to the oxidative phosphorylation KEGG pathway (hsa00190) were among the genes with high expression correlation with COPS5 out of 106 total genes ($p < 1.1e-16$). A number of GO pathways involving mitochondrial functions were also found among the over-represented pathways. These included respiratory chain (GO:0070469), mitochondrial electron transport (GO:0006120), NADH dehydrogenase activity (GO:0003954), mitochondrial respiratory chain complex I (GO:0005747). In fact, all of the 20 most over-represented pathways are directly related to major mitochondrial and energy derivation functions.

Table 2-11: Association of COPS5 with mitochondrial pathways in normal oral tissues

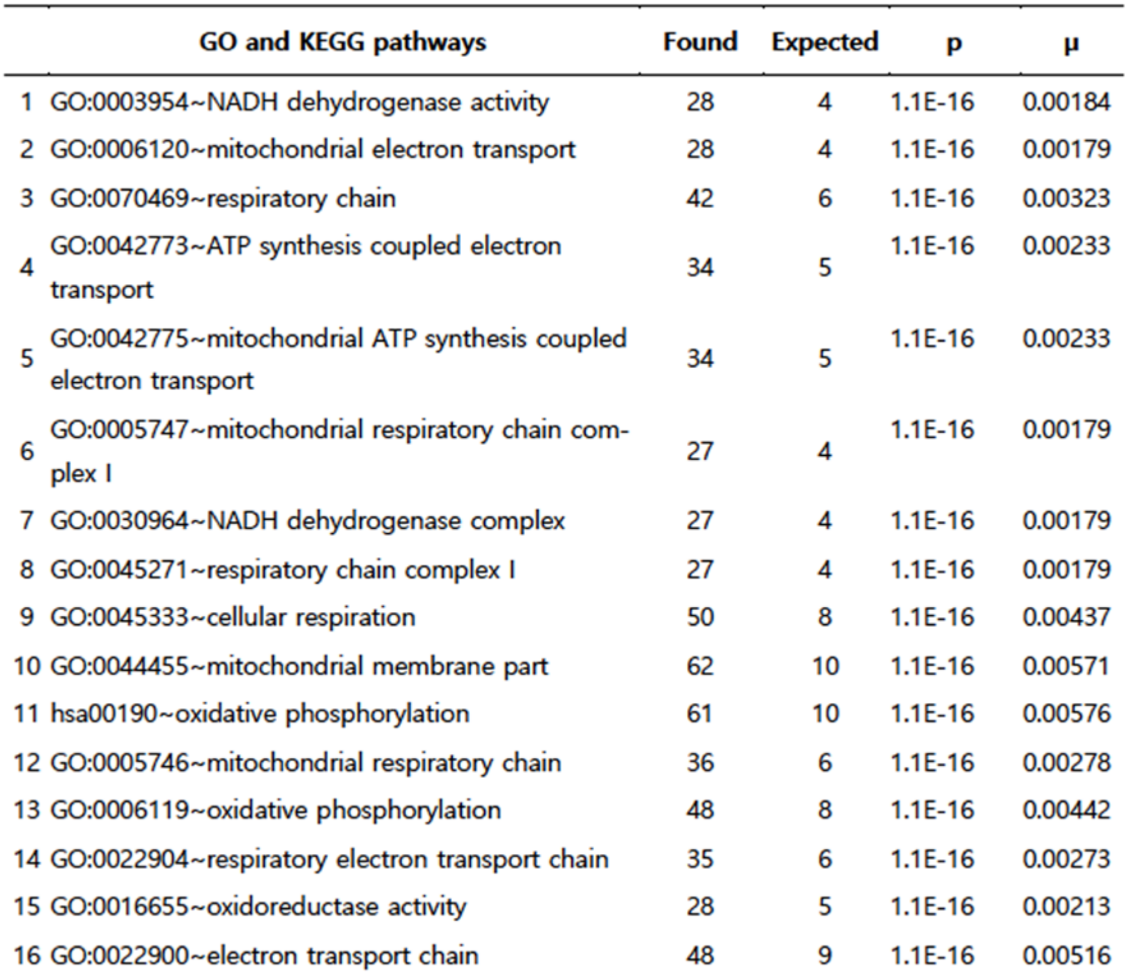

	GO and KEGG pathways	Found	Expected	p	μ
1	GO:0003954~NADH dehydrogenase activity	28	4	1.1E-16	0.00184
2	GO:0006120~mitochondrial electron transport	28	4	1.1E-16	0.00179
3	GO:0070469~respiratory chain	42	6	1.1E-16	0.00323
4	GO:0042773~ATP synthesis coupled electron transport	34	5	1.1E-16	0.00233
5	GO:0042775~mitochondrial ATP synthesis coupled electron transport	34	5	1.1E-16	0.00233
6	GO:0005747~mitochondrial respiratory chain complex I	27	4	1.1E-16	0.00179
7	GO:0030964~NADH dehydrogenase complex	27	4	1.1E-16	0.00179
8	GO:0045271~respiratory chain complex I	27	4	1.1E-16	0.00179
9	GO:0045333~cellular respiration	50	8	1.1E-16	0.00437
10	GO:0044455~mitochondrial membrane part	62	10	1.1E-16	0.00571
11	hsa00190~oxidative phosphorylation	61	10	1.1E-16	0.00576
12	GO:0005746~mitochondrial respiratory chain	36	6	1.1E-16	0.00278
13	GO:0006119~oxidative phosphorylation	48	8	1.1E-16	0.00442
14	GO:0022904~respiratory electron transport chain	35	6	1.1E-16	0.00273
15	GO:0016655~oxidoreductase activity	28	5	1.1E-16	0.00213
16	GO:0022900~electron transport chain	48	9	1.1E-16	0.00516

Dataset includes the top 1000 functional pathways found in high correlation with Found: number of genes in a particular GO or KEGG pathway found in the top 1000 r_{COPS5} list; Expected: number of expected genes to yield $p < 0.05$ appearing in 1000 genes based on the average appearance per gene (μ); μ values were calculated by the total appearance of individual pathways in the entire gene list of 20,154. P values were calculated using binomial distribution in R. Expected occurrences in a list of 1000 genes to provide $p < 0.05$ are listed.

At the time this study was carried out, gene ontology database had not yet linked COPS5 to any of mitochondrial-related pathways. Expression values were examined in pair-plots for COPS5 and mitochondrial genes of the five highest r_{COPS5}, NDUFB6, MRPS36, ATP5F1, TMEM126A, NDUFB3 (**Figure 2-4**). The results illustrate high integrity of the data and the coordination of the expression of the COPS5 with the mitochondria related genes.

Dependency on the anatomical sites and smoking history were tested with the same subgroups as described above (**Supplemental Table D-3**). The mRNA expression data from the two major anatomical sites, oral cavity and oral tongue, resulted in almost identical over-representation of the mitochondrial pathways with COPS5. The same conclusion was made with the subgroup containing only the current smokers.

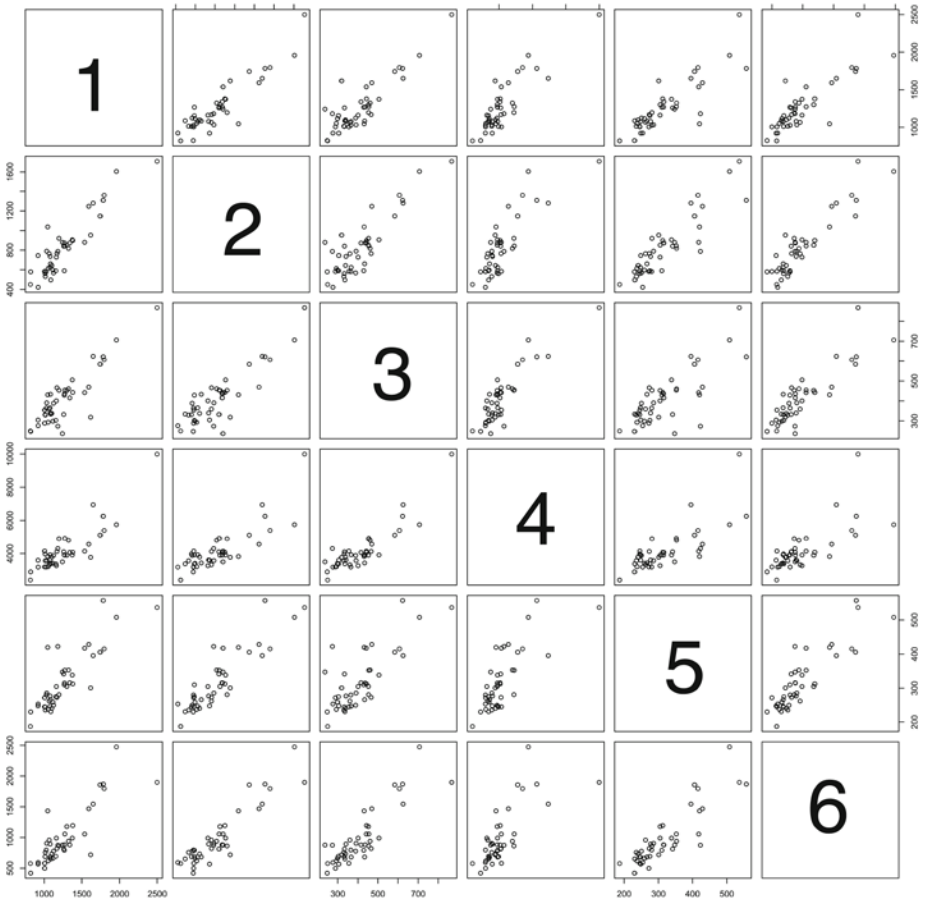

Figure 2-4: Pair-wise plot for RNA expression 5 mitochondrial genes

The five genes with the highest r_{COPS5} in the normal oral tissues are plotted. 1: COPS5, 2: NDUFB6, 3: MRPS36, 4: ATP5F1, 5: TMEM126A, 6: NDUFB3.

2.4.7 Alteration of COPS5 expression coordination in cancer tissues

The gene expression coordination between the COPS5 gene and the mitochondrial pathways was elucidated with tumor tissues **(Table 2-13 and Supplemental Table D-4).** Although a few GO pathways related to mitochondrial functions were over-represented, major pathways associated with the COPS5 expression were those involved in ribosome processing and RNA binding as well as membrane lumen pathways.

The possibility that tissues from a particular anatomical site with high dysregulation caused the bias was addressed. Oral cavity, tongue, and larynx are the major 3 sites that together contribute to about 80% of the donated head and neck cancer tissues. COPS5-associated GO and KEGG pathways were determined for the tissues from the particular sites, and confirmed that correlation of COPS5 expression with mitochondria associated genes were not as predominant as in the normal tissues.

To further support the finding, enrichment score (ES) was calculated for the genes in the oxidative phosphorylation KEGG pathway (hsa00190) using RNA-Seq data of 44 normal head and neck tissues deposited in TCGA (198) **(Figure 2-5 A).** The obtained ES value, 0.797, was much higher than the average ES value based on randomly assigned gene pools **(Figure 2-5 B).**

In addition, ES values corresponding to all the other KEGG pathways were calculated for the 42 matched normal and tumor tissues **(Table 2-14).** The ES values of the oxidative phosphorylation pathway (hsa00190) were found to be among the highest. The ubiquinone biosynthesis pathway generated the highest

Table 2-12: Loss of coordinated expression of COPS5 with mitochondria related genes in the tumor tissues

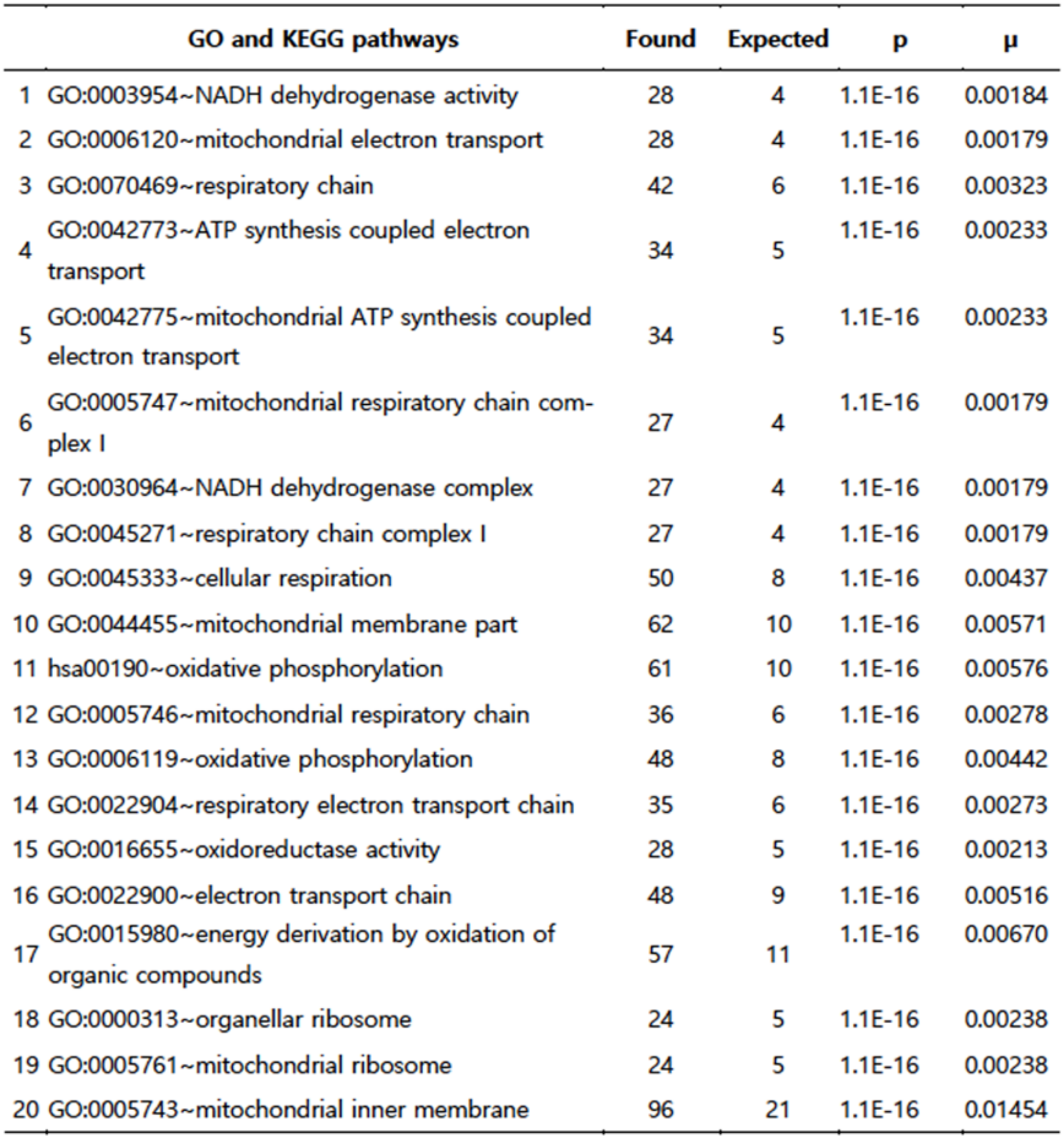

	GO and KEGG pathways	Found	Expected	p	μ
1	GO:0003954~NADH dehydrogenase activity	28	4	1.1E-16	0.00184
2	GO:0006120~mitochondrial electron transport	28	4	1.1E-16	0.00179
3	GO:0070469~respiratory chain	42	6	1.1E-16	0.00323
4	GO:0042773~ATP synthesis coupled electron transport	34	5	1.1E-16	0.00233
5	GO:0042775~mitochondrial ATP synthesis coupled electron transport	34	5	1.1E-16	0.00233
6	GO:0005747~mitochondrial respiratory chain complex I	27	4	1.1E-16	0.00179
7	GO:0030964~NADH dehydrogenase complex	27	4	1.1E-16	0.00179
8	GO:0045271~respiratory chain complex I	27	4	1.1E-16	0.00179
9	GO:0045333~cellular respiration	50	8	1.1E-16	0.00437
10	GO:0044455~mitochondrial membrane part	62	10	1.1E-16	0.00571
11	hsa00190~oxidative phosphorylation	61	10	1.1E-16	0.00576
12	GO:0005746~mitochondrial respiratory chain	36	6	1.1E-16	0.00278
13	GO:0006119~oxidative phosphorylation	48	8	1.1E-16	0.00442
14	GO:0022904~respiratory electron transport chain	35	6	1.1E-16	0.00273
15	GO:0016655~oxidoreductase activity	28	5	1.1E-16	0.00213
16	GO:0022900~electron transport chain	48	9	1.1E-16	0.00516
17	GO:0015980~energy derivation by oxidation of organic compounds	57	11	1.1E-16	0.00670
18	GO:0000313~organellar ribosome	24	5	1.1E-16	0.00238
19	GO:0005761~mitochondrial ribosome	24	5	1.1E-16	0.00238
20	GO:0005743~mitochondrial inner membrane	96	21	1.1E-16	0.01454

The analysis was carried out in the same way as for Table 2-11

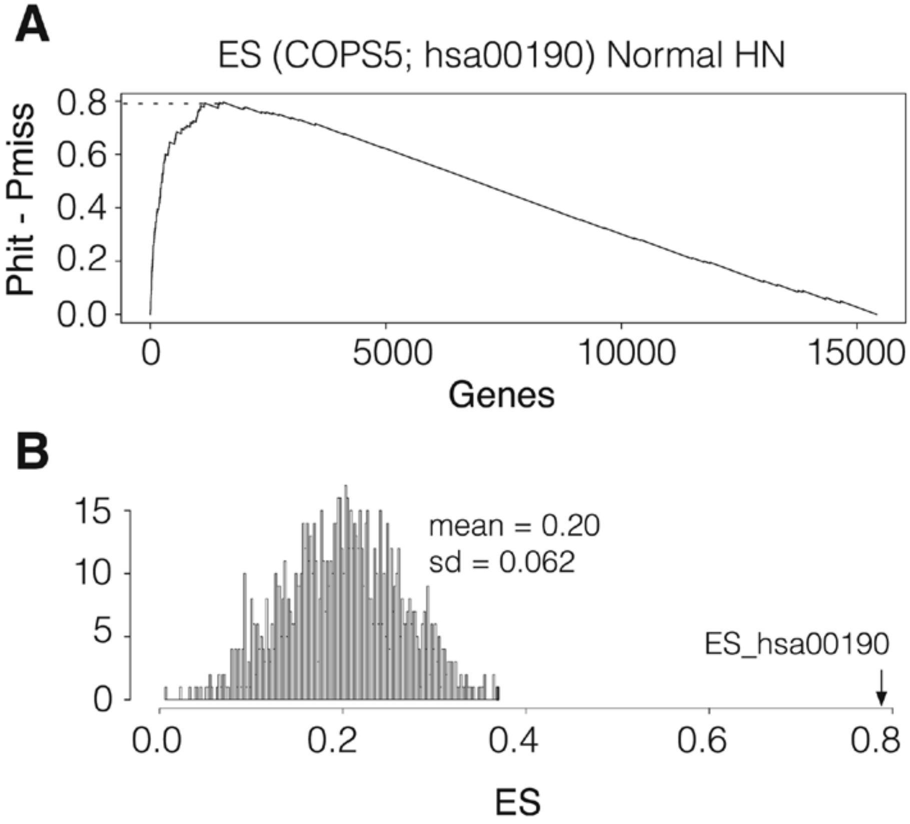

Figure 2-5: Enrichment score for KEGG oxidative phosphorylation pathway

(**A**) The enrichment score was calculated for the oxidative phosphorylation KEGG pathway (hsa00190). Genes are aligned on x-axis based on their correlation coefficients to the COPS5 expression. The hsa00190 pathway contained 106 genes in the entire list. (**B**) 106 randomly selected genes were used to calculate ES using the r_{COPS5} gene list as in A. The histogram was generated by iteration of 1000 times. The arrow indicates the ES for hsa00190.

Table 2-13: Enrichment scores for the COPS5 gene on KEGG pathways

		KEGG pathways	ES	Min	Nh	p
1	hsa00130	Ubiquinone and other terpenoid-quinone biosynthesis	0.919	-0.004	6	0.001
2	hsa00400	Phenylalanine	0.811	-0.028	3	0.038
3	hsa00190	Oxidative phosphorylation	0.797	0.000	106	0.000
4	hsa00630	Glyoxylate and dicarboxylate metabolism	0.752	-0.014	13	0.001
5	hsa00053	Ascorbate and aldarate metabolism	0.750	-0.083	6	0.001
6	hsa00062	Fatty acid elongation in mitochondria	0.745	-0.027	8	0.004
7	hsa03050	Proteasome	0.734	-0.004	41	0.000
8	hsa00640	Propanoate metabolism	0.698	-0.003	29	0.000
9	hsa00620	Pyruvate metabolism	0.691	-0.006	34	0.000
10	hsa04260	Cardiac muscle contraction	0.676	-0.001	56	0.000

All KEGG pathways found in the entire gene list of TCGA RNA expression database (199) were individually scanned through the r_{COPS5} alignment, and the maximum (ES) as well as minimum (P_{hit} - P_{miss}) were calculated as previously described (198). The KEGG pathways that generated the 10 highest ES values are shown. N_h: number of genes belonging to a KEGG pathway in the entire list. A p value for a particular KEGG pathway with an N_h (= N_o) was determined using mean and standard deviation obtained by the following method. N_o genes were randomly selected from the r_{COPS5} list and calculated an ES value, which was reiterated for 1,000 times to generate the mean and standard deviation of ES.

ES value, which is an essential factor in the respiratory chain and requires phenylalanine (generating the second highest ES) for its synthesis. Thus, the enrichment of genes involved in mitochondria-related pathway based on the COPS5 correlation was exceptionally high.

To elucidate the significance of the COP9 coordination with oxidative phosphorylation compared to other genes, we calculated ES values relative to the hsa00190 KEGG pathway for the entire gene list in the RNA-Seq data of the matched normal and tumor tissues to obtain FDR (**Table 2-15, 2-16**). Except for the COPS7B gene, all the COP9 subunit genes showed highly significant correlations with the genes in the oxidative phosphorylation pathway. Remarkably, while most of the genes belonging to the oxidative phosphorylation pathway resulted in the high ES/low FDR values, the COP9 genes (except for COPS7B) were ranked comparably with these genes. Again, the p as well as FDR values were increased for all the COP9 genes with the tumor specimen set, indicating that tumor tissues have lost the link of COP9 expression to the oxidative phosphorylation related genes. Taken all together, there results imply that the normal physiological function of the COP9 may be inseparable from the mitochondrial activity

2.4.8 Analysis of gene expression of other cancers in TCGA

Finally, the question was addressed whether the association of the expressions of COP9 genes with those of mitochondrial genes was unique in head and neck tissues. To probe this, the RNA expression data of TCGA for the lung squamous cell carcinoma tissues were analyzed. Tumors originating from

Table 2-14: ES for COP9 genes for all KEGG pathways

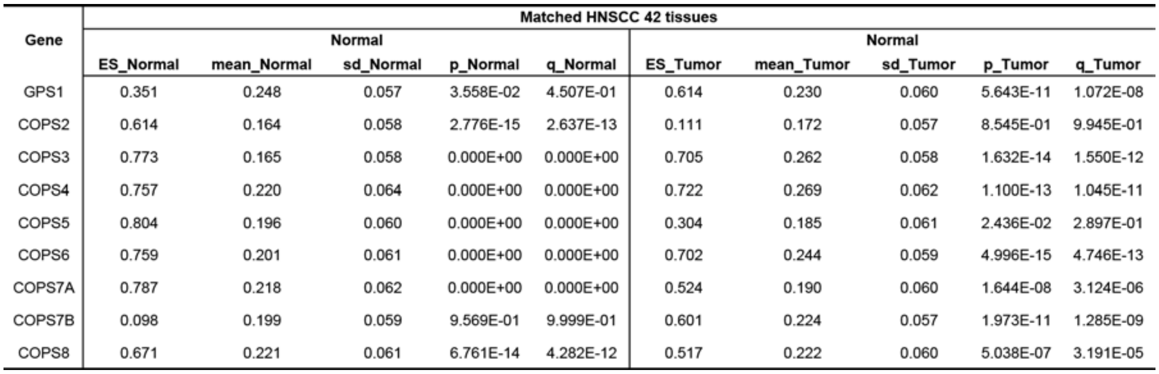

Gene	Matched HNSCC 42 tissues									
	Normal					Normal				
	ES_Normal	mean_Normal	sd_Normal	p_Normal	q_Normal	ES_Tumor	mean_Tumor	sd_Tumor	p_Tumor	q_Tumor
GPS1	0.351	0.248	0.057	3.558E-02	4.507E-01	0.614	0.230	0.060	5.643E-11	1.072E-08
COPS2	0.614	0.164	0.058	2.776E-15	2.637E-13	0.111	0.172	0.057	8.545E-01	9.945E-01
COPS3	0.773	0.165	0.058	0.000E+00	0.000E+00	0.705	0.262	0.058	1.632E-14	1.550E-12
COPS4	0.757	0.220	0.064	0.000E+00	0.000E+00	0.722	0.269	0.062	1.100E-13	1.045E-11
COPS5	0.804	0.196	0.060	0.000E+00	0.000E+00	0.304	0.185	0.061	2.436E-02	2.897E-01
COPS6	0.759	0.201	0.061	0.000E+00	0.000E+00	0.702	0.244	0.059	4.996E-15	4.746E-13
COPS7A	0.787	0.218	0.062	0.000E+00	0.000E+00	0.524	0.190	0.060	1.644E-08	3.124E-06
COPS7B	0.098	0.199	0.059	9.569E-01	9.999E-01	0.601	0.224	0.057	1.973E-11	1.285E-09
COPS8	0.671	0.221	0.061	6.761E-14	4.282E-12	0.517	0.222	0.060	5.038E-07	3.191E-05

For each COP9 gene correlation coefficient table, ES values were calculated for all KEGG pathways. Mean, standard deviation (sd), p and q values were calculated as described in the method section. Extremely high correlations of the COP9 genes (except for GPS1 and COPS7B) found in normal tissues were decreased significantly in tumor tissues (especially for COPS2 and COPS5).

Table 2-15: ES for COP9 genes for the oxidative phosphorylation pathway

Gene	Matched HNSCC tissues (42)									
	Normal					Tumor				
	ES	mean	sd	p	q	ES	mean	sd	p	q
GPS1	0.710	0.177	0.057	0.00E+00	0.00E+00	0.743	0.245	0.062	3.33E-16	5.14E-15
COPS2	0.586	0.170	0.058	6.20E-13	6.73E-12	0.417	0.170	0.059	1.61E-05	7.35E-05
COPS3	0.770	0.167	0.058	0.00E+00	0.00E+00	0.637	0.198	0.060	1.83E-13	1.53E-12
COPS4	0.753	0.211	0.062	0.00E+00	0.00E+00	0.178	0.212	0.063	7.07E-01	1.00
COPS5	0.809	0.196	0.063	0.00E+00	0.00E+00	0.300	0.182	0.061	2.60E-02	0.09
COPS6	0.746	0.194	0.059	0.00E+00	0.00E+00	0.632	0.213	0.063	1.12E-11	7.40E-11
COPS7A	0.787	0.209	0.060	0.00E+00	0.00E+00	0.066	0.214	0.061	9.92E-01	1.00
COPS7B	0.117	0.194	0.057	0.91	1.00	0.512	0.166	0.057	5.68E-10	3.33E-09
COPS8	0.671	0.211	0.062	6.92E-14	8.96E-13	0.561	0.182	0.060	1.75E-10	1.06E-09

ES values for all genes in RNAseq data were calculated for the oxidative phosphorylation KEGG pathway (hsa00190). Mean, standard deviation (sd), p and q values were calculated as described in the method section.

The extremely high correlations of the COP9 genes with hsa00190 were found among normal tissues, whereas such correlations were decreased significantly among tumor tissues, especially for the COPS4, COPS5, and COPS7A genes.

the lung upper airway epithelia share similarity with HNSCC in its etiology and its involvement of smoking as an important risk factor. First, the synergistic expression pattern of COP9 genes in the normal tissues (n = 50) was examined, and found to be highly synergistic with one another **(Table 2-16 and Figure 2-2).** Exceptions were GPS1 and COPS7B, which showed lower correlation coefficients to other COP9 factors. The high positive correlations were again lost in the tumor tissues. These results showed a remarkable coincidence with those of head and neck normal and tumor tissues.

The functional pathway analysis with the entire gene list resulted in the high correlation of the COPS5 expression with the mitochondrial genes **(Supplemental Table D-4).** Unlike the case of head and neck squamous cell carcinoma, however, the coordinated expression of COP9 and the mitochondrial genes was maintained well in the lung squamous cell carcinoma tissues **(Supplemental Table D-4).**

2.5 Discussion

Cancer genetics and analyses of the TCGA database mainly focus on the loss of genomic integrity. Mutations and single nucleotide polymorphism in DNA show the high rate of permanent alteration of the genome, epigenetic modification of the genome, RNA and miRNA expression alterations. TCGA data sets are available publicly for these types of analyses. The database is highly reliable and allowed us to examine cancer genomics with more than 500 tumor specimens (200).

Table 2-16: Synchronized expression of the COP9 genes in the matched tissues of normal and lung squamous cell carcinoma

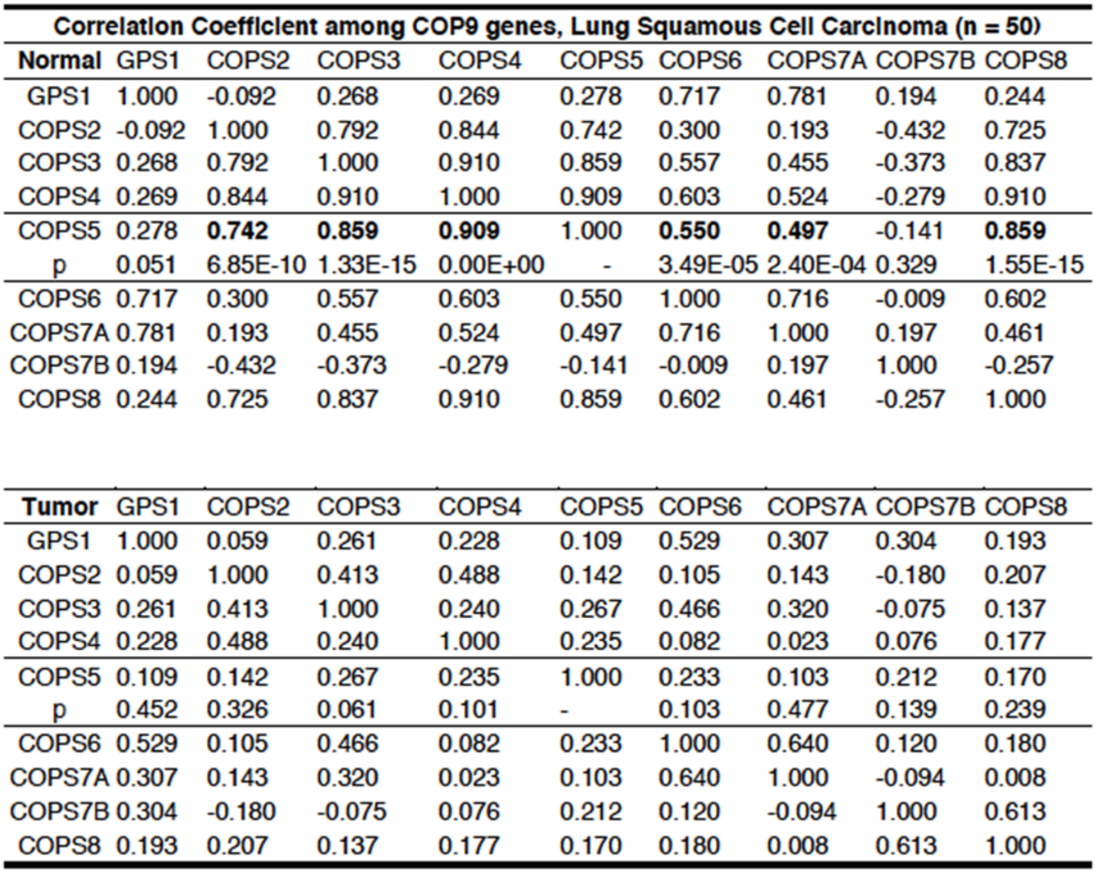

Correlation Coefficient among COP9 genes, Lung Squamous Cell Carcinoma (n = 50)

Normal	GPS1	COPS2	COPS3	COPS4	COPS5	COPS6	COPS7A	COPS7B	COPS8
GPS1	1.000	-0.092	0.268	0.269	0.278	0.717	0.781	0.194	0.244
COPS2	-0.092	1.000	0.792	0.844	0.742	0.300	0.193	-0.432	0.725
COPS3	0.268	0.792	1.000	0.910	0.859	0.557	0.455	-0.373	0.837
COPS4	0.269	0.844	0.910	1.000	0.909	0.603	0.524	-0.279	0.910
COPS5	0.278	**0.742**	**0.859**	**0.909**	1.000	**0.550**	**0.497**	-0.141	**0.859**
p	0.051	6.85E-10	1.33E-15	0.00E+00	-	3.49E-05	2.40E-04	0.329	1.55E-15
COPS6	0.717	0.300	0.557	0.603	0.550	1.000	0.716	-0.009	0.602
COPS7A	0.781	0.193	0.455	0.524	0.497	0.716	1.000	0.197	0.461
COPS7B	0.194	-0.432	-0.373	-0.279	-0.141	-0.009	0.197	1.000	-0.257
COPS8	0.244	0.725	0.837	0.910	0.859	0.602	0.461	-0.257	1.000

Tumor	GPS1	COPS2	COPS3	COPS4	COPS5	COPS6	COPS7A	COPS7B	COPS8
GPS1	1.000	0.059	0.261	0.228	0.109	0.529	0.307	0.304	0.193
COPS2	0.059	1.000	0.413	0.488	0.142	0.105	0.143	-0.180	0.207
COPS3	0.261	0.413	1.000	0.240	0.267	0.466	0.320	-0.075	0.137
COPS4	0.228	0.488	0.240	1.000	0.235	0.082	0.023	0.076	0.177
COPS5	0.109	0.142	0.267	0.235	1.000	0.233	0.103	0.212	0.170
p	0.452	0.326	0.061	0.101	-	0.103	0.477	0.139	0.239
COPS6	0.529	0.105	0.466	0.082	0.233	1.000	0.640	0.120	0.180
COPS7A	0.307	0.143	0.320	0.023	0.103	0.640	1.000	-0.094	0.008
COPS7B	0.304	-0.180	-0.075	0.076	0.212	0.120	-0.094	1.000	0.613
COPS8	0.193	0.207	0.137	0.177	0.170	0.180	0.008	0.613	1.000

The analysis was carried out in the same way as for Table 2-3.

In addition to the tumor specimens, data from about 40 to 50 normal tissues are made available for most types of cancers with a notable exception for glioblastoma. Although the data sizes are smaller than those for the cancer tissues, they are arguably one of the most comprehensive data for genomics of human specimens of non-disease status with pathological scrutiny, which should provide valuable information for elucidating functions of a gene under the normal physiology. We hypothesized that a synergistic expression of genes may be observed in the normal tissues, when expressions of a group of genes need to be coordinated for their proper cellular activities. COP9 signalosome is an ideal subject to test this possibility, because all 8 subunits are essential for the proper COP9 function; deficiency in one of the COP9 genes decreased stability of the other subunits and caused lethality (199,201). In this study the COP9 signalosome genes showed highly synergistic expressions in the normal head and neck tissues, except for GPS1 and COPS7B. Remarkably, these characteristics, including the lower r-values for GPS1 and COPS7b, were maintained well even in the lung and breast (data not shown) normal tissues. The coordinated expression of the COP9 genes decreased in the tumor tissues. Therefore, this coordination could not have been detected by analyzing tumor tissues. Likewise, because all cells cultured *in vitro* are under non-physiological conditions and thus transformed at some extent, it would have been difficult to obtain convincing evidence for the expression correlation of the COP9 subunit genes based on *in vitro* cell biological studies alone.

It is interesting to observe the lowest coordination of GPS1 expression compared to the other COP9 components (excluding COPS7B). Besides being a subunit of COP9, GPS1 is known for its function in suppression of G-protein and mitogen-activated signal transduction in mammalian cells (202). This COP9-independent function quite likely requires a regulation of the GPS1 gene separate from the other COP9 genes.

COPS7B not only had the lowest *r*-value, but also significantly lower expression compared to COPS7A **(Figure 2-2).** While COPS7A and COPS7B genes are encoded in different human chromosomes, chromosome 12 and 2 respectively, there is a high homology between COPS7A and COPS7B in the amino acid sequence (78% identical). Thus, COPS7B may have only a minor functional role for COP9, which may be compensated by COPS7A.

To our knowledge, one of the approaches in this study, using the exact physical map of the transcription start sites available from the Ensemble genome database, has not been applied previously to elucidate effects of the relative locations of genes on the gene expression correlations. In this study, we used this approach to find the chromosomal locations of the genes as a dominant factor causing the loss of the coordinated expressions of the COP9 genes. This cis-effect was not found in the normal tissues in most genes, an indication that expression of most genes in normal tissues are regulated based on their functions and independently from their chromosomal locations. Therefore, important implications derived from this analysis are that 1) analyzing tumor tissue data may not identify a function of a protein family such as COP9, and 2) the qualities of the normal tissue data available in TCGA are high enough to help identifying unknown expressional linkages with functional pathways. Although the primary focus of this study was COP9 expression profiling, we expanded the analysis of the influence of the chromosomal location for all the genes that were analyzable in the RNA-Seq data, and the data for cancer genes (hsa05200) are shown in **Supplemental Table D-5.** It may be interesting to elucidate whether these proto-oncogenes show tight association with the chromosomal locations in other types of tumor tissues available in TCGA.

The observation that the expression of the COPS5 gene (and therefore the other COP9 genes) was synchronized with those involved in mitochondrial function was unexpected. The correlation coefficients of the COPS5 and top ranked genes such as NDUFB6 and MRPS36 **(Figure 2-4)** were remarkably high with statistical significance. Moreover, not only a handful of genes involved in mitochondria but also the total pathway analysis revealed that mitochondria-related cellular functions and pathways were predominantly over-represented in the COPS5 correlation coefficient table. Although there have not been reports that show direct function of COP9 for mitochondria, correlation analyses with the genes of which functions have been extensively studied (i.e. TP53 and CDKN2A) linked these genes with predicted cellular functions. These results validate the approach in this study and support the prediction that the COP9 signalosome has a novel functional link to mitochondrial activities **(Supplemental Table D-6).**

Few studies have linked COP9 to mitochondria-related cellular activities. Jab1/COPS5 was previously identified as an apoptosis inducing factor through modulation of mitochondrial BH3-domain containing protein BclGs (203). A study found that in Neurospora crassa, 3 subunits of the COP9 were required to recover from deficiency of alternative oxidase function, which is important for mitochondrial function (204). However, no follow-up studies have been carried out for mammalian cells. On the other hand, pathways involved in ribosomal functions were associated with the COPS5 expression in the tumor tissues. The significance of this link is currently unclear. However, the COP9 structure is homologous to translation initiation factor 3 (eIF3), another high-ordered complex in the cells (205), and our speculation is that COPS5 may have an overlapping function in the protein synthesis in transformed cells.

The quantity and quality of the genomics database will only be improved. The present study underscores the importance and usefulness of examining the genomics of normal tissues. The results would provide novel functional links of a gene, which was not possible by analyzing the data set of pathophysiological specimens. This approach can reasonably be applied to other genes to identify pathways that have not been known due to scarce information for genomics information of normal tissues.

2.6 Conclusions

The present study investigated COPS5 gene expression using the TCGA database. The analysis revealed the highly synergistic mRNA expression pattern among COP9 genes in normal oral tissues. The coordination was abrogated in the tumor tissues, and the regulatory mechanism was taken over by a *cis*-acting gene regulation. Further analysis revealed an unexpected expression correlation between the COPS5 gene and a number of mitochondria-related genes, postulating the possible functional role of the COP9 signalosome for mitochondrial activities. The quality of the RNA expression data available in TCGA is high enough to allow us gene expression analysis in normal tissues to identify gene functions under normal physiology, which may not be recognized by the data obtained from tumor tissues.

Chapter 3: Polyubiquitination of Apurinic/apyrimidinic Endonuclease 1 by Parkin

Original citation: Scott, TL*; Wicker, CA*; Suganya, R; Dhar, B; Pittman, T; Horbinski, C; Izumi, T. Polyubiquitiniation of apurinic/apyrimidinic endonuclease 1 by Parkin. Mol Carcinog. 2017 Feb; 56(2): 252-336. Minor adjustments were made to comply with ETD formatting requirements.

*Denotes co-first author

Document is verbatim to that of published paper except where needed for clarification and to meet ETD formatting requirements.

From Molecular Carcinogenesis. Copyright © 2016 Wiley Periodicals, Inc. by John Wiley Sons, Inc. Reprinted by permission of John Wiley & Sons, Inc.

Copyright © Christina Ann Wicker 2017

3.1 Synopsis

Apurinic/apyrimidinic endonuclease 1 (APE1) is an essential protein crucial for repair of oxidized DNA damage not only in genomic DNA but also in mitochondrial DNA. Parkin, a tumor suppressor and Parkinson's disease (PD) associated gene, is an E3 ubiquitin ligase crucial for mitophagy. While DNA damage is known to induce mitochondrial stress, Parkin's role in regulating DNA repair proteins has not been elucidated. In this study, we examined the possibility of Parkin-dependent ubiquitination of APE1.

Ectopically expressed APE1 was degraded by Parkin and PINK1 via polyubiquitination in mouse embryonic fibroblast cells. PD-causing mutations in Parkin and PINK1 abrogated APE1 ubiquitination. Interaction of APE1 with Parkin was observed by co-immunoprecipitation, proximity ligation assay, and co-localization in the cytoplasm. N-terminal deletion of 41 amino acid residues in APE1 abrogated the Parkin-dependent APE1 degradation. These results suggested that Parkin directly ubiquitinated N-terminal Lys residues in APE1 in the cytoplasm. Modulation of Parkin and PINK1 activities under mitochondrial or oxidative stress caused moderate but statistically significant decrease of endogenous APE1 in human cell lines including SH-SY5Y, HEK293, and A549 cells. Analyses of glioblastoma tissues showed an inverse relation between the expression levels of APE1 and Parkin. These results suggest that degradation of endogenous APE1 by Parkin occur when cells are stressed to activate Parkin, and imply a role of Parkin in maintaining the quality of APE1, and loss of Parkin may contribute to elevated APE1 levels in glioblastoma.

3.2 Introduction

Oxidatively damaged DNA is primarily repaired by DNA base excision repair. In the mammalian DNA base excision repair pathway, apurinic/apyrimidinic (AP) endonuclease (APE1) incises DNA upstream of AP sites to generate single-strand breaks (SSBs) with 3'-OH termini for subsequent DNA repair synthesis reactions (206). APE1 is shown to be essential during mouse embryonic development and is the only active AP-endonuclease in mammals. Studies also demonstrated that APE1 was indispensable for cultured cells (123,207), although recent studies demonstrated that cells derived from a B lymphocyte line could survive without APE1 (208,209). APE1 also functions as a gene expression regulator by redoxically activating oncogenic and pro-survival transcription factors such as AP-1 and NF-κB, and is also involved in gene regulation necessary for calcium homeostasis (39,117). Therefore, APE1 is a pro-survival multifunctional protein. Drug and radiation resistance of tumor tissues have been linked to increased APE1 expression (165,210-213).

APE1 is post-translationally modified by phosphorylation, acetylation, and ubiquitination (115,214-219). APE1 was found to be ubiquitinated by MDM2 (220,221), the major p53 regulator (222,223). However, APE1 ubiquitination was later observed in mouse embryonic fibroblast defective of MDM2 (220), implying existence of backup activities for APE1 ubiquitination other than MDM2. Meisenberg et al. identified UBR3 as another E3 ubiquitin ligase for APE1 (224).

Properly maintained mitochondrial membrane potential is critical to meet cellular energy demands through oxidative phosphorylation. Electron leaks from the respiratory chain complexes result in the generation of superoxide (O_2^-). The mitochondrial superoxide dismutase is extremely efficient in scavenging O_2^- (225), and thus cells at normal growth conditions maintain the oxidative stress at a manageable level. This status quo may be broken by exogenous reagents, genotoxic stresses, and gene mutations that impair mitochondria (226-228). Damaged mitochondria elevate intracellular reactive oxygen species (ROS), and result in further impairment of mitochondria (229). To avoid this vicious cycle, a salvaging process named mitophagy is initiated to break down damaged mitochondria and generate new mitochondria (230). It is becoming apparent that mitophagy is modulated by DNA damage responses. Recent studies found that activation of poly (ADP-ribose) polymerase 1 (PARP1) by DNA strand breaks plays a pivotal role in the energy metabolism (231,232). In the process of DNA repair, oxidative DNA damage are converted to DNA strand breaks as intermediate lesions (233). The suppression of mitophagy by the activated PARP may be a self-feedback system during the repair of endogenous DNA damage. However, understanding the interplay among factors for mitophagy and DNA repair proteins is far from complete.

During mitophagy, proteins in damaged mitochondria are degraded via polyubiquitination, which is mainly carried out by Parkin, a RING domain-containing E3 ubiquitin ligase (234). PINK1 (PTEN-induced-kinase 1) is a critical activator of Parkin (230,234). PINK1 phosphorylates ubiquitin and Parkin (235) (236-238) and recruits Parkin from cytoplasm to mitochondrial surfaces to facilitate ubiquitination of its target proteins such as mitofusin 2 (Mfn2), Miro, and VDAC1

(239,240). Mutations in the Parkin and the PINK1 genes cause mitochondrial degeneration and are associated with Parkinson’s disease and glioblastoma (GBM) (230,241,242).

Considering that Parkin expression is induced by p53 (243,244) which enhances APE1 ubiquitination (221), it is possible that Parkin ubiquitinates APE1. Moreover, a recent proteomics study for identifying Parkin's substrates and interacting proteins revealed APE1 as one of possible targets of Parkin (245). These observations prompted us to investigate the activity of Parkin for APE1 ubiquitination. In this study, we investigated functional and physical interactions between APE1, Parkin, and PINK1.

3.3 Materials and Methods

3.3.1 DNA, Cell Culture And Transient Transfection

All cDNAs in plasmid expression vectors used in this study are of humans. Expression vectors for YFP-Parkin (23955) and cMyc-PINK1 (13314) (246,247) were obtained from Addgene. Non-tagged wild-type (wt) PINK1 was then cloned by PCR amplification into pcDNA3.1 (Invitrogen). The full-length human Parkin and its specific E2 ligase UbcH7 were cloned for this study by PCR cloning from quick cDNA clone (Clontech) using Phusion Taq DNA polymerase (NEB) with appropriate primers synthesized (Integrated DNA Technology) into the pcDNA3.1Zeo (+) expression vector (Invitrogen). Mutations (R275W and C431F in Parkin and G309D in PINK1) were introduced by PCR subcloning. The pBi16, a mammalian expression vector with a flippase recognition target (FRT) site and a doxycycline (Dox) inducible-dual promoter (248), is a generous gift from Dr.

Grabczyk. The human Parkin and PINK1 cDNAs were cloned into pBi16 (named pBi16-PaPi, **Figure 3-1**) for inducing both proteins together with doxycycline. All sequences of DNA amplified by PCR were confirmed by DNA sequencing (ACGT Inc. and GenScript Inc).

MEF^{la}, a mouse embryonic fibroblast cells, deficient in mouse Ape1 (mApe1) and expressing hAPE1 was described previously for its extremely low APE1 expression (122). The MEF^{la} cells were cultured in DMEM High Glucose medium (Hyclone) supplemented with 10% fetal bovine serum (Gemini Inc.), 1% penicillin/streptomycin, 1% L-glutamine (Hyclone). SH-SY5Y (a human neuroblastoma) and A549 (a human lung adenocarcinoma) were purchased from ATCC. The HEK293 derivative T-Rex 293 was purchased from Invitrogen. The T-Rex 293 cells were transfected with pBi16-PaPi and pOG44 expressing flippase (Flp). 293/pBI16-PaPi (293-PaPi) stable transfectants were selected with 150-µg/mL hygromycin. The 293-PaPi cells were plated on 60 mm dishes (1x10^{6}/dish). After overnight incubation, Parkin and PINK1 were induced with 2 µg/mL doxycycline. At the same time, drugs indicated in the results were added in the culture medium, and together incubated for 16 hours. Cells were then harvested for immunoblot analyses.

For transient transfection, cells were plated on 60 mm dishes at 4x10^{5} - 1x10^{6} and incubated for overnight. Lipofectamine 2000 (Invitrogen) was used for transfection using OptiMEM-I (Invitrogen) with the vendors' manual. PINK1 siRNA was purchased from Applied Biosystems. Introduction of siRNA was standardized for minimum cytotoxicity as the following method. Semi-confluent SH-SY5Y cells were suspended in the DMEM medium at 1×10^7 cells/mL, and mixed with 200 nM siRNA. Cell/siRNA suspensions in 0.1 cm cuvettes were then electroporated using ECM 830 square wave electroporation system (BTX) at 920V, 120 μF, 2 pulses at 0.1 sec interval. After 15 minutes at room temperature, cells were transferred to 100 mm dishes (Corning) containing complete DMEM-High Glucose media (Gibco) and incubated for 72 hours. When necessary, 10 μM carbonyl cyanide 3-chlorophenylhydrazone (CCCP) was added after 48 h, and further incubated for 24 hours (total 72 hours after the electroporation). Cells were then harvested and examined with immunoblot.

3.3.2 Immunoblot (Western blot) assay

Whole cell extracts were prepared from cells detached by scraping after being washed with PBS twice, and resuspended in RIPA buffer (249) supplemented with proteinase inhibitor cocktail (Roche) and 40 μM MG132. After adjusting protein concentration, the extracts were run in 10% acrylamide SDS-PAGE, transferred to PVDF membrane (Bio-Rad), and blotted with appropriate antibodies. SDS-PAGE samples were run with a pre-stained protein size marker (NEB, P7709).

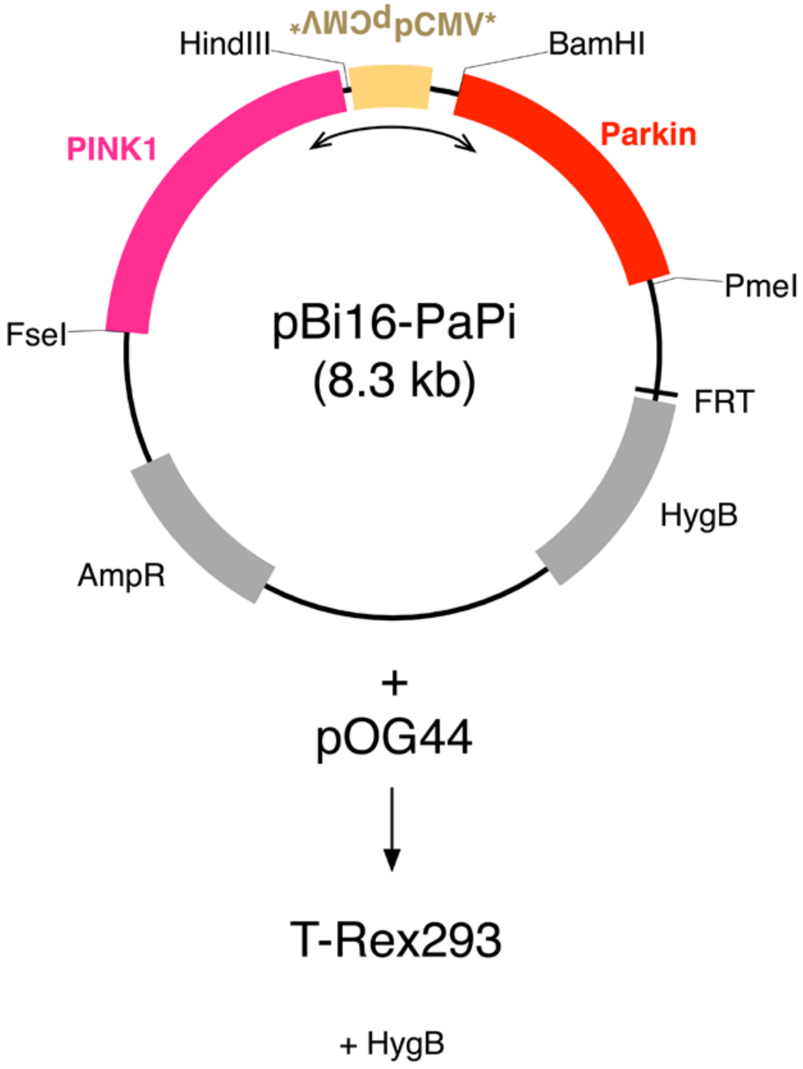
HindIII
pCMV*
pCMV*
BamHI
PINK1
Parkin
PmeI
FseI
pBi16-PaPi
(8.3 kb)
FRT
HygB
AmpR
+
pOG44
T-Rex293
+ HygB

Figure 3-1: Dual expression vector pBi16-PaPi

The human Parkin and PINK1 cDNA were cloned into pBi16 [1] and stably integrated using FRT site-directed recombination in the T-Rex 293 cells by hygromycin B (HygB) selection (Invitrogen). pCMV*: doxycycline-inducible CMV promoter; pOG44: Flp site-specific recombinase expression vector (Invitrogen).

3.3.3 Detection of Ubiquitinated APE1 in A549

Histidine hexamer-tagged ubiquitin (6xHis-ub) cDNA was transfected with APE1, Parkin, and PINK1 in A549 cells and incubated for 24 hours. The cells were lysed in the binding buffer (20 mM Tris pH 8.0, 0.5 M NaCl, 0.1 % NP-40, 10 mM imidazole) with 40 μM MG132 (Sigma) and proteinase inhibitor cocktail without EDTA (Roche). The crude cell extracts (total fraction) were incubated with Ni-NTA magnetic beads (Qiagen) for 15 minutes at 4℃, washed with the binding buffer, and eluted with binding buffer with 120 mM imidazole. The total and eluted (His-tagged protein-enriched) fractions were analyzed by immunoblot using anti-APE1 antibody.

3.3.4 Analysis of Localization of YFP-Parkin and APE1

MEF^{la} cells were spread on coverslips a day before DNA transfection. The cDNA carrying YFP-Parkin and APE1 were co-transfected in the same way as described above, and incubated for 24 hours. If necessary, MG132 was added and incubated. Cells were incubated in the presence of Mitotracker Red (Invitrogen), fixed in 3.7% formaldehyde, and then permeabilized in PBS containing 0.2% TritonX-100 for 15 minutes. After washing with PBS twice, cells were blotted with anti-APE1 antibody, stained with anti-mouse IgG antibody conjugated to Alexa Fluor 488 (Invitrogen) followed by DAPI staining, and mounted on glass plates with Vector Lab mounting reagent. Cells were then analyzed with Leica TSP SP5 Confocal Microscope confocal microscopy at the Imaging Core facility of University of Kentucky.

3.3.5 Co-Immunoprecipitation (CO-IP) of Recombinant APE1-FLAG and Parkin

E. coli BLR (DE3) strain (EMD Biosciences) was transformed with a pRSF-Duet1 derivative (EMD) carrying Parkin and either of APE1-FLAG or APE1 (negative control) cDNAs. The cells were grown until OD600 reached 0.6 to 0.8, and then expressions of the proteins were induced with 0.5 mM IPTG (Fisher) at 16˚C for 16 hours (220,250). Cells were lysed in a co-IP buffer (120 mM NaCl, 2mM EDTA, 0.1mM EGTA, 0.05% NP40, 1 mM DTT, 50mM HEPES pH 7.9) supplemented with proteinase inhibitor cocktail (Complete Ultra Mini, Roche). After centrifugation for 20 minutes at 4˚C, small portions of supernatants were kept separately as total fractions (inputs), and the remaining samples were subjected to immunoprecipitation with agarose resin conjugated to the anti-FLAG antibody M2 (Sigma). The resin was washed in the co-IP buffer, and eluted in 100 µg/mL FLAG peptide (Sigma), and both total and IP fractions were analyzed by immunoblotting using anti-APE1 and anti-Parkin antibodies.

3.3.6 Proximity Ligation Assay (PLA)

A549 cells were spread on coverslips and incubated for overnight before transfection of the APE1 and Parkin cDNA. The cells were then incubated with 1 µM Mitotracker RED for 1 hour and fixed in 100% methanol at -20˚C and then in 100% ice-cold acetone.

The samples were processed according to the OLINK Bioscience DuoLink In Situ protocol. Briefly, the coverslips were rehydrated in PBS (pH7.5) containing 0.1% Triton X-100 (v/v) for at least 30 minutes at room temperature. The samples were then blocked with 5% BSA in PBS+ Triton X-100 for 30 minutes. The primary antibodies were applied (1:200 ms-anti-parkin, 1:250 rb-anti-APE1) and incubated overnight at 4°C in a humidity chamber; all other incubations were carried out in a 37°C humidity chamber unless otherwise noted. The samples were washed and incubated with the Duolink secondary antibodies (anti-mouse and anti-rabbit IgG) for 1 hour. After washing, the samples were incubated with the ligation reaction mixture for 30 minutes, washed, and then further incubated with the green amplification reagent for 90 minutes. After the final wash, the samples were mounted with Duolink In Situ mounting medium containing DAPI. The fluorescent signals in the cells were analyzed using an Olympus inverted fluorescence microscope.

3.3.7 Tissue Extract Preparation

Snap-frozen GBM specimens were obtained from male patients (50-75 years old) in accordance with IRB regulations. Whole cell lysates of the tissues were prepared using the Fisher Cryo-homogenizing system. Briefly, the samples were disaggregated through grinding with a clean pre-chilled mortar and pestle. The samples were then transferred to a micro-centrifuge tube and RIPA buffer, containing 40 µM MG132 and protease inhibitors, was added to an approximate concentration of 10 mg/µL pre-ground weight. The samples were then centrifuged to collect large debris, and the supernatant was used to prepare a stock in SDS-PAGE loading buffer and to determine final protein concentration. The SDS-PAGE stock was sonicated and incubated at 70° C for 5 minutes and stored at -80° C until use. Before SDS-PAGE, the samples were diluted to a final concentration of 3 µg/µL in SDS-PAGE loading buffer.

3.3.8 Immunohistochemistry for GBM and Control Tissues

A combined total of 17 GBMs and control brain tissues were obtained from the Markey Cancer Center Biospecimen and Tissue Procurement Shared Resource Facility (BSTP SRF). Formaldehyde-fixed paraffin embedded 5 µm sections were deparaffinized in xylene and rehydrated stepwise using graded ethanol and finally water. Dako antigen retrieval buffer was used with a Biocare Medical decloaking chamber for antigen retrieval following the manufacturer's protocol. Dako peroxidase blocking reagent was used to inhibit endogenous peroxidase activity. Sections were incubated with primary antibody for 1 hour at room temperature: APE1, Parkin. Next, sections were incubated with polymer linked secondary antibody, either mouse (Dako K4007) or rabbit (Dako K4003) for 30 min at room temperature followed by development with diaminobenzodine. Following washing, slides were counterstained with Meyer's hematoxylin and allowed to Blue in ammonia water before dehydration in graded ethanol. Slides were incubated in xylene before affixing coverslip.

High-resolution digital image slides of GBM and control brain tissue were obtained by scanning with the Aperio ScanScope (Leica) at 20x magnification. Aperio ImageScope software V 11.2.0.780 and the software's algorithms for Positive Pixel Count V9 and Nuclear V9 were used to analyze these images for % total intensities for APE1 and Parkin in tissue and nuclear localization respectively.

3.3.9 Chemicals and Other Reagents

CCCP and MG132 were purchased from Sigma. Antibodies used in this study are those for APE1 (Santa Cruz, sc-55498), PINK1 (Novus BC100-494 and Protein Tech 23274-1-AP), Parkin (Santa Cruz, sc-32282), β-tubulin (Santa Cruz, sc58884), GAPDH (Invitrogen, AM4300), p53 (Santa Cruz, sc-126). Pre-stained protein molecular weight marker was purchased from New England Biolab (P7709).

3.4 Results

3.4.1 Direct Involvement of Parkin in APE1 ubiquitination

To test whether APE1 is ubiquitinated by Parkin, protein extracts from A549 expressing histidine hexamer-tagged ubiquitin (His-Ub), APE1, Parkin and PINK1 were subjected to enrichment of His-Ub through nickel resin purification (251). Monoubiquitinated as well as polyubiquitinated APE1 were detected in the His-Ub enriched fraction when Parkin was expressed (**Figure 3-2 A lane 2 vs. lane 1**). The results indicated Parkin was capable of ubiquitinating APE1. The His-Ub diminished when PINK1 was co-expressed while intact APE1 decreased **(lane 3 v.s. lane 4**), suggesting that PINK1 was required for polyubiquitination and degradation of APE1.

To understand functional requirements of Parkin and PINK1 for APE1 ubiquitination, a mouse embryonic fibroblast cell line MEF^{la} (MEF^{lowAPE1}) was transiently transfected with Parkin, PINK1, and APE1. APE1 levels were not altered when either Parkin or PINK1 was expressed alone (**Figure 3-2 B lanes 3 and 4 v.s. lane 2)** (122)**.** However, expressing both Parkin and PINK1

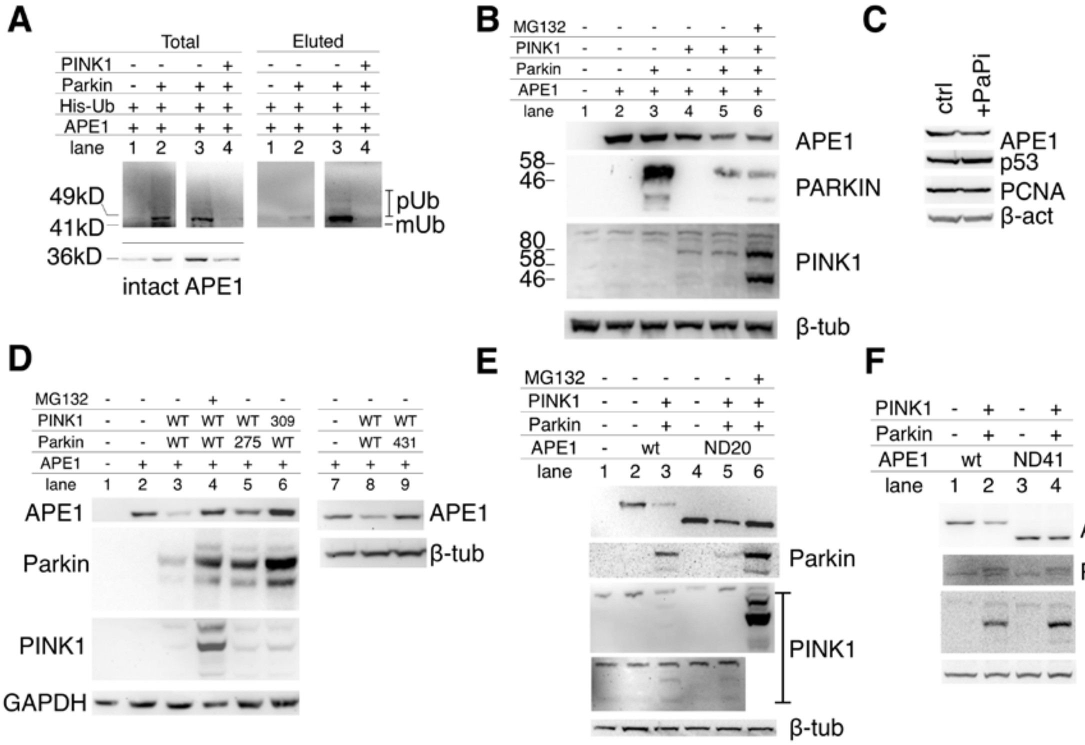
A
Total
Eluted
PINK1 - - - + - - - +
Parkin - + + + - + + +
His-Ub + + + + + + + +
APE1 + + + + + + + +
lane 1 2 3 4 1 2 3 4
49kD
41kD
36kD
pUb
mUb
intact APE1
B
MG132 - - - - - +
PINK1 - - - + + +
Parkin - - + - + +
APE1 - + + + + +
lane 1 2 3 4 5 6
APE1
58
46
PARKIN
80
58
46
PINK1
β-tub
C
ctrl
+PaPi
APE1
p53
PCNA
β-act
D
MG132 - - - + - - - - -
PINK1 - - WT WT WT 309 - WT WT
Parkin - - WT WT 275 WT - WT 431
APE1 - + + + + + + + +
lane 1 2 3 4 5 6 7 8 9
APE1
Parkin
PINK1
GAPDH
APE1
β-tub
E
MG132 - - - - - +
PINK1 - - + - + +
Parkin - - + - + +
APE1 - wt ND20
lane 1 2 3 4 5 6
Parkin
PINK1
β-tub
F
PINK1 - + - +
Parkin - + - +
APE1 wt ND41
lane 1 2 3 4
APE1
PINK1
Parkin
β-tub

Figure 3-2: Functional requirements for APE1 ubiquitination

(**A**) Detection of monoubiquitinated and polyubiquitinated APE1. A549 was transfected with APE1 (lane 1), APE1 and Parkin (lane 2), His-tagged Ubiquitin (His-Ub), APE1, and Parkin (lane 3), His-Ub, APE1, Parkin, and PINK1 (lane 4). Total protein lysates and eluted fractions (enriched with His-Ub) were analyzed with APE1 antibody as described in Materials and Methods. (**B**) MEF^{la} transfected with 1: empty vector, 2: APE1, 3: APE1 and PARKIN, 4: APE1 and PINK1, 5: APE1, PINK1, and PARKIN, 6: APE1, PINK1, PARKIN with 10 μM MG132 for 6 hours. (**C**) MEF^{la} transfected with APE1, PCNA, p53 without (ctrl) or with Parkin and PINK1 (PaPi) and the stabilities of APE1, PCNA, p53 were monitored after 24 hours. (**D**) Mutant Parkin (275 = R275W, 431 = C431F) and PINK1 (309 = G309D) were co-transfected in MEF^{la} as shown in the table. Protein levels were examined after 24 hours incubation. MG132 was at 3 μM for 16 hours. (**E**) The WT (full-length) or ND20 (N-terminal 20 a.a. truncation) APE1 was co-transfected with Parkin and PINK1 in MEF^{la}. Lane 6: MG132 was added at 3 μM for overnight incubation. Expression of PINK1 in lanes 3 and 5 was confirmed separately from lane 6 which otherwise caused a halo effect. (**F**) ND41 (41 a.a. N-terminal truncation) APE1 was examined after Parkin and PINK1 expression.

caused a marked APE1 decrease (**Figure 3-2 B** lane 5; also in **Figure 3-2 D** lane 3, **Figure 3-2 E lane 3E, and Figure 3-2 F lane 2).** p53 is a well-known target of ubiquitination by other E3 ubiquitin ligases (252-254). We tested whether p53 was also efficiently ubiquitinated by Parkin. However, the stability of p53 was unaffected by Parkin and PINK1 (**Figure 3-2 C**). Similarly, proliferating cell nuclear antigen (PCNA), highly susceptible to mono- and poly-ubiquitination (254), was not modified by Parkin (**Figure 3-2 C**). The unaltered stabilities of p53 and PCNA as well as β-tubulin and β-actin indicated a high specificity of the reaction of Parkin on APE1. Incubating cells with a 26S proteasome inhibitor MG132 restored the APE1 level (**Figure 3-2 D**, lane 4 v.s. lane 3).

The Parkin polypeptide contains two RING domains (**Figure 3-3**). R275W and C431F missense mutations, which are located in the first and second RING domains in Parkin respectively (**Figure 3-3**), abrogate its E3 ligase activity and cause early onset Parkinson’s disease (255,256). These Parkin mutants failed to degrade APE1 (**Figure 3-2 D lanes 5 and 9; Table 3-1).** PINK1 carrying G309D missense mutation is defective in its kinase activity (**Figure 3-3**), and incapable of activating Parkin (247,255,257). The G309D PINK1 did not activate APE1 degradation (**Figure 3-2 D** lane 6; **Table 3-1**). These results suggested that the ligase activity of Parkin was required for APE1 degradation, for which the kinase activity of PINK1 was also critical.

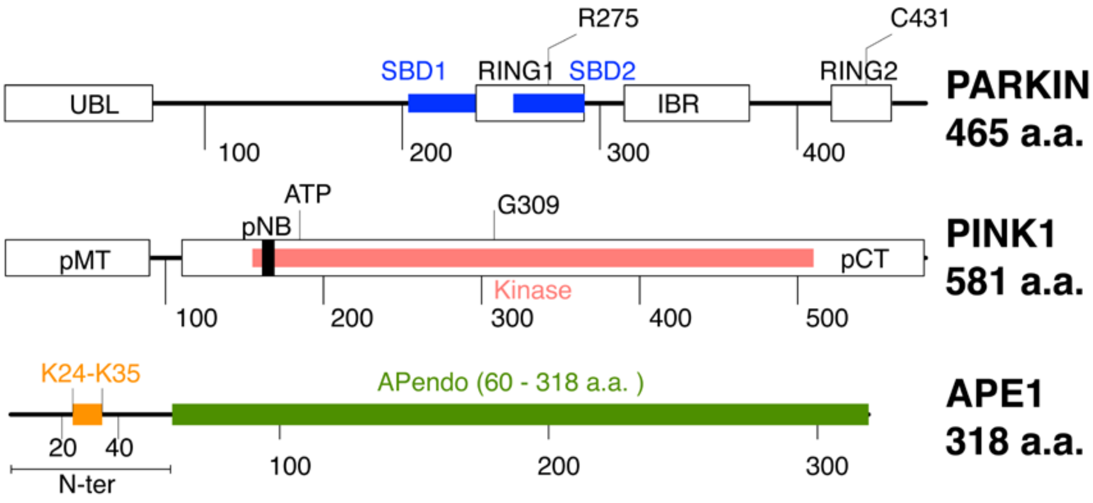
R275
C431
SBD1
RING1
SBD2
RING2
UBL
IBR
PARKIN 465 a.a.
100
200
300
400
ATP
G309
pNB
pMT
pCT
Kinase
PINK1 581 a.a.
100
200
300
400
500
K24-K35
APendo (60 - 318 a.a.)
APE1 318 a.a.
20
40
N-ter
100
200
300

Figure 3-3: Parkin, PINK1, and APE1 Functional Domains

3.4.2 Interaction of APE1 with Parkin

Sarraf et al. recently identified proteins interacting with Parkin and their possible ubiquitination sites, and APE1 was found to be a protein interacting with Parkin through its N-terminal segment, i.e., 20-30th amino acids from N-terminus (245). To probe the importance of the N-terminal region of APE1 for the stability, MEF^{la} cells were transiently transfected with N-terminally truncated APE1, ND20 and ND41 (N-terminal 20 and 41 amino acids deletions), along with Parkin and PINK1. While ND20 APE1 was efficiently degraded by Parkin (**Figure 3-2 E** and **Table 3-1**), ND41 APE1 was significantly more resistant to Parkin dependent degradation compared to those of the full-length and ND20 APE1 (**Figure 3-2 F** and **Table 3-1**). It is likely that APE1 is mainly ubiquitinated at the amino acid residues 20-41 which contains two Lys clusters (24K-25K-27K and 31K-32K-35K), which is consistent with the previous studies showing that the N-terminal residues contained major ubiquitin acceptor Lys residues catalyzed by MDM2 and UBR3 (221,224).

In the normal condition, APE1 in MEF^{la} was localized predominantly in the nuclei (**Figure 3-4 A**, control). When the cells were treated with MG132, cytoplasmic APE1 was visibly increased 3 hours after the treatment, and became indistinguishable from the nuclear APE1 after overnight incubation of the cells with MG132 (**Figure 3-4 A**). The major fraction of Parkin is present in the cytoplasm (240).

Table 3-1: Effect of Parkin and PINK1 on the stability of APE1

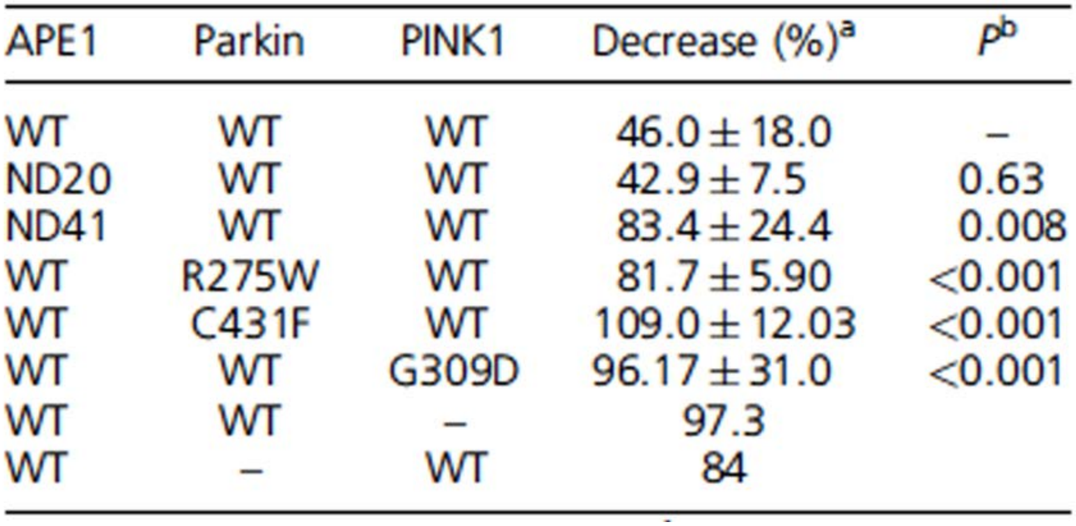

APE1	Parkin	PINK1	Decrease (%)[a]	*P*[b]
WT	WT	WT	46.0 ± 18.0	–
ND20	WT	WT	42.9 ± 7.5	0.63
ND41	WT	WT	83.4 ± 24.4	0.008
WT	R275W	WT	81.7 ± 5.90	<0.001
WT	C431F	WT	109.0 ± 12.03	<0.001
WT	WT	G309D	96.17 ± 31.0	<0.001
WT	WT	–	97.3	
WT	–	WT	84	

Relative APE1 intensities (%) in MEF^{la} with the wild-type or mutant Parkin and PINK1 expressions were calculated by comparing with those without Parkin nor PINK1. [a]APE1 amounts were normalized by β-tubulin, and compared with that without Parkin and PINK1. Values based on more than three independent experiments. [b]P values by Student's t-test. Each value (more than three experiments) calculated with the result of the first row (with wt-APE1, wt-Parkin, and wt-PINK1).

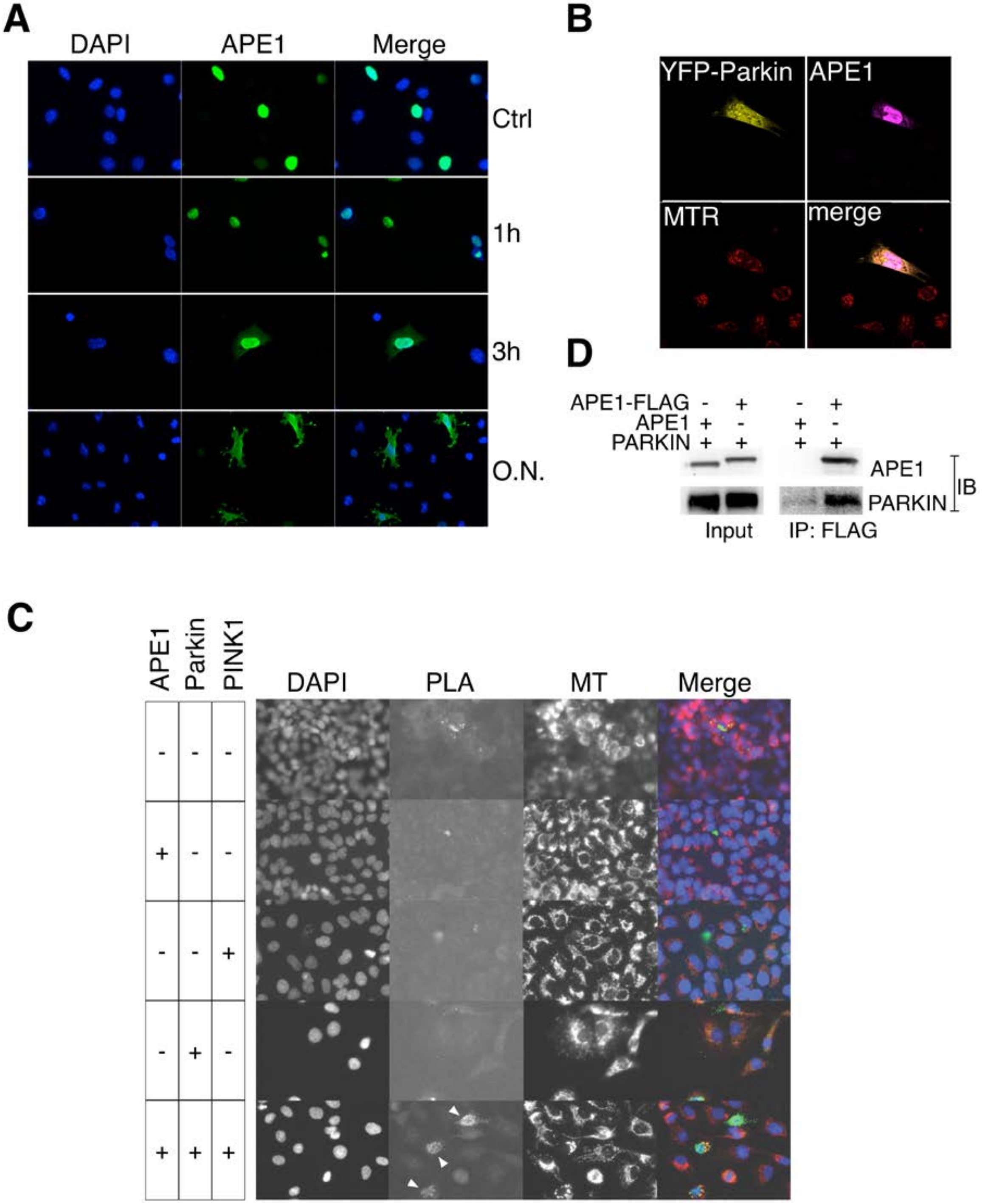
A
DAPI
APE1
Merge
Ctrl
1h
3h
O.N.
B
YFP-Parkin
APE1
MTR
merge
D
APE1-FLAG - + - +
APE1 + - + -
PARKIN + + + +
APE1
PARKIN
IB
Input
IP: FLAG
C
APE1
Parkin
PINK1
DAPI
PLA
MT
Merge
- - -
+ - -
- - +
- + -
+ + +

Figure 3-4: Interaction of APE1 with Parkin in the cytoplasm

(**A**) Accumulation of APE1 in the presence of MG132. MEF^{la} cells expressing the wild-type APE1 were incubated with MG132 for indicated time periods. MG132 concentrations were 40 μM (0 - 3 hours) and 3 μM (overnight). APE1 was labeled with anti-APE1 antibody and AlexaFluor 488 and analyzed in fluorescence microscopy. (**B**) MEF^{la} transfected with APE1 and YFP-Parkin were incubated with MG132 40 μM for 3 hours, fixed, labeled with anti-APE1 and AlexaFluor 633 (shown in purple), and then analyzed by confocal microscopy. Z-series pictures were taken for a detailed analysis (**Figure 3-5**). (**C**) Proximity ligation assay (PLA) between APE1 and Parkin in A549. A549 expressing APE1, Parkin, PINK1 as indicated. APE1 and Parkin specific antibodies were used to probe the interactions of the two proteins as described in Materials and Methods. Positive signals were seen only in the cells co-transfected with APE1, Parkin, and PINK1 (bottom panel shown with arrows). MT: fluorescent signals by MitoTracker Red (Invitrogen). (**D**) Co-immunoprecipitation of APE1 and Parkin. Parkin and APE1 (lane 1) or Parkin and APE1-FLAG (lane 2) co-expressed in *E. coli* BLR were subjected to immunoprecipitation using FLAG antibody, and the total and eluted fractions were analyzed in immunoblot using APE1 and Parkin antibodies.

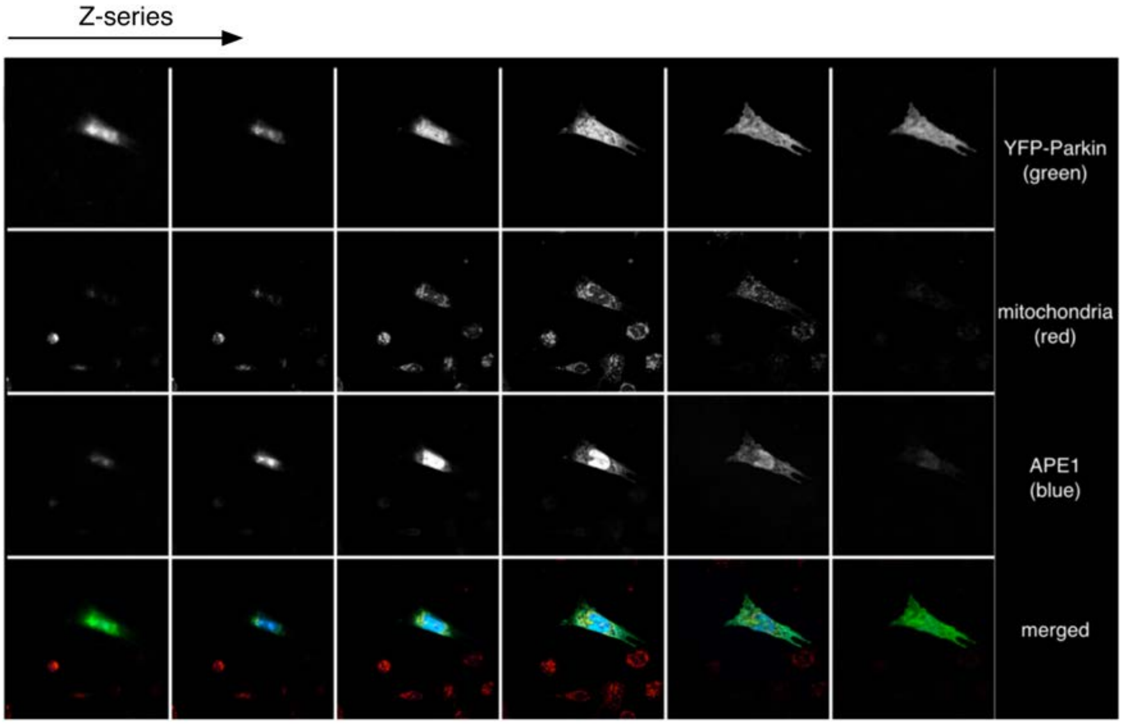
Z-series
YFP-Parkin (green)
mitochondria (red)
APE1 (blue)
merged

Figure 3-5: Colocalization of YFP-Parkin and APE1

MEF^{la} cells were transfected with YFP-Parkin and APE1, and incubated in 40 μM MG132 for 3 hours Cells were then stained with MitoTracker Red, anti-APE1 and anti-IgG-AlexaFluor 633, and then analyzed by confocal microscopy (Leica) to analyze co-localization of YFP-Parkin and APE1. Colors in Merged pictures: red: MitoTracker Red, green: YFP-Parkin, blue: APE1. Z-series photographs showing co-localization of YFP-Parkin and APE1.

The possibility of cytosolic co-localization of APE1 with Parkin was elucidated, using YFP-Parkin and APE1. After MG132 treatment, APE1 was found to be co-localized with YFP-Parkin in the cytoplasm (**Figure 3-4 B and Figure 3-1**). The cytoplasmic co-localization of APE1 and YFP-Parkin suggested that the physical interaction occurred in the cytoplasm. This possibility was examined with proximity ligation assay (PLA) (233). Antibodies specific to APE1 and Parkin were used to label the two proteins and signals were detected when the two proteins were in the proximate location to each other (**Figure 3-4 C**). The PLA signal was detected when APE1 and Parkin were co-expressed. Importantly, the PLA was observed mainly in the cytoplasm but not in the nuclei or inside of mitochondria. The absence of Parkin-APE1 interaction in the nuclei is consistent with the cytosolic localization of Parkin in previous studies (258-260). To test whether APE1 directly interacts with Parkin without involvement of other cellular factors such as ubiquitin or PINK1, recombinant Parkin was expressed with APE1 or with FLAG-APE1 simultaneously in *E. coli*, and performed FLAG-immunoprecipitation to detect Parkin in the FLAG-APE1 enriched fraction. Parkin was specifically detected in the FLAG-APE1 containing fraction (**Figure 3-4 D**). The result indicated that APE1 directly interacts with Parkin. Co-immunoprecipitation of Parkin by ND41 APE1-FLAG was significantly decreased **(Figure 3-6)** compared to that by full-length APE1, indicating that the N-terminal segment is pivotal for the interaction. However, it should be noted that Parkin signal was not completely disappeared in the ND41-FLAG IP fraction, and we

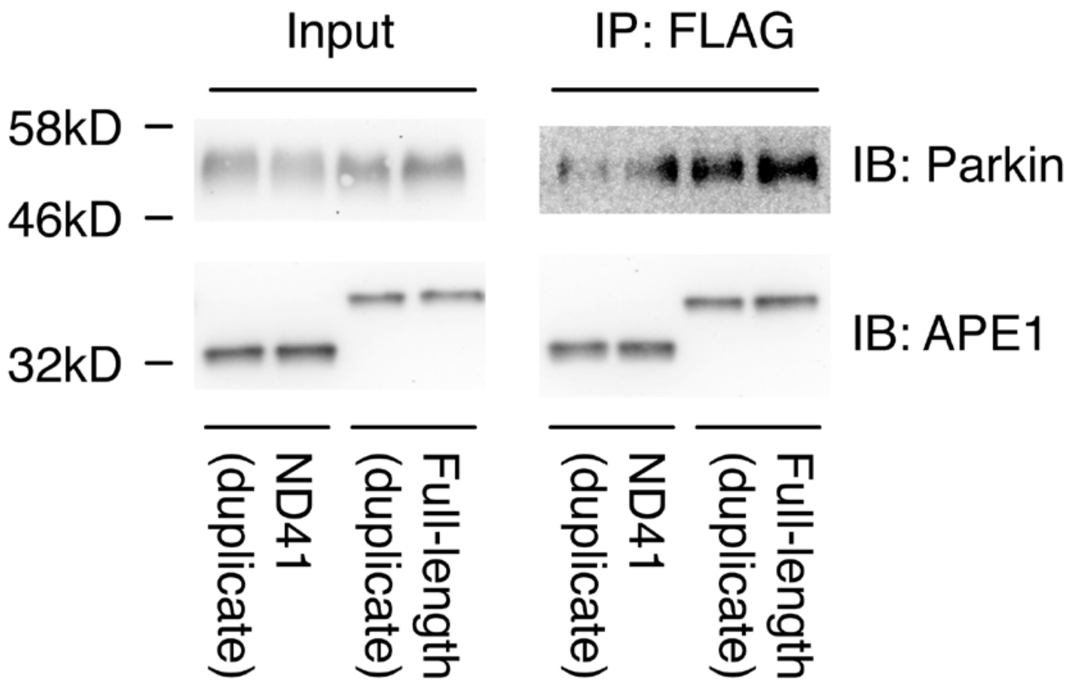
Input
IP: FLAG
58kD
46kD
32kD
IB: Parkin
IB: APE1
ND41 (duplicate)
Full-length (duplicate)
ND41 (duplicate)
Full-length (duplicate)

Figure 3-6: APE1 and Parkin Interaction

Interaction of full-length and ND41 APE1 with Parkin. Parkin and APE1-FLAG, or Parkin and ND41 APE1-FLAG, were co-expressed in *E. coli* BLR, and FLAG immunoprecipitation was carried out as described in the Materials and Methods. Ratios of [Parkin]/[APE1] in the IP fraction was determined using the signal intensities. Relative ratios for the full-length APE1 versus ND41 APE1 was 2.61±0.62 $p < 0.5$). Total 3 immunoprecipitation experiments were carried out to determine the mean and standard deviation.

could not exclude the possibility that the downstream APE1 polypeptide is also involved in the interaction of APE1 with Parkin.

3.4.3 Ubiquitination and Degradation of Endogenous APE1 by Parkin and PINK1

To examine the effect of Parkin expression on endogenous APE1, a lung adenocarcinoma cell line A549 was transiently co-transfected with Parkin and its cofactors (255,261-264), namely, Uba1 (E1 ligase), UbcH7 (Parkin-specific E2 ligase), and PINK1 (**Figure 3-7 A**). The level of endogenous APE1 decreased in a does-dependent manner (**Figure 3-7 B**). Densitometry of the immunoblot revealed that the level of the endogenous APE1 was down to 60% of the control cells transfected with the vector plasmid DNA alone.

Levels of the endogenous p53 and PCNA as well as housekeeping proteins β-tubulin and GAPDH were unaltered by the expression of Parkin and its cofactors (**Figure 3-7 B**). These results indicated a high specificity of the reaction of Parkin on APE1, consistent with the results with the ectopically expressed proteins (**Figure 3-7 C**). Total protein extracts from A549 were analyzed for ubiquitination of endogenous APE1. A specific band appeared at the position for monoubiquitinated APE1 after cells were transiently transfected with Parkin (**Figure 3-2 C**). Therefore, endogenous APE1 was ubiquitinated and degraded by Parkin.

Inducible expression of Parkin and PINK1 without transient transfection would provide a more refined experimental condition. To achieve this, a derivative of HEK 293 cell line 293-PaPi was used. The 293-PaPi is a stable transfectant of HEK293, and enables simultaneous induction of Parkin and

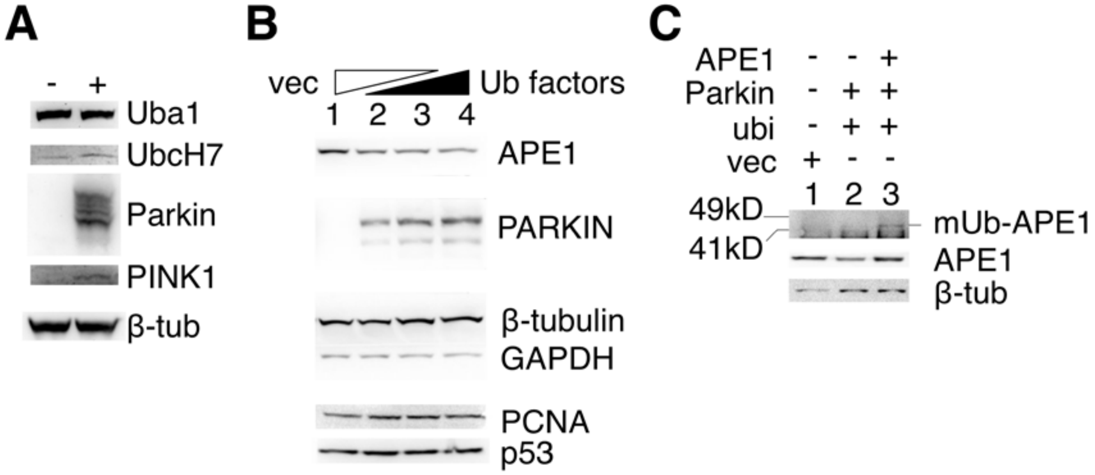
A
-
+
Uba1
UbcH7
Parkin
PINK1
β-tub
B
vec
Ub factors
1
2
3
4
APE1
PARKIN
β-tubulin
GAPDH
PCNA
p53
C
APE1
Parkin
ubi
vec
49kD
41kD
mUb-APE1
APE1
β-tub

Figure 3-7: Parkin targets APE1 for degradation

(**A**) Expression of Parkin and its cofactors, Uba1, UbcH7, Parkin and PINK1 in A549. A549 was transfected with (-) empty vector alone or (+) the vectors carrying Parkin, PINK1, Uba1, and UbcH7 cDNAs. β-tub: β-tubulin. Note that there was no change in the Uba1 probably due to its abundance. (**B**) A549 cells were transfected with cDNA expression vectors for ubiquitin, UBA1, UBCH7, Parkin, and PINK1. Amount of each DNA: 1: 0 µg, 2: 0.17 µg, 3: 0.35 µg, 4: 0.7 µg. Empty vector DNA (vec) was added to each to make the total amount of DNA equal among samples. Cells were then incubated for 16 h, and harvested for immunoblot examination. (**C**) A549 transfected with vector alone (1) or ubiquitin, Uba1, UbcH7, Parkin and PINK1 as in (B) and incubated with MG132 (3 µM for 16 hr), and APE1 (middle) and its ubiquitinated forms (top), as well as β-tubulin (bottom) were analyzed by immunoblot separately.

PINK1 by doxycycline from a bidirectional promoter (248) (**Figure 3-1**). Induction of Parkin and PINK1 (**Figure 3-8 A**) did not alter APE1 or β-tubulin while Mfn2 decreased clearly (**Figure 3-8 B**). Because Parkin's E3 ligase function is active at mitochondria, the 293-PaPi cells were treated with H_2O_2 to increase APE1 in mitochondria(265). Treatment of the cells with H_2O_2 decreased APE1 to approximately 70% of the control while the amount of β-tubulin was still unchanged (**Figure 3-8 B**). Although the change of APE1 level by H_2O_2 in the doxycycline-treated 293-PaPi was statistically significant, doxycycline or H_2O_2 alone did not show significant difference from the untreated control cells (**Figure 3-8 B**). These results indicated that degradation of APE1 by Parkin was limited compared to the transiently expressed APE1, suggesting that a large portion of APE1 is not in contact with the Parkin and PINK1 without induction of stresses such as oxidative stress.

3.4.4 Loss of Parkin is associated with elevated APE1 levels in GBM

Parkin deficiency has been associated with GBM (241,242). To elucidate the correlation between Parkin and APE1 in brain tumors, expression levels of Parkin and APE1 in both GBM and non-neoplastic brain tissues were examined. Qualities of the monoclonal antibodies for Parkin and APE1 were confirmed in Western blot to detect the corresponding proteins specifically (**Figure 3-9 A**). Interestingly, the GBM tissues showed increased APE1 levels while decreasing the Parkin levels (**Figure 3-9 A**). Parkin and APE1 levels were examined in detail by immunohistochemistry (**Figure 3-9 B**). Parkin levels in the non-neoplastic brain tissues were higher than those of GBM tissues (**Figure 3-9 C**, $p = 0.0009$),

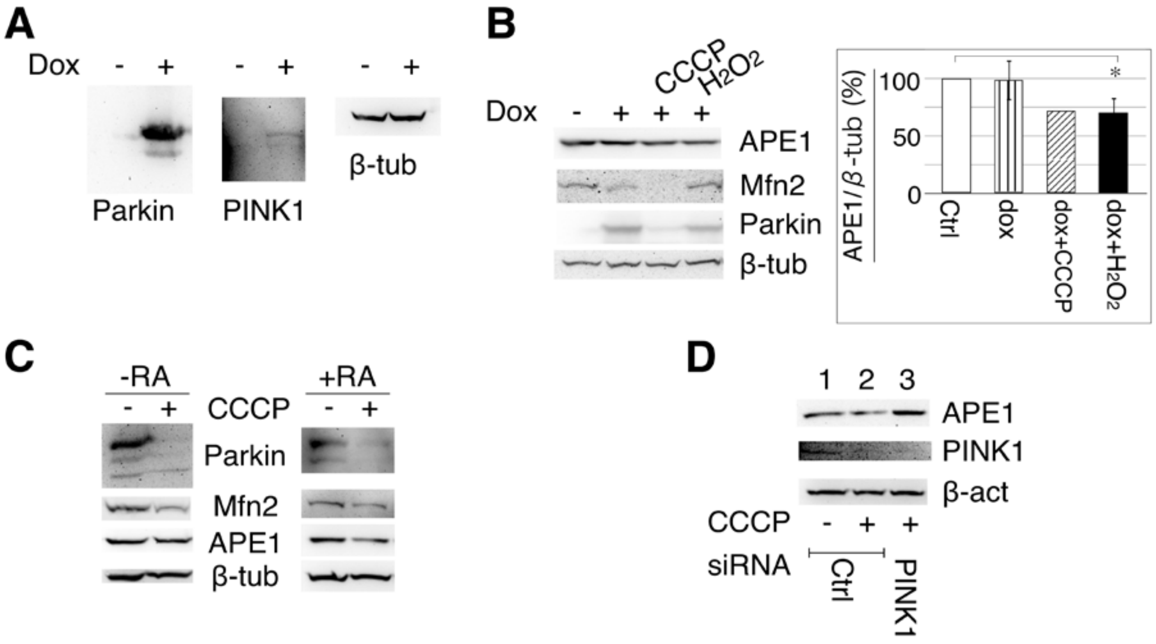

Figure 3-8: Effect of Parkin and PINK1 co-expression on APE1

(A) Parkin and PINK1 expressions examined in 293-PaPi cell lysates after 16 hours of treatment without (lane 1) or with (lane 2) doxycycline (2 μg/mL). (**B**) (Top) Immunoblot for APE1, Parkin, Mfn2, and β-tubulin levels in 293-PaPi cells treated with doxycycline for 16 hours. CCCP: 10 μM; H_2O_2: 50 μM. (Bottom) Averages of APE1/β-tubulin ratios with the treatments as indicated. *$p < 0.05$. (**C**) SH-SY5Y cells were incubated with DMSO only (-) or with 10 μM CCCP (+), and incubated for 24 hours at 37˚C and analyzed by immunoblot. In the right panel, SH-SY5Y cells were differentiated by the 5-days treatment with 10 μM retinoic acid (RA), and then incubated with 10 μM CCCP for 24 hours. (**D**) Scrambled control (lanes 1 and 2) or PINK1 siRNA (lane 3) were electroporated in SH-SY5Y, and the level of APE1 was examined after 72 hours incubation with 24 hours treatment of DMSO (lanes 1 and 3) or 10 μM CCCP (lane 2).

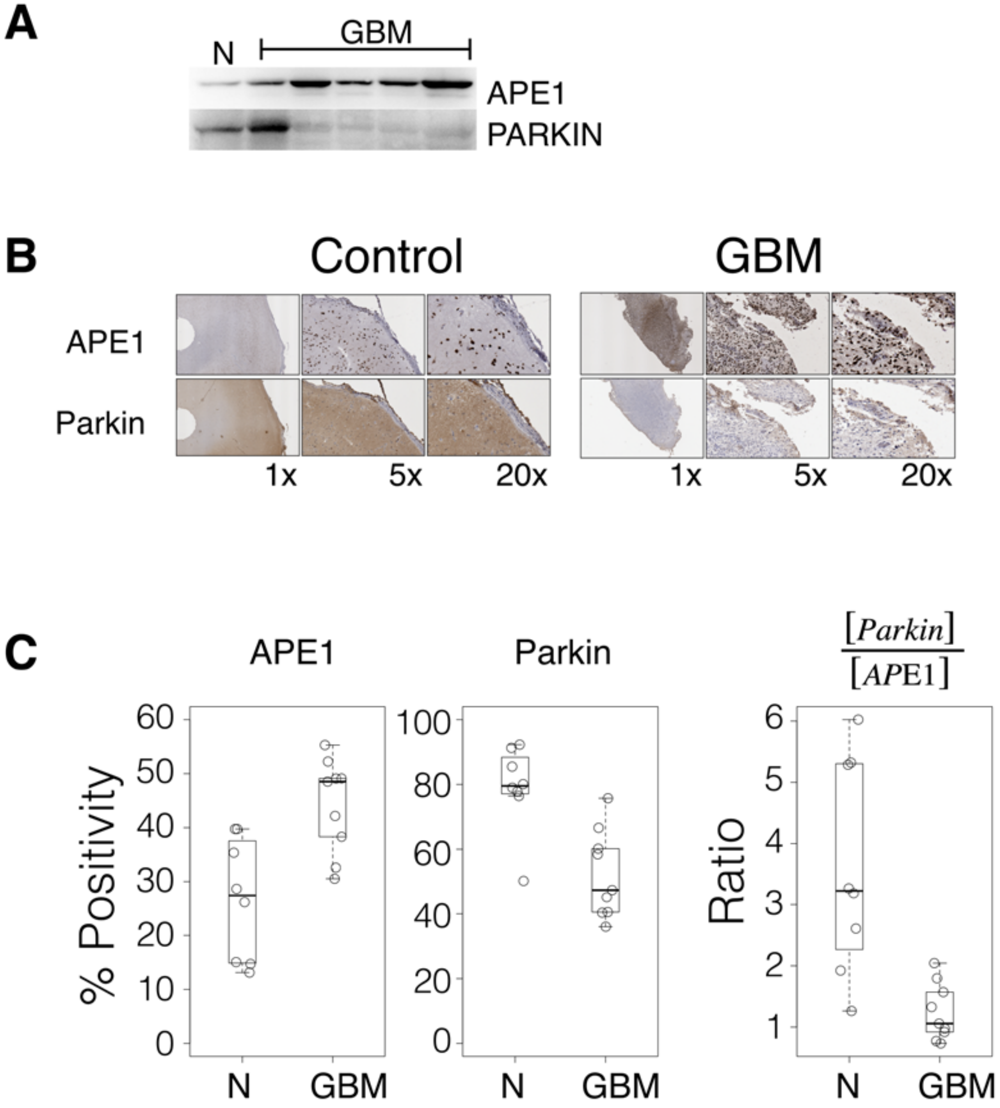

Figure 3-9: Parkin and APE1 expressions in GBM

(**A**) Five glioma and one non-neoplastic (from epilepsy surgery) brain tissues were processed for protein extraction and analyzed in immunoblot assays. (B) Representative results of immunohistochemistry from non-neoplastic (Control) and GBM tissues. Magnifications: 1x, 5x, and 20x. (**C**) Total levels of APE1 (**Left** panel) and Parkin (**Middle** panel) were measured and normalized by nuclear counts using Aperio analytical software (Leica), and are shown as box plots for the non-neoplastic (N) and GBM brain tissues. (**Right** panel) Parkin levels were divided by APE1 levels of the corresponding tissues, and the calculated ratios are plotted. Each box plot shows the median value (bold horizontal line), the first and third quartile (box), and 1.5x interquartile range (whiskers). Individual values are also shown as circles. The p values (Student's t-test) are 0.009, 0.0025, 0.0013 for the left, middle, and the right panel, respectively.

while APE1 signals were higher in GBM tissues than the non-neoplastic tissues ($p = 0.0025$). Parkin/APE1 ratios were calculated, and were significantly lower in the GBM tissues than in the non-neoplastic brain tissues (**Figure 3-9 C,** $p = 0.0013$). Notably, the variance of Parkin/APE1 ratios was significantly lower than that of either APE1 or Parkin levels, implying that the loss of Parkin and the gain of APE1 expression during the tumorigenesis are associated with each other.

3.5 Discussion

APE1 is primarily known for repair of oxidized and alkylated DNA damage, but also is an important gene expression regulator that activates transcription factors such as AP-1 and NFκB (119). Both APE1 functions are pro-proliferation and advantageous to cell survival, which explains elevated APE1 expression in tumor tissues. Indeed, tumor cells with high APE1 levels acquire drug and radiation resistance (165,210-213). Therefore, identifying factors that control APE1 levels should provide information relevant to the cancer therapeutics, particularly those causing cytotoxicity via DNA damage generation.

We speculated a possible role of Parkin for controlling intracellular levels of APE1, because (1) backup E3 ligase activity was detected in cells defective in MDM2 (220), (2) Parkin is induced by p53, and (3) a proteomics study detected APE1 as a possible substrate of Parkin (243-245). The present results show that Parkin is a quite efficient and highly specific E3 ligase to ubiquitinate APE1. The examination of mutant Parkin and PINK1 supports that the ubiquitination reaction is dependent on the E3 ligase activity of Parkin and the kinase activity of PINK1. Evidence for the direct interaction of APE1 with Parkin was obtained with co-immunoprecipitation of APE1 and Parkin and by proximity ligation assay. Based on these results, we conclude that Parkin directly ubiquitinates APE1. While monoubiquitinated APE1 was readily detected by MDM2 and UBR3 (221,224), detection of monoubiquitinated APE1 catalyzed by Parkin and PINK1 was relatively difficult. This observation implies that monoubiquitinated APE1 immediately undergoes polyubiquitination process by Parkin, and APE1 is efficiently degraded after the reaction by Parkin. Inhibiting the 26S proteasome by MG132 resulted in increase of monoubiquitinated APE1 in a manner dependent on Parkin and PINK1. Thus, Parkin with its cofactors Uba1, UbcH7, and PINK1 ubiquitinates directly, and degrades APE1 through 26S proteasome more efficiently than those processed by MDM2 and UBR3.

While ND20 APE1 (N-terminal 20 a.a. truncation) was degraded by Parkin as effectively as the full-length APE1, the stability of ND41 APE1 in the presence of Parkin and PINK1 was significantly increased. The results indicated that the N-terminal polypeptide between 20 to 40 amino residues in APE1 is important for the Parkin-dependent ubiquitination.

The N-terminal 60 amino acid segment in APE1 is not defined well functionally and structurally. This domain is unique in the mammalian AP endonuclease (266), and is dispensable for the AP-endonuclease activity (267), and thus it has been speculated that the N-terminal domain has an uncharacterized function unique to mammalian cells. In this context, it is interesting that the segment is rich in Lys, the major acceptor for acetylation and ubiquitination. The N-terminal segment between 20 and 41 amino acid residues contains six Lys residues, namely, 24K, 25K, 27K, 31K, 32K, and 35K. Acetylation of APE1 at these Lys residues was reported (39,215,219,268). These N-terminal Lys residues were also the main ubiquitin acceptors for MDM2 and UBR3 E3 ligases (221,224). Based on a recent quantitative proteomics study, the APE1 segment 18-RTEPEAKKSKTAA-30, containing Lys 24, 25 and 27, was identified to be a possible target of ubiquitination catalyzed by Parkin (245). Therefore, Lys residues in the N-terminus may be essential for the post-translational modifications that modulates APE1's gene regulatory function (39) and for altering its stability by polyubiquitination.

Although activating Parkin resulted in decrease of endogenous APE1 in three cell lines, SH-SY5Y, A549, and 293-PaPi, it should be noted that Parkin was active on endogenous APE1 only when stressful conditions (CCCP and H_2O_2) were invoked. We speculate that the modest effect of Parkin on endogenous APE1 is due to the fact that the majority of endogenous APE1 is compartmentalized in the nuclei, which may prevent Parkin from reacting on APE1. Stresses induced in the cells activated Parkin system (CCCP in SH-SY5Y) or facilitated mitochondrial localization of APE1 from nuclei (H_2O_2 in 293) (265). Although endogenous APE1 significantly decreased in A549 without any treatments, transient transfection is known to induce stress responses (269,270). Thus, APE1 ubiquitination by Parkin is unique in that the main site of the reaction is the cytoplasm, which is supported by the proximity ligation assay. In contrast, APE1 ubiquitination by MDM2 and UBR3 occurred mainly in the nuclei (220,224). It should be noted that APE1 was co-purified with mitochondria, but majority of this APE1 fraction was found to be on the surface of mitochondria (271), which is the major platform for the Parkin driven protein degradation. However, it is highly plausible in the event of mitophagy, APE1 in the mitochondria becomes the target of Parkin as well.

Although APE1 has been studied for its activities in the nuclei, there is an increasing interest in APE1‘s presence in the cytoplasm and its cancer-promoting effect (109,272,273). Kakolyris et al. found that APE1 was present in the cytoplasm of the normal human tissues (274). More recently, malignant cancer cells in the lung exhibited cytoplasmic APE1 at unusually high levels, and was linked to a poor prognosis of cancer treatment (109). Vascott et al. found that treatment of cells with an APE1 inhibitor E3330 caused cytoplasmic translocation of APE1 (275). Frossi also found that H_2O_2 induced translocation of APE1 into mitochondria (265). These studies suggest a cellular mechanism to export APE1 from nuclei. Based on these previous studies and present results, it is postulated that APE1 ubiquitination by Parkin is active in the cytoplasm, in which damaged APE1 proteins are ubiquitinated and degraded by Parkin to protect cells from undergoing malignant transformation. Meanwhile, undamaged, properly folded APE1 in the nucleus may be protected from this salvage system by the compartmentalization.

Originally identified as a gene of which deficiency is responsible for PD, Parkin was recently reported as a tumor suppressor gene of which loss of heterozygosity was frequently found in GBM (241). Analysis of Parkin and APE1 expressions in normal and GBM specimens revealed that Parkin/APE1 ratios (expression of Parkin relative to that of APE1) in the GBM tissues were uniformly low, while those in the non-neoplastic brain tissues showed much higher values and larger variance than those in GBM. This observation implies a correlation between the loss of Parkin and the high expression of APE1 in the brain tumor tissues. It is possible that a lack of Parkin activity either by loss of heterozygosity or by p53 mutation may lead to deficiency in regular APE1 degradation, and may accumulate in the cytoplasm as well as in the nuclei. However, the results do not determine whether Parkin deficiency is the direct cause of high APE1 activities in GBM, or vice versa. More recently, Hu et al. reported that melanoma specific inactivation of the Parkin gene (276). According to the study, melanoma specific Parkin alterations were observed at significantly high odds ratios over healthy control tissues. The alterations included copy number variations, splicing mutations, and putatively inactivating mutations including N273S, R275W, and P437L which are adjacent to the missense mutations that cause early onset Parkinson's disease (R275W and C431F). Further studies are necessary to investigate whether Parkin is crucial for the tight regulation of the intracellular level and subcellular distribution of APE1 to prevent cells from becoming malignant tumors.

3.6 Chapter 3 acknowledgements

This study was supported by NCI grant CA098664 (T.I.) and Cancer Center Supporting Grant (P30CA17758) by the Markey Cancer Center at the University of Kentucky. We thank Dr. E. Grabczyk for his providing the pBi16 vector and acknowledge D. Napier’s expertise on immunohistochemistry, which was crucial for this study. We would like to thank Ms. Chawsheen and Martinez-Traverso for their technical assistance.

Chapter 4: Summary and Future Directions

4.1 Summary

Genetic alterations have long been linked to tumorigenesis. In the first study, we discuss the discovery of potential biomarkers for head and neck cancer, and a potential mechanism for how APE1 mediates inhibition of antioxidants and tumor suppressors. In the second study, we discuss using TCGA transcriptome database to identify genetic alterations between matched normal and tumor tissues. In addition, we discuss the discovery of a dominant physical effect that leads to synchronization of genes at the same chromosomal location. In the third study, we identified that Parkin and PINK1 are necessary for ubiquitination and degradation of APE1. The loss of Parkin was associated with aberrant APE1 in glioblastoma multiforme.

4.1.1 Chapter 1 summary

The study in **chapter 1** identified multiple, potential biomarkers for use in HNSCC. Most importantly, we identified potential biomarkers in the early stages of cancer that were associated with lymph node invasion, poorly differentiated tumors, and decreased survival **(Figure 1-7, 1-9, 1-10).** This is important because identifying patients with poor prognosis in the early stages of cancer allows the best opportunity to prevent progression to invasive cancer. Biomarkers that predict patient survival, and aggressive phenotypes may lead to improved patient survival. By alerting physicians to patients at high-risk for worsened prognosis, treatment strategies could be altered to improve patient survival. Additionally, identifying these factors provides insight into novel treatment targets. Researchers are already exploring the use of APE1 inhibitors to overcome the treatment resistance associated with APE1 overexpression (175).

We examined for differences in protein expression with regards to clinical factors such as survival rates, presence of lymph node invasion, tumor grade, and age at diagnosis. We identified reduced protein levels of antioxidant SOD3 in the benign tissues in smokers, and in individuals with p16 positive tumors **(Figure 1-9, 1-11, 1-12).** Both tobacco usage and HPV are associated with increased oxidative risk. Depletion of antioxidants likely led to increased oxidative stress and cellular damage, which supported tumor development. We also observed that individuals with increased SOD3 protein in benign tissue, typically developed cancer later in life **(Figure 1-13).** Therefore, treatments that upregulate SOD3 in individuals with depleted SOD3 may delay cancer development in high-risk patients such as tobacco users.

In **chapter 1**, we examined possible mechanisms for how APE1 overexpression contributes to tumor development and treatment resistance. Previously, APE1 gene expression has been linked to decreased gene expression of tumor suppression DCN in mouse embryonic fibroblasts (122). Because loss of DCN has been associated with increased metastasis and mortality, we examined if and how APE1 suppresses DCN expression in HNSCC (124-132). Focusing on APE1's redox dependent transcriptional regulator activities, we examined the relationship between APE1 and factors involved in antioxidant pathways including NRF2, PPARGC1A, SOD2, and SOD3. Importantly, we identified that APE1 protein levels are significantly elevated in CIS. Overexpression of APE1 has been linked to genomic instability (109,110). Therefore, overexpression of APE1 in CIS may lead to increased genomic instability, which allows CIS to progress to invasive cancer. Though speculative, therapeutics that regulate APE1 levels may prevent patients with early stage cancers from ever developing invasive cancer. We identified a negative correlation between NRF2 gene expression and expression of DCN, SOD2, and SOD3. In addition, we observed diminished SOD2 and SOD3 gene expression in cancerous tissues. Decreased expression of these important antioxidants may lead to increased oxidative stress within tissues and in turn drive further APE1 overexpression.

4.1.2 Chapter 2 summary

In **chapter 2**, we utilized TCGA transcriptome database to identify genes that were coordinated synergistically with genes of the COP9 signalosome. The COP9 signalosome is involved has been implicated in tumorigenesis. In particular, the deneddylase activity of CSN5 regulates key proteins associated with cell cycle control including tumor suppressor p53 (180). Despite the COP9 signalosome being studied, little is known about its role in normal tissues. Therefore, this study examined COP9 signalosome gene coordination in matched normal and tumor tissues to identify if gene coordination differs between normal and tumor tissues. Analysis in normal tissues identified significantly coordinated expression of COP9 genes to that of genes involved in mitochondria-related functional pathways. Because this coordination was lost in the matched HNSCC tissues, we speculated that COP9 signalosome function is required for coordinated mitochondrial activity.

The COP9 signalosome is also associated with regulating DNA repair pathways. Although unpublished, observations made by the Izumi lab support a functional link between APE1 and the COP9 signalosome as COP9 subunits were found to interact with APE1. Additionally USP15, a deubiquitinase that is associated with COP9, demonstrated a specific deubiquitinase activity on mono-ubiquitinated APE1. Recent studies found that COP9 can regulate nucleotide excision repair (277,278). These observations including ours indicate that the COP9 signalosome is an important cellular factor in the cellular stress response and oncogenesis. This study highlights the usefulness of the transcriptome data of the matched normal and tumor tissues accessible in TCGA, as the association of COP9 genes and mitochondrial gene expression would not have been identified using traditional cell culture systems.

Another unique knowledge we obtained in **chapter 2,** was the effects of chromosomal location on gene expression correlation in tumor tissues. In this study, highly synchronized to the COPS5 subunits were enriched in physical proximity to the COPS5 gene had the highest correlation relative to the COP9 genes. This dominant chromosomal cis-effect on gene expression coordination may be another mechanism by which gene expression becomes altered in cancer tissues. Use of this technique may identify gene expression linkages that promote tumor development and treatment resistance.

4.1.3 Chapter 3 summary

In **chapter 3**, we identified post-translational modification of APE1 by tumor suppressor Parkin. As in other cancers, APE1 overexpression is linked to treatment resistance and increased mortality of patients with glioblastoma multiforme (165,210,211). Parkin is a tumor suppressor and E3 ubiquitin ligase (234). Ubiquitination of APE1 is critical for APE1's function, and degradation (116). Therefore, we hypothesized that Parkin's E3 ubiquitin ligase function regulates APE1 protein levels. In this study, we identified interaction between APE1 and Parkin. We identified that Parkin along with PINK1, are needed for efficient APE1 degradation through post-translational modification. Using digital image analysis of immunohistochemistry slides; we identified an inverse relationship between Parkin and APE1 in glioblastoma multiforme (**Figure 3-9**). APE1 overexpression in glioblastoma multiforme is linked to treatment resistance and increased mortality (116). The loss of Parkin in glioblastoma multiforme likely prevents proper degradation of APE1, contributing to APE1 overexpression. Therapeutics increasing Parkin expression may restore normal ubiquitination and degradation of APE1, which would normalize APE1 expression. Normalization of APE1 expression may restore treatment sensitivity and increase patient survival.

4.2 Future directions

4.2.1 Explore if APE1 gene has a dominant physical effect on the transcription of nearby genes In HNSCC

In **chapter 2**, we identified a dominant cis-chromosomal effect of COP9 genes on transcription of nearby genes (153). Using TCGA transcriptome data from tumor tissues, we identified that COPS5 gene expression was highly correlated with genes in the same chromosomal region. This correlated gene expression is thought to be a result of a dominant physical effect of the physical gene location. Therefore, we hypothesize that there is a chromosomal cis-effect with genes located near APE1 and that this may upregulate expression of genes that contribute to cancer development, and treatment resistance.

To examine the presence of a chromosomal cis-effect of genes having the same chromosomal location of APE1, we employed techniques utilized in **chapter 2**. A preliminary examination was performed using TCGA transcriptome data from matched normal and HNSCC tumor samples. This analysis revealed highly correlated expressions of genes involved in DNA repair, and drug-resistance relative to APE1. This correlation was observed in HNSCC tissues, but not in non-neoplastic tissues **(Figure 4-1, Table 4-1).** Multiple genes involved in DNA repair were significantly correlated to APE1 in tumor tissues including poly ADP-ribose polymerase (PARP2), SPT homolog facilitates chromatin remodeling subunit (SUPT16H), methyltransferase like 3 (METTL3), and protein arginine methyltransferases (PRMT5) **(Table 4-1).** SUPT16H is involved in the chromatin reorganization needed to allow DNA repair proteins to access DNA damage sites (279). METTL3 and PRMT5 methyltransferases are involved in recruitment of DNA repair factors to DNA damage sites (280,281). Therefore, these genes may facilitate increased DNA repair capabilities and contribute to treatment resistance.

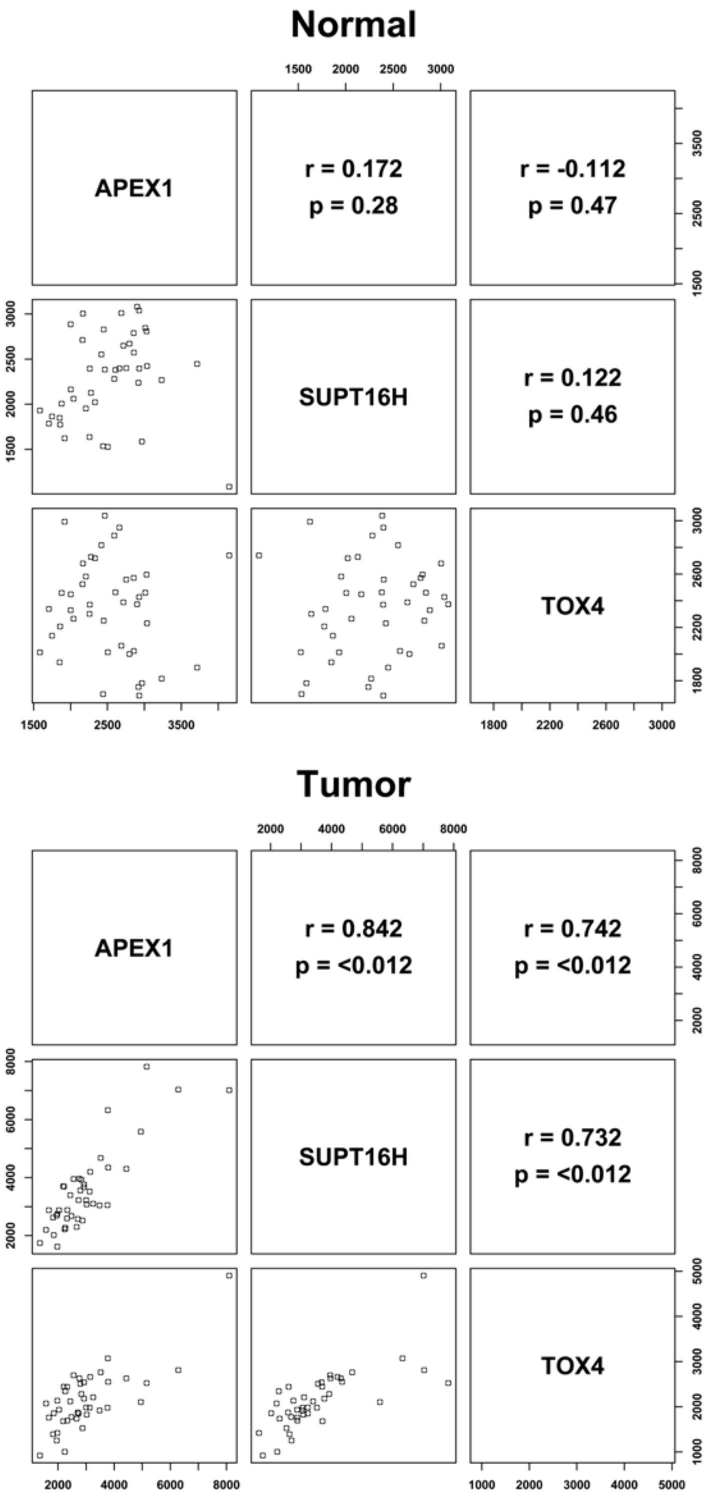

Figure 4-1: Synchronized gene expression of genes involved in DNA repair and cisplatin-resistance

Pairwise plots were generated for DNA repair proteins APEX1 and SUPT16H, as well as TOX4. The later of which is implicated in cisplatin-resistance. Genes are located near 14q11. Data was obtained from TCGA for matched non-neoplastic and HNSCC tumors (n=43).

Table 4-1: Synchronization of DNA repair and survival genes physically located near APE1 in HNSCC

		Correlation Coefficient Relative to APE1			
Gene	**Mbps**	**Non-neoplastic**	**Tumor**	**Role in Repair**	**Reference**
PARP2	-0.112	-0.266	0.802**	BER, DSBR	Scott et al. 2014 (20)
APEX1	0.000	1.000	1.000**	BER, Redox gene regulation	Seibold et al. 2015 (283)
SUPT16H	0.896	0.171	0.845**	HR	Oliveira et al. 2014 (279)
TOX4	1.021	-0.113	0.743**	Cisplatin-resistance	Bounaix Morand du Puch et al. 2011 (282)
METTL3	1.043	-0.008	0.512*	NER	Xiang et al. 2017 (280)
PRMT5	2.465	0.322	0.639**	HR	Clarke et al. 2017 (281)

Correlation coefficients were generated for genes involved in DNA repair and cell survival relative to APE1. Mbps: location in Chr 14 relative to APEX1. 42 matched non-neoplastic and tumor tissues. Role in Repair: BER: DNA base excision repair; DSBR: DNA double-strand break repair; HR: DSBR via homologous recombination; NER: DNA nucleotide excision repair. *p < 1E-3 in; **p < 1E-6. No genes in non-neoplastic tissues demonstrated statistically significant correlation.

If APE1 overexpression induces expression of genes involved in DNA repair, then cells may have enhanced DNA repair capabilities. This increased DNA repair may minimize the DNA damaging effects of chemoradiotherapy, which is necessary to kill tumor cells. In addition, we found that APE1 was significantly correlated to TOX high mobility group box family member 4 (TOX4), which has been implicated in cisplatin drug resistance (282). Cisplatin is commonly used in the treatment of head and neck cancers.

Overexpression of APE1 has been linked to cisplatin resistance, which contributes to poor patient outcome (284). The dominant chromosomal cis-effect observed between APE1 and TOX4 may be one way that APE1 is contributing towards treatment resistance **(Table 4-1)** (210). It is likely that tumors lose coordinated gene regulation and that the chromosomal location becomes a dominant factor in regulating gene expression. Newer research has established that genes are encapsulated locally in a chromosomal conformation named topologically associated domains (TADs) that consist of transcriptionally regulated units (285,286). Alterations of TAD structures were associated with tumorigenesis. Identifying TAD structures specific to HNSCC may identify tumors that are more sensitive to certain cancer treatments, which could improve patient survival.

4.2.2 Assessing if APE1 increases NRF2 activity to promote downregulation of DCN, and SOD3

In **chapter 1**, we originally hypothesized that APE1 suppressed DCN and SOD3 indirectly through NRF2. The proposed model in this study is largely based on correlative analysis of protein and gene expression data. This model could be more firmly supported by the addition of *in vitro* experiments including promoter assays and chromatin immunoprecipitation. Despite a positive correlation between APE1 and NRF2 protein expression, no correlation was observed between APE1 and NRF2 gene expression **(Table 1-2, Table 1-3).** However, APE1 is known to interact with NRF2 and increase NRF2's transcriptional regulatory activity (141). APE1 may still modulate expression of DCN and SOD3 by increasing NRF2 activity. In **chapter 3** we utilized the proximity ligation assay technique to detect interaction between APE1 and Parkin in cell lines (116). This same technique can be used in fixed tissues. To support our hypothesis that NRF2 interacts with APE1, the proximity ligation assay in HNSCC tissue samples can be used to identify interaction between APE1 and NRF2. Although APE1 and NRF2 physical interaction supports that APE1 binds to NRF2 and potentially increases NRF2 activity, more direct *in vitro* assays are needed to confirm this. Using head and neck cancer cell lines, I would perform immunoprecipitation to confirm APE1 and NRF2 binding. In addition, I would need to assess if transcription of known NRF2 downstream targets are decreased in cells with wildtype APE1 as compared to cells with loss of APE1.

We propose that NRF2 suppresses transcription of DCN, SOD2, and SOD3. This was supported by our results where we identified negative gene correlation between NRF2, DCN, and SOD3 (**Table 1-2**). As previously mentioned in the discussion section of **chapter 1**, there are NRF2 binding sites within the promoter region of DCN, and SOD3 **(Table 1-1).** Chromatin immunoprecipitation assay (ChIP) is a technique commonly used to assess binding of proteins to specific DNA regions. In addition, transcription of DCN, and SOD3 can be measured using luciferase promoter assay in cells with wildtype NRF2 and NRF2 knockdown. These assays combined can confirm whether NRF2 binds to DCN, and SOD3 promoter regions, and whether the presence of NRF2 is associated with decreased transcription of DCN, and SOD3.

Previous studies have supported that NRF2 suppresses SOD2 (121). We observed a negative correlation between NRF2 and SOD2 gene correlation in HNSCC (**Table 1-1**). However, it is not clear how NRF2 mediates SOD2 suppression. Unlike SOD3, transcription factor binding site analysis demonstrated no NRF2 binding site within the SOD2 promoter regions. PPARGC1A is a known transcriptional coactivator of NRF2 (287). If NRF2 is suppressing SOD2 gene transcription, it is possible that PPARGC1A is modulating this effect. However, studies have reported a positive regulatory role between PPARGC1A and SOD2 (152). If NRF2 is suppressing SOD2 gene expression, PPARGC1A may enhance this through acting as an NRF2 coactivator. To examine whether PPARGC1A enhances NRF2-mediated inhibition of SOD2, transcription of SOD2 should be assessed using luciferase promoter assay in cells with wildtype PPARGC1A and PPARGC1A knockdown.

Copyright © Christina Ann Wicker 2017

Appendix A: List of Supplemental Figures and Tables

Supplemental Figures

Supplemental Figure C-1: Ki-67 and Desmin as representative controls for nuclear and total cellular staining........173
Supplemental Figure C-2: APE1 survival analysis: low versus high protein expression........174
Supplemental Figure C-3: PPARGC1A survival analysis: low versus high protein expression........175
Supplemental Figure C-4: DCN survival analysis: low versus high protein expression176
Supplemental Figure C-5: SOD3 survival analysis: low versus high protein expression........177
Supplemental Figure C-6: NRF2 survival analysis: low versus high protein expression........178
Supplemental Figure C-7: Gene expression survival analysis for APEX1, PPARGC1A, DCN, SOD1, SOD2, and SOD3........179

Supplemental Tables

Supplemental Table D-1: The COPS5 correlation coefficient table list includes 1000 highest |*r*| values relative to the expression of COPS5 in the normal and tumor tissues of head and neck....180

Supplemental Table D-2: GO and KEGG pathways that are over-represented in the normal and tumor oral tissues based on the COPS5 correlation coefficient table. (XLSX 147 kb)....180

Supplemental Table D-3: GO and KEGG pathways over-represented by COPS5 expression correlation in the two major anatomical sites in the head and neck (oral cavity and tongue)....180

Supplemental Table D-4: GO and KEGG pathways over-represented in the normal and tumor lung tissues based on the COPS5 correlation coefficient table....180

Supplemental Table D-5: Genes under the chromosomal cis-effect in the HNSCC tissues....180

Supplemental Table D-6: KEGG pathway analysis for the TP53 genes....180

Appendix B: List of Abbreviations

Abbreviation	Meaning
APE1	Apurinic/apyrimidic endonuclease 1
BSTP SRF	Biospecimen and Tissue Procurement Shared Resource Facility
CDC	Centers for Disease Control and Prevention
CIS	Carcinoma in Situ
CRT	chemoradiotherapy
DAVID	Database for Annotation, Visualization and Integrated Discovery
DCN	decorin
DMEM	Dulbecco's Modified Eagle Medium
ES	enrichment score
FBS	fetal bovine serum
FDR	false discovery rate
FFPE	formalin fixed paraffin embedded
HE	Hematoxylin and Eosin
HNSCC	head and neck squamous cell carcinoma
HPV	Human Pappilomavirus
IHC	Immunohistochemistry
KCR	Kentucky Cancer Registry
KEGG	Kyoto Encyclopedia of Genes and Genomes
MDM2	mouse double minute 2 homolog
MMS	methyl methanesulfonate
NCI	National Cancer Institute
NEDD5	neural precursor cell expressed developementally down-regulated protein 5
NFE2L2/NRF2	Nuclear Factor, Erythroid 2-Like 2
NPCR	National Program of Cancer Registries
PARP1	poly(ADP-ribose) polymerase 1
PBS	phosphate buffer saline
PGC1-alpha/PPARGC1A	peroxisome proliferator-activated receptorgGamma
PINK1	PTEN-induced putative kinase 1
PLA	proximity ligation assay
PTEN	phosphatase and tensin homolog
ROS	reactive oxygen species
SAS	statistical analysis system
SEER	Surveillance, Epidemiology, and End Results Program
SOD2	superoxide dismutase 2
SOD3/ecSOD	Extracellular Superoxide Dismutase
SPSS	Statistical Package for the Social Science
TAD	Topologically associated domains
TCGA	The Cancer Genome Atlas

Appendix C: Supplemental Material for Chapter 1

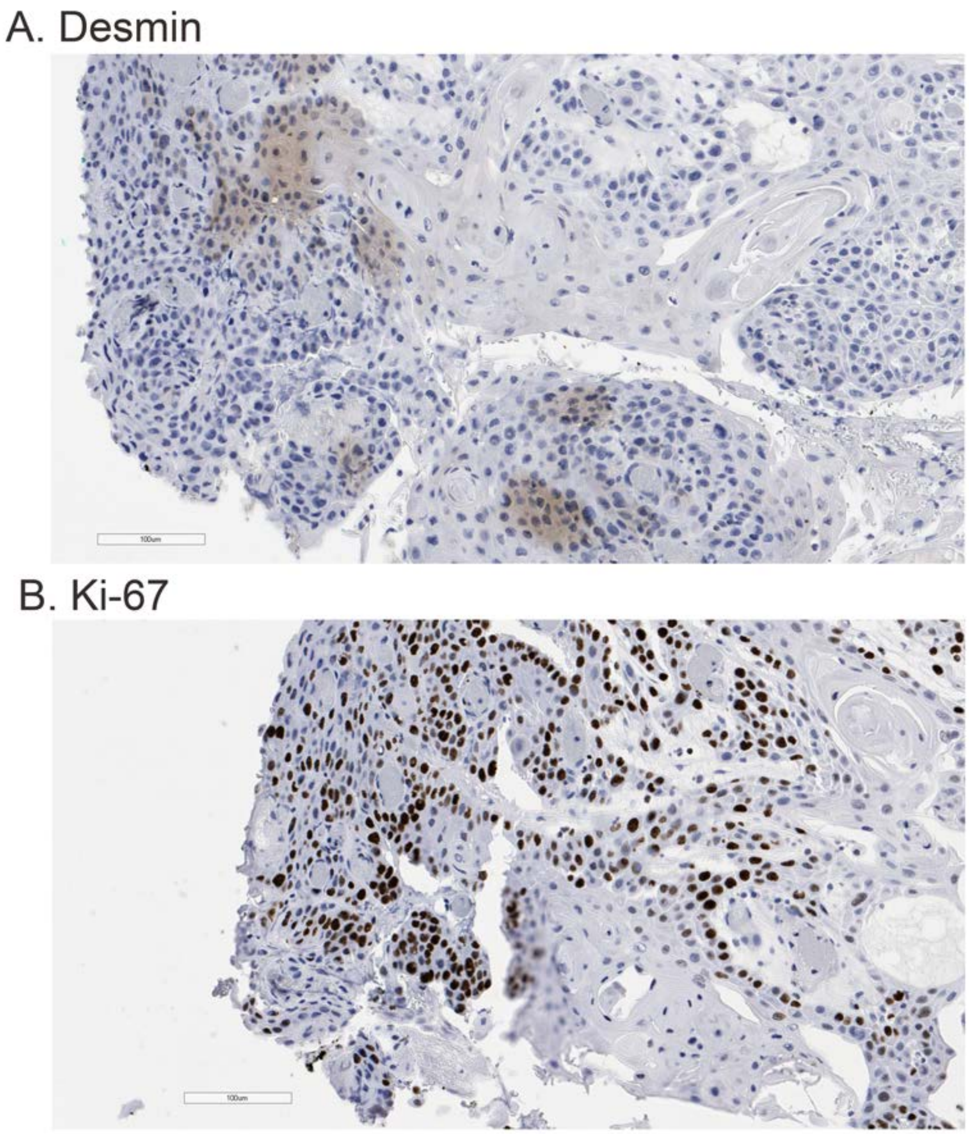

Supplemental Figure C-1: Ki-67 and Desmin as representative controls for nuclear and total cellular staining.

IHC for Ki-67 and Desmin were analyzed to determine the accuracy of Aperio's nuclear, and the positive pixel count algorithm used for total cellular protein.

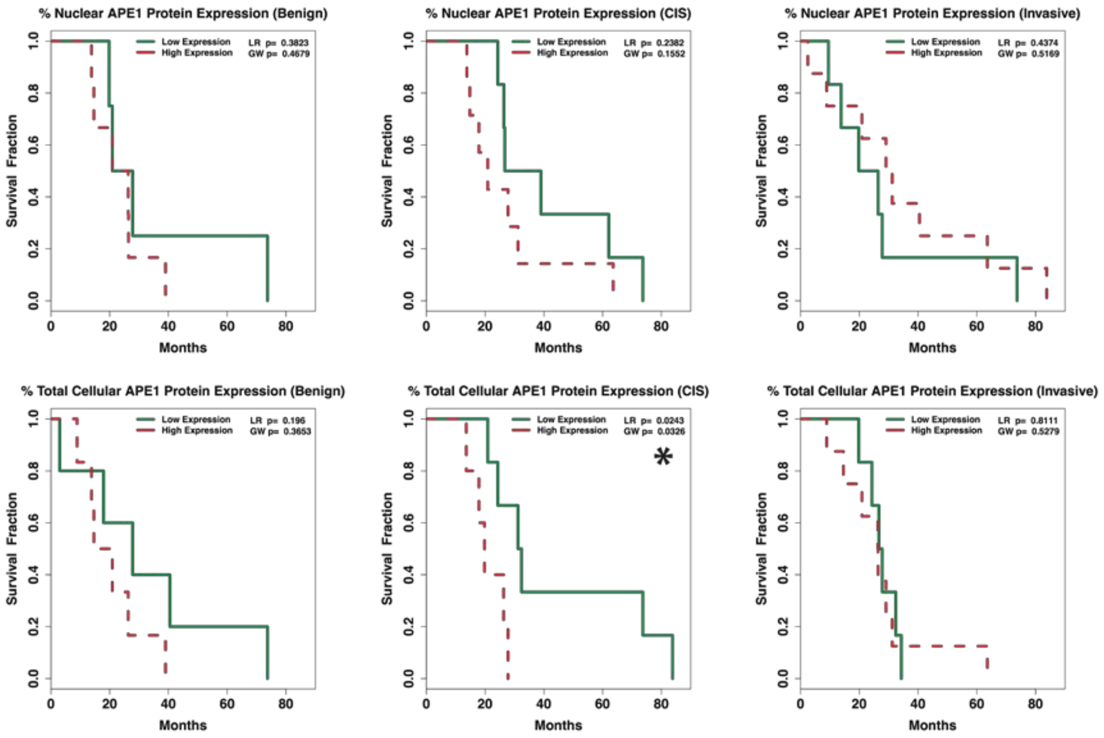

Supplemental Figure C-2: APE1 survival analysis: low versus high protein expression

Graphs represent the top significant Kaplan Meier survival curves comparing low vs. high protein expression. Top Row: % Nuclear APE1 protein expression in benign, CIS, and invasive tissue. Bottom Row: % Total Cellular APE1 protein expression in benign, CIS, and invasive tissue. * Denotes significance $p<0.05$ LR: Mantel-Haenszel Log-Rank, GW= Peto & Peto modification of the Gehan-Wilcoxon statistical tests.

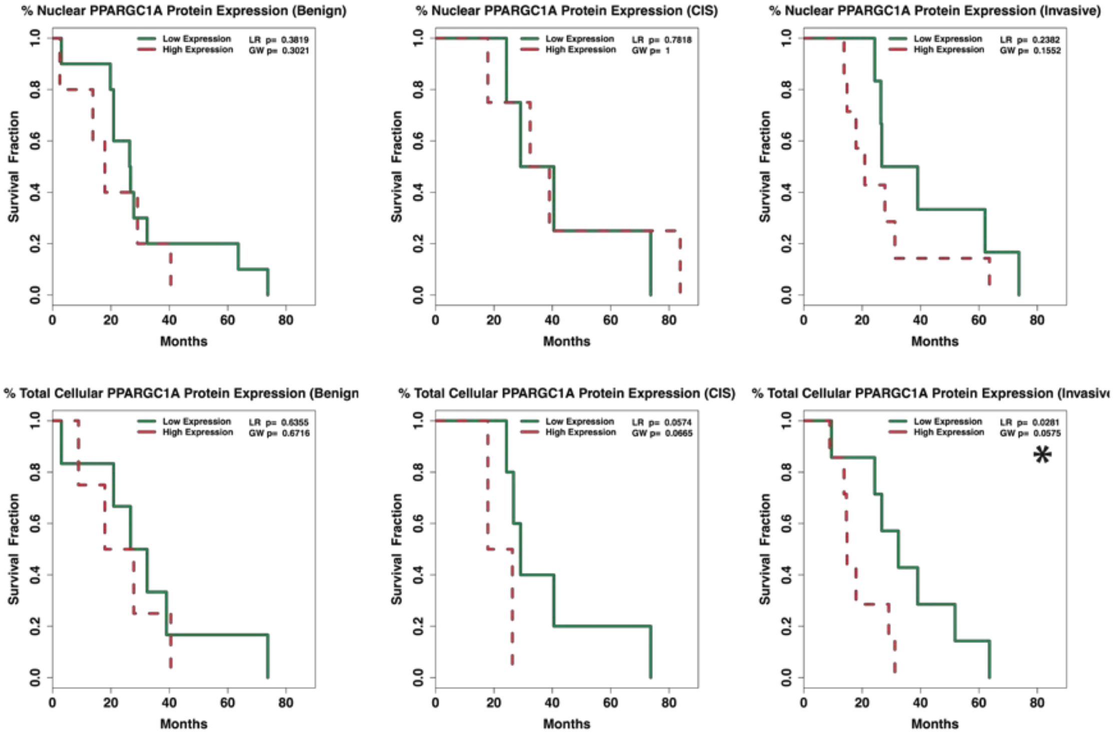

Supplemental Figure C-3: PPARGC1A survival analysis: low versus high protein expression

Graphs represent the top significant Kaplan Meier survival curves comparing low vs. high protein expression. Top Row: % Nuclear PPARGC1A protein expression in benign, CIS, and invasive tissue. Bottom Row: % Total Cellular PPARGC1A protein expression in benign, CIS, and invasive tissue. * Denotes significance p=0.057 LR: Mantel-Haenszel Log-Rank, GW= Peto & Peto modification of the Gehan-Wilcoxon statistical tests.

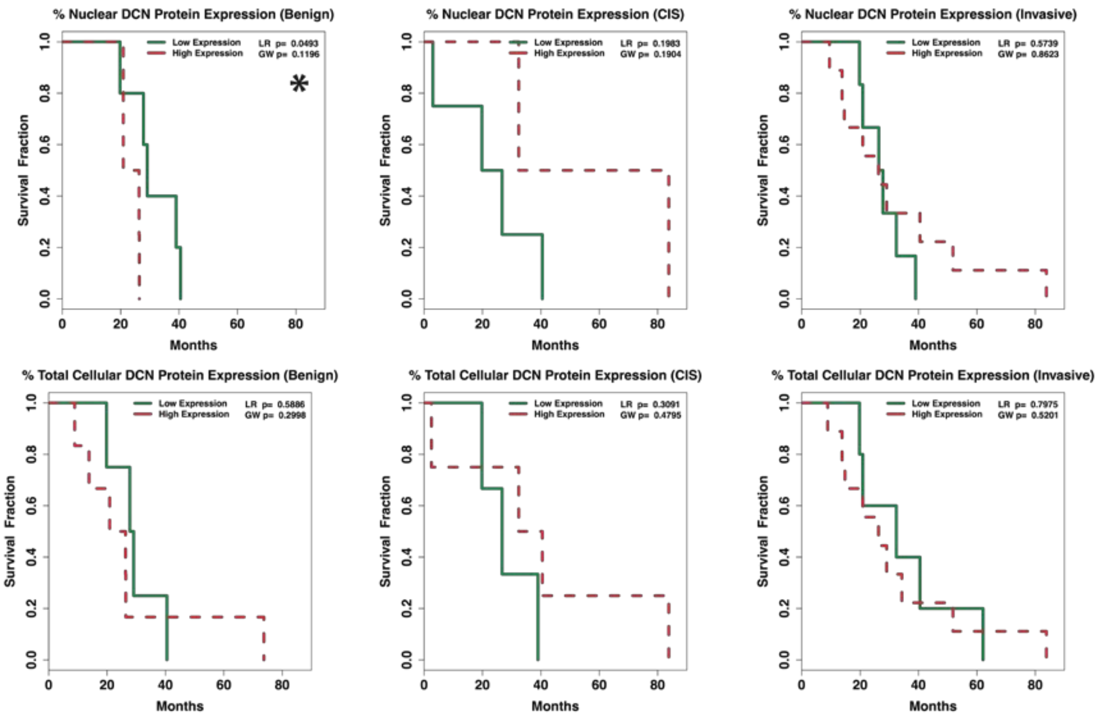

Supplemental Figure C-4: DCN survival analysis: low versus high protein expression

Graphs represent the top significant Kaplan Meier survival curves comparing low vs. high protein expression. Top Row: % Nuclear DCN protein expression in benign, CIS, and invasive tissue. Bottom Row: % Total Cellular DCN protein expression in benign, CIS, and invasive tissue. * Denotes significance $p<0.05$LR: Mantel-Haenszel Log-Rank, GW= Peto & Peto modification of the Gehan-Wilcoxon statistical tests.

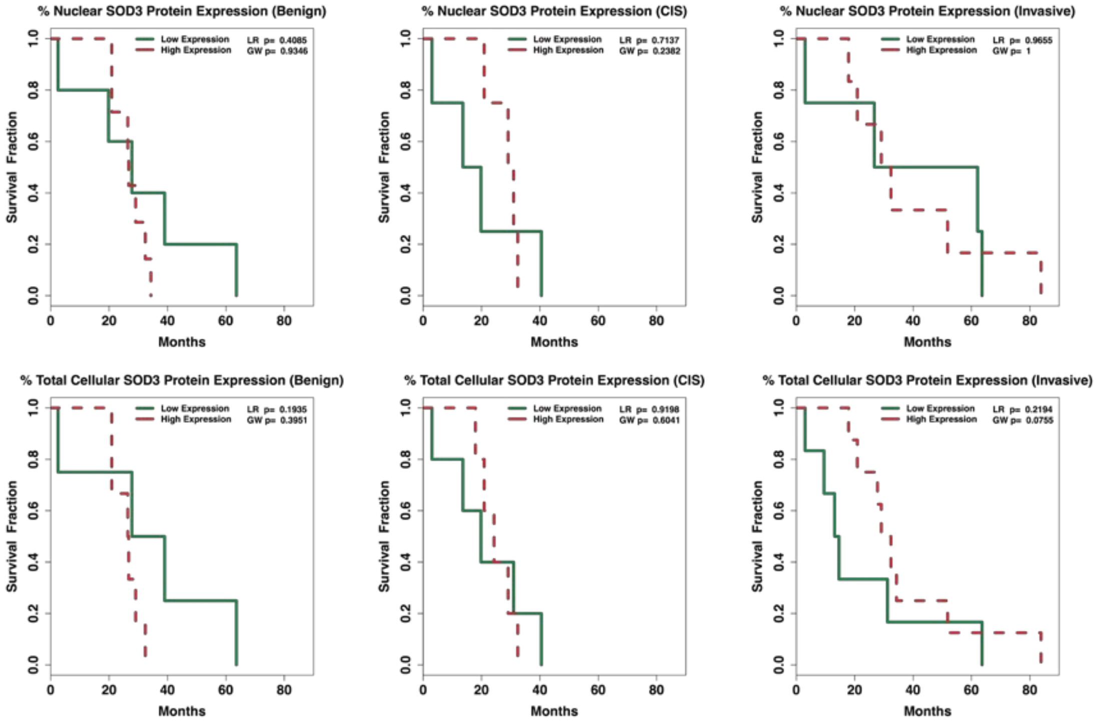

Supplemental Figure C-5: SOD3 survival analysis: low versus high protein expression

Graphs represent the top significant Kaplan Meier survival curves comparing low vs. high protein expression. Top Row: % Nuclear SOD3 protein expression in benign, CIS, and invasive tissue. Bottom Row: % Total Cellular SOD3 protein expression in benign, CIS, and invasive tissue. * Denotes significance $p<0.05$LR: Mantel-Haenszel Log-Rank, GW= Peto & Peto modification of the Gehan-Wilcoxon statistical tests.

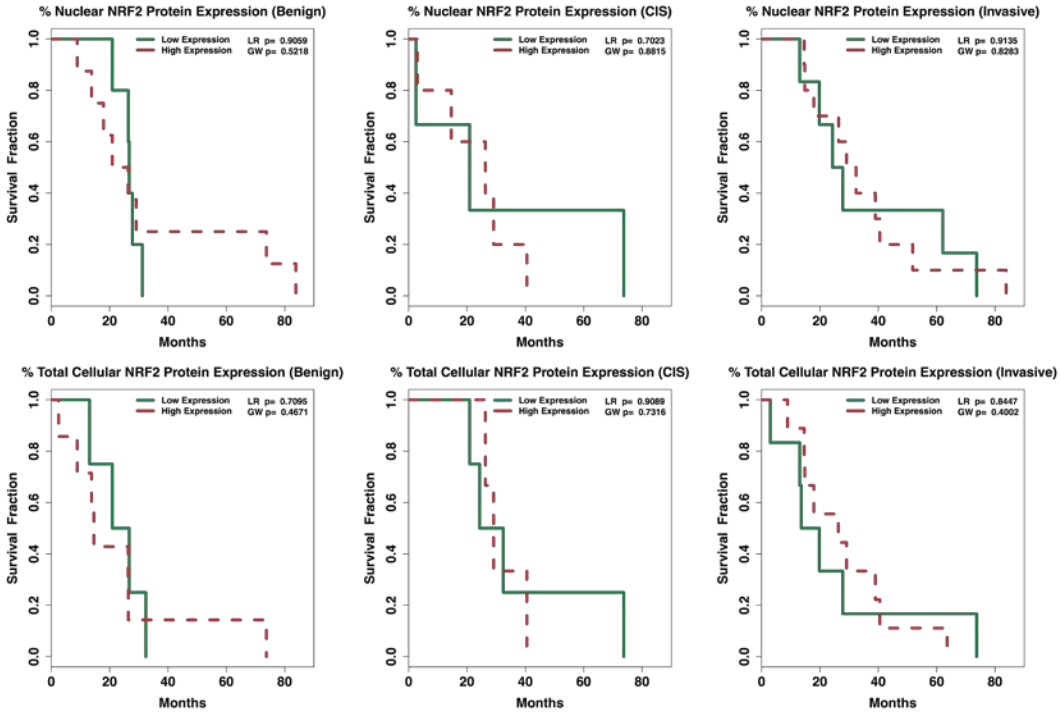

% Nuclear NRF2 Protein Expression (Benign)

% Nuclear NRF2 Protein Expression (CIS)

% Nuclear NRF2 Protein Expression (Invasive)

% Total Cellular NRF2 Protein Expression (Benign)

% Total Cellular NRF2 Protein Expression (CIS)

% Total Cellular NRF2 Protein Expression (Invasive)

Supplemental Figure C-6: NRF2 survival analysis: low versus high protein expression

Graphs represent the top significant Kaplan Meier survival curves comparing low vs. high protein expression. Top Row: % Nuclear NRF2 protein expression in benign, CIS, and invasive tissue. Bottom Row: % Total Cellular NRF2 protein expression in benign, CIS, and invasive tissue. * Denotes significance p<0.05 LR: Mantel-Haenszel Log-Rank, GW= Peto & Peto modification of the Gehan-Wilcoxon statistical tests.

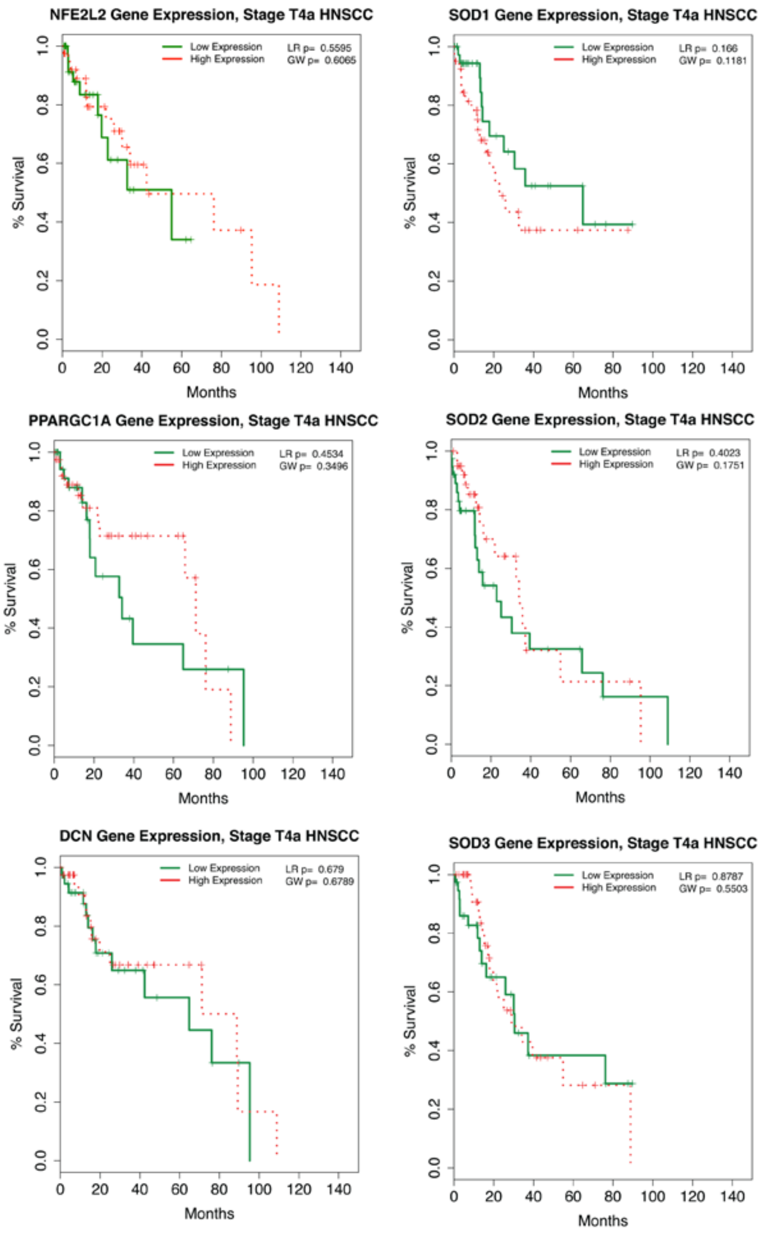

Supplemental Figure C-7: Gene expression survival analysis for APEX1, PPARGC1A, DCN, SOD1, SOD2, and SOD3

Survival analysis was performed and compared low versus high gene expression in patients with pathology stage T4a HNSCC. Gene expression data obtained from TCGA database. * Denotes significance p<0.05 LR: Mantel-Haenszel Log-Rank, GW= Peto & Peto modification of the Gehan-Wilcoxon statistical tests.

Appendix D: Chapter 2 Supplemental Material

Excel files for supplemental tables D-1 through D-6 can be found here:

https://doi.org/10.1186/s12864-016-3313-y

Supplemental Table D-1: The COPS5 correlation coefficient table list includes 1000 highest |*r*| values relative to the expression of COPS5 in the normal and tumor tissues of head and neck.

Supplemental Table D-2: GO and KEGG pathways that are over-represented in the normal and tumor oral tissues based on the COPS5 correlation coefficient table. (XLSX 147 kb)

Supplemental Table D-3: GO and KEGG pathways over-represented by COPS5 expression correlation in the two major anatomical sites in the head and neck (oral cavity and tongue).

Supplemental Table D-4: GO and KEGG pathways over-represented in the normal and tumor lung tissues based on the COPS5 correlation coefficient table.

Supplemental Table D-5: Genes under the chromosomal cis-effect in the HNSCC tissues

Supplemental Table D-6: KEGG pathway analysis for the TP53 genes

Appendix E: Chapter 1 Summary of Conclusions

Overall protein expression (Figure 1-6):

- Nuclear and total APE1 increased in CIS and more so in invasive tissue.
- Nuclear and total DCN decreased in CIS and invasive.
- Slight increase in total NRF2 in invasive as compared to benign.
- Nuclear and total SOD3 decreased in CIS and more so in invasive.
- Nuclear PPARGC1A decreased in CIS and invasive.

Correlation of Protein Expression (Table 1-3):

- There was a positive correlation with total cellular APE1 and DCN in benign tissue ($p<0.05$). However, there was a negative correlation in CIS ($p<0.01$). This suggests loss of coordination between APE1 and DCN within the tumor environment.
- Positive correlation between total cellular PPARGC1A and SOD3 in invasive ($p<0.05$) as well as between nuclear PPARGC1A and SOD3 ($p<0.01$).
- Positive correlation between nuclear APE1 and NRF2 in benign ($p<0.01$) and invasive tissue ($p<0.05$). Additionally there is a positive correlation between nuclear APE1 in benign tissue with nuclear NRF2 in CIS ($p<0.01$). This supports the link between APE1 and NRF2 expression.
- There was a positive correlation found between nuclear NRF2 and PPARGC1A protein expression in benign tissue ($p<0.01$). This was also observed between nuclear NRF2 in invasive and PPARGC1A in CIS ($p<0.05$). Total NRF2 in benign with total PPARGC1A in benign, and invasive ($p<0.01$). As well as total NRF2 in CIS tissue with total PPARGC1A in benign and invasive ($p<0.01$) as well as CIS ($p<0.05$).

- A significant negative correlation was observed between total APE1 in benign with total SOD3 in CIS ($p<0.05$). Additionally, there was a significant negative correlation between total APE1 and nuclear SOD3 in benign tissue ($p<0.05$).

Correlation of gene expression (Table 1-2):

- Comparing APEX1 in non-neoplastic tissue to SOD3 in non-neoplastic, there was a negative correlation observed ($p=0.09$). There was also a negative correlation between APEX1 and PPARGC1A in non-neoplastic tissues ($p=0.095$).
- There was a negative correlation between APEX1 in tumor and SOD3 in non-neoplastic tissue ($p=0.059$). There was a positive link between APEX1 with PPARGC1A in tumor ($p<0.05$).
- DCN in non-neoplastic tissue was positively associated with SOD3 in tumor ($p<0.01$). This positive correlation was maintained between DCN and SOD3 in tumor tissues ($p<0.01$).
- In non-neoplastic tissue, NFE2L2 had a negative correlation with DCN, SOD3, SOD2, and PPARGC1A ($p<0.01$).

Multivariate analysis of clinical factors:

- Elevated total and nuclear DCN as well as total SOD3 in benign tissue of patients with poorly differentiated tumors. Decreased PPARGC1A in CIS tissue of patients with poorly differentiated tumors **(Figure 1-10).**
- Elevated total and nuclear APE1 in CIS tissue within the primary tumor of patients who also had lymph node invasion **(Figure 1-9).**

Survival Data with Protein Expression:

- Significantly reduced survival in patients with high total APE1 in CIS tissue (LR $p=0.0243$, GW $p=0.0326$) **(Figure 1-7).**
- Patients with high total PPARGC1A in invasive tissue had significantly reduced survival (LR $p=0.0281$, GW $p=0.0575$)**(Figure 1-7).**

- High nuclear DCN in benign tissue was linked to reduced survival (LR p=0.0493) **(Figure 1-7).**
- Low levels of total SOD3 in invasive tissue was linked to reduced survival (LR p=0.0797, GW p=0.0377) **(Figure 1-7).**

Survival data based on gene expression in T4a HNSCC

- Significantly reduced survival with high APE1 gene expression in pathology stage T4a tissues (LR p=0.0148, GW p=0.0101) **(Figure 1-8).**
- There was no significant difference in survival in the gene expression of NRF2, DCN, PPARGC1A, SOD1, SOD2, or SOD3 in pathology stage T4a tissues **(Figure C-7).**

References

1. Kentucky Cancer Registry. (2016) Age-Adjusted Invasive Oral Cavity and Pharynx Cancer Incidence Rates by Appalachian Region in Kentucky, 2009 - 2013. Kentucky Cancer Registry, Cancer-Rates.info
2. Institute, N. C. SEER Cancer Statistics Factsheets: Oral Cavity and Pharynx Cancer.
3. Chi, A. C., Day, T. A., and Neville, B. W. (2015) Oral cavity and oropharyngeal squamous cell carcinoma--an update. *CA Cancer J Clin* 65, 401-421
4. Chau, N. G., Rabinowits, G., and Haddad, R. I. (2014) Human papillomavirus-associated oropharynx cancer (HPV-OPC): treatment options. *Curr Treat Options Oncol* 15, 595-610
5. Vermorken, J. B., and Specenier, P. (2010) Optimal treatment for recurrent/metastatic head and neck cancer. *Ann Oncol* 21 Suppl 7, vii252-261
6. Marur, S., and Forastiere, A. A. (2016) Head and Neck Squamous Cell Carcinoma: Update on Epidemiology, Diagnosis, and Treatment. *Mayo Clin Proc* 91, 386-396
7. Haubner, F. O., E ; Phol, F ; Strutz, J ; Gassner , H. (2012) Wound healing after radiation therapy: Review of the literature. *Radiation Oncology* 7, 1-9
8. Tibbs, M. (1997) Wound healing following radiation therapy: a review. *Radiation and Oncology* 42, 99-106
9. O'Sullivan, B. D., A ; Turcotte, R ; Bell, R; Catton, C; Chabot, P; Wunder, J; Kander, R; Goddard, K; Sadura, A; Pater, J; Zee, B. (2002) Preoperative versus postoperative radiotherapy in soft-tissue sarcoma of the limbs: a randomised trial. *The Lancet* 359, 2235-2241
10. Wick, C. C., Rezaee, R. P., Wang, T., Garcia-Jarchow, A. M., Zender, C. A., Gibson, M., Yao, M., and Lavertu, P. (2016) Use of concurrent chemoradiation in advanced staged (T4) laryngeal cancer. *Am J Otolaryngol*
11. Sacco, A. G., and Cohen, E. E. (2015) Current Treatment Options for Recurrent or Metastatic Head and Neck Squamous Cell Carcinoma. *J Clin Oncol* 33, 3305-3313
12. Nesher, L., and Rolston, K. V. (2014) The current spectrum of infection in cancer patients with chemotherapy related neutropenia. *Infection* 42, 5-13
13. Wurtmann, E. J., and Wolin, S. L. (2009) RNA under attack: cellular handling of RNA damage. *Crit Rev Biochem Mol Biol* 44, 34-49
14. Sultana, R., and Butterfield, D. A. (2010) Role of oxidative stress in the progression of Alzheimer's disease. *Journal of Alzheimer's disease : JAD* 19, 341-353
15. Ramana, K. V., Srivastava, S., and Singhal, S. S. (2013) Lipid peroxidation products in human health and disease. *Oxidative medicine and cellular longevity* 2013, 583438
16. Rasheed, M. H., Beevi, S. S., and Geetha, A. (2007) Enhanced lipid peroxidation and nitric oxide products with deranged antioxidant status in patients with head and neck squamous cell carcinoma. *Oral Oncol* 43, 333-338
17. Kong, Q., and Lin, C. L. (2010) Oxidative damage to RNA: mechanisms, consequences, and diseases. *Cellular and molecular life sciences : CMLS* 67, 1817-1829
18. Milonski, J., Zielinska-Blizniewska, H., Olszewski, J., Majsterek, I., and Mrowicka, M. (2015) DNA damage and oxidant-antioxidant status in blood of patients with head and neck cancer. *DNA Cell Biol* 34, 213-219

19. Reuter, S., Gupta, S. C., Chaturvedi, M. M., and Aggarwal, B. B. (2010) Oxidative stress, inflammation, and cancer: how are they linked? *Free radical biology & medicine* 49, 1603-1616
20. Scott, T. L., Rangaswamy, S., Wicker, C. A., and Izumi, T. (2014) Repair of oxidative DNA damage and cancer: recent progress in DNA base excision repair. *Antioxidants & redox signaling* 20, 708-726
21. Lau, A. T., Wang, Y., and Chiu, J. F. (2008) Reactive oxygen species: current knowledge and applications in cancer research and therapeutic. *J Cell Biochem* 104, 657-667
22. Phaniendra, A., Jestadi, D. B., and Periyasamy, L. (2015) Free radicals: properties, sources, targets, and their implication in various diseases. *Indian J Clin Biochem* 30, 11-26
23. Cadet, J., and Wagner, J. R. (2013) DNA base damage by reactive oxygen species, oxidizing agents, and UV radiation. *Cold Spring Harb Perspect Biol* 5
24. Holley, A. K., Miao, L., St Clair, D. K., and St Clair, W. H. (2014) Redox-modulated phenomena and radiation therapy: the central role of superoxide dismutases. *Antioxidants & redox signaling* 20, 1567-1589
25. Kesarwala, A. H., Krishna, M. C., and Mitchell, J. B. (2016) Oxidative stress in oral diseases. *Oral Dis* 22, 9-18
26. Berlett, B. S., and Stadtman, E. R. (1997) Protein Oxidation in Aging, Disease, and Oxidative Stress. *The Journal of biological chemistry* 272, 20313-20316
27. Li, Z., Wu, J., and Deleo, C. J. (2006) RNA damage and surveillance under oxidative stress. *IUBMB Life* 58, 581-588
28. Gottfredsen, R. H., Larsen, U. G., Enghild, J. J., and Petersen, S. V. (2013) Hydrogen peroxide induce modifications of human extracellular superoxide dismutase that results in enzyme inhibition. *Redox Biol* 1, 24-31
29. Salo, D. C., Pacifici, R. E., Lin, S. W., Giulivi, C., and Davies, K. J. (1990) Superoxide Dismutase Undergoes Proteolysis and Fragmentation following Oxidative Modification and Inactivation. *The Journal of biological chemistry* 20, 11919-11927
30. Niki, E., Yoshida, Y., Saito, Y., and Noguchi, N. (2005) Lipid peroxidation: mechanisms, inhibition, and biological effects. *Biochemical and biophysical research communications* 338, 668-676
31. Gupta, A., Bhatt, M. L. B., and Misra, M. K. (2009) Lipid peroxidation and antioxidant status in head and neck squamous cell carcinoma patients. *Oxidative medicine and cellular longevity* 2, 68-72
32. Salzman, R., Pácal, L., Tomandal, J., Kánkova, K., Tóthova, E., Gál, B., Kostřica, R., and Salzman, P. (2009) Elevated Malondialdehyde Correlates with the Extent of Primary Tumor and Predicts Poor Prognosis of Oropharyngeal Cancer. *Anticancer Res* 29, 4227-4232
33. Evans, M. D., Dizdaroglu, M., and Cooke, M. S. (2004) Oxidative DNA damage and disease: induction, repair and significance. *Mutation research* 567, 1-61
34. Neeley, W. L., and Essigmann, J. M. (2006) Mechanisms of Formation, Genotoxicity, and Mutation of Guanine Oxidation Products. *Chemical Research in Toxicology* 19, 491-505
35. Wang, Z., Rhee, D. B., Lu, J., Bohr, C. T., Zhou, F., Vallabhaneni, H., de Souza-Pinto, N. C., and Liu, Y. (2010) Characterization of oxidative guanine damage and repair in mammalian telomeres. *PLoS genetics* 6, e1000951
36. Hatem, E. A., S. (2015) Oxidative Stress in Carcinogenesis and Therapy *Journal of Cell Signaling* 1, 1-10

37. Klaunig, J. E., Kamendulis, L. M., and Hocevar, B. A. (2010) Oxidative stress and oxidative damage in carcinogenesis. *Toxicol Pathol* 38, 96-109
38. Jacobs, A. L., and Schar, P. (2012) DNA glycosylases: in DNA repair and beyond. *Chromosoma* 121, 1-20
39. Bhakat, K. K., Mantha, A. K., and Mitra, S. (2009) Transcriptional regulatory functions of mammalian AP-endonuclease (APE1/Ref-1), an essential multifunctional protein. *Antioxidants & redox signaling* 11, 621-638
40. Fortini, P., Pascucci, B., Parlanti, E., D'Errico, M., Simonelli, V., and Dogliotti, E. (2003) 8-Oxoguanine DNA damage: at the crossroad of alternative repair pathways. *Mutation Research/Fundamental and Molecular Mechanisms of Mutagenesis* 531, 127-139
41. Ide, H., and Kotera, M. (2004) Human DNA Glycosylases Involved in the Repair of Oxidatively Damaged DNA. *Biol Pharm Bull* 27, 480-485
42. Sattler, U., Frit, P., Salles, B., and Calsou, P. (2003) Long-patch DNA repair synthesis during base excision repair in mammalian cells. *EMBO reports* 4, 363-367
43. Demple, B., and Sung, J. S. (2005) Molecular and biological roles of Ape1 protein in mammalian base excision repair. *DNA repair* 4, 1442-1449
44. Fortini, P., Parlanti, E., Sidorkina, O. M., Laval, J., and Dogliotti, E. (1999) The Type of DNA Glycosylase Determines the Base Excision Repair Pathway in Mammalian Cells. *The Journal of biological chemistry* 274, 15230-15236
45. Liou, G. Y., and Storz, P. (2010) Reactive oxygen species in cancer. *Free Radic Res* 44, 479-496
46. Fukai, T., and Ushio-Fukai, M. (2011) Superoxide dismutases: role in redox signaling, vascular function, and diseases. *Antioxidants & redox signaling* 15, 1583-1606
47. Sheng, Y., Abreu, I. A., Cabelli, D. E., Maroney, M. J., Miller, A. F., Teixeira, M., and Valentine, J. S. (2014) Superoxide dismutases and superoxide reductases. *Chem Rev* 114, 3854-3918
48. Zelko, I. N., Mariani, T. J., and Folz, R. J. (2002) Superoxide Dismutase Multigene Family: A Comparison of The CuZn-SOD (SOD1), Mn-SOD (SOD2), And Ec-SOD3 (SOD3) Gene Structures, Evolution, And Expression. *Free radical biology & medicine* 33, 337-349
49. Waris, G., and Ahsan, H. (2006) Reactive oxygen species: role in the development of cancer and various chronic conditions. *J Carcinog* 5, 14
50. Robbins, D., and Zhao, Y. (2014) Manganese superoxide dismutase in cancer prevention. *Antioxidants & redox signaling* 20, 1628-1645
51. Rakhit, R., Cunningham, P., Furtos-Matei, A., Dahan, S., Qi, X. F., Crow, J. P., Cashman, N. R., Kondejewski, L. H., and Chakrabartty, A. (2002) Oxidation-induced misfolding and aggregation of superoxide dismutase and its implications for amyotrophic lateral sclerosis. *The Journal of biological chemistry* 277, 47551-47556
52. Miao, L., and St Clair, D. K. (2009) Regulation of superoxide dismutase genes: implications in disease. *Free radical biology & medicine* 47, 344-356
53. Malafa, M., Margenthaler, J., Webb, B., Neitzel, L., and Christophersen, M. (2000) MnSOD expression is increased in metastatic gastric cancer. *J Surg Res* 88, 130-134
54. Cullen, J. J., Weydert, C., Hinkhouse, M. M., Ritche, J., Domann, F. E., and Spitz, D. R. (2003) The Role of Manganese Superoxide Dismutase in the Growth of Pancreatic Adenocarcinoma. *Cancer research* 63, 1297-1303

55. Janssen, A. M. L., Bosman, C. B., Oostendorp-van de Ruit, M. M., Kubben, F. J. G. M., Griffioen, G., and Lamers, C. B. H. W. (2000) Superoxide Dismutases in Gastric and Esophageal Cancer and the Prognostic Impact in Gastric Cancer. *Clinical Cancer Research* 6, 3183-3192
56. Soini, Y., Vakkala, M., Kahlos, K., Paakko, P., and Kinnula, V. (2001) MnSOD expression is less frequent in tumour cells of invasive breast carcinomas than in in situ carcinomas or non-neoplastic breast epithelial cells. *J Pathol* 195, 156-162
57. Ho, J. C., Zheng, S., Comhair, S. A. A., Farver, C., and Erzurum, S. (2001) Differential Expression of Manganese Superoxide Dismutase and Catalase in Lung Cancer. *Cancer research* 61, 8578-8585
58. Sandstrom, J. K., K. Edlund, T. Marklund, S. . (1993) Heparin-affinity patterns and composition of extracellular superoxide dismutase in human plasma and tissues. *Biochem J.* 294, 853-857
59. Johnson, W. T., Johnson, L. A., and Lukaski, H. C. (2005) Serum superoxide dismutase 3 (extracellular superoxide dismutase) activity is a sensitive indicator of Cu status in rats. *J Nutr Biochem* 16, 682-692
60. Singh, B., and Bhat, H. K. (2012) Superoxide dismutase 3 is induced by antioxidants, inhibits oxidative DNA damage and is associated with inhibition of estrogen-induced breast cancer. *Carcinogenesis* 33, 2601-2610
61. Chu, Y., Piper, R., Richardson, S., Watanabe, Y., Patel, P., and Heistad, D. D. (2006) Endocytosis of extracellular superoxide dismutase into endothelial cells: role of the heparin-binding domain. *Arterioscler Thromb Vasc Biol* 26, 1985-1990
62. Ookawara, T., Eguchi, H., Nishimura, M., Kizaki, T., Eiji, T., Saitoh, D., Ohno, H., and Suzuki, K. (2003) Effects of oxidative stress on the nuclear translocation of extracellular superoxide dismutase. *Biochemical and biophysical research communications* 303, 914-919
63. Ookawara, T., Kizaki, T., Takayama, E., Imazeki, N., Matsubara, O., Ikeda, Y., Suzuki, K., Ji, L. L., Tadakuma, T., Taniguchi, N., and Ohno, H. (2002) Nuclear translocation of extracellular superoxide dismutase. *Biochemical and biophysical research communications* 296, 54-61
64. Ueda, J., Starr, M. E., Takahashi, H., Du, J., Chang, L. Y., Crapo, J. D., Evers, B. M., and Saito, H. (2008) Decreased pulmonary extracellular superoxide dismutase during systemic inflammation. *Free radical biology & medicine* 45, 897-904
65. Slaughter, D. S., HW ; Smejkal, W. (1953) "Field Cancerization" in Oral Stratified Squamous Epithelium *Cancer* 6, 963-968
66. WATSON, J. C., FH. . (1953) Genetical implications of the structure of deoxyribonucleic acid. *Nature* 171, 964-967
67. Ashwini, B., Chitra, S., Sharada, P., and Hema, K. (2015) Oral field cancerization: An update of evidences. *Journal of Dr. NTR University of Health Sciences* 4, 141
68. Aparna, M., Shenai, P., Chatra, L., Veena, K. M., Rao, P. K., Prabhu, R. V., and Shahin, K. A. (2013) Field cancerization: A review. *Archives of Medicine and Health Sciences* 1, 136
69. Mohan, M., and Jagannathan, N. (2014) Oral field cancerization: an update on current concepts. *Oncol Rev* 8, 244
70. Simple, M. S., A; Das, D; Kuriakose, M. (2015) Cancer stem cells and field cancerization of Oral squamous cell carcinoma. *Oral Oncol* 51, 643-651
71. Pieras, E., Frontera, G., Ruiz, X., Vicens, A., Ozonas, M., and Piza, P. (2010) Concomitant carcinoma in situ and tumour size are prognostic factors for bladder

recurrence after nephroureterectomy for upper tract transitional cell carcinoma. *BJU Int* 106, 1319-1323
72. Shariat, S. F., Palapattu, G. S., Karakiewicz, P. I., Rogers, C. G., Vazina, A., Bastian, P. J., Schoenberg, M. P., Lerner, S. P., Sagalowsky, A. I., and Lotan, Y. (2007) Concomitant carcinoma in situ is a feature of aggressive disease in patients with organ-confined TCC at radical cystectomy. *Eur Urol* 51, 152-160
73. Angadi, P. V., Savitha, J. K., Rao, S. S., and Sivaranjini, Y. (2012) Oral field cancerization: current evidence and future perspectives. *Oral Maxillofac Surg* 16, 171-180
74. Holcomb, N., Goswami, M., Han, S. G., Clark, S., Orren, D. K., Gairola, C. G., and Mellon, I. (2016) Exposure of Human Lung Cells to Tobacco Smoke Condensate Inhibits the Nucleotide Excision Repair Pathway. *PloS one* 11, e0158858
75. Singh, A. K., Pandey, P., Tewari, M., Pandey, H. P., Gambhir, I. S., and Shukla, H. S. (2016) Free radicals hasten head and neck cancer risk: A study of total oxidant, total antioxidant, DNA damage, and histological grade. *J Postgrad Med* 62, 96-101
76. Hecht, S. S. (2012) Lung carcinogenesis by tobacco smoke. *International journal of cancer. Journal international du cancer* 131, 2724-2732
77. Vu, A. T., K; Holman, M; Ding, Y; Hearn, B; Watson, C. (2015) Polycyclic Aromatic Hydrocarbons in the Mainstream Smoke of Popular U.S. Cigarettes. *Chem Res Toxicol* 28, 1616-1626
78. van der Vaart, H., Postma, D. S., Timens, W., and ten Hacken, N. H. (2004) Acute effects of cigarette smoke on inflammation and oxidative stress: a review. *Thorax* 59, 713-721
79. Goel, R., Bitzer, Z., Reilly, S. M., Trushin, N., Foulds, J., Muscat, J., Liao, J., Elias, R. J., and Richie, J. P., Jr. (2017) Variation in Free Radical Yields from U.S. Marketed Cigarettes. *Chem Res Toxicol* 30, 1038-1045
80. Cao, C., Lai, T., Li, M., Zhou, H., Lv, D., Deng, Z., Ying, S., Chen, Z., Li, W., and Shen, H. (2016) Smoking-promoted oxidative DNA damage response is highly correlated to lung carcinogenesis. *Oncotarget* 7, 18919-18926
81. Juul, K., Tybjærg-Hansen, A., Marklund, S., Lange, P., and Nordestgaard, B. G. (2006) Genetically Increased Antioxidative Protection and Decreased Chronic Obstructive Pulmonary Disease. *American Journal of Respiratory and Critical Care Medicine* 173, 858-864
82. Oberley-Deegan, R. E., Regan, E. A., Kinnula, V., and Crapo, J. D. (2009) Extracellular Superoxide Dismutase and Risk of COPD. *COPD* 6, 307-312
83. Ganguly, K., Depner, M., Fattman, C., Bein, K., Oury, T. D., Wesselkamper, S. C., Borchers, M. T., Schreiber, M., Gao, F., von Mutius, E., Kabesch, M., Leikauf, G. D., and Schulz, H. (2009) Superoxide dismutase 3, extracellular (SOD3) variants and lung function. *Physiol Genomics* 37, 260-267
84. Tollefson, A. K., Oberley-Deegan, R. E., Butterfield, K. T., Nicks, M. E., Weaver, M. R., Remigio, L. K., Decsesznak, J., Chu, H. W., Bratton, D. L., Riches, D. W., and Bowler, R. P. (2010) Endogenous enzymes (NOX and ECSOD) regulate smoke-induced oxidative stress. *Free radical biology & medicine* 49, 1937-1946
85. Young, R. P., Hopkins, R., Black, P. N., Eddy, C., Wu, L., Gamble, G. D., Mills, G. D., Garrett, J. E., Eaton, T. E., and Rees, M. I. (2006) Functional variants of antioxidant genes in smokers with COPD and in those with normal lung function. *Thorax* 61, 394-399
86. Dahl, M., Bowler, R. P., Juul, K., Crapo, J. D., Levin, S., and Nordestgaard, B. G. (2008) Superoxide Dismutase 3 Polymorphism Associated with Reduced Lung

Function in Two Large Populations. *American journal of respiratory cell and molecular biology* 178

87. Yoo, D. G., Song, Y. J., Cho, E. J., Lee, S. K., Park, J. B., Yu, J. H., Lim, S. P., Kim, J. M., and Jeon, B. H. (2008) Alteration of APE1/ref-1 expression in non-small cell lung cancer: the implications of impaired extracellular superoxide dismutase and catalase antioxidant systems. *Lung Cancer* 60, 277-284
88. Guo, T., Eisele, D. W., and Fakhry, C. (2016) The potential impact of prophylactic human papillomavirus vaccination on oropharyngeal cancer. *Cancer* 122, 2313-2323
89. Lin, B. W., H; D'Souza, G ; Zhang, Z ; Fakhry, C; Joseph, A; Drake, V; Sanguineti, G; Westra, W; Pai, S. (2013) Long term prognosis and risk factors among HPV-associated oropharyngeal squamous cell carcinoma patients. *Cancer* 119, 3462-2471
90. Schantz, S. P. Y., Guo-Pei. (2002) Head and Neck Cancer Incidence Trends in Young Americans, 1973-1997, With a Special Analysis for Tongue Cancer. *Arch Otolaryngol Head Neck Surg.* 128, 268-274
91. Pytynia, K. B., Dahlstrom, K. R., and Sturgis, E. M. (2014) Epidemiology of HPV-associated oropharyngeal cancer. *Oral Oncol* 50, 380-386
92. Chaturvedi, A. K., Engels, E. A., Pfeiffer, R. M., Hernandez, B. Y., Xiao, W., Kim, E., Jiang, B., Goodman, M. T., Sibug-Saber, M., Cozen, W., Liu, L., Lynch, C. F., Wentzensen, N., Jordan, R. C., Altekruse, S., Anderson, W. F., Rosenberg, P. S., and Gillison, M. L. (2011) Human papillomavirus and rising oropharyngeal cancer incidence in the United States. *J Clin Oncol* 29, 4294-4301
93. Goldstone, S. E., Jessen, H., Palefsky, J. M., Giuliano, A. R., Moreira, E. D., Vardas, E., Aranda, C., Hillman, R. J., Ferris, D. G., Coutlee, F., Marshall, J. B., Vuocolo, S., Haupt, R. M., Guris, D., and Garner, E. (2013) Quadrivalent HPV vaccine efficacy against disease related to vaccine and non-vaccine HPV types in males. *Vaccine* 31, 3849-3855
94. Viens, L. J., Henley, S. J., Watson, M., Markowitz, L. E., Thomas, C. C., Thompson, T. D., Razzaghi, H., and Saraiya, M. (2016) Human Papillomavirus-Associated Cancers - United States, 2008-2012. *MMWR Morb Mortal Wkly Rep* 65, 661-666
95. Gillison, M. L. K., Wayne M.; Shah, Keerti V. (May 1999) Human papillomavirus in head and neck squamous cell carcinoma: are some head and neck cancers a sexually transmitted disease? *Curr Opin Oncol.* 11, 191-199
96. Miller, C. S., and Johnstone, B. M. (2001) Human papillomavirus as a risk factor for oral squamous cell carcinoma: a meta-analysis, 1982-1997. *Oral Surg Oral Med Oral Pathol Oral Radiol Endod* 91, 622-635
97. Poling, J. S., Ma, X. J., Bui, S., Luo, Y., Li, R., Koch, W. M., and Westra, W. H. (2014) Human papillomavirus (HPV) status of non-tobacco related squamous cell carcinomas of the lateral tongue. *Oral Oncol* 50, 306-310
98. Vigneswaran, N., and Williams, M. D. (2014) Epidemiologic trends in head and neck cancer and aids in diagnosis. *Oral Maxillofac Surg Clin North Am* 26, 123-141
99. Mallen-St Clair, J., Alani, M., Wang, M. B., and Srivatsan, E. S. (2016) Human papillomavirus in oropharyngeal cancer: The changing face of a disease. *Biochimica et biophysica acta* 1866, 141-150
100. Nishat, R., Behura, S. S., Ramachandra, S., Kumar, H., and Bandyopadhyay, A. (2015) Human Papilloma Virus (HPV) Induced Head & Neck Squamous Cell Carcinoma: A Comprehensive Retrospect. *J Clin Diagn Res* 9, ZE01-04

101. Miller, D. L., Puricelli, M. D., and Stack, M. S. (2012) Virology and molecular pathogenesis of HPV (human papillomavirus)-associated oropharyngeal squamous cell carcinoma. *The Biochemical journal* 443, 339-353
102. Williams, V. M., Filippova, M., Filippov, V., Payne, K. J., and Duerksen-Hughes, P. (2014) Human papillomavirus type 16 E6* induces oxidative stress and DNA damage. *J Virol* 88, 6751-6761
103. Longworth, M. S., and Laimins, L. A. (2004) Pathogenesis of human papillomaviruses in differentiating epithelia. *Microbiol Mol Biol Rev* 68, 362-372
104. Marullo, R., Werner, E., Zhang, H., Chen, G. Z., Shin, D. M., and Doetsch, P. W. (2015) HPV16 E6 and E7 proteins induce a chronic oxidative stress response via NOX2 that causes genomic instability and increased susceptibility to DNA damage in head and neck cancer cells. *Carcinogenesis* 36, 1397-1406
105. Romagosa, C., Simonetti, S., Lopez-Vicente, L., Mazo, A., Lleonart, M. E., Castellvi, J., and Ramon y Cajal, S. (2011) p16(Ink4a) overexpression in cancer: a tumor suppressor gene associated with senescence and high-grade tumors. *Oncogene* 30, 2087-2097
106. Knudsen, K., Weber, E., Arden, K., Cavenee, W., Feramisco, J., and Knudson, E. (1999) The retinoblastoma tumor suppressor inhibits cellular proliferation through two distinct mechanisms: inhibition of cell cycle progression and induction of cell death. *Oncogene* 18, 5239-5245
107. Shi, W., Kato, H., Perez-Ordonez, B., Pintilie, M., Huang, S., Hui, A., O'Sullivan, B., Waldron, J., Cummings, B., Kim, J., Ringash, J., Dawson, L. A., Gullane, P., Siu, L., Gillison, M., and Liu, F. F. (2009) Comparative prognostic value of HPV16 E6 mRNA compared with in situ hybridization for human oropharyngeal squamous carcinoma. *J Clin Oncol* 27, 6213-6221
108. Majchrzak, E., Szybiak, B., Wegner, A., Pienkowski, P., Pazdrowski, J., Luczewski, L., Sowka, M., Golusinski, P., Malicki, J., and Golusinski, W. (2014) Oral cavity and oropharyngeal squamous cell carcinoma in young adults: a review of the literature. *Radiol Oncol* 48, 1-10
109. Wu, H. H., Cheng, Y. W., Chang, J. T., Wu, T. C., Liu, W. S., Chen, C. Y., and Lee, H. (2010) Subcellular localization of apurinic endonuclease 1 promotes lung tumor aggressiveness via NF-kappaB activation. *Oncogene* 29, 4330-4340
110. Wu, H., Chu, Y., Wang, L., Tsai, L., Lee, M., Chen, C., Shleh, S., Cheng, Y., and Lee, H. (2013) Cytoplasmic Ape1 Expression Elevated by p53 Aberration May Predict Survival and Relapse in Resected Non-Small Cell Lung Cancer. *Ann Surg Oncol* 20, S336–S347
111. Tell, G., Fantini, D., and Quadrifoglio, F. (2010) Understanding different functions of mammalian AP endonuclease (APE1) as a promising tool for cancer treatment. *Cellular and molecular life sciences : CMLS* 67, 3589-3608
112. Tell, G., Damante, G., Caldwell, D., and Kelley, M. R. (2005) The intracellular localization of APE1/Ref-1: more than a passive phenomenon? *Antioxidants & redox signaling* 7, 367-384
113. Ramana, C. V., Boldogh, I., Izumi, T., and Mitra, S. (1998) Activation of apurinic/apyrimidinic endonuclease in human cells by reactive oxygen species and its correlation with their adaptive response to genotoxicity of free radicals. *Proceedings of the National Academy of Sciences of the United States of America* 95, 5061-5066
114. Teoh-Fitzgerald, M. L., Fitzgerald, M. P., Jensen, T. J., Futscher, B. W., and Domann, F. E. (2012) Genetic and epigenetic inactivation of extracellular superoxide dismutase promotes an invasive phenotype in human lung cancer by disrupting ECM homeostasis. *Molecular cancer research : MCR* 10, 40-51

115. Busso, C. S., Lake, M. W., and Izumi, T. (2010) Posttranslational modification of mammalian AP endonuclease (APE1). *Cellular and molecular life sciences : CMLS* 67, 3609-3620
116. Scott, T. L., Wicker, C. A., Suganya, R., Dhar, B., Pittman, T., Horbinski, C., and Izumi, T. (2017) Polyubiquitination of apurinic/apyrimidinic endonuclease 1 by Parkin. *Mol Carcinog* 56, 325-336
117. Tell, G., Quadrifoglio, F., Tiribelli, C., and Kelley, M. R. (2009) The many functions of APE1/Ref-1: not only a DNA repair enzyme. *Antioxidants & redox signaling* 11, 601-620
118. Li, Y., Liu, X., Zhou, T., Kelley, M. R., Edwards, P., Gao, H., and Qiao, X. (2014) Inhibition of APE1/Ref-1 redox activity rescues human retinal pigment epithelial cells from oxidative stress and reduces choroidal neovascularization. *Redox Biol* 2, 485-494
119. Kelley, M. R., Georgiadis, M. M., and Fishel, M. L. (2012) APE1/Ref-1 role in redox signaling: translational applications of targeting the redox function of the DNA repair/redox protein APE1/Ref-1. *Curr Mol Pharmacol* 5, 36-53
120. Stadler, M. E., Patel, M. R., Couch, M. E., and Hayes, D. N. (2008) Molecular biology of head and neck cancer: risks and pathways. *Hematol Oncol Clin North Am* 22, 1099-1124, vii
121. Reddy, N. M., Kleeberger, S. R., Yamamoto, M., Kensler, T. W., Scollick, C., Biswal, S., and Reddy, S. P. (2007) Genetic dissection of the Nrf2-dependent redox signaling-regulated transcriptional programs of cell proliferation and cytoprotection. *Physiol Genomics* 32, 74-81
122. Suganya, R., Chakraborty, A., Miriyala, S., Hazra, T. K., and Izumi, T. (2015) Suppression of oxidative phosphorylation in mouse embryonic fibroblast cells deficient in apurinic/apyrimidinic endonuclease. *DNA repair* 27, 40-48
123. Izumi, T., Brown, D. B., Naidu, C. V., Bhakat, K. K., Macinnes, M. A., Saito, H., Chen, D. J., and Mitra, S. (2005) Two essential but distinct functions of the mammalian abasic endonuclease. *Proceedings of the National Academy of Sciences of the United States of America* 102, 5739-5743
124. Gubbiotti, M. A., Vallet, S. D., Ricard-Blum, S., and Iozzo, R. V. (2016) Decorin interacting network: A comprehensive analysis of decorin-binding partners and their versatile functions. *Matrix Biol* 55, 7-21
125. Bi, X., Pohl, N. M., Qian, Z., Yang, G. R., Gou, Y., Guzman, G., Kajdacsy-Balla, A., Iozzo, R. V., and Yang, W. (2012) Decorin-mediated inhibition of colorectal cancer growth and migration is associated with E-cadherin in vitro and in mice. *Carcinogenesis* 33, 326-330
126. Shi, X., Liang, W., Yang, W., Xia, R., and Song, Y. (2015) Decorin is responsible for progression of non-small-cell lung cancer by promoting cell proliferation and metastasis. *Tumour Biol* 36, 3345-3354
127. Araki, K., Wakabayashi, H., Shintani, K., Morikawa, J., Matsumine, A., Kusuzaki, K., Sudo, A., and Uchida, A. (2009) Decorin suppresses bone metastasis in a breast cancer cell line. *Oncology* 77, 92-99
128. Cawthorn, T. R., Moreno, J. C., Dharsee, M., Tran-Thanh, D., Ackloo, S., Zhu, P. H., Sardana, G., Chen, J., Kupchak, P., Jacks, L. M., Miller, N. A., Youngson, B. J., Iakovlev, V., Guidos, C. J., Vallis, K. A., Evans, K. R., McCready, D., Leong, W. L., and Done, S. J. (2012) Proteomic analyses reveal high expression of decorin and endoplasmin (HSP90B1) are associated with breast cancer metastasis and decreased survival. *PloS one* 7, e30992

129. Li, S. J., Chen, D. L., Zhang, W. B., Shen, C., and Che, G. W. (2015) Prognostic value of stromal decorin expression in patients with breast cancer: a meta-analysis. *J Thorac Dis* 7, 1939-1950
130. Reed, C. C., Waterhouse, A., Kirby, S., Kay, P., Owens, R. T., McQuillan, D. J., and Iozzo, R. V. (2005) Decorin prevents metastatic spreading of breast cancer. *Oncogene* 24, 1104-1110
131. Zou, Y., Yu, X., Lu, J., Jiang, Z., Zuo, Q., Fan, M., Huang, S., and Sun, L. (2015) Decorin-Mediated Inhibition of Human Trophoblast Cells Proliferation, Migration, and Invasion and Promotion of Apoptosis In Vitro. *Biomed Res Int* 2015, 201629
132. Nayak, S., Goel, M. M., Bhatia, V., Chandra, S., Makker, A., Kumar, S., Agrawal, S. P., Mehrotra, D., and Rath, S. K. (2013) Molecular and phenotypic expression of decorin as modulator of angiogenesis in human potentially malignant oral lesions and oral squamous cell carcinomas. *Indian J Pathol Microbiol* 56, 204-210
133. Bi, X.-L., and Yang, W. (2013) Biological functions of decorin in cancer. *Chinese Journal of Cancer* 32, 266-269
134. Takeda, D., Hasegawa, T., Ueha, T., Sakakibara, A., Kawamoto, T., Minamikawa, T., Sakai, Y., and Komori, T. (2016) Decreased mitochondrial copy numbers in oral squamous cell carcinoma. *Head Neck* 38, 1170-1175
135. Bhalla, K., Hwang, B. J., Dewi, R. E., Ou, L., Twaddel, W., Fang, H. B., Vafai, S. B., Vazquez, F., Puigserver, P., Boros, L., and Girnun, G. D. (2011) PGC1alpha promotes tumor growth by inducing gene expression programs supporting lipogenesis. *Cancer research* 71, 6888-6898
136. Bellance, N., Benard, G., Furt, F., Begueret, H., Smolkova, K., Passerieux, E., Delage, J. P., Baste, J. M., Moreau, P., and Rossignol, R. (2009) Bioenergetics of lung tumors: alteration of mitochondrial biogenesis and respiratory capacity. *Int J Biochem Cell Biol* 41, 2566-2577
137. LeBleu, V. S., O'Connell, J. T., Gonzalez Herrera, K. N., Wikman, H., Pantel, K., Haigis, M. C., de Carvalho, F. M., Damascena, A., Domingos Chinen, L. T., Rocha, R. M., Asara, J. M., and Kalluri, R. (2014) PGC-1alpha mediates mitochondrial biogenesis and oxidative phosphorylation in cancer cells to promote metastasis. *Nature cell biology* 16, 992-1003, 1001-1015
138. Kim, J., and Keum, Y. S. (2016) NRF2, a Key Regulator of Antioxidants with Two Faces towards Cancer. *Oxidative medicine and cellular longevity* 2016, 2746457
139. Ganan-Gomez, I., Wei, Y., Yang, H., Boyano-Adanez, M. C., and Garcia-Manero, G. (2013) Oncogenic functions of the transcription factor Nrf2. *Free radical biology & medicine* 65, 750-764
140. Gurusamy, N., Malik, G., Gorbunov, N. V., and Das, D. K. (2007) Redox activation of Ref-1 potentiates cell survival following myocardial ischemia reperfusion injury. *Free radical biology & medicine* 43, 397-407
141. Iwasaki, K., Mackenzie, E. L., Hailemariam, K., Sakamoto, K., and Tsuji, Y. (2006) Hemin-mediated regulation of an antioxidant-responsive element of the human ferritin H gene and role of Ref-1 during erythroid differentiation of K562 cells. *Molecular and cellular biology* 26, 2845-2856
142. Fishel, M. L., Wu, X., Devlin, C. M., Logsdon, D. P., Jiang, Y., Luo, M., He, Y., Yu, Z., Tong, Y., Lipking, K. P., Maitra, A., Rajeshkumar, N. V., Scandura, G., Kelley, M. R., and Ivan, M. (2015) Apurinic/apyrimidinic endonuclease/redox factor-1 (APE1/Ref-1) redox function negatively regulates NRF2. *The Journal of biological chemistry* 290, 3057-3068
143. Wang, T., Hu, P., Li, B., Zhang, J. P., Cheng, Y. F., and Liang, Y. M. (2017) Role of Nrf2 signaling pathway in the radiation tolerance of patients with head and

neck squamous cell carcinoma: an in vivo and in vitro study. *Onco Targets Ther* 10, 1809-1819

144. Kim, Y. R., Oh, J. E., Kim, M. S., Kang, M. R., Park, S. W., Han, J. Y., Eom, H. S., Yoo, N. J., and Lee, S. H. (2010) Oncogenic NRF2 mutations in squamous cell carcinomas of oesophagus and skin. *J Pathol* 220, 446-451
145. Santana, T., Sa, M. C., de Moura Santos, E., Galvao, H. C., Coletta, R. D., and Freitas, R. A. (2017) DNA base excision repair proteins APE-1 and XRCC-1 are overexpressed in oral tongue squamous cell carcinoma. *J Oral Pathol Med* 46, 496-503
146. Huang, C. F., Zhang, L., Ma, S. R., Zhao, Z. L., Wang, W. M., He, K. F., Zhao, Y. F., Zhang, W. F., Liu, B., and Sun, Z. J. (2013) Clinical significance of Keap1 and Nrf2 in oral squamous cell carcinoma. *PloS one* 8, e83479
147. Miller, C. J., Gounder, S. S., Kannan, S., Goutam, K., Muthusamy, V. R., Firpo, M. A., Symons, J. D., Paine III, R., Hoidal, J. R., and Rajasekaran, N. S. (2012) Disruption of Nrf2/ARE signaling impairs antioxidant mechanisms and promotes cell degradation pathways in aged skeletal muscle. *Biochimica et biophysica acta* 1822, 1038-1050
148. Lee, C., and Huang, C. H. (2013) LASAGNA-Search: an integrated web tool for transcription factor binding site search and visualization. *Biotechniques* 54, 141-153
149. Lee, C., and Huang, C. H. (2013) LASAGNA: a novel algorithm for transcription factor binding site alignment. *BMC Bioinformatics* 14, 108
150. Lee, C., and Huang, C. H. (2014) LASAGNA-Search 2.0: integrated transcription factor binding site search and visualization in a browser. *Bioinformatics* 30, 1923-1925
151. Castilho, R. M., Squarize, C. H., and Almeida, L. O. (2017) Epigenetic Modifications and Head and Neck Cancer: Implications for Tumor Progression and Resistance to Therapy. *Int J Mol Sci* 18
152. Marmolino, D., Manto, M., Acquaviva, F., Vergara, P., Ravella, A., Monticelli, A., and Pandolfo, M. (2010) PGC-1alpha down-regulation affects the antioxidant response in Friedreich's ataxia. *PloS one* 5, e10025
153. Wicker, C. A., and Izumi, T. (2016) Analysis of RNA expression of normal and cancer tissues reveals high correlation of COP9 gene expression with respiratory chain complex components. *BMC Genomics* 17, 983
154. Rizzardi, A. E., Johnson, A. T., Vogel, R. I., Pambuccian, S. E., Henriksen, J., Skubitz, A. P., Metzger, G. J., and Schmechel, S. C. (2012) Quantitative comparison of immunohistochemical staining measured by digital image analysis versus pathologist visual scoring. *Diagn Pathol* 7, 1-10
155. Rizzardi, A. E., Zhang, X., Vogel, R. I., Kolb, S., Geybels, M. S., Leung, Y. K., Henriksen, J. C., Ho, S. M., Kwak, J., Stanford, J. L., and Schmechel, S. C. (2016) Quantitative comparison and reproducibility of pathologist scoring and digital image analysis of estrogen receptor beta2 immunohistochemistry in prostate cancer. *Diagn Pathol* 11, 63
156. Bouzin, C., Saini, M. L., Khaing, K. K., Ambroise, J., Marbaix, E., Gregoire, V., and Bol, V. (2016) Digital pathology: elementary, rapid and reliable automated image analysis. *Histopathology* 68, 888-896
157. Ko, J. J., Klimowicz, A. C., Jagdis, A., Phan, T., Laskin, J., Lau, H. Y., Siever, J. E., Petrillo, S. K., Thomson, T. A., Rose, M. S., Bebb, G., Magliocco, A. M., and Hao, D. (2016) ATM, THMS, and RRM1 protein expression in nasopharyngeal carcinomas treated with curative intent. *Head Neck* 38 Suppl 1, E384-391

158. Sand, J. M., Leeming, D. J., Byrjalsen, I., Bihlet, A. R., Lange, P., Tal-Singer, R., Miller, B. E., Karsdal, M. A., and Vestbo, J. (2016) High levels of biomarkers of collagen remodeling are associated with increased mortality in COPD - results from the ECLIPSE study. *Respir Res* 17, 125
159. Team, R. C. (2016) R: A Language and Environment for Statistical Computing. R Foundation for Statistical Computing, Vienna, Austria
160. Dragulescu, A. A. (2014) xlsxjars: Package required POI jars for the xlsx package.
161. Dragulescu, A. A. (2014) xlsx: Read, write, format Excel 2007 and Excel 97/2000/XP/2003 files.
162. Urbanek, S. (2016) rJava: Low-Level R to Java Interface. R package version 0.9-8
163. T, T. (2015) _A Package for Survival Analysis in S_.
164. Lou, R., Martinez, M. C., and Naranjo, J. D. (2010) A pretest for choosing between logrank and wilcoxon tests in the two-sample problem. *International Journal of Statistics* LXVIII, 111-125
165. Bobola, M. S. B., A.; Berger, M.S.; Stevens, B.A.; Silber, J.R. (2001) Apurininc/Apyrimidinic Endonuclease Activity Is Elevated in Human Adult Gliomas. *Clinical Cancer Research* 7, 3510-3518
166. Seyfried, T. N., and Huysentruyt, L. C. (2013) On the Origin of Cancer Metastasis. *Crit Rev Oncog* 18, 43-73
167. Jogi, A., Vaapil, M., Johansson, M., and Pahlman, S. (2012) Cancer cell differentiation heterogeneity and aggressive behavior in solid tumors. *Ups J Med Sci* 117, 217-224
168. Zhao, N., Ang, M. K., Yin, X. Y., Patel, M. R., Fritchie, K., Thorne, L., Muldrew, K. L., Hayward, M. C., Sun, W., Wilkerson, M. D., Chera, B. S., Hackman, T., Zanation, A. M., Grilley-Olson, J. E., Couch, M. E., Shockley, W. W., Weissler, M. C., Shores, C. G., Funkhouser, W. K., Olshan, A. F., and Hayes, D. N. (2012) Different cellular p16(INK4a) localisation may signal different survival outcomes in head and neck cancer. *Br J Cancer* 107, 482-490
169. Martinez, M. E., Jacobs, E. T., Baron, J. A., Marshall, J. R., and Byers, T. (2012) Dietary supplements and cancer prevention: balancing potential benefits against proven harms. *J Natl Cancer Inst* 104, 732-739
170. Wei, X., Li, Y. B., Li, Y., Lin, B. C., Shen, X. M., Cui, R. L., Gu, Y. J., Gao, M., Li, Y. G., and Zhang, S. (2017) Prediction of Lymph Node Metastases in Gastric Cancer by Serum APE1 Expression. *J Cancer* 8, 1492-1497
171. Bauer, S. R., Richman, E. L., Sosa, E., Weinberg, V., Song, X., Witte, J. S., Carroll, P. R., and Chan, J. M. (2013) Antioxidant and vitamin E transport genes and risk of high-grade prostate cancer and prostate cancer recurrence. *Prostate* 73, 1786-1795
172. Rajarman, P., Hutchinson, A., Rothman, N., Black, P., Fine, H., Loeffler, J., Selker, R., Shapiro, W., Linet, M., and Inskip, P. (2008) Oxidative response gene polymorphisms and risk of adult brain tumors. *Neuro-Oncology* 10, 709-715
173. Griess, B., Tom, E., Domann, F., and Teoh-Fitzgerald, M. (2017) Extracellular superoxide dismutase and its role in cancer. *Free radical biology & medicine* 112, 464-479
174. Poletto, M., Legrand, A. J., Fletcher, S. C., and Dianov, G. L. (2016) p53 coordinates base excision repair to prevent genomic instability. *Nucleic acids research* 44, 3165-3175
175. Poletto, M., Malfatti, M. C., Dorjsuren, D., Scognamiglio, P. L., Marasco, D., Vascotto, C., Jadhav, A., Maloney, D. J., Wilson, D. M., Simeonov, A., and Tell,

G. (2016) Inhibitors of the apurinic/apyrimidinic endonuclease 1 (APE1)/nucleophosmin (NPM1) interaction that display anti-tumor properties. *Mol Carcinog* 55, 688-704

176. Dubiel, D., Rockel, B., Naumann, M., and Dubiel, W. (2015) Diversity of COP9 signalosome structures and functional consequences. *FEBS letters* 589, 2507-2513
177. Lingaraju, G. M., Bunker, R. D., Cavadini, S., Hess, D., Hassiepen, U., Renatus, M., Fischer, E. S., and Thomä, N. H. (2014) Crystal structure of the human COP9 signalosome. *Nature* 512, 161-165
178. Chamovitz, D. A., Wei, N., Osterlund, M. T., von Arnim, A. G., Staub, J. M., Matsui, M., and Deng, X. W. (1996) The COP9 complex, a novel multisubunit nuclear regulator involved in light control of a plant developmental switch. *Cell* 86, 115-121
179. Emberley, E. D., Mosadeghi, R., and Deshaies, R. J. (2012) Deconjugation of Nedd8 from Cul1 is directly regulated by Skp1-F-box and substrate, and the COP9 signalosome inhibits deneddylated SCF by a noncatalytic mechanism. *The Journal of biological chemistry* 287, 29679-29689
180. Terry J Shackleford, F. X. C. (2010) JAB1/CSN5: a new player in cell cycle control and cancer. *Cell Div.* 5
181. Schweitzer, K., Bozko, P. M., Dubiel, W., and Naumann, M. (2007) CSN controls NF-kappaB by deubiquitinylation of IkappaBalpha. *The EMBO journal* 26, 1532-1541
182. Huang, X., Langelotz, C., Hetfeld-Pechoc, B. K., Schwenk, W., and Dubiel, W. (2009) The COP9 signalosome mediates beta-catenin degradation by deneddylation and blocks adenomatous polyposis coli destruction via USP15. *Journal of molecular biology* 391, 691-702
183. Bae, M. K., Ahn, M. Y., Jeong, J. W., Bae, M. H., Lee, Y. M., Bae, S. K., Park, J. W., Kim, K. R., and Kim, K. W. (2002) Jab1 interacts directly with HIF-1alpha and regulates its stability. *The Journal of biological chemistry* 277, 9-12
184. Tomoda, K., Kato, J. Y., Tatsumi, E., Takahashi, T., Matsuo, Y., and Yoneda-Kato, N. (2005) The Jab1/COP9 signalosome subcomplex is a downstream mediator of Bcr-Abl kinase activity and facilitates cell-cycle progression. *Blood* 105, 775-783
185. Lee, M.-H., Zhao, R., Phan, L., and Yeung, S.-C. J. (2011) Roles of COP9 signalosome in cancer. *Cell Cycle* 10, 3057-3066
186. Bech-Otschir, D., Kraft, R., Huang, X., Henklein, P., Kapelari, B., Pollmann, C., and Dubiel, W. (2001) COP9 signalosome-specific phosphorylation targets p53 to degradation by the ubiquitin system. *The EMBO journal* 20, 1630-1639
187. Wei, N., and Deng, X. W. (2003) The COP9 signalosome. *Annual review of cell and developmental biology* 19, 261-286
188. Kato, J. Y., and Yoneda-Kato, N. (2009) Mammalian COP9 signalosome. *Genes to cells : devoted to molecular & cellular mechanisms* 14, 1209-1225
189. Kotiguda, G. G., Weinberg, D., Dessau, M., Salvi, C., Serino, G., Chamovitz, D. A., and Hirsch, J. A. (2012) The organization of a CSN5-containing subcomplex of the COP9 signalosome. *The Journal of biological chemistry* 287, 42031-42041
190. Sharon, M., Mao, H., Boeri Erba, E., Stephens, E., Zheng, N., and Robinson, C. V. (2009) Symmetrical modularity of the COP9 signalosome complex suggests its multifunctionality. *Structure* 17, 31-40
191. Christmann, M., Schmaler, T., Gordon, C., Huang, X., Bayram, O., Schinke, J., Stumpf, S., Dubiel, W., and Braus, G. H. (2013) Control of multicellular

development by the physically interacting deneddylases DEN1/DenA and COP9 signalosome. *PLoS genetics* 9, e1003275

192. Zhang, W., Qin, Z., Zhang, X., and Xiao, W. (2011) Roles of sequential ubiquitination of PCNA in DNA-damage tolerance. *FEBS letters* 585, 2786-2794
193. Yoshida, A., Yoneda-Kato, N., Panattoni, M., Pardi, R., and Kato, J. Y. (2010) CSN5/Jab1 controls multiple events in the mammalian cell cycle. *FEBS letters* 584, 4545-4552
194. Schütz, A. K., Hennes, T., Jumpertz, S., Fuchs, S., and Bernhagen, J. (2012) Role of CSN5/JAB1 in Wnt/β-catenin activation in colorectal cancer cells. *FEBS letters* 586, 1645-1651
195. Meir, M., Galanty, Y., Kashani, L., Blank, M., Khosravi, R., Fernández-Ávila, M. J., Cruz-García, A., Star, A., Shochot, L., Thomas, Y., Garrett, L. J., Chamovitz, D. A., Bodine, D. M., Kurz, T., Huertas, P., Ziv, Y., and Shiloh, Y. (2015) The COP9 signalosome is vital for timely repair of DNA double-strand breaks. *Nucleic acids research* 43, 4517-4530
196. Leppert, U., Henke, W., Huang, X., Müller, J. M., and Dubiel, W. (2011) Post-transcriptional fine-tuning of COP9 signalosome subunit biosynthesis is regulated by the c-Myc/Lin28B/let-7 pathway. *Journal of molecular biology* 409, 710-721
197. Deng, X. W., Dubiel, W., Wei, N., Hofmann, K., Mundt, K., Colicelli, J., Kato, J., Naumann, M., Segal, D., Seeger, M., Carr, A., Glickman, M., and Chamovitz, D. A. (2000) Unified nomenclature for the COP9 signalosome and its subunits: an essential regulator of development. *Trends Genet* 16, 202-203
198. Subramanian, A., Tamayo, P., Mootha, V. K., Mukherjee, S., Ebert, B. L., Gillette, M. A., Paulovich, A., Pomeroy, S. L., Golub, T. R., Lander, E. S., and Mesirov, J. P. (2005) Gene set enrichment analysis: a knowledge-based approach for interpreting genome-wide expression profiles. *Proceedings of the National Academy of Sciences of the United States of America* 102, 15545-15550
199. Tomoda, K., Yoneda-Kato, N., Fukumoto, A., Yamanaka, S., and Kato, J. Y. (2004) Multiple functions of Jab1 are required for early embryonic development and growth potential in mice. *The Journal of biological chemistry* 279, 43013-43018
200. Network, C. G. A. (2015) Comprehensive genomic characterization of head and neck squamous cell carcinomas. *Nature* 517, 576-582
201. Mundt, K. E., Liu, C., and Carr, A. M. (2002) Deletion mutants in COP9/signalosome subunits in fission yeast Schizosaccharomyces pombe display distinct phenotypes. *Molecular biology of the cell* 13, 493-502
202. Spain, B. H., Bowdish, K. S., Pacal, A. R., Staub, S. F., Koo, D., Chang, C. Y., Xie, W., and Colicelli, J. (1996) Two human cDNAs, including a homolog of Arabidopsis FUS6 (COP11), suppress G-protein- and mitogen-activated protein kinase-mediated signal transduction in yeast and mammalian cells. *Molecular and cellular biology* 16, 6698-6706
203. Liu, X., Pan, Z., Zhang, L., Sun, Q., Wan, J., Tian, C., Xing, G., Yang, J., Jiang, J., and He, F. (2008) JAB1 accelerates mitochondrial apoptosis by interaction with proapoptotic BclGs. *Cellular signalling* 20, 230-240
204. Nargang, F. E., Adames, K., Rüb, C., Cheung, S., Easton, N., Nargang, C. E., and Chae, M. S. (2012) Identification of genes required for alternative oxidase production in the Neurospora crassa gene knockout library. *G3 (Bethesda)* 2, 1345-1356
205. des Georges, A., Dhote, V., Kuhn, L., Hellen, C. U., Pestova, T. V., Frank, J., and Hashem, Y. (2015) Structure of mammalian eIF3 in the context of the 43S preinitiation complex. *Nature* 525, 491-495

206. Izumi, T., Wiederhold, L. R., Roy, G., Roy, R., Jaiswal, A., Bhakat, K. K., Mitra, S., and Hazra, T. K. (2003) Mammalian DNA base excision repair proteins: their interactions and role in repair of oxidative DNA damage. *Toxicology* 193, 43-65
207. Fung, H., and Demple, B. (2005) A vital role for Ape1/Ref1 protein in repairing spontaneous DNA damage in human cells. *Molecular cell* 17, 463-470
208. Masani, S., Han, L., and Yu, K. (2013) Apurinic/apyrimidinic endonuclease 1 is the essential nuclease during immunoglobulin class switch recombination. *Molecular and cellular biology* 33, 1468-1473
209. Xu, J., Husain, A., Hu, W., Honjo, T., and Kobayashi, M. (2014) APE1 is dispensable for S-region cleavage but required for its repair in class switch recombination. *Proceedings of the National Academy of Sciences of the United States of America* 111, 17242-17247
210. Bobola, M. S., Finn, L. S., Ellenbogen, R. G., Geyer, J. R., Berger, M. S., Braga, J. M., Meade, E. H., Gross, M. E., and Silber, J. R. (2005) Apurinic/apyrimidinic endonuclease activity is associated with response to radiation and chemotherapy in medulloblastoma and primitive neuroectodermal tumors. *Clin Cancer Res* 11, 7405-7414
211. Silber, J. R., Bobola, M. S., Blank, A., Schoeler, K. D., Haroldson, P. D., Huynh, M. B., and Kolstoe, D. D. (2002) The apurinic/apyrimidinic endonuclease activity of Ape1/Ref-1 contributes to human glioma cell resistance to alkylating agents and is elevated by oxidative stress. *Clin Cancer Res* 8, 3008-3018
212. Curtis, C. D., Thorngren, D. L., and Nardulli, A. M. (2010) Immunohistochemical analysis of oxidative stress and DNA repair proteins in normal mammary and breast cancer tissues. *BMC Cancer* 10, 9
213. Koukourakis M, G. A., Kakolyris S, Sivridis E, Georgoulias V, Funtzilas G, Hickson I, Gatter K, Harris A. (2001) Nuclear Expression of Human Apurinic/Apyrimidinic Endonuclease (HAP1/REF-1) in Head-And-Neck Cancer is Associated with Resistance To Chemoradiatherapy And Poor Outcome. *Head and Neck* 50, 27-36
214. Yacoub, A., Kelley, M. R., and Deutsch, W. A. (1997) The DNA repair activity of human redox/repair protein APE/Ref-1 is inactivated by phosphorylation. *Cancer research* 57, 5457-5459
215. Lirussi, L., Antoniali, G., Vascotto, C., D'Ambrosio, C., Poletto, M., Romanello, M., Marasco, D., Leone, M., Quadrifoglio, F., Bhakat, K. K., Scaloni, A., and Tell, G. (2012) Nucleolar accumulation of APE1 depends on charged lysine residues that undergo acetylation upon genotoxic stress and modulate its BER activity in cells. *Molecular biology of the cell* 23, 4079-4096
216. Fritz, G., and Kaina, B. (1999) Phosphorylation of the DNA repair protein APE/REF-1 by CKII affects redox regulation of AP-1. *Oncogene* 18, 1033-1040
217. Huang, E., Qu, D., Zhang, Y., Venderova, K., Haque, M. E., Rousseaux, M. W., Slack, R. S., Woulfe, J. M., and Park, D. S. (2010) The role of Cdk5-mediated apurinic/apyrimidinic endonuclease 1 phosphorylation in neuronal death. *Nature cell biology* 12, 563-571
218. Bhakat, K. K., Izumi, T., Yang, S. H., Hazra, T. K., and Mitra, S. (2003) Role of acetylated human AP-endonuclease (APE1/Ref-1) in regulation of the parathyroid hormone gene. *The EMBO journal* 22, 6299-6309
219. Yamamori, T., DeRicco, J., Naqvi, A., Hoffman, T. A., Mattagajasingh, I., Kasuno, K., Jung, S. B., Kim, C. S., and Irani, K. (2010) SIRT1 deacetylates APE1 and regulates cellular base excision repair. *Nucleic acids research* 38, 832-845

220. Busso, C. S., Wedgeworth, C. M., and Izumi, T. (2011) Ubiquitination of human AP-endonuclease 1 (APE1) enhanced by T233E substitution and by CDK5. *Nucleic acids research* 39, 8017-8028
221. Busso, C. S., Iwakuma, T., and Izumi, T. (2009) Ubiquitination of mammalian AP endonuclease (APE1) regulated by the p53-MDM2 signaling pathway. *Oncogene* 28, 1616-1625
222. Clegg, H. V., Itahana, Y., Itahana, K., Ramalingam, S., and Zhang, Y. (2012) Mdm2 RING mutation enhances p53 transcriptional activity and p53-p300 interaction. *PloS one* 7, e38212
223. Itahana, K., Mao, H., Jin, A., Itahana, Y., Clegg, H. V., Lindström, M. S., Bhat, K. P., Godfrey, V. L., Evan, G. I., and Zhang, Y. (2007) Targeted inactivation of Mdm2 RING finger E3 ubiquitin ligase activity in the mouse reveals mechanistic insights into p53 regulation. *Cancer Cell* 12, 355-366
224. Meisenberg, C., Tait, P. S., Dianova, II, Wright, K., Edelmann, M. J., Ternette, N., Tasaki, T., Kessler, B. M., Parsons, J. L., Kwon, Y. T., and Dianov, G. L. (2012) Ubiquitin ligase UBR3 regulates cellular levels of the essential DNA repair protein APE1 and is required for genome stability. *Nucleic acids research* 40, 701-711
225. Dhar, S. K., and St Clair, D. K. (2012) Manganese superoxide dismutase regulation and cancer. *Free radical biology & medicine* 52, 2209-2222
226. Mouchiroud, L., Houtkooper, R. H., Moullan, N., Katsyuba, E., Ryu, D., Cantó, C., Mottis, A., Jo, Y. S., Viswanathan, M., Schoonjans, K., Guarente, L., and Auwerx, J. (2013) The NAD(+)/Sirtuin Pathway Modulates Longevity through Activation of Mitochondrial UPR and FOXO Signaling. *Cell* 154, 430-441
227. Houtkooper, R. H., Mouchiroud, L., Ryu, D., Moullan, N., Katsyuba, E., Knott, G., Williams, R. W., and Auwerx, J. (2013) Mitonuclear protein imbalance as a conserved longevity mechanism. *Nature* 497, 451-457
228. Ohsawa, S., Sato, Y., Enomoto, M., Nakamura, M., Betsumiya, A., and Igaki, T. (2012) Mitochondrial defect drives non-autonomous tumour progression through Hippo signalling in Drosophila. *Nature* 490, 547-551
229. Kazak, L., Reyes, A., and Holt, I. J. (2012) Minimizing the damage: repair pathways keep mitochondrial DNA intact. *Nat Rev Mol Cell Biol* 13, 659-671
230. Youle, R. J., and Narendra, D. P. (2011) Mechanisms of mitophagy. *Nat Rev Mol Cell Biol* 12, 9-14
231. Fouquerel, E., Goellner, E. M., Yu, Z., Gagné, J. P., Barbi de Moura, M., Feinstein, T., Wheeler, D., Redpath, P., Li, J., Romero, G., Migaud, M., Van Houten, B., Poirier, G. G., and Sobol, R. W. (2014) ARTD1/PARP1 negatively regulates glycolysis by inhibiting hexokinase 1 independent of NAD+ depletion. *Cell Rep* 8, 1819-1831
232. Fang, E. F., Scheibye-Knudsen, M., Brace, L. E., Kassahun, H., SenGupta, T., Nilsen, H., Mitchell, J. R., Croteau, D. L., and Bohr, V. A. (2014) Defective mitophagy in XPA via PARP-1 hyperactivation and NAD(+)/SIRT1 reduction. *Cell* 157, 882-896
233. Hegde, M. L., Izumi, T., and Mitra, S. (2012) Oxidized base damage and single-strand break repair in mammalian genomes: role of disordered regions and posttranslational modifications in early enzymes. *Prog Mol Biol Transl Sci* 110, 123-153
234. Pickrell, A. M., and Youle, R. J. (2015) The roles of PINK1, parkin, and mitochondrial fidelity in Parkinson's disease. *Neuron* 85, 257-273
235. Koyano, F., Okatsu, K., Kosako, H., Tamura, Y., Go, E., Kimura, M., Kimura, Y., Tsuchiya, H., Yoshihara, H., Hirokawa, T., Endo, T., Fon, E. A., Trempe, J. F.,

Saeki, Y., Tanaka, K., and Matsuda, N. (2014) Ubiquitin is phosphorylated by PINK1 to activate parkin. *Nature* 510, 162-166

236. Wauer, T., Swatek, K. N., Wagstaff, J. L., Gladkova, C., Pruneda, J. N., Michel, M. A., Gersch, M., Johnson, C. M., Freund, S. M., and Komander, D. (2015) Ubiquitin Ser65 phosphorylation affects ubiquitin structure, chain assembly and hydrolysis. *The EMBO journal* 34, 307-325
237. Kane, L. A., Lazarou, M., Fogel, A. I., Li, Y., Yamano, K., Sarraf, S. A., Banerjee, S., and Youle, R. J. (2014) PINK1 phosphorylates ubiquitin to activate Parkin E3 ubiquitin ligase activity. *The Journal of cell biology* 205, 143-153
238. Kazlauskaite, A., Kondapalli, C., Gourlay, R., Campbell, D. G., Ritorto, M. S., Hofmann, K., Alessi, D. R., Knebel, A., Trost, M., and Muqit, M. M. (2014) Parkin is activated by PINK1-dependent phosphorylation of ubiquitin at Ser65. *The Biochemical journal* 460, 127-139
239. Wang, X., Winter, D., Ashrafi, G., Schlehe, J., Wong, Y. L., Selkoe, D., Rice, S., Steen, J., LaVoie, M. J., and Schwarz, T. L. (2011) PINK1 and Parkin target Miro for phosphorylation and degradation to arrest mitochondrial motility. *Cell* 147, 893-906
240. Geisler, S., Holmström, K. M., Skujat, D., Fiesel, F. C., Rothfuss, O. C., Kahle, P. J., and Springer, W. (2010) PINK1/Parkin-mediated mitophagy is dependent on VDAC1 and p62/SQSTM1. *Nature cell biology* 12, 119-131
241. Veeriah, S., Taylor, B. S., Meng, S., Fang, F., Yilmaz, E., Vivanco, I., Janakiraman, M., Schultz, N., Hanrahan, A. J., Pao, W., Ladanyi, M., Sander, C., Heguy, A., Holland, E. C., Paty, P. B., Mischel, P. S., Liau, L., Cloughesy, T. F., Mellinghoff, I. K., Solit, D. B., and Chan, T. A. (2010) Somatic mutations of the Parkinson's disease-associated gene PARK2 in glioblastoma and other human malignancies. *Nat Genet* 42, 77-82
242. Gong, Y., Zack, T. I., Morris, L. G., Lin, K., Hukkelhoven, E., Raheja, R., Tan, I. L., Turcan, S., Veeriah, S., Meng, S., Viale, A., Schumacher, S. E., Palmedo, P., Beroukhim, R., and Chan, T. A. (2014) Pan-cancer genetic analysis identifies PARK2 as a master regulator of G1/S cyclins. *Nat Genet* 46, 588-594
243. Zhang, C., Lin, M., Wu, R., Wang, X., Yang, B., Levine, A. J., Hu, W., and Feng, Z. (2011) Parkin, a p53 target gene, mediates the role of p53 in glucose metabolism and the Warburg effect. *Proceedings of the National Academy of Sciences of the United States of America* 108, 16259-16264
244. Viotti, J., Duplan, E., Caillava, C., Condat, J., Goiran, T., Giordano, C., Marie, Y., Idbaih, A., Delattre, J. Y., Honnorat, J., Checler, F., and Alves da Costa, C. (2014) Glioma tumor grade correlates with parkin depletion in mutant p53-linked tumors and results from loss of function of p53 transcriptional activity. *Oncogene* 33, 1764-1775
245. Sarraf, S. A., Raman, M., Guarani-Pereira, V., Sowa, M. E., Huttlin, E. L., Gygi, S. P., and Harper, J. W. (2013) Landscape of the PARKIN-dependent ubiquitylome in response to mitochondrial depolarization. *Nature* 496, 372-376
246. Narendra, D., Tanaka, A., Suen, D. F., and Youle, R. J. (2008) Parkin is recruited selectively to impaired mitochondria and promotes their autophagy. *The Journal of cell biology* 183, 795-803
247. Beilina, A., Van Der Brug, M., Ahmad, R., Kesavapany, S., Miller, D. W., Petsko, G. A., and Cookson, M. R. (2005) Mutations in PTEN-induced putative kinase 1 associated with recessive parkinsonism have differential effects on protein stability. *Proceedings of the National Academy of Sciences of the United States of America* 102, 5703-5708

248. Sammarco, M. C., and Grabczyk, E. (2005) A series of bidirectional tetracycline-inducible promoters provides coordinated protein expression. *Anal Biochem* 346, 210-216
249. Collett, M. S., and Erikson, R. L. (1978) Protein kinase activity associated with the avian sarcoma virus src gene product. *Proceedings of the National Academy of Sciences of the United States of America* 75, 2021-2024
250. Izumi, T., Malecki, J., Chaudhry, M. A., Weinfeld, M., Hill, J. H., Lee, J. C., and Mitra, S. (1999) Intragenic suppression of an active site mutation in the human apurinic/apyrimidinic endonuclease. *Journal of molecular biology* 287, 47-57
251. <Oncogene 28(13)Suppl, 2009 Busso etal.pdf>.
252. Scheffner, M., Werness, B. A., Huibregtse, J. M., Levine, A. J., and Howley, P. M. (1990) The E6 oncoprotein encoded by human papillomavirus types 16 and 18 promotes the degradation of p53. *Cell* 63, 1129-1136
253. Marchenko, N. D., Wolff, S., Erster, S., Becker, K., and Moll, U. M. (2007) Monoubiquitylation promotes mitochondrial p53 translocation. *The EMBO journal* 26, 923-934
254. Lee, K. Y., and Myung, K. (2008) PCNA modifications for regulation of post-replication repair pathways. *Mol Cells* 26, 5-11
255. Wang, H. L., Chou, A. H., Wu, A. S., Chen, S. Y., Weng, Y. H., Kao, Y. C., Yeh, T. H., Chu, P. J., and Lu, C. S. (2011) PARK6 PINK1 mutants are defective in maintaining mitochondrial membrane potential and inhibiting ROS formation of substantia nigra dopaminergic neurons. *Biochimica et biophysica acta* 1812, 674-684
256. Chung, K. K., Zhang, Y., Lim, K. L., Tanaka, Y., Huang, H., Gao, J., Ross, C. A., Dawson, V. L., and Dawson, T. M. (2001) Parkin ubiquitinates the alpha-synuclein-interacting protein, synphilin-1: implications for Lewy-body formation in Parkinson disease. *Nature medicine* 7, 1144-1150
257. Haque, M. E., Thomas, K. J., D'Souza, C., Callaghan, S., Kitada, T., Slack, R. S., Fraser, P., Cookson, M. R., Tandon, A., and Park, D. S. (2008) Cytoplasmic Pink1 activity protects neurons from dopaminergic neurotoxin MPTP. *Proceedings of the National Academy of Sciences of the United States of America* 105, 1716-1721
258. Joo, J. H., Dorsey, F. C., Joshi, A., Hennessy-Walters, K. M., Rose, K. L., McCastlain, K., Zhang, J., Iyengar, R., Jung, C. H., Suen, D. F., Steeves, M. A., Yang, C. Y., Prater, S. M., Kim, D. H., Thompson, C. B., Youle, R. J., Ney, P. A., Cleveland, J. L., and Kundu, M. (2011) Hsp90-Cdc37 chaperone complex regulates Ulk1- and Atg13-mediated mitophagy. *Molecular cell* 43, 572-585
259. Tanaka, A. (2010) Parkin-mediated selective mitochondrial autophagy, mitophagy: Parkin purges damaged organelles from the vital mitochondrial network. *FEBS letters* 584, 1386-1392
260. Lazarou, M., Jin, S. M., Kane, L. A., and Youle, R. J. (2012) Role of PINK1 binding to the TOM complex and alternate intracellular membranes in recruitment and activation of the E3 ligase Parkin. *Developmental cell* 22, 320-333
261. Narendra, D. P., Jin, S. M., Tanaka, A., Suen, D. F., Gautier, C. A., Shen, J., Cookson, M. R., and Youle, R. J. (2010) PINK1 is selectively stabilized on impaired mitochondria to activate Parkin. *PLoS Biol* 8, e1000298
262. Brooks, J., Ding, J., Simon-Sanchez, J., Paisan-Ruiz, C., Singleton, A. B., and Scholz, S. W. (2009) Parkin and PINK1 mutations in early-onset Parkinson's disease: comprehensive screening in publicly available cases and control. *J Med Genet* 46, 375-381

263. Beasley, S. A., Hristova, V. A., and Shaw, G. S. (2007) Structure of the Parkin in-between-ring domain provides insights for E3-ligase dysfunction in autosomal recessive Parkinson's disease. *Proceedings of the National Academy of Sciences of the United States of America* 104, 3095-3100
264. Wenzel, D. M., Lissounov, A., Brzovic, P. S., and Klevit, R. E. (2011) UBCH7 reactivity profile reveals parkin and HHARI to be RING/HECT hybrids. *Nature* 474, 105-108
265. Frossi, B., Tell, G., Spessotto, P., Colombatti, A., Vitale, G., and Pucillo, C. (2002) H(2)O(2) induces translocation of APE/Ref-1 to mitochondria in the Raji B-cell line. *J Cell Physiol* 193, 180-186
266. Gorman, M. A., Morera, S., Rothwell, D. G., de La Fortelle, E., Mol, C. D., Tainer, J. A., Hickson, I. D., and Freemont, P. S. (1997) The crystal structure of the human DNA repair endonuclease HAP1 suggests the recognition of extra-helical deoxyribose at DNA abasic sites. *The EMBO journal* 16, 6548-6558
267. Izumi, T., and Mitra, S. (1998) Deletion analysis of human AP-endonuclease: minimum sequence required for the endonuclease activity. *Carcinogenesis* 19, 525-527
268. Fantini, D., Vascotto, C., Marasco, D., D'Ambrosio, C., Romanello, M., Vitagliano, L., Pedone, C., Poletto, M., Cesaratto, L., Quadrifoglio, F., Scaloni, A., Radicella, J. P., and Tell, G. (2010) Critical lysine residues within the overlooked N-terminal domain of human APE1 regulate its biological functions. *Nucleic acids research* 38, 8239-8256
269. Fiszer-Kierzkowska, A., Vydra, N., Wysocka-Wycisk, A., Kronekova, Z., Jarząb, M., Lisowska, K. M., and Krawczyk, Z. (2011) Liposome-based DNA carriers may induce cellular stress response and change gene expression pattern in transfected cells. *BMC Mol Biol* 12, 27
270. Jacobsen, L., Calvin, S., and Lobenhofer, E. (2009) Transcriptional effects of transfection: the potential for misinterpretation of gene expression data generated from transiently transfected cells. *Biotechniques* 47, 617-624
271. Szczesny, B., and Mitra, S. (2005) Effect of aging on intracellular distribution of abasic (AP) endonuclease 1 in the mouse liver. *Mech Ageing Dev* 126, 1071-1078
272. Mitra, S., Izumi, T., Boldogh, I., Bhakat, K. K., Chattopadhyay, R., and Szczesny, B. (2007) Intracellular trafficking and regulation of mammalian AP-endonuclease 1 (APE1), an essential DNA repair protein. *DNA repair* 6, 461-469
273. Li, M., Zhong, Z., Zhu, J., Xiang, D., Dai, N., Cao, X., Qing, Y., Yang, Z., Xie, J., Li, Z., Baugh, L., Wang, G., and Wang, D. (2010) Identification and characterization of mitochondrial targeting sequence of human apurinic/apyrimidinic endonuclease 1. *The Journal of biological chemistry* 285, 14871-14881
274. Kakolyris, S., Kaklamanis, L., Giatromanolaki, A., Koukourakis, M., Hickson, I. D., Barzilay, G., Turley, H., Leek, R. D., Kanavaros, P., Georgoulias, V., Gatter, K. C., and Harris, A. L. (1998) Expression and subcellular localization of human AP endonuclease 1 (HAP1/Ref-1) protein: a basis for its role in human disease. *Histopathology* 33, 561-569
275. Vascotto, C., Bisetto, E., Li, M., Zeef, L. A., D'Ambrosio, C., Domenis, R., Comelli, M., Delneri, D., Scaloni, A., Altieri, F., Mavelli, I., Quadrifoglio, F., Kelley, M. R., and Tell, G. (2011) Knock-in reconstitution studies reveal an unexpected role of Cys-65 in regulating APE1/Ref-1 subcellular trafficking and function. *Molecular biology of the cell* 22, 3887-3901

276. Hu, H. H., Kannengiesser, C., Lesage, S., André, J., Mourah, S., Michel, L., Descamps, V., Basset-Seguin, N., Bagot, M., Bensussan, A., Lebbé, C., Deschamps, L., Saiag, P., Leccia, M. T., Bressac-de-Paillerets, B., Tsalamlal, A., Kumar, R., Klebe, S., Grandchamp, B., Andrieu-Abadie, N., Thomas, L., Brice, A., Dumaz, N., and Soufir, N. (2016) PARKIN Inactivation Links Parkinson's Disease to Melanoma. *J Natl Cancer Inst* 108
277. Groisman, R., Polanowska, J., Kuraoka, I., Sawada, J., Saijo, M., Drapkin, R., Kisselev, A. F., Tanaka, K., and Nakatani, A. F. (2003) The Ubiquitin Ligase Activity in the DDB2 and CSA Complexes Is Differentially Regulated by the COP9 Signalosome in Response to DNA Damage. *Cell* 113, 357-367
278. Fousteri, M., Vermeulen, W., van Zeeland, A. A., and Mullenders, L. H. (2006) Cockayne Syndrome A and B Proteins Differentially Regulate Recruitment of Chromatin Remodeling and Repair Factors to Stalled RNA Polymerase II In Vivo. *Molecular cell* 23, 471-482
279. Oliveira, D. V., Kato, A., Nakamura, K., Ikura, T., Okada, M., Kobayashi, J., Yanagihara, H., Saito, Y., Tauchi, H., and Komatsu, K. (2014) Histone chaperone FACT regulates homologous recombination by chromatin remodeling through interaction with RNF20. *J Cell Sci* 127, 763-772
280. Xiang, Y., Laurent, B., Hsu, C. H., Nachtergaele, S., Lu, Z., Sheng, W., Xu, C., Chen, H., Ouyang, J., Wang, S., Ling, D., Hsu, P. H., Zou, L., Jambhekar, A., He, C., and Shi, Y. (2017) RNA m6A methylation regulates the ultraviolet-induced DNA damage response. *Nature* 543, 573-576
281. Clarke, T. L., Sanchez-Bailon, M. P., Chiang, K., Reynolds, J. J., Herrero-Ruiz, J., Bandeiras, T. M., Matias, P. M., Maslen, S. L., Skehel, J. M., Stewart, G. S., and Davies, C. C. (2017) PRMT5-Dependent Methylation of the TIP60 Coactivator RUVBL1 Is a Key Regulator of Homologous Recombination. *Molecular cell* 65, 900-916 e907
282. Bounaix Morand du Puch, C., Barbier, E., Kraut, A., Coute, Y., Fuchs, J., Buhot, A., Livache, T., Seve, M., Favier, A., Douki, T., Gasparutto, D., Sauvaigo, S., and Breton, J. (2011) TOX4 and its binding partners recognize DNA adducts generated by platinum anticancer drugs. *Arch Biochem Biophys* 507, 296-303
283. Seibold, P., Schmezer, P., Behrens, S., Michailidou, K., Bolla, M. K., Wang, Q., Flesch-Janys, D., Nevanlinna, H., Fagerholm, R., Aittomaki, K., Blomqvist, C., Margolin, S., Mannermaa, A., Kataja, V., Kosma, V. M., Hartikainen, J. M., Lambrechts, D., Wildiers, H., Kristensen, V., Alnaes, G. G., Nord, S., Borresen-Dale, A. L., Hooning, M. J., Hollestelle, A., Jager, A., Seynaeve, C., Li, J., Liu, J., Humphreys, K., Dunning, A. M., Rhenius, V., Shah, M., Kabisch, M., Torres, D., Ulmer, H. U., Hamann, U., Schildkraut, J. M., Purrington, K. S., Couch, F. J., Hall, P., Pharoah, P., Easton, D. F., Schmidt, M. K., Chang-Claude, J., and Popanda, O. (2015) A polymorphism in the base excision repair gene PARP2 is associated with differential prognosis by chemotherapy among postmenopausal breast cancer patients. *BMC Cancer* 15, 978
284. Zhang, Y., Wang, J., Xiang, D., Wang, D., and Xin, X. (2009) Alterations in the expression of the apurinic/apyrimidinic endonuclease-1/redox factor-1 (APE1/Ref-1) in human ovarian cancer and identification of the therapeutic potential of APE1/Ref-1 inhibitor. *International Journal of Oncology* 35, 1069-1079
285. Achinger-Kawecka, J., and Clark, S. J. (2017) Disruption of the 3D cancer genome blueprint. *Epigenomics* 9, 47-55
286. Bradner, J. E., Hnisz, D., and Young, R. A. (2017) Transcriptional Addiction in Cancer. *Cell* 168, 629-643

287. Wenz, T. (2009) PGC-1alpha activation as a therapeutic approach in mitochondrial disease. *IUBMB Life* 61, 1051-1062

Vita

Education

Institution	**Concentration**	**Degree Date**
Wright State University	Neuroscience and Physiology M.S.	2006-2008
Wright State University	Biology B.S.	2000-2006

Professional Positions Held

Institution	**Department**	**Position**	**Duration**
University of Kentucky	Toxicology and Cancer Biology	Research Assistant	Fall 2012-Present
University of Kentucky	Toxicology and Cancer Biology	Teaching Assistant	Fall 2016
University of Cincinnati	University of Cincinnati Cancer Institute Tumor Bank	Tumor Bank Coordinator	FEB 2011-JUL 2012
University of Cincinnati	Cancer Biology	Research Assistant	JUL 2008-AUG 2010
Wright State University	Neuroscience, Cell Biology, and Physiology	Research Assistant	Fall 2006-Spring 2008
Wright State University	Biology	Laboratory Assistant	JAN -OCT 2007

Scholastic and Professional Honors

2016-Present	Molecular Mechanisms of Toxicity Training Grant (T32ES007266)
2008	Nomination for Midwestern Association of Graduate Schools (MAGS) Distinguished Thesis Awards
2006-2008	Wright State University Department of Neuroscience, Cell Biology, and Physiology Tuition Scholarship

Professional Publications

Original Articles

Wicker, C.A. and Izumi, T. (2016) Analysis of RNA expression of normal and cancer tissues reveal high expression correlation of the COPS5 gene with mitochondrial genes. BMC Genomics 17:983

Scott, T. L.**, **Wicker, C. A**.**, Rangaswamy, S, Dhar, B., Pittman, T. Horbinski, C. and Izumi, T. (2016) Polyubiquitination of Apurinic/Apyrimidinic Endonuclease 1 by Parkin Mol Carcinog e-pub ahead of print **co-first author

Wicker, C.A.; Kulkarni-Datar, K.; Srivastava, S.; Brown, T. (2010) BITC sensitizes pancreatic Adenocarcinoma to TRAIL-induced Apoptosis. *Cancer Growth and Metastasis* 2: 45-55

Review Articles

Scott, T. L., Rangaswamy, S., **Wicker, C. A.,** and Izumi, T. (2014) Repair of oxidative DNA damage and cancer: recent progress in DNA base excision repair. *Antioxidants & redox signaling* 20, 708-726

Poster and Platform Presentations

Wicker, C.A.*; Scott, T.L.; Rangaswamy, S.; Arnold, S.; Brill, Y.; Chen, L.; Horbinski, C.; Napier, D.; Valentino, J.; Kudrimoti, M.; Yu, G.; Izumi, T. (April 2017). “Regulation of tumor suppressor decorin by APE1 in head and neck squamous cell carcinoma” Presented at AACR; Washington DC

Wicker, C.A.; Scott, T.L.; Rangaswamy, S.; Arnold, S.; Brill, Y.; Chen, L.; Horbinski, C.; Napier, D.; Valentino, J.; Kudrimoti, M.; Yu, G.; Izumi, T.* (May 2017).**“**Regulation of tumor suppressor decorin by APE1 in head and neck squamous cell carcinoma” Presented at the Markey Cancer Center Research Day; Lexington, KY.

Wicker, C.A.*; Scott, T.L.; Rangaswamy, S.; Arnold, S.; Brill, Y.; Chen, L.; Horbinski, C.; Napier, D.; Valentino, J.; Kudrimoti, M.; Yu, G.; Izumi, T. (2016) “Downregulation of Tumor Suppressor Decorin by APE1 in Head and Neck Squamous Cell Carcinoma” Presented at the Markey Cancer Center Research Day; Lexington, KY

Wicker, C.A.; Rangaswamy, S.; Arnold, S.; Brill, Y.; Horbinski, C.; Napier, D.; Valentino, J.; Kudrimoti, M.; Yu, G.; Izumi, T. (June 2015) “APE1’s Regulation of Decorin and its Role in Cancer”; Presented at Ohio Valley Society of Toxicology Summer Meeting; University of Cincinnati; Cincinnati, Ohio ***

Wicker, C.A.*; Scott, T.L.; Rangaswamy, S.; Arnold, S.; Brill, Y.; Chen, L.; Horbinski, C.; Napier, D.; Valentino, J.; Kudrimoti, M.; Yu, G.; Izumi, T. (2016) “Downregulation of Tumor Suppressor Decorin by APE1 in Head and Neck Squamous Cell Carcinoma” Presented at the Markey Cancer Center Research Day; Lexington, KY

Wicker, C.A.*; Rangaswamy, S.; Arnold, S.; Brill, Y.; Horbinski, C.; Napier, D.; Valentino, J.; Kudrimoti, M.; Yu, G.; Izumi, T. “APE1’s Regulation of Decorin and its Role in Cancer”; (Nov. 2015) Presented at Ohio Valley Society of Toxicology Annual Meeting; Northern Kentucky University; Highland Heights, KY

Wicker, C.A.*; Rangaswamy, S.; Arnold, S.; Brill, Y.; Horbinski, C.; Napier, D.; Valentino, J.; Kudrimoti, M.; Yu, G.; Izumi, T. (June 2015) “APE1’s Regulation of Decorin and its Role in Cancer”; Presented at Ohio Valley Society of Toxicology Summer Meeting; University of Cincinnati; Cincinnati, Ohio

Wicker, C.A.*; Scott,T.; Dhar, B.; Saito, H.; Horbinski, C.; Chen, L.; Orren, D.; Valentino, J.; Arnold, S.; Kudrimoti, M.; Yu, G.; Izumi, T. (Sept. 2014) “Expression and Subcellular Distribution of AP Endonuclease 1 in Head and Neck Tumors. Presented at the Ohio Valley Society of Toxicology Annual Meeting; Wright State University; Dayton, Ohio

Wicker, C.A.*; Scott, T.L.; Dhar, B.; Saito, H.; Horbinski, C.; Chen, L.; Orren, D.; Valentino, J.; Arnold, S.; Kudrimoti, M.; Yu, G.; Izumi, T (2014) “Expression and Subcellular Distribution of AP Endonuclease 1 in Head and Neck Tumors. Presented at the Markey Cancer Center Research Day; Lexington, KY

Rangaswamy, S.*; Chakraborty, A.; Scott,T.L..; Dhar, B.; **Wicker, C.A.**; Hazra, T.; Izumi, T. (2014) “Viability of Cells with Extremely Low Levels of APE1, An Essential DNA Base Excision Repair Protein” Presented at the Markey Cancer Center Research Day; Lexington, KY

Clark, S.*; **Wicker, C.A.**; Valentino, J.; Izumi, T.; Orren, D.; Machwe, A. (2014) “Relationships Between Tobacco Use, DNA Damage Biomarkers, and the Etiology of Head and Neck Cancers” Presented at the Markey Cancer Center Research Day; Lexington, KY

Sagin, F.*; Winstead, K.; **Wicker, C.A.**; Fathallah; H. (2012) “Standardization of Consent Practices at the University of Cincinnati Cancer Institute Tumor Bank: Challenge in Specimen Banking” Presented at the 5th Annual Biospecimen Research Network (BRN) Symposium; Bethesda, MD

Wicker, C.A.; Winstead, K.; Sagin; F.*; Fathallah; H. (2012) “Improving Biospecimen Collection Practices at the University of Cincinnati Cancer Institute Tumor Bank” Presented at the 5th Annual Biospecimen Research Net-work (BRN) Symposium; Bethesda, MD

Wicker, C.A.*; Kulkarni-Datar, K.; Sahu, R.; Srivastava, S.; Brown, T. (2008) “Effects of BITC on TRAIL Sensitization in Human Pancreatic Adenocarcinoma” Experimental Biology; April 5-9, 2008; San Diego, CA

Wicker, C.A.; Kulkarni-Datar, K.; Sahu, R*.; Srivastava, S.; Brown, T. (2008) “Benzyl isothiocyanate sensitizes human pancreatic cells to TRAIL-induced apoptosis” American Association for Cancer Research (AACR) ; April 12-16, 2008; San Diego, CA.

Wicker, C.A.*; Kulkarni-Datar, K.; Srivastava, S.; Brown, T. (2007) “Effects of BITC on TRAIL Sensitization in Human Pancreatic Adenocarcinoma” Presented at WSU Research Forum; Dayton, OH ***

Wicker, C.A.*; Kulkarni-Datar, K.; Srivastava, S.; Brown, T. (2007) “Effects of BITC on TRAIL Sensitization in Human Pancreatic Adenocarcinoma” Presented at 22nd Annual Meeting of the Ohio Physiological Society; Athens, OH

*Presenting author
** co-first author
***Platform presentation